ESCOLA POLITÉCNICA
PROGRAMA DE PÓS-GRADUAÇÃO
ENGENHARIA E TECNOLOGIA DE MATERIAIS - PGETEMA

VICTOR HUGO JACKS MENDES DOS SANTOS

DESENVOLVIMENTO DE MÉTODO QUANTITATIVO E ESTUDO DE GEOQUÍMICA ISOTÓPICA PARA MONITORAR A INTEGRIDADE DAS PASTAS DE CIMENTO DE POÇOS EXPOSTOS A AMBIENTES RICOS EM CO_2

Porto Alegre
2022

PÓS-GRADUAÇÃO - *STRICTO SENSU*

Pontifícia Universidade Católica
do Rio Grande do Sul

Ficha Catalográfica

S237d Santos, Victor Hugo Jacks Mendes dos

Desenvolvimento de método quantitativo e estudo de geoquímica isotópica para monitorar a integridade das pastas de cimento de poços expostos a ambientes ricos em CO2 / Victor Hugo Jacks Mendes dos Santos. – 2022.
214 f.
Tese (Doutorado) – Programa de Pós-Graduação em Engenharia e Tecnologia de Materiais, PUCRS.

Orientador: Prof. Dr. Felipe Dalla Vecchia.
Coorientadora: Profa. Dra. Sandra Mara Oliveira Einloft.

1. Integridade de poços. 2. Degradação por CO2. 3. Monitoramento de poços. 4. Análise multivariada. 5. Geoquímica isotópica. I. Dalla Vecchia, Felipe. II. Einloft, Sandra Mara Oliveira. III. , . IV. Título.

Elaborada pelo Sistema de Geração Automática de Ficha Catalográfica da PUCRS
com os dados fornecidos pelo(a) autor(a).
Bibliotecária responsável: Loiva Duarte Novak CRB-10/2079

Pontifícia Universidade Católica do Rio Grande do Sul
ESCOLA POLITÉCNICA
PROGRAMA DE PÓS-GRADUAÇÃO EM ENGENHARIA E TECNOLOGIA DE MATERIAIS

DESENVOLVIMENTO DE MÉTODO QUANTITATIVO E ESTUDO DE GEOQUÍMICA ISOTÓPICA PARA MONITORAR A INTEGRIDADE DAS PASTAS DE CIMENTO DE POÇOS EXPOSTOS A AMBIENTES RICOS EM CO2

CANDIDATO: VICTOR HUGO JACKS MENDES DOS SANTOS

Esta Tese de Doutorado foi julgada para obtenção do título de DOUTOR EM ENGENHARIA E TECNOLOGIA DE MATERIAIS e aprovada em sua forma final pelo Programa de Pós-Graduação em Engenharia e Tecnologia de Materiais da Pontifícia Universidade Católica do Rio Grande do Sul.

DR. FELIPE DALLA VECCHIA - ORIENTADOR

DRA. SANDRA MARA OLIVEIRA EINLOFT - COORIENTADORA

BANCA EXAMINADORA

DRA. ANA MARIA PIMENTEL MIZUSAKI - PROGRAMA DE PÓS-GRADUAÇÃO EM GEOCIÊNCIAS - UFRGS

DR. MAURICIO MANCIO - PROGRAMA DE PÓS-GRADUAÇÃO EM ENGENHARIA CIVIL - PPGEC - UNISINOS

DRA. ELEANI MARIA DA COSTA - PGETEMA - PUCRS

PUCRS
Campus Central
Av. Ipiranga, 6681 - Prédio 32 - Sala 507 - CEP: 90619-900
Telefone: (51) 3353.4059 - Fax: (51) 3320.3625
E-mail: engenharia.pg.materiais@pucrs.br
www.pucrs.br/politecnica

Pontifícia Universidade Católica do Rio Grande do Sul
Programa de Pós-Graduação em Engenharia e Tecnologia de Materiais

DESENVOLVIMENTO DE MÉTODO QUANTITATIVO E ESTUDO DE GEOQUÍMICA ISOTÓPICA PARA MONITORAR A INTEGRIDADE DAS PASTAS DE CIMENTO DE POÇOS EXPOSTOS A AMBIENTES RICOS EM CO_2

VICTOR HUGO JACKS MENDES DOS SANTOS
BACHAREL EM QUÍMICA INDUSTRIAL
MESTRE EM ENGENHARIA E TECNOLOGIA DE MATERIAIS

PROPOSTA DE TESE PARA A OBTENÇÃO DO TÍTULO DE DOUTOR EM ENGENHARIA E TECNOLOGIA DE MATERIAIS

Porto Alegre

Maio, 2022

Pontifícia Universidade Católica do Rio Grande do Sul
Programa de Pós-Graduação em Engenharia e Tecnologia de Materiais

DESENVOLVIMENTO DE MÉTODO QUANTITATIVO E ESTUDO DE GEOQUÍMICA ISOTÓPICA PARA MONITORAR A INTEGRIDADE DAS PASTAS DE CIMENTO DE POÇOS EXPOSTOS A AMBIENTES RICOS EM CO_2

VICTOR HUGO JACKS MENDES DOS SANTOS
BACHAREL EM QUÍMICA INDUSTRIAL
MESTRE EM ENGENHARIA E TECNOLOGIA DE MATERIAIS

ORIENTADOR: PROF. DR. FELIPE DALLA VECCHIA
CO-ORIENTADORA: PROFA. DRA. SANDRA MARA OLIVEIRA EINLOFT

Proposta de Tese realizada no Programa de Pós-Graduação em Engenharia e Tecnologia de Materiais (PGETEMA) da Pontifícia Universidade Católica do Rio Grande do Sul, como parte dos requisitos para a obtenção do título de Doutor em Engenharia e Tecnologia de Materiais.

Trabalho vinculado aos Projetos – Convênio PUCRS/ Petrobras nº 2017/00742-8 e n° 2018/00235-1

Porto Alegre

Maio, 2022

“Never express yourself more clearly than you are able to think.”
(Niels Bohr)

DEDICATÓRIA

Dedico este trabalho aos meus pais, por todo incentivo e confiança depositados em mim, e a todos aqueles que em gestos, pensamentos e/ou orações mantiveram-se presentes.

AGRADECIMENTOS

Aos meus pais, Luiz Alfredo Mendes dos Santos e Fátima Regina Jacks Mendes dos Santos, por todo incentivo, conselhos e amor.

A minha família e aos meus amigos por todo carinho e compreensão com meus momentos de ausência.

Aos meus orientadores Felipe Dalla Vecchia e Sandra Mara Oliveira Einloft, bem como ao Professor Marcus Seferin (orientador de mestrado), por todas as oportunidades, ensinamentos, conselhos, dedicação, confiança depositada, anos de amizade e empenho ao longo do meu ensino e desenvolvimento profissional.

Ao Instituto do Petróleo e dos Recursos Naturais (IPR) da PUCRS pelo acolhimento, auxílio financeiro, oportunidades, aprendizados e sensibilidade ao me liberar para o desenvolvimento deste trabalho.

Aos meus colegas e amigos do IPR de hoje e de outrora, em especial aos meus colegas de projeto, Darlan Pontin, Gabriela Gonçalves Dias Ponzi, Amanda Sofia de Guimarães e Stepanha, Renan Bordulis Martel e Marta Kerber Schütz, por todo o apoio, anos de amizade, pelas conversas edificantes e cafés compartilhados.

Aos colegas Pâmela de Medeiros Engelmann, Victor Kovaski Cescani, João Pedro Tauscheck Zielinski, Rosalia Barili da Cunha, Clarissa Lovato Melo pelo auxílio prestado durante a etapa de execução do presente trabalho e pela troca de experiências.

À Petrobras, que financiou significativamente a execução das atividades de pesquisa desenvolvidas.

E a todos que direta ou indiretamente fizeram parte do desenvolvimento deste trabalho.

SUMÁRIO

LISTA DE FIGURAS

LISTA DE TABELAS

LISTA DE SÍMBOLOS

A	Absorbância	% A
$CaCO_3$	Concentração de $CaCO_3$ na pasta de cimento	mg $CaCO_3$/g cimento
P	Pressão	bar
DIC	Carbono inorgânico dissolvido	Na_2CO_3-eq ppm
EC	Condutividade elétrica	$\mu s.cm^{-1}$
T	Transmitância	% T
Temp.	Temperatura	°C
Tc	Taxa de corrosão	mm/ano
wt. %	Percentual mássico	%
$\delta^{13}C$	Assinatura isotópica do carbono	‰ (per mil)
ε	Fator de enriquecimento isotópico	‰ (per mil)
θ-2θ	Ângulo de difração de Raios-X	°

LISTA DE ABREVIAÇÕES

A	Óxido de Alumínio (Al_2O_3)
Afm	Monosulfato
Aft	Trisulfato
ANOVA	Análise de Variância (do inglês, *Analysis of Variance*)
API	Instituto Americano do Petróleo *(*do inglês, *American Petroleum Institute)*
ATR	Reflectância Total Atenuada (do inglês, *Atenuated Total Reflectance*)
C	Óxido de Cálcio (CaO)
C_2S	Silicato Dicálcico
C_3A	Aluminato Tricálcico
C_3S	Silicato Tricálcico
C_4AF	Aluminoferratos Tetracálcico
CA	Análise de Correlação (do inglês, *Correlation Analysis*)
C-A-S-H	Silicato-Aluminato de Cálcio
CCS	Captura e Armazenamento de Carbono (do inglês, *Carbon Capture and Storage*)
CCUS	Captura, Utilização e Armazenamento de Carbono (do inglês, *Carbon Capture, Utilization and Storage*)
CH	Portlandita
C-S-H	Silicato de Cálcio Hidratado
DIC	Carbono Inorgânico Dissolvido (do inglês, *Dissolved Inorganic Carbon*)
DRX	Difração de Raios-X (do inglês, *X-ray Diffraction – XRD*)
EC	Condutividade Elétrica (do inglês, *electrical conductivity)*
EDS	Espectroscopia de Energia Dispersiva de Raios-X (do inglês, *Energy-Dispersive X-ray Spectroscopy*)
F	Óxido Férrico (Fe_2O_3)
FID	Detector de Ionização de Chama (do inglês, *Flame Ionization Detector*)
FTIR	Espectroscopia de Infravermelho com Transformada de Fourier (do inglês, *Fourier-Transform Infrared Spectroscopy*)
GB	*GasBench II*
GC	Cromatografia Gasosa (do inglês, *Gas Chromatography*)

GHG	Gases do Efeito Estufa (do inglês, *Greenhouse Gases*)
HPHT	Alta Pressão e Alta Temperatura (do inglês, *High Pressure-High Temperature*)
IRMS	Espectrômetro de Massas com Razão Isotópica (do inglês, *Isotope Ratio Mass Spectrometer*)
K	Óxido de Potássio (K_2O)
M	Óxido de Magnésio (MgO)
MCS	Materiais Cimentícios Suplementares (do inglês, *Supplementary Cementitious Materials* – SCM)
MEV	Microscopia Eletrônica de Varredura (do inglês, *Scanning Electron Microscopy* - SEM)
MicroCT	Microtomografia de Raios-X (do inglês, *X-ray Microtomography*)
MVA	Análise Multivariada (do inglês, *Multivariate Analysis*)
N	Óxido de Sódio (Na_2O)
N.A	Unidade Normalizada de Área (do inglês, *Normalized Unit of Area*)
NMR	Espectroscopia de Ressonância Magnética Nuclear (do inglês, *Nuclear Magnetic Resonance Spectroscopy*)
O&G	Óleo e Gás (do inglês, *Oil and Gas*)
PCA	Análise de Componentes Principais (do inglês, *Principal Component Analysis*)
PLS	Regressão Parcial de Mínimos Quadrados (do inglês, *Partial Least Squares Regression*)
S	Dióxido de Silício (SiO_2)
$\bar{S}$	Trióxido de Enxofre (SO_3)
TCD	Detector de Condutividade Térmica (do inglês, *Thermal Conductivity Detector*)
TEM	Microscopia Eletrônica de Transmissão (do inglês, *Transmission Electron Microscopy*)
TGA	Análise Termogravimétrica (do inglês, *Thermogravimetric Analysis*)
U.A	Unidades de Área (do inglês, *Units of Area*)
USGS	Serviço Geológico dos Estados Unidos (do inglês, *United States Geological Survey*)
VPDB	*Vienna Pee Dee Belemnite*
XRF	Fluorescência de Raios-X (do inglês, *X-ray Florescence*)

RESUMO

SANTOS, Victor Hugo Jacks Mendes dos. **Desenvolvimento de método quantitativo e estudo de geoquímica isotópica para monitorar a integridade das pastas de cimento de poços expostos a ambientes ricos em CO_2**. Porto Alegre. 2022. Tese. Programa de Pós-Graduação em Engenharia e Tecnologia de Materiais, PONTIFÍCIA UNIVERSIDADE CATÓLICA DO RIO GRANDE DO SUL.

Os métodos de monitoramento são essenciais para a obtenção de informações relevantes para as empresas tomarem decisões. Nesse contexto, propôs-se estudar soluções para monitorar a integridade das pastas de cimentos de poços expostos a ambientes ricos em CO_2. No estudo de desenvolvimento de método quantitativo, foram calibrados e validados modelos de regressão parcial de mínimos quadrados (PLS), quantificando, com base nos dados de espectroscopia de infravermelho com transformada de Fourier (FTIR), o conteúdo de $CaCO_3$ em pastas de cimento que passaram pelo processo de carbonatação. No estudo de geoquímica isotópica, identificou-se que o pH do meio reacional e a solubilidade e pH das fases minerais dos materiais cimentícios são os principais parâmetros que influenciam nos fatores cinéticos e termodinâmicos e no equilíbrio/distribuição dos isótopos de carbono (^{13}C e ^{12}C) ao longo do sistema reacional e observou-se o potencial dos métodos de isótopos estáveis para discriminar a origem do CO_2. Assim, na presente tese de doutorado: (*i*) foram desenvolvidas soluções rápidas e confiáveis para monitorar o conteúdo de $CaCO_3$ em pastas de cimento carbonatado por FTIR e (*ii*) foi confirmado o potencial dos dados de isótopos estáveis de carbono ($\delta^{13}C$) para diferenciar a origem do CO_2 que induziu o processo de degradação das pastas de cimento de poços. A partir dos resultados, pode-se concluir que foram obtidos dados consistentes que levaram à proposição de novas alternativas para estudar e monitorar a integridade das pastas de cimento de poços expostos a ambientes ricos em CO_2. Dessa forma, o presente trabalho pôde contribuir para o desenvolvimento da área de engenharia e tecnologia de materiais cimentícios para aplicação em poços de óleo e gás (O&G) e no contexto de Captura e Armazenamento de Carbono (CCS).

Palavras-Chaves: Integridade de poços; degradação por CO_2; monitoramento de poços, análise multivariada; geoquímica isotópica.

ABSTRACT

SANTOS, Victor Hugo Jacks Mendes dos. **Development of a quantitative method and study of isotopic geochemistry to monitor the integrity of cement pastes from wells exposed to CO_2-rich environments**. Porto Alegre. 2022. PhD Thesis. Graduation Program in Materials Engineering and Technology, PONTIFICAL CATHOLIC UNIVERSITY OF RIO GRANDE DO SUL.

Monitoring methods are essential for obtaining relevant information for companies to make decisions. In this context, it was proposed to study solutions to monitor the integrity of cement pastes from wells exposed to CO_2-rich environments. In the quantitative method development study, partial least squares (PLS) regression models were calibrated and validated, quantifying, based on Fourier-transform infrared spectroscopy (FTIR) data, the $CaCO_3$ content in cement pastes that underwent the carbonation process. In the isotopic geochemistry study, it was identified that the pH of the reaction medium and the solubility and pH of the mineral phases of cementitious materials are the main parameters that influence the kinetic and thermodynamic factors and the balance/distribution of carbon isotopes (^{13}C and ^{12}C) throughout the reaction system, and it was observed the potential of the stable isotope methods to discriminate the origin of CO_2. Thus, in the present doctoral thesis: (*i*) rapid and reliable solutions were developed to monitor the $CaCO_3$ content in carbonated cement pastes by FTIR and (*ii*) it was confirmed the potential of stable carbon isotopes ($\delta^{13}C$) data to differentiate the origin of CO_2 that induced the degradation process of the well cement pastes. From the results, it can be concluded that consistent data were obtained that led to the proposition of new alternatives to study and monitor the integrity of cement pastes from wells exposed to CO_2-rich environments. In this way, the present work could contribute to the development of the area of engineering and technology of cementitious materials for application in oil and gas (O&G) wells and in the Carbon Capture and Storage (CCS) context.

Keywords: Wellbore integrity; CO_2 degradation; well monitoring; multivariate data analysis; isotope geochemistry

1. INTRODUÇÃO

A influência dos gases de efeito estufa no meio ambiente é uma das maiores preocupações da humanidade no século XXI (BAI; ZHANG; FU, 2016; TIONG; GHOLAMI; RAHMAN, 2019). O aumento da atividade econômica e da industrialização intensificou as emissões de gases de efeito estufa, como metano (CH_4) e dióxido de carbono (CO_2), e estão entre os principais elementos motrizes do aquecimento global (BAI *et al.*, 2015b; LIU *et al.*, 2021b; WILBERFORCE *et al.*, 2021). Nesse contexto, há um crescente apelo pela adoção de tecnologias de baixa emissão de carbono que favoreçam a descarbonização do setor industrial, bem como o atendimento das metas de redução de emissões de gases do efeito estufa e a mitigação de impactos ambientais (BAI; ZHANG; FU, 2016). Atualmente, as principais fontes de emissões de gases de efeito estufa estão relacionadas a: (*i*) geração de energia proveniente de combustíveis fósseis, (*ii*) mudança no uso da terra e desmatamento e (*iii*) decomposição de minerais (carbonatos) (ANDREW, 2018; METZ *et al.*, 2005; WILBERFORCE *et al.*, 2021). Nesse contexto, a cadeia produtiva do cimento é a maior fonte de emissões derivadas da decomposição de carbonatos e representa cerca de 5 a 7% do quantitativo global de CO_2 emitido (BENHELAL; SHAMSAEI; RASHID, 2021; MAZURANA *et al.*, 2021).

O cimento é um dos materiais mais importantes na construção civil e é aplicado como aglomerante hidráulico em fundações estruturais ou como elemento de proteção de engenharia (SHI *et al.*, 2019). No contexto da indústria de óleo e gás (O&G), os poços são estruturas de engenharia desenvolvidas para acessar as camadas geológicas subsuperficiais para uma ampla variedade de propósitos, incluindo a exploração de hidrocarbonetos e a operação de projetos de Captura e Armazenamento Geológico de Carbono (CCS) (GARCIA FERNANDEZ *et al.*, 2019). Ao longo do ciclo de vida de um poço, as pastas de cimentos Portland são aplicados

para operações de cimentação primária, isolamento hidráulico do meio, atividades corretivas da tubulação, desvios de fluxos de fluidos e/ou como material de *plugs* para realizar o abandono temporário ou permanente das estruturas (KHALIFEH *et al.*, 2018; TIONG; GHOLAMI; RAHMAN, 2019). Porém, é amplamente relatado pela literatura que as pastas de cimento Portland são química e mecanicamente vulneráveis em condições de reservatórios e podem perder sua integridade quando: (*i*) a cura do material ocorre em temperaturas elevadas (> 110 °C), (*ii*) sofram os efeitos dos ciclos térmicos de aquecimento/resfriamento e (*iii*) forem expostos a ambientes ricos em CO_2 (BU *et al.*, 2017; KUZIELOVÁ *et al.*, 2018; TIONG; GHOLAMI; RAHMAN, 2019).

Devido à sua composição química, todo o material à base de cimento sofre com certo nível de carbonatação ao longo de seu ciclo de vida (ASHRAF, 2016; COSTA *et al.*, 2019). Assim, a carbonatação é um tema de grande interesse em diversos segmentos (COSTA *et al.*, 2019; LIU *et al.*, 2019). Enquanto os tópicos de pesquisa: (*i*) carbonatação natural (carbonatação atmosférica), (*ii*) carbonatação acelerada e (*iii*) carbonatação da pasta de cimento de poços, enfocam questões de integridade de material (ANDRADE *et al.*, 2018; BATISTA *et al.*, 2021; BENHELAL; SHAMSAEI; RASHID, 2021; DALLA VECCHIA *et al.*, 2020; EKOLU, 2016; LEDESMA *et al.*, 2020; LIU *et al.*, 2021a; MORAES; COSTA, 2022; PONZI *et al.*, 2021; SILVA; DE OLIVEIRA ANDRADE, 2017), os campos de estudo: (*iv*) cura por carbonatação (cura acelerada) e (*v*) mineralização de CO_2 (sequestro mineral), avaliam os materiais dentro do contexto de Captura, Utilização e Armazenamento de Carbono (CCUS) (LIU *et al.*, 2021a; YADAV; MEHRA, 2021; ZHANG; GHOULEH; SHAO, 2017).

Os atuais desafios técnico-econômicos para viabilizar o desenvolvimento sustentável da economia mundial requerem a liberação de recursos para fomentar pesquisas na área de integridade de materiais (MARSHDI, 2018). Dessa forma, a compreensão científica sobre o desempenho da pasta de cimento e a influência das variáveis ambientais sobre a integridade dos materiais são questões essenciais para acelerar o desenvolvimento de novos materiais cimentícios capazes de resistir às condições extremas dos poços (OMOSEBI *et al.*, 2016). Para tanto, apesar do aumento expressivo de estudos envolvendo a integridade das pastas de cimento em ambientes ricos em CO_2, ainda há espaços para desenvolvimentos técnicos

importantes (FAROOQUI *et al.*, 2017). Nesse contexto, este trabalho propôs-se a desenvolver soluções para estudar e monitorar a integridade das pastas de cimentos de poços expostos a ambientes ricos em CO_2. Assim, a presente tese divide-se em duas áreas a fim de: (*i*) desenvolver um método quantitativo de monitoramento do processo de carbonatação de materiais cimentícios e (*ii*) avaliar o potencial dos métodos de geoquímica isotópica para aprofundar os conhecimentos sobre o processo de carbonatação das pastas de cimento em ambientes ricos em CO_2.

Devido à complexidade dos materiais cimentícios, é necessário empregar várias técnicas analíticas complementares para caracterizar estes materiais de forma completa (BJØRGE *et al.*, 2019; HORGNIES; CHEN; BOUILLON, 2013). Nesse contexto, a análise quantitativa do carbonato de cálcio ($CaCO_3$) na matriz cimentícia é um dos pontos centrais em todos os estudos que envolvem o processo de carbonatação das pastas de cimento. No entanto, os métodos de caracterização sofrem de uma ou mais restrições relacionadas a: (*i*) disponibilidade de equipamento, (*ii*) sensibilidade e especificidade do método, (*iii*) falta de recursos humanos especializados, (*iv*) custo de análise e/ou (*v*) procedimentos elaborados para realizar o preparo e análise de amostras (HENRY; WATSON; JOHN, 2017; REBOUÇAS; ROHWEDDER; PASQUINI, 2018; SCHNEIDER DOS SANTOS; ROLIM; HEPP PULGATI, 2015). A fim de contornar estas restrições, o presente trabalho propôs-se a desenvolver um método rápido e confiável para quantificar carbonato de cálcio ($CaCO_3$) nas pastas de cimento a partir da espectroscopia de infravermelho com transformada de Fourier (FTIR) acoplada com modelos de regressão multivariada. Neste contexto, o método desenvolvido poderá ser utilizado para: (*i*) quantificar os produtos da reação de carbonatação, (*ii*) controlar o processo de carbonatação e (*iii*) compreender os seus efeitos na integridade e propriedades das pastas de cimento.

Além disso, há um número significativo de estudos recentes que avaliam o processo de carbonatação das pastas de cimentos de poços utilizando abordagens experimentais e numéricas (ABID; GHOLAMI; MUTADIR, 2020; BATISTA *et al.*, 2021; DONG; DUAN; GAO, 2020; LEDESMA *et al.*, 2020; MORAES; COSTA, 2022; PONZI *et al.*, 2021; SCHÜTZ *et al.*, 2019; SZABÓ-KRAUSZ *et al.*, 2020). Porém, ainda existem na literatura questões importantes não resolvidas relacionadas à dinâmica do

processo de carbonatação dos materiais cimentícios em meios ricos em CO_2. Até o momento, a assinatura isotópica do carbono ($\delta^{13}C$) já foi utilizada como traçador químico para monitorar o processo de injeção de CO_2 em reservatórios utilizados para operações de Captura e Armazenamento de Carbono (CCS) e estudar a dinâmica do transporte reativo da pluma de gás (CO_2) ao longo da percolação dos fluidos no reservatório (BARTH *et al.*, 2015; MAYER *et al.*, 2015; WIESE *et al.*, 2013; ZIMMER *et al.*, 2018). Por outro lado, há um número limitado de estudos que realizaram a análise isotópica da pasta de cimento de poços carbonatados (CAREY *et al.*, 2007; GABOREAU *et al.*, 2012; MANCEAU *et al.*, 2016), sendo que nenhum dos autores se discorreu sobre a importância dos resultados obtidos. Dessa forma, o presente trabalho também propôs avaliar o potencial dos métodos de geoquímica isotópica para aprofundar os conhecimentos sobre o processo de carbonatação das pastas de cimento de poços expostos a ambientes ricos em CO_2. Assim, será estudado o potencial dos métodos de isótopos estáveis de carbono ($\delta^{13}C$) para discriminar a origem do CO_2 consumido no processo de carbonatação das pastas de cimento, avaliando a ocorrência dos fenômenos de fracionamento isotópico ao longo das etapas do processo de degradação do material.

2. OBJETIVOS

Estudar soluções para monitorar a integridade das pastas de cimentos de poços expostos a ambientes ricos em CO_2.

2.1. Objetivos Específicos

- Desenvolver um método rápido e confiável para quantificar o carbonato de cálcio ($CaCO_3$) em pastas de cimento carbonatados a partir da espectroscopia de infravermelho com transformada de Fourier (FTIR) acoplada com modelos de regressão multivariada;

- Avaliar o potencial dos métodos de geoquímica isotópica para aprofundar os conhecimentos sobre o processo de carbonatação das pastas de cimentos de poços expostos a ambientes ricos em CO_2.

3. REVISÃO BIBLIOGRÁFICA

Há um aumento constante de demanda energética devido ao crescimento econômico e populacional do mundo, o que resulta em uma maior exploração de combustíveis fósseis (BAI; ZHANG; FU, 2016). Apesar da maior participação de fontes de energia alternativas e renováveis, o petróleo ainda compõe majoritariamente a matriz energética mundial (BU *et al.*, 2017). Dessa forma, ainda não é possível substituir integralmente os recursos fósseis da matriz energética mundial por energias renováveis, como a produção de biocombustíveis, a exploração da energia solar fotovoltaica, a produção de energia hídrica e o aproveitamento da energia eólica (BAI; ZHANG; FU, 2016; TIONG; GHOLAMI; RAHMAN, 2019).

O esgotamento das reservas convencionais de óleo e gás (O&G) e a redução da produtividade dos poços existentes levam as empresas do setor a investir na exploração de novas áreas até então inexploradas e inacessíveis, enfrentando barreiras tecnológicas (WANG *et al.*, 2017). Nesse contexto, os novos empreendimentos de óleo e gás (O&G) estão sendo instalados em reservatórios cada vez mais profundos, com condições extremas de temperatura e pressão e operando em meios consideravelmente mais agressivos (KIRAN *et al.*, 2017; WANG *et al.*, 2017). Ao avançar as fronteiras de exploração, o desenvolvimento de novas tecnologias passa a ser mais desafiador e as empresas passam a lidar com maiores riscos, custos de exploração e incertezas de empreendimento (KIRAN *et al.*, 2017).

Dentro dos recentes avanços de fronteiras de exploração, o Pré-Sal é uma das descobertas mais significativas do setor de O&G (MOCZYDLOWER *et al.*, 2012). O

Pré-Sal da Bacia de Santos é um cenário único, sendo definido como reservatórios carbonáticos com origem e propriedades não convencionais (ARAUJO RODRIGUES; LUÍS SAUER, 2015; DA COSTA FRAGA *et al.*, 2015; DE ALMEIDA *et al.*, 2010; MOCZYDLOWER *et al.*, 2012). Entre os desafios de exploração da área estão: (*i*) a espessa camada selo de sal, (*ii*) as elevadas distâncias da costa, (*iii*) a profundidade dos reservatórios e (*iv*) o conteúdo variável, porém frequentemente elevado de CO_2 (BAI *et al.*, 2015a; BAI; ZHANG; FU, 2016). Nesse contexto, uma vez que os reservatórios do Pré-Sal se encontram em ambientes agressivos, há necessidade de realizar um estudo abrangente de integridade de todas as estruturas que estão envolvidas nas operações de comissionamento de poços de O&G, o que requer o desenvolvimento de materiais e tecnologias para operar e monitorar as intervenções nos reservatórios com meio agressivo (elevadas pressões, temperaturas e concentrações de CO_2) (BAI *et al.*, 2015a; BAI; ZHANG; FU, 2016; KIRAN *et al.*, 2017; MARSHDI, 2018; TIONG; GHOLAMI; RAHMAN, 2019).

Os poços são estruturas desenvolvidas para realizar o acesso às camadas geológicas profundas, sendo utilizados para realizar a exploração de hidrocarbonetos e/ou viabilizar o armazenamento geológico de CO_2 (GARCIA FERNANDEZ *et al.*, 2019). Sendo assim, a integridade do poço é uma questão chave para o desenvolvimento seguro e sustentável de qualquer processo de perfuração de seções geológicas profundas (KIRAN *et al.*, 2017). Nesse contexto, falhas na integridade do poço podem levar a ocorrência de impactos ambientais significativos e/ou à consequências financeiras negativas (CARROLL *et al.*, 2016; KIRAN *et al.*, 2017; LI; NYGAARD, 2018; TIONG; GHOLAMI; RAHMAN, 2019).

O cimento é um dos materiais mais importantes da humanidade e é utilizado por muitas décadas na indústria de óleo e gás, cumprindo o papel de garantir a integridade dos poços e de servir de barreira física contra qualquer fluxo indesejado de O&G entre formações geológicas (KIRAN *et al.*, 2017; MISHRA *et al.*, 2017). No contexto da indústria de óleo e gás, os poços são estruturas desenvolvidas para

acessar as camadas geológicas subsuperficiais (GARCIA FERNANDEZ *et al.*, 2019) Além de resistir às ações do meio agressivo, a pasta de cimento também deve manter a integridade das formações rochosas e proteger a tubulação de aço de ataques químicos e físicos (BAI; ZHANG; FU, 2016).

Ao longo do ciclo de vida de um poço, os materiais cimentícios, principalmente cimentos Portland, são aplicados para operações de cimentação primária, operações corretivas, realizar o isolamento hidráulico do meio, desviar os fluxos de O&G e viabilizar o abandono temporário ou permanente dos poços (*plug*) (KHALIFEH *et al.*, 2018; TIONG; GHOLAMI; RAHMAN, 2019). Nesse contexto, a pasta de cimento cumpre a função de proteger os materiais do poço de fluidos corrosivos (como CO_2 e H_2S), fornecer suporte mecânico (tubulação de aço e formação rochosa), isolar as zonas produtoras e impedir o vazamento de óleo e gás para a superfície (AJAYI; GUPTA, 2019; KIRAN *et al.*, 2017; OMOSEBI *et al.*, 2016, 2017; WAKEEL *et al.*, 2019).

Do ponto de vista prático, fatores químicos, mecânicos e operacionais podem afetar a integridade de poços (KIRAN *et al.*, 2017). Porém, as pastas de cimentos Portland, comumente utilizados para estas aplicações, são materiais instáveis nas condições de reservatórios e podem perder sua integridade, ainda mais rapidamente, se sofrerem com retrogressão (meio acima de 110 °C), forem submetidos a ciclos térmicos de aquecimento/resfriamento ou forem expostos ao CO_2 no estado supercrítico (BU *et al.*, 2017; KUZIELOVÁ *et al.*, 2018; TIONG; GHOLAMI; RAHMAN, 2019). Estas mesmas condições ambientais são comumente identificadas em poços perfurados para realizar a Captura e Armazenamento de CO_2 (CCS) (ABID *et al.*, 2018; KIRAN *et al.*, 2017; KOUKOUZAS *et al.*, 2017; LESTI; TIEMEYER; PLANK, 2013). Em ambos os casos, uma eventual falha de integridade pode resultar em vazamento de hidrocarbonetos e a danos ambientais incalculáveis (FAROOQUI *et al.*, 2017; KIRAN *et al.*, 2017; TIONG; GHOLAMI; RAHMAN, 2019).

A Captura e Armazenamento de CO_2 (CCS) é definida como uma tecnologia de transição para uma economia de baixo carbono, sendo capaz de mitigar parcialmente as emissões de gases do efeito estufa e reduzir a pegada de carbono das atividades industriais que fazem uso intensivo de energia fóssil (ABID *et al.*, 2018; BAI; ZHANG; FU, 2016). Dessa forma, o objetivo das tecnologias de CCS é limitar a emissão de gases de efeito estufa, e, por sua vez, o aquecimento global, que é uma das questões ambientais críticas do século XXI (BAI *et al.*, 2015a; TIONG; GHOLAMI; RAHMAN, 2019). Nesse contexto, o requisito mínimo para uma operação de sequestro de CO_2 é a garantia de que o armazenamento geológico é seguro, confiável e de longo prazo (BAGHERI; SHARIATIPOUR; GANJIAN, 2018; LI; NYGAARD, 2018).

Uma vez implementado, o CCS pode armazenar cerca de 5 bilhões de toneladas de CO_2 por ano de maneira eficaz e segura (TIONG; GHOLAMI; RAHMAN, 2019). Entre as formações geológicas potenciais, têm-se: aquíferos salinos profundos, reservas de carvão inacessíveis e reservatórios de O&G depletados (KOUKOUZAS *et al.*, 2017). Porém, após o processo de injeção, existem vários caminhos pelos quais o CO_2 pode migrar e/ou vazar do reservatório para outras formações geológicas ou para a superfície (LESTI; TIEMEYER; PLANK, 2013). Entre os caminhos de escape preferencias, têm-se: (*i*) vazamento através da formação geológica, (*ii*) retornar a superfície pela tubulação do poço, (*iii*) percolar através das interfaces (pasta de cimento/formação e pasta de cimento/tubulação de aço) e/ou (*iv*) permear através do tampão de pasta de cimento de poços abandonados (ABID *et al.*, 2018; LESTI; TIEMEYER; PLANK, 2013).

A maioria dos vazamentos associados à pasta de cimento podem ser atribuídos à perda ocasional da integridade do material, resultantes da degradação da bainha de cimento exposta à pluma de CO_2 e levando a formação de caminhos preferenciais (microfraturas e espaço microanular) (ABID *et al.*, 2018). Assim, a fim de evitar falhas catastróficas, é necessário realizar estudos abrangentes para compreender o mecanismo de degradação dos materiais cimentícios e encontrar maneiras de reduzir

e/ou retardar o processo de perda de integridade (OMOSEBI *et al.*, 2017). Portanto, o desenvolvimento de novas formulações de cimento ainda é uma área de pesquisa muito ativa, com uma demanda substancial por novas soluções que possam atender os critérios técnicos dos novos reservatórios de petróleo e empreendimentos de CCS, ao mesmo tempo em que atendam aos requisitos de sustentabilidade ambiental (MISHRA *et al.*, 2017). Dessa forma, a consolidação do saber científico sobre o comportamento das pastas de cimento em meios agressivos é o lastro necessário para acelerar o desenvolvimento de novas formulações de cimento, capazes de resistir às condições cada vez mais adversas dos poços (OMOSEBI *et al.*, 2016).

3.1. Cimento Portland

A classe dominante de materiais cimentícios é composta pelos cimentos Portland, amplamente utilizados em todas as etapas do ciclo de vida da construção, operação e abandono de poços (SALEHI *et al.*, 2019). Os cimentos Portland são constituídos majoritariamente pelo silicato tricálcico (C_3S - Ca_3SiO_5 - alita), silicato dicálcico (C_2S - Ca_2SiO_4 - belita,), aluminato tricálcico (C_3A - $Ca_3Al_2O_6$ - celita) e o aluminoferratos tetracálcico (C_4AF - $Ca_4Al_2Fe_2O_{10}$ - brownmillerita) (OMOSEBI *et al.*, 2016; PARIS *et al.*, 2016; SALEHI *et al.*, 2019; ŠILER *et al.*, 2016).

O Instituto Americano do Petróleo (API, do inglês *American Petroleum Institute*) define oito tipos diferentes de cimento Portland (cimento Portland API de A a H) como sendo adequados para a aplicação em poços com diferentes faixas de temperatura e pressão (API SPECIFICATION, 2010; BAI *et al.*, 2015a). Também podem ser encontrados cimentos com composição similares classificados por outras agências normatizadoras como a *American Society for Testing and Materials* (ASTM INTERNATIONAL, 2019). Na Tabela 3-1, encontram-se descritos os óxidos que compõem os principais tipos de cimentos aplicados em operações de cimentação de poços para a exploração de óleo e gás e para a o desenvolvimento de projetos de CCS.

Tabela 3-1. Descrição dos principais óxidos que compõem os materiais cimentícios

Notação	Fórmula Química	Nome
S	SiO_2	Dióxido de silício
A	Al_2O_3	Óxido de alumínio
F	Fe_2O_3	Óxido férrico
C	CaO	Óxido de cálcio
M	MgO	Óxido de magnésio
$\bar{S}$	SO_3	Trióxido de enxofre
N	Na_2O	Óxido de sódio
K	K_2O	Óxido de potássio

Quanto às características dos cimento Portland, muitas das propriedades dos materiais serão definidas pela composição percentual do óxido de cálcio (CaO), do óxido de alumínio (Al_2O_3) e do dióxido de silício (SiO_2) (SUWAN, 2018). A concentração destes elementos nos compósitos cimentícios, em conjunto com os óxidos minoritários, tamanho de partícula, quantidade de fases reativas e quantidade de água de hidratação, vão regular a cinética da reação do material e definir a sua aplicação (LOTHENBACH; SCRIVENER; HOOTON, 2011). A partir do diagrama ternário CaO-Al_2O_3-SiO_2 (Figura 3-1), é possível visualizar a composição dos cimentos anidros e dos principais materiais cimentícios suplementares (MCS) e avaliar as fases do cimento que poderão se formar ao longo do processo de hidratação.

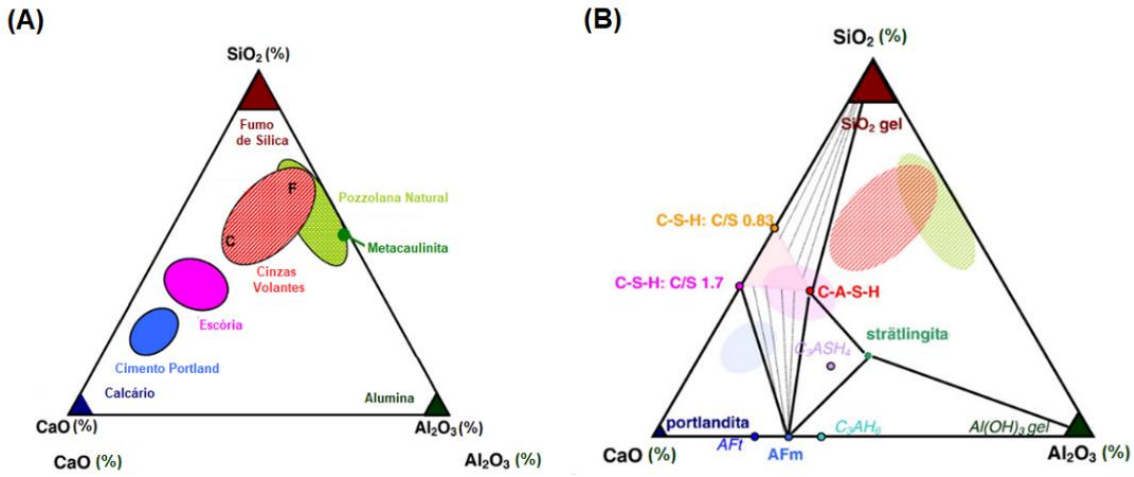

Figura 3-1. Diagrama ternário CaO-Al_2O_3-SiO_2 de materiais cimentícios**.** Adaptado de Lothenbach; Scrivener e Hooton, (2011)

3.1.1. Hidratação do cimento Portland

Compreender os mecanismos de hidratação das pastas de cimento é um objeto de interesse comum dos meios acadêmico e industrial (BULLARD *et al.*, 2011). A hidratação da pasta de cimento trata-se da combinação de todos os processos químicos e físicos que ocorrem após o contato do material sólido anidro com a água de mistura (STARK, 2011). De acordo com Bullard *et al.* (2011), a hidratação do cimento envolve um conjunto de processos de transformação categorizados como:

(i) Dissolução/dissociação: processos que envolvem o fluxo de materiais das frações sólidas do cimento para a solução quando em contato com a água;

(ii) Difusão: processos de transferência de massa que ocorrem na solução, ao longo das fases dos materiais ou através dos poros da pasta de cimento;

(iii) Nucleação: processos que iniciam a precipitação de sólidos que servirão de indutores dos processos subsequentes de crescimento e de aumento do volume de solidos das pasta de cimento;

(iv) Crescimento: processos de incorporação/fixação de unidades moleculares na estrutura das fases sólidas da pasta de cimento (cristalinas ou amorfas) resultando no desenvolvimento da consistência do material.

(v) Complexação: processos reativos de formação de complexos de íons ou complexos moleculares adsorvidos em superfícies sólidas ou que estejam presentes de maneira estável em solução;

(vi) Adsorção: processos de acúmulo de íons ou outras unidades moleculares ao longo da interface sólido-líquido da pasta de cimento.

A hidratação da pasta de cimento ainda é fruto de muito debate, mas entende-se que o processo pode ser descrito em 5 etapas, definidas com base no fluxo de calor observado no decorrer do processo de desenvolvimento das propriedades do material. Ao longo do processo de cura da pasta de cimento, os componentes (C_3S, C_2S, C_3A e C_4AF) do cimento são hidratados e resultam na consolidação do material com baixa permeabilidade e resistência mecânica necessária (DESHPANDE; PATIL, 2017; HWANG *et al.*, 2018; SALEHI *et al.*, 2019; TIONG; GHOLAMI; RAHMAN, 2019). O processo de cura da pasta de cimento ocorre ao longo de vários meses e é caracterizado como um processo exotérmico (BAGHERI; SHARIATIPOUR; GANJIAN, 2018). Assim, o processo de hidratação é dividido nas etapas de: (*i*) período de indução, (*ii*) período de reação lenta, (*iii*) período de aceleração, (*iv*) período de desaceleração e (*v*) hidratação lenta contínua e é representado na Figura 3-2.

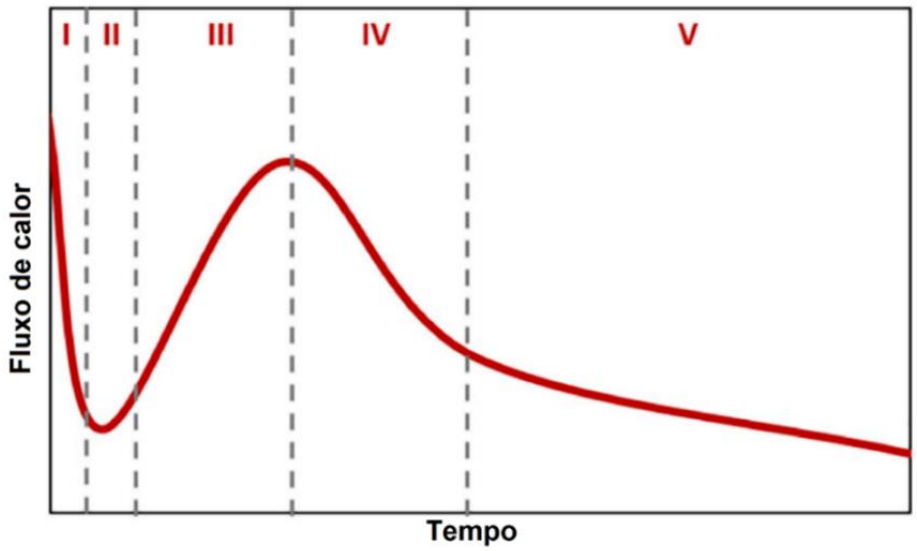

Figura 3-2. Processo de hidratação da pasta de cimento considerando o fluxo de calor ao longo do tempo: (*i*) período de indução, (*ii*) período de reação lenta, (*iii*) período de aceleração, (*iv*) período de desaceleração e (*v*) hidratação lenta contínua. Adaptado de John; Matschei e Stephan, (2018)

A hidratação da pasta de cimento inicia com a dissolução do aluminato tricálcico (C_3A), gerando hidróxidos de alumínio e cálcio e elevando o valor do pH do meio para uma faixa entre 11 e 13 (HEINZ; HEINZ, 2021). O C_3A hidrata (Equação 3.1) mais rapidamente e contribui para o desenvolvimento do endurecimento/pega inicial, sendo

necessário utilizar-se de gipsita (Equação 3.2) a fim de evitar a consolidação precoce do material (BAGHERI; SHARIATIPOUR; GANJIAN, 2018). Essa reação é acompanhada pela hidratação inicial mais lenta do silicato tricálcico (C_3S), o principal componente do cimento Portland. A hidratação do C_3S resulta na produção do silicato de cálcio hidratado (C-S-H), caracterizado como uma fase majoritariamente semi-amorfa, e a portlandita [CH - $Ca(OH)_2$ - hidróxido de cálcio], caracterizada pela estrutura cristalina e alcalinidade (Equação 3.3) (ABID *et al.*, 2018; GU *et al.*, 2017; OMOSEBI *et al.*, 2016). Enquanto o silicato tricálcico (C_3S) contribui para a pega/resistência inicial do material, o silicato dicálcico (C_2S) hidrata muito lentamente durante o período de alguns meses e contribui para o desenvolvimento das propriedades finais da pasta de cimento e aumentam a fração de C-S-H e CH, conforme Equação 3.4 (DORN; BLASK; STEPHAN, 2022; HEINZ; HEINZ, 2021). A fase de C_4AF hidrata (Equação 3.5) com uma taxa semelhante ao C_3S e é considerada menos influente devido a sua pequena contribuição (5 a 15%) em peso e a relativa inércia dos óxidos e hidróxidos de ferro (HEINZ; HEINZ, 2021; TIONG; GHOLAMI; RAHMAN, 2019). Ao longo do processo de hidratação, a transformação de fases ricas em alumínio (C_3A, C_4AF) na presença de sulfato de cálcio resultam na formação de fases adicionais de etringita e sulfoaluminato (HEINZ; HEINZ, 2021).

$$2C_3A + 21H \rightarrow C_4AH_{13} + C_2AH_8 \rightarrow 2C_3AH_6 + 9H \quad (3.1)$$

$$C_3A + 3C\bar{S}H_2 + 26H \rightarrow C_6A\bar{S}_3H_{32} \quad (3.2)$$

$$2C_3S + 6H \rightarrow C - S - H + 3CH \quad (3.3)$$

$$2C_2S + 4H \rightarrow C - S - H + CH \quad (3.4)$$

$$C_4AF + 10H \rightarrow C_3AH_6 + FH_3 + CH \quad (3.5)$$

O gel de silicato de cálcio hidratado (C–S–H) é o principal elemento ligante da pasta de cimento Portland e governa a maioria das propriedades físico-químicas do

material (HEINZ; HEINZ, 2021; JOHN; MATSCHEI; STEPHAN, 2018). O C-S-H se forma pela precipitação dos íons presentes na solução dos poros da pasta de cimento, principalmente devido à dissolução de silicatos de cálcio anidro (C_3S, C_2S) e outros materiais siliciosos solúveis que podem estar presentes em cimentos misturados com MCS, como a microsílica (HEINZ; HEINZ, 2021). Após o processo de cura, o C-S-H chega a compor 70% da fração mássica da pasta de cimento, atuando como agente ligante e mantendo coesa a estrutura do material. O C-S-H é um mineral com elevada área superficial, sendo o principal responsável pela porosidade e permeabilidade dos materiais cimentícios (WAKEEL *et al.*, 2019). Já a portlandita (CH) compõe entre 15-20% da fração mássica da pasta de cimento e atua como reserva alcalina do material, servindo como um elemento protetivo da matriz cimentícia, elevando o pH da matriz cimentícia e retardando os processos de degradação por fluidos ácidos (CO_2 e H_2S) (GU *et al.*, 2017; WAKEEL *et al.*, 2019). O C-S-H e a CH são responsáveis pelo desenvolvimento das propriedades químicas e mecânicas finais dos materiais cimentícios (BAGHERI; SHARIATIPOUR; GANJIAN, 2018; WAKEEL *et al.*, 2019). Na Figura 3-3, estão representados alguns dos principais elementos que compõem a estrutura da pasta de cimento hidratado, que são: a base de C-S-H com a presença de um cristal hexagonal característico da portlandita (CH) (3-3A) e os cristais prismáticos aciculares de etringita crescendo nos grãos de clínquer (3-3B).

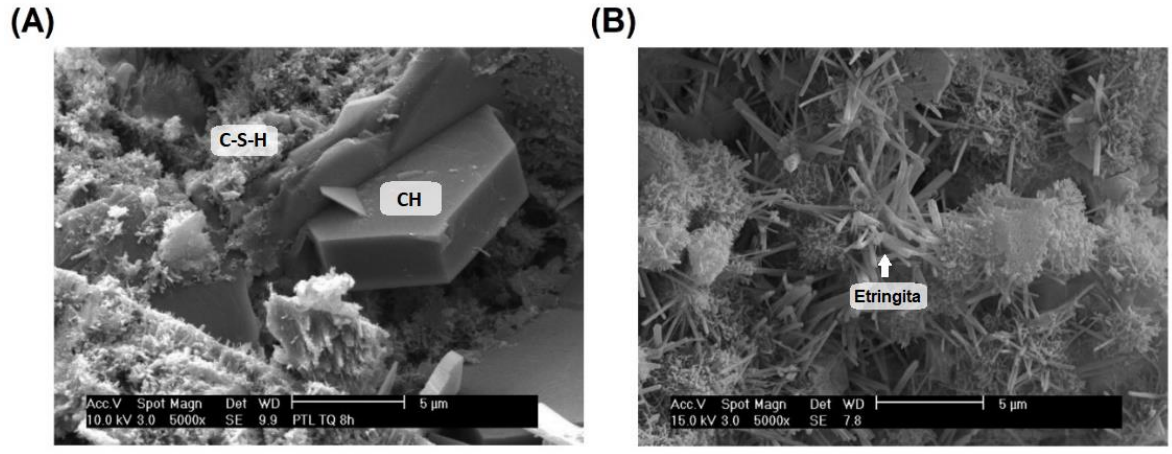

Figura 3-3. Estrutura da pasta de cimento Portland. (A) Estrutura hexagonal de portlandita e base de C-S-H (magnificação: 5000x) e (B) cristais aciculares de etringita (magnificação: 5000x). Adaptado de Artioli; Bullard, (2013)

3.2. Cimentação de poços

A pasta de cimento desempenha um papel chave ao longo do ciclo de vida dos poços (OMOSEBI *et al.*, 2017), sendo necessário que os materiais cimentícios mantenham sua integridade por longos períodos de tempo (AJAYI; GUPTA, 2019; OMOSEBI *et al.*, 2017). Dessa forma, pode-se dividir o tempo de vida útil do poço das estruturas em duas fases, sendo elas: (*i*) a construção/operação e (*ii*) o tamponamento/abandono (AJAYI; GUPTA, 2019). Mais detalhadamente, as operações de poços de O&G podem ser divididas nas seguintes etapas: (a) perfuração, (b) completação, (c) recuperação primária de petróleo, (d) recuperação secundária de petróleo (repressurização do reservatório), (e) recuperação terciária de petróleo (*e.g.*, recuperação avançada de petróleo), (f) armazenamento geológico de carbono, (g) tamponamento e (h) abandono do poço (AJAYI; GUPTA, 2019; BAGHERI; SHARIATIPOUR; GANJIAN, 2018; BAI *et al.*, 2015a; BAI; ZHANG; FU, 2016; HWANG *et al.*, 2018; KIRAN *et al.*, 2017). Ao longo destas etapas, uma série de ações de intervenções corretivas podem ser realizadas para assegurar a integridade dos poços (AJAYI; GUPTA, 2019; BAI *et al.*, 2015a). Ainda, faz-se necessário a realização de monitoramento de longo prazo para avaliar a integridade do poço e os riscos associados a eventuais falhas estruturais (BAGHERI; SHARIATIPOUR; GANJIAN, 2018; BAI *et al.*, 2015a; BAI; ZHANG; FU, 2016; HWANG *et al.*, 2018), uma vez que os todos os elementos do poço estão sujeitos a uma série de processos de degradação ao longo de seu ciclo de vida.

A perfuração é um processo essencial para os empreendimentos que envolvem a exploração de seções geológicas subsuperficiais, como reservatórios de O&G e de armazenamento geológico de carbono (CCS). Assim, a complexidade e dificuldade dos processos de perfuração e de cimentação de poços aumenta à medida que a indústria avança para reservatórios com condições operacionais mais severas (mais profundos, com pressões mais elevadas e com ambientes mais agressivos) (MURTAZA *et al.*, 2019). Os poços são compostos basicamente por: (*i*) uma tubulação

de aço (*casing*) e (*ii*) uma bainha de cimento entre a formação rochosa e o tubo de produção (GARCIA FERNANDEZ *et al.*, 2019; TREMOSA *et al.*, 2017). Para o caso particular da indústria de O&G, a operação de cimentação se procede bombeando a pasta de cimento para seções profundas subsuperficiais, a fim de cumprir sua função de estabilizar e fornecer o selo hidráulico da estrutura do poço (SHAHRIAR; NEHDI, 2014). Ainda, para os poços fechados temporariamente ou abandonados, o cimento pode ser utilizado para o preenchimento interno da tubulação de aço a fim de formar um tampão (*plug*), que impede o escape de fluidos do reservatório e isola o meio geológico da superfície (TREMOSA *et al.*, 2017).

Uma das etapas essenciais da operação de poços é a cimentação adequada das seções subsuperficiais, a fim de garantir a integridade das estruturas e a longevidade do empreendimento (AHDAYA *et al.*, 2019). Porém, a perfuração é uma operação complexa e resulta na formação da lama de perfuração, que deve ser constantemente removida de maneira eficiente pelo fluido de perfuração (KIRAN *et al.*, 2017). À medida que o processo avança, o poço passa a ser preenchido com o fluido de perfuração, uma mistura densa de água, argilominerais e outros minerais, que estabiliza a estrutura do poço, refrigera os componentes da broca e lixivia os resíduos (calha) (BAI; ZHANG; FU, 2016). Após um determinado avanço da perfuração, um tubo de aço é colocado no lugar e cimentado (AHDAYA *et al.*, 2019). Para a operação de cimentação, a pasta de cimento é injetada através do tubo de aço, deslocando o fluido de perfuração e ocupando o espaço anular existente entre a tubulação de aço e a formação rochosa (TORSÆTER; TODOROVIC; LAVROV, 2015). Então, a pasta de cimento preenche completamente o espaço anular entre a tubulação e o reservatório e retira o fluido de perfuração e os materiais residuais da formação geológica (MURTAZA *et al.*, 2019; PAIVA *et al.*, 2018). Nesse processo, o fluido de perfuração deve ser removido de maneira eficiente a fim de evitar que ocorra problemas locais de ligação entre a pasta de cimento, a formação rochosa e a tubulação de aço (AGBASIMALO; RADONJIC, 2012; BAI; ZHANG; FU, 2016; CHOI *et al.*, 2013).

Após o endurecimento, a pasta de cimento se ligará fortemente à formação rochosa e à parede da tubulação de aço, fornecendo o selo hidráulico e a proteção necessária para os elementos do poço (PAIVA *et al.*, 2018). Assim, o sucesso desta operação depende diretamente de utilizar-se de materiais que apresentem uma elevada resistência de ligação entre a pasta de cimento/tubulação de aço e entre a pasta de cimento e a formação geológica (MURTAZA *et al.*, 2019). Na Figura 3-4 é apresentado um esquema do processo de cimentação dos poços de O&G e de CCS.

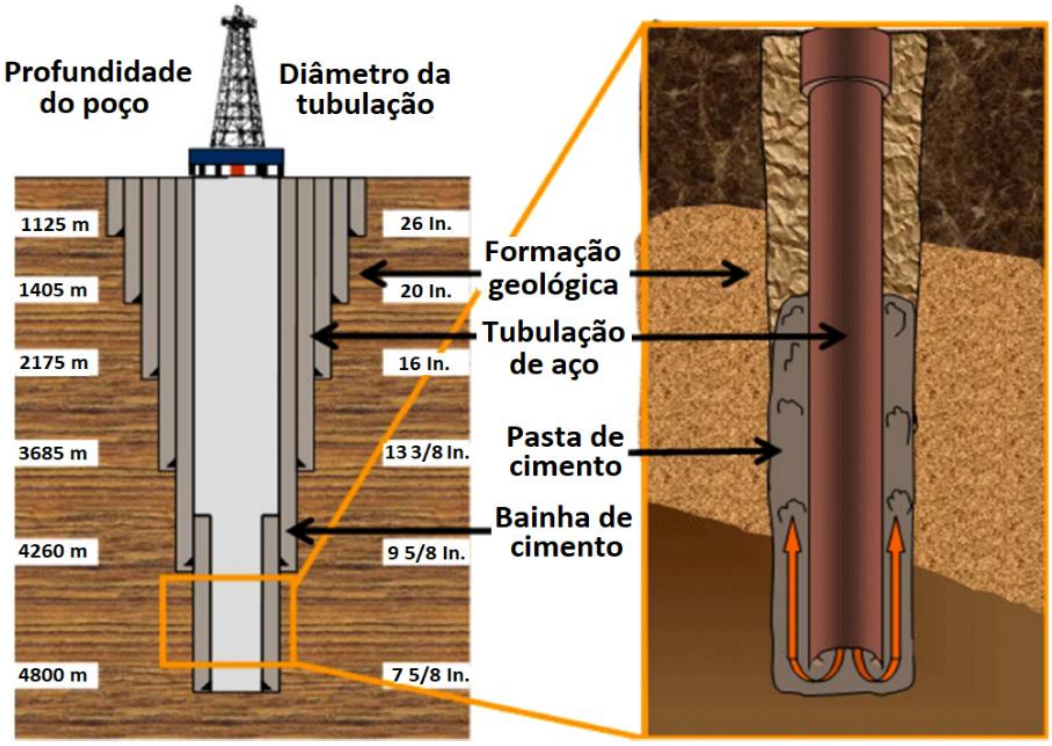

Figura 3-4. Representação esquemática de uma perfuração e da aplicação da pasta de cimento em uma seção de poços. Adaptado de Mangadlao; Cao e Advincula, (2015)

Ao longo do processo de perfuração de poços, as principais falhas de operação de cimentação são: (*i*) colocação inadequada ou incompleta da pasta de cimento, especialmente em poços não verticais, (*ii*) baixa qualidade do material (pasta de cimentos com alta porosidade-permeabilidade), (*iii*) vazamentos entre as juntas de seções da bainha de cimento (possivelmente representando 90% de todas as falhas tubulares), (*iv*) falha em remover adequadamente a lama de perfuração do poço, entre

outros problemas associados a uma ligação fraca entre a formação rochosa/pasta de cimento e a pasta de cimento/tubulação de aço, (*v*) desenvolvimento de canais de lama ou gás no cimento e (*vi*) danos causados à formação durante a perfuração (CARROLL *et al.*, 2016).

3.3. Integridade de poços

Garantir a integridade do poço e sua eficiência durante todo o período de operação, além de centenas de anos após o abandono das atividades econômicas, é uma das maiores preocupações da indústria de O&G e de CCS. Embora o cimento Portland seja muito utilizado, ele apresenta uma série de desvantagens que podem resultar em falhas operacionais e impactos ambientais (AHDAYA *et al.*, 2019). Sendo assim, considerando que é impossível evitar que ocorram processos de degradação ao longo do tempo, é essencial que se desenvolvam materiais que apresentem elevada estabilidade química e mecânica em meios agressivos (AJAYI; GUPTA, 2019; FAROOQUI *et al.*, 2017; TIONG; GHOLAMI; RAHMAN, 2019). Mesmo com longo histórico de utilização, ainda pouco se sabe sobre a dinâmica do processo de degradação da pasta de cimento e como que a reação do CO_2 pode impactar no desempenho do material e nos fenômenos interfaciais a longo prazo (HEINZ; HEINZ, 2021). Assim, há uma necessidade de ampliar a compreensão dos efeitos dos parâmetros dos processos de degradação, como a temperatura, pressão e agressividade dos fluidos, sobre as interações/alterações que a pasta de cimento pode sofrer em contato com a formação geológica (FAROOQUI *et al.*, 2017).

A perda de integridade dos poços é um processo relacionado ao tempo, em que: (*i*) o fluxo de fluidos, (*ii*) as reações químicas, (*iii*) o transporte de solutos, (*iv*) a qualidade da cimentação do anular, (*v*) o estresse mecânico, (*vi*) a corrosão da tubulação de aço (*casing*), (*vii*) a degradação do *plug* de cimento e (*viii*) os defeitos nas operações de abandono, podem ocorrer ao longo de todo o ciclo de vida do poço (KIRAN *et al.*, 2017). Nesse contexto, atenção especial é prestada à degradação da bainha de cimento e à corrosão tubulação de aço, que constituem-se como os

principais e mais frágeis componentes dos poços (BAI; ZHANG; FU, 2016). Adicionalmente, processos como a retração da pasta de cimento durante a hidratação, eventuais choques mecânicos e os defeitos de cimentação, também podem levar a formação de fraturas e caminhos preferenciais para o vazamento de fluidos do reservatório (WIGAND *et al.*, 2009).

As interfaces pasta de cimento/formação geológica e pasta de cimento/tubulação de aço são os pontos críticos dos poços, podendo sofrer falhas devido a uma ineficiente aplicação da pasta de cimento, ao ataque de fluidos corrosivos, como os gases H_2S e CO_2 e/ou a uma baixa eficiência de remoção da lama de perfuração (TORSÆTER; TODOROVIC; LAVROV, 2015). Na literatura, encontram-se inúmeros relatos de problemas de vazamentos ao longo das interfaces de poços, o que alerta para a suscetibilidade desses pontos às falhas de integridade e às ações de degradação (AJAYI; GUPTA, 2019; HWANG *et al.*, 2018). Porém, experimentos com interfaces (pasta de cimento/aço e pasta de cimento/rocha) indicam resultados contraditórios, em que, a depender do tempo de evolução do processo e às condições a que os materiais estão expostos, o mesmo processo químico pode ter um efeito positivo ou negativo sobre a integridade do material (CARROLL *et al.*, 2016). Assim, uma vez que não há um debate sobre a representatividade das condições dos experimentos de integridade dos materiais de poços frente ao CO_2, os resultados da literatura podem indicar que os aspectos reacionais/experimentais não padronizados podem levar ao contraditório e expõem a necessidade de discussões sobre as condições dos ensaios (TEODORIU; BELLO, 2020).

Além das falhas de interface, a ação do ciclo térmico, das condições de cura da pasta de cimento e do efeito das condições HPHT (*High Pressure-High Temperature*), podem resultar na formação de falhas de integridade (BAGHERI; SHARIATIPOUR; GANJIAN, 2018; GARCIA FERNANDEZ *et al.*, 2019; LI; NYGAARD, 2018). Na Tabela 3-2, são apresentadas algumas fases primárias da pasta de cimento e os respectivos produtos de degradação resultantes das diversas alterações que os materiais estão sujeitos a sofrer ao longo do seu ciclo de vida.

Tabela 3-2. Fases primárias da pasta de cimento Portland e os respectivos produtos de degradação associados às alterações do material submetido à salmoura saturada com CO_2, H_2S e SO_2 (CARROLL *et al.*, 2016)

Fases primárias do cimento	
Fase	**Fórmula**
Silicato de cálcio-hidrato (C-S-H)	$Ca_rSiO_{2+x}•nH_2O$
Portlandita (CH)	$Ca(OH)_2$
Monosulfato (AFm)	$Ca_4Al_2(OH)_{12}SO_4•6H_2O$ $Ca_4Fe_2(OH)_{12}SO_4•6H_2O$
Trisulfato (AFt)	$Ca_6Al_2(OH)_{12}(SO_4)_3•26H_2O$ $Ca_6Fe_2(OH)_{12}(SO_4)_3•26H_2O$
Katoite	$Ca_3Al_2(OH)_{12}$
Gipsita	$CaSO_4•2H_2O$
Produtos secundários de alteração	
Fase	**Fórmula**
Carbonato de cálcio	$CaCO_3$
C-S-H descalcificado	$Ca_{r-y}SiO_{2+x-y}•(x-y)H_2O$
Sal de Friedel's	$Ca_4Al_2(OH)_{12}Cl_2•6H_2O$
Gipsita	$CaSO_4•2H_2O$
Silicato amorfo	SiO_2
Alumina amorfa	$Al(OH)_3$
Hidróxido férrico amorfo	$Fe(OH)_3$
Brucita	$Mg(OH)_2$
Pirita	FeS_2
Sulfeto de ferro amorfo	FeS

As propriedades de resistência a compressão, porosidade e permeabilidade das pastas de cimento podem ser alteradas devido às mudanças de composição do material ao longo dos diferentes processos de degradação (KIRAN *et al.*, 2017). Nesse contexto, as falhas de integridade podem levar ao comprometimento da estrutura mecânica das pastas de cimento, o que pode resultar na formação de caminhos preferenciais para o vazamento de fluidos e expor as frações internas do material à ação de químicos como o cloreto (Cl^-), o sulfato (SO_4^{2-}) e o CO_2 (ABID *et al.*, 2018; BAGHERI; SHARIATIPOUR; GANJIAN, 2018; GARCIA FERNANDEZ *et al.*, 2019). Assim, esses aspectos serão discutidos brevemente a seguir.

3.3.1. Interface bainha de cimento/tubulação de aço

O desempenho das tubulações de aço à corrosão varia muito a depender da sua composição, do processo de fabricação e do tipo de agente químico ao qual forem expostas, podendo sofrer fenômenos de transformação associados à presença de sulfatos, cloretos, H_2S e CO_2 (AJAYI; GUPTA, 2019; CARROLL *et al.*, 2016; KIRAN *et al.*, 2017). Nesse contexto, a corrosão representa o processo de degradação mais importante resultante da interação entre a tubulação de aço e a bainha de cimento (AJAYI; GUPTA, 2019). Fundamentalmente, a corrosão pode ser descrita como um processo destrutivo que envolve a reação de um metal/liga com os fluidos que compõem o meio (AJAYI; GUPTA, 2019; KIRAN *et al.*, 2017). Assim, a corrosão da tubulação de aço pode resultar em uma série de defeitos de integridade, como a presença de fraturas na interface (pasta de cimento-aço), o que leva a formação de caminhos preferenciais para o vazamento de fluidos do reservatório (KIRAN *et al.*, 2017). Além disso, é comum observar a formação de espaço microanular ou fissuras associadas ao estresse térmico, ou seja, falhas induzidas pelas diferentes propriedades de expansão térmica da pasta de cimento e do aço (BU *et al.*, 2017). Ainda que a pasta de cimento possa apresentar propriedades de reparação (*self-healing*) das microfraturas do material, apenas os defeitos de integridade de pequena dimensão podem ser corrigidos por esse processo (GARCIA FERNANDEZ *et al.*, 2019). Assim, a fim de prever o comportamento das interfaces da pasta de cimento-aço e de garantir a integridade do poço, é necessário realizar o estudo dos fenômenos de degradação interfaciais cimento-aço (AJAYI; GUPTA, 2019; ASHRAF, 2016).

O fluxo de fluidos na interface da pasta de cimento-aço normalmente é pouco expressivo, uma vez que não é muito provável a existência de grandes falhas contínuas (TEODORIU; BELLO, 2020). Apesar do baixo fluxo na interface, fatores como a temperatura elevada acabam por favorecer a cinética de degradação dos materiais do poço (pasta de cimento e aço) (AJAYI; GUPTA, 2019). Teoricamente, o CO_2 deveria acelerar a corrosão do aço e induzir o processo de degradação da pasta de cimento Portland, resultando na transformação química das frações reativas de

portlandita (CH) e de silicato de cálcio hidratado (C-S-H) em uma mistura de carbonato de cálcio ($CaCO_3$) e frações silicosas (C-S-H descalcificada e sílica amorfa) (ASHRAF, 2016; BAGHERI; SHARIATIPOUR; GANJIAN, 2018). Porém, o processo de perda de integridade do poço ocorre em etapas com diferentes características e cinéticas de transformação.

Inicialmente, o pH elevado da pasta de cimento (12-13) resulta na proteção dos materiais, ao induzir a precipitação de carbonato nos poros da pasta de cimento e a formação de uma camada passivadora de siderita ($FeCO_3$) sobre o aço. A precipitação de $FeCO_3$ na superfície do aço reduz a taxa de corrosão de 20 mm/ano para 0,2 mm/ano (ASHRAF, 2016; CHOI *et al.*, 2013; HAN *et al.*, 2012; TAVARES *et al.*, 2015). Na interface da pasta de cimento-aço, a solução rica em CO_2 corrói o aço, lixiviando íons Fe^{2+} para a solução e promovendo precipitação de $FeCO_3$ na superfície da tubulação, enquanto na bainha de cimento, dois processos estão ocorrendo: (*i*) a dissolução da portlandita (CH) e (*ii*) o processo de carbonatação da pasta de cimento. Em seguida, ferro (Fe^{2+}) e cálcio (Ca^{2+}) reagem com o CO_2 levando a uma formação de carbonato de cálcio ($CaCO_3$), siderita ($FeCO_3$) e carbonatos mistos ($Fe_xCa_yCO_3$) em ambas as fases (pasta de cimento e aço) (DALLA VECCHIA *et al.*, 2020). Esse processo é apresentado na Figura 3-5.

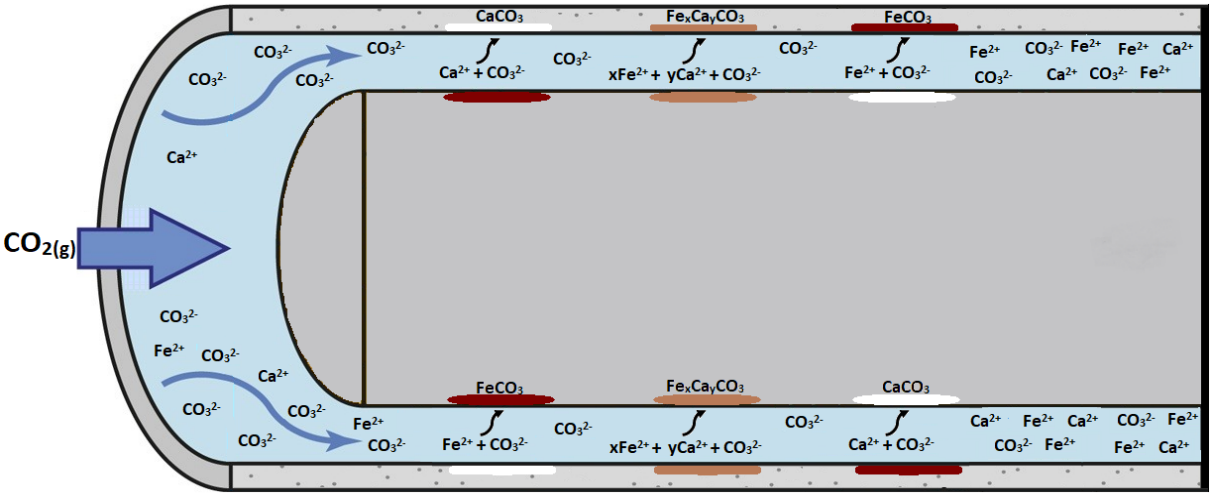

Figura 3-5. Dinâmica da degradação do sistema interfacial pasta de cimento-aço em poços ricos em CO_2. Adaptado de Dalla Vecchia *et al.*, (2020)

3.3.2. Interface cimento/formação geológica

A interface pasta de cimento-formação rochosa representa outro ponto de atenção importante das operações em subsuperfície. Nesse contexto, os fenômenos de degradação podem resultar no comprometimento das propriedades interfaciais do sistema (cimento-formação) e na perda da integridade do poço. Para tanto, estudar as características das formações rochosas é essencial, uma vez que cada extrato geológico tende a interagir de maneira diferente com os materiais cimentícios. Assim, as diferentes interações entre o cimento e as rochas do reservatório levam a formação de ligações cimento-rocha com diferentes características e qualidades ao longo de toda a seção perfurada (AJAYI; GUPTA, 2019). Esse processo ocorre pois a rocha do reservatório interage diretamente com a camada mais externa da bainha de cimento, levando a troca de materiais (migração de íons e fluidos) entre as fases (pasta de cimento e formação) e a consolidação da interface rocha-cimento (CONDE SILVA; MILESTONE, 2018b). Nesse contexto, tanto a porosidade, quanto a composição química da formação geológica, têm um impacto considerável na resistência de ligação entre a pasta de cimento e a rocha (CONDE SILVA; MILESTONE, 2018b).

A penetração da pasta de cimento na rocha é regulada pela porosidade do reservatório, o que, posteriormente, também limita a quantidade de fluidos ricos em CO_2 que podem entrar em contato com a pasta de cimento ou permear pelas falhas de interface (AJAYI; GUPTA, 2019; CONDE SILVA; MILESTONE, 2018b). Uma vez que o processo de cimentação tenha sido bem sucedido, é improvável que os fluidos do reservatório migrem através da interface pasta de cimento/rocha (XIAO *et al.*, 2017). Porém, as tensões na formação geológica no entorno do poço mudam ao longo do ciclo de vida do poço, podendo induzir alterações que podem afetar a permeabilidade dos materiais do poço (CARROLL *et al.*, 2016; XIAO *et al.*, 2017). Assim, se houver alguma falha na interface da pasta de cimento/formação, uma série de processos geoquímicos podem resultar na perda da integridade da estrutura e na formação de caminhos preferenciais para a migração de fluidos (BAGHERI;

SHARIATIPOUR; GANJIAN, 2018; CONDE SILVA; MILESTONE, 2018a; XIAO *et al.*, 2017). Na Figura 3-6, são resumidos os principais caminhos de fuga de fluidos dos reservatórios, estando estes principalmente relacionados com a ocorrência de defeitos interfaciais (pasta de cimento-aço e pasta de cimento-formação geológica). Entre os pontos de vazamentos, têm-se: (A) as falhas entre a tubulação de aço e a pasta de cimento, (B) entre a tubulação de aço e o *plug* de cimento, (C) através da estrutura porosa da pasta de cimento, (D) através da tubulação de aço, (E) através das fraturas da pasta de cimento e (F) entre a pasta de cimento e a formação rochosa (CELIA *et al.*, 2005; KMIEĆ *et al.*, 2018).

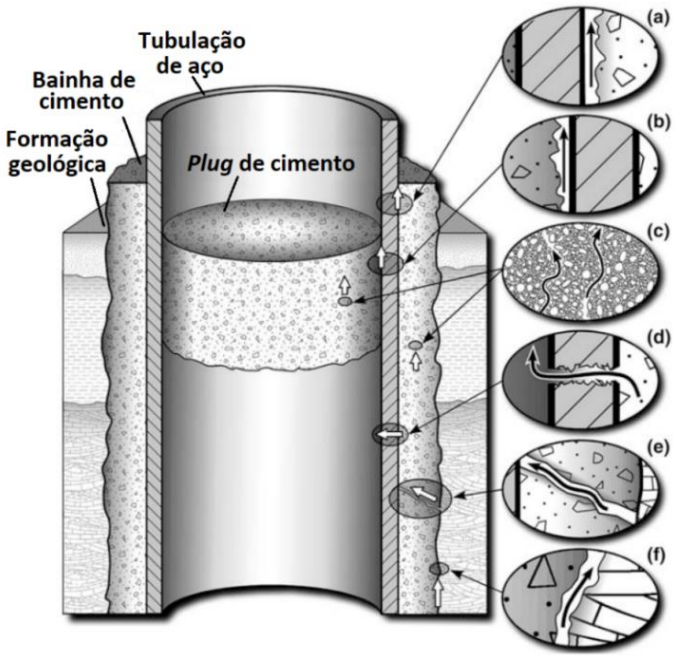

Figura 3-6. Potenciais vias de fuga de fluidos em um poço: (A) entre a tubulação de aço e a pasta de cimento, (B) entre a tubulação de aço e o *plug* de cimento, (C) através da estrutura porosa da pasta de cimento, (D) através da tubulação de aço, (E) através das fraturas da pasta de cimento, (F) entre a pasta de cimento e a formação rochosa. Adaptado de Celia *et al.*, (2005) e Kmieć *et al.*, (2018)

3.3.3. Efeito térmico

O efeito térmico sobre a integridade dos materiais é um dos pontos críticos de atenção na especificação de projetos, uma vez que pode ser prejudicial para as

propriedades finais dos materiais do poço (pasta de cimento, aço e interfaces). Nesse contexto, muitos dos problemas estão relacionados à composição do cimento, às condições de cura do material e a forma como o ciclo de aquecimento-resfriamento impacta na integridade da pasta de cimento (KUZIELOVÁ *et al.*, 2019). Na Figura 3-7, é apresentado como as formações de microanular e de microfissuras podem estar associadas aos mecanismos de degradação induzidos pela temperatura e aos diferentes coeficientes de expansão térmica dos materiais (pasta de cimento e aço). Ao longo do ciclo térmico de aquecimento-resfriamento (Figura 3-7A), os materiais (pasta de cimento e aço) sofrem uma série de processos de expansão e retração que levam a formação de fraturas e de microanular (Figura 3-7B) (KIRAN *et al.*, 2017; PAIVA *et al.*, 2018). Uma vez que a tubulação de aço apresenta maior coeficiente de expansão térmica quando comparados com a pasta de cimento Portland (Figura 3-7C), espera-se que poços submetidos à oscilações intensas de temperatura venham a apresentar descolamento da interface e por sua vez, perda de integridade do poço ao longo do tempo (KIRAN *et al.*, 2017). Assim, a formação do microanular e de microfissuras geram caminhos preferenciais para a migração de fluidos ao longo do poço e podem representar riscos ao meio ambiente e prejuízo financeiros para o operador das unidades de exploração.

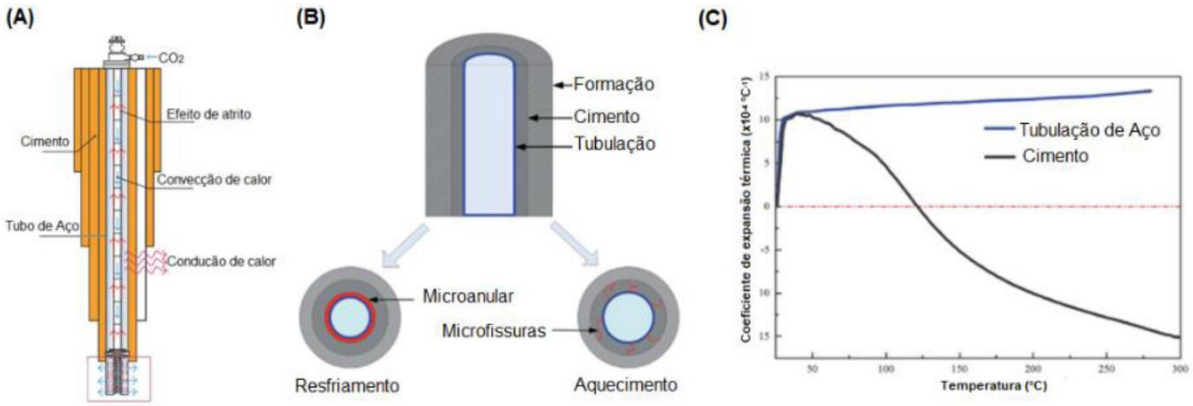

Figura 3-7. A influência do ciclo de aquecimento e resfriamento na pasta de cimento: (A) ciclo térmico da operação de poços (PIAO *et al.*, 2018), (B) comprometimento da vedação do poço (BU *et al.*, 2017) e (C) coeficiente de expansão térmica (BU *et al.*, 2017)

Adicionalmente, uma intensificação nas falhas de interface pode ser observada quando o processo de cimentação ocorre em temperaturas elevadas (> 110 °C) (BU *et al.*, 2017; KUZIELOVÁ *et al.*, 2018). Nessas condições, a pasta de cimento passa pelo processo de retrogressão, que resulta na perda de resistência do material associada à transformação estrutural dos silicatos de cálcio hidratados (C-S-H) amorfos para formas cristalinas de C-S-H, como a jaffeíta e a α-C_2SH (HWANG *et al.*, 2018; KUZIELOVÁ *et al.*, 2018; SALEHI *et al.*, 2019). Porém, o efeito da temperatura sobre o processo de retrogressão e a formação de fissuras/microanular podem ser suavizados/mitigados a partir da modificação das formulações de cimento (PAIVA *et al.*, 2018). Nesse contexto, a solução da indústria de O&G passa pela adição de 25 a 45% em massa de materiais cimentícios suplementares (MCS) com elevada atividade pozolânica na pasta de cimento, a fim de consumir a fração de portlandita (CH) e modificar a relação Ca/Si do C-S-H, reduzindo os efeitos da temperatura na integridade dos materiais (HWANG *et al.*, 2018; KUZIELOVÁ *et al.*, 2019).

3.3.4. Efeito do cloreto e do sulfato

Nos poços e reservatórios existem quantidades significativas de componentes químicos que podem causar problemas de integridade e que estão associados aos fluidos do meio. Nesse contexto, os íons cloreto (Cl^-) e sulfato (SO_4^{2-}) estão entre os elementos dissolvidos que podem promover o ataque químico e levar a modificação dos minerais da pasta de cimento, à corrosão do aço e às falhas de integridade (PARIS *et al.*, 2016; QIN; GAO; CHEN, 2019). A intrusão de cloreto na matriz cimentícia está entre os principais gatilhos que levam à corrosão da tubulação de aço, além de promover alterações na estrutura da pasta de cimento (SHAH *et al.*, 2018). Quando ambos os íons se encontram no meio (Cl^- e SO_4^{2-}), os íons cloreto acabam por tamponar a ação do SO_4^{2-} a partir da reação rápida do Cl^- com os aluminatos de cálcio na pasta de cimento para produzir uma série de fases sólidas que incluem os hidratos de monosulfato (AFm) e o sal de Friedel ($C_3A.CaCl_2.10H_2O$ - cloro-aluminato de cálcio hidratado) (MÁRQUEZ *et al.*, 2011). Dessa forma, evitar a percolação de

cloretos através da matriz cimentícia é uma das principais áreas de interesse no estudo de materiais cimentícios (ZHUANG *et al.*, 2016).

Já o ataque de sulfato (SO_4^{2-}) na pasta de cimento Portland tem um mecanismo complexo (SUKMAK *et al.*, 2015). Ao longo desse processo, o sulfato pode reagir com produtos de hidratação da pasta de cimento, alterando a composição química das fases e a morfologia do material, resultando na degradação da pasta de cimento e na perda de integridade dos poços (DING *et al.*, 2018). Assim, a matriz cimentícia passa por um processo de descalcificação (C-S-H) e desaluminização do silicato-aluminato de cálcio (C-A-S-H) induzida pelo SO_4^{2-}, o que resulta na diminuição das relações Ca/Si e Al/Si (DING *et al.*, 2018; MÁRQUEZ *et al.*, 2011). Adicionalmente, o C_3A e C_4AF podem ser consumidos pelo ataque do SO_4^{2-}, levando a produção de etringita secundária expansiva (AFt), a fissuração da pasta de cimento e ao aumento da porosidade da matriz cimentícia, facilitando a percolação de fluidos agressivos (Cl^-, SO_4^{2-}, H_2S e CO_2) (MÁRQUEZ *et al.*, 2011). Quando a pasta de cimento é exposta a ambientes ricos em sulfato, a formação de etringita, gipsita e brucita pode ser detectada como um indicativo do processo de degradação (ZHUANG *et al.*, 2016).

3.3.5. Degradação da pasta de cimento pelo CO_2

A reação do CO_2 com a pasta de cimento é conhecida como carbonatação. Este processo é caracterizado pelo ataque das espécies de carbono inorgânicos dissolvidas (DIC), formadas a partir da dissolução do CO_2 em meio aquoso, aos componentes hidratados reativos da pasta de cimento (AJAYI; GUPTA, 2019). A depender do pH do sistema, a dissolução de CO_2 em água resulta na produção das espécies de DIC: ácido carbônico (H_2CO_3), bicarbonato (HCO_3^-) e/ou carbonato (CO_3^{2-}), como mostrado na Equação 3.6 (BAI *et al.*, 2015a; DUGUID; RADONJIC; SCHERER, 2011; KIRAN *et al.*, 2017).

$$CO_{2(g)} + H_2O_{(l)} \leftrightarrow H_2CO_{3(aq)} \leftrightarrow HCO_3^-{}_{(aq)} + H^+{}_{(aq)} \leftrightarrow CO_3^{2-}{}_{(aq)} + 2H^+{}_{(aq)} \quad (3.6)$$

As concentrações relativas das espécies de DIC, [H_2CO_3], [HCO_3^-] e [CO_3^{2-}], são governadas pelo pH da solução, conforme plotado na Figura 3-8. O ácido carbônico (H_2CO_3) é a espécie dominante em valores de pH menores que 6, enquanto o bicarbonato (HCO_3^-) é a espécie majoritária entre os valores de pH de 6 a 9 e o íon carbonato (CO_3^{2-}) domina em valores de pH acima de 9 (MIDDELBURG, 2019). No caso de sistemas reacionais contendo minerais carbonáticos, as espécies de DIC desempenham um papel importante na capacidade de tamponamento do pH do meio, devido à sua alta solubilidade, alta reatividade e a sua participação em processos de dissolução, precipitação e degasificação do meio (MIDDELBURG, 2019).

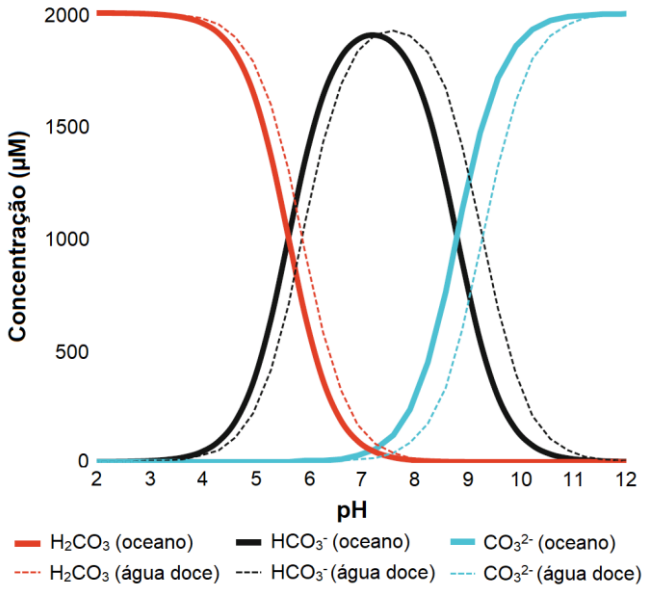

Figura 3-8. Diagrama de Bjerrum da distribuição das espécies de DIC em função do pH. Adaptado de Middelburg, (2019)

Assim, todos os processos reativos que consomem alguma espécie de DIC são acompanhados pelo um rearranjo na concentração/especiação das espécies de carbono dissolvidos e na manutenção da atividade hidrogeniônica (pH) da solução (BACHU; ADAMS, 2003; MIDDELBURG, 2019). A temperatura, salinidade e presença de outros íons no meio também podem contribuir para pequenas mudanças na composição das espécies de DIC, embora não apresentem, inicialmente, grande efeito sobre o pH da solução (MIDDELBURG, 2019). Nas temperaturas e pressões

elevadas encontradas em reservatórios e poços de CCS, os sólidos dissolvidos na água, o complexo poroso das rochas e uma variedade de espécies minerais, resultam em sistemas químicos complexos que podem dificultar a previsão das propriedades e características geoquímicas dos processos reativos na presença de CO_2 (BACHU; ADAMS, 2003).

A solubilidade dos gases, incluindo o CO_2, sofre influência da temperatura, salinidade e pressão. No geral, o aumento da salinidade e da temperatura resultam na redução da capacidade de dissolução das soluções aquosas (MIDDELBURG, 2019). Além disso, em condições comuns em poços, o CO_2 encontra-se em estado supercrítico, uma condição especial em que o CO_2 apresenta densidade similar a fluidos e viscosidade similar a gases (BAI; ZHANG; FU, 2016). Nesse contexto, o CO_2 supercrítico configura-se como um fluido extremamente reativo e capaz de permear através da matriz cimentícia porosa. No presente trabalho, o processo de degradação em meio aquoso foi realizado para simular as condições de reservatórios de O&G e de CCS. Na Figura 3-9, são apresentados os gráfico de solubilidade de CO_2 com a pressão e o diagrama de fases para o CO_2, em que a condição supercrítica é alcançada em temperaturas acima de 31 °C e pressões superiores a 73,8 bar (ZHA *et al.*, 2015).

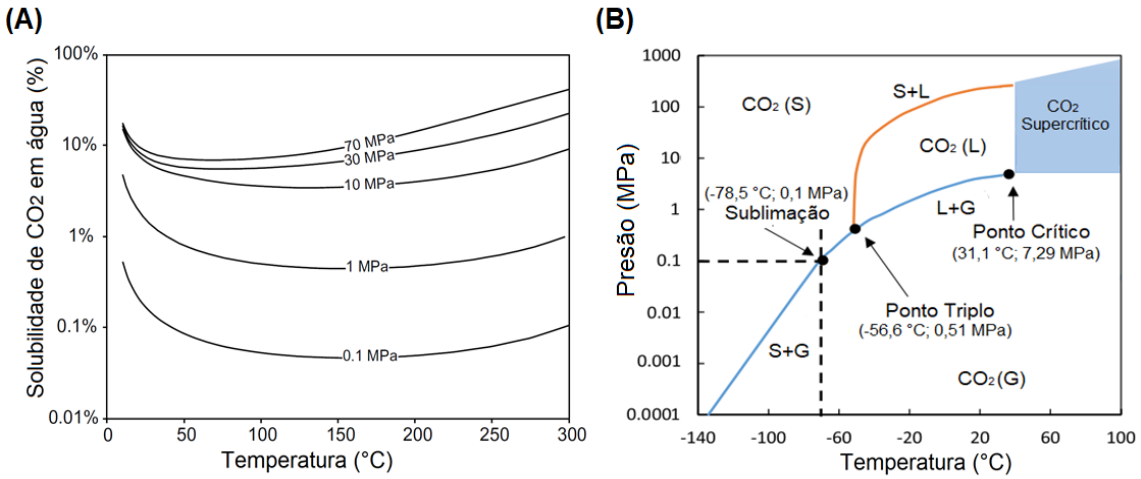

Figura 3-9. Solubilidade (A) e diagrama de fases (B) do CO_2. Adaptado de Bachu e Adams, (2003); De Sena Costa *et al.*, (2018) e Tiong; Gholami e Rahman, (2019)

Considerando que o fluxo de fluidos ao longo do poço é extremamente baixo, o sistema estático acaba sendo normalmente utilizado nos estudos que investigam a carbonatação da pasta de cimento (BAGHERI; SHARIATIPOUR; GANJIAN, 2018; TEODORIU; BELLO, 2020; TIONG; GHOLAMI; RAHMAN, 2019). Assim, a Figura 3-10 apresenta o sistema reacional estático, em que estão representados: (*i*) o reator e o sistema de pressurização (Figura 3-10A) e (*ii*) o efeito da exposição das amostras ao CO_2 supercrítico após o processo de degradação (Figura 3-10B). Ainda, na Figura 3-10B, o resultado convencional do teste de fenolftaleína pode ser observado, em que a área pigmentada em cor lilás é utilizada como técnica para estimar a extensão da camada degradada.

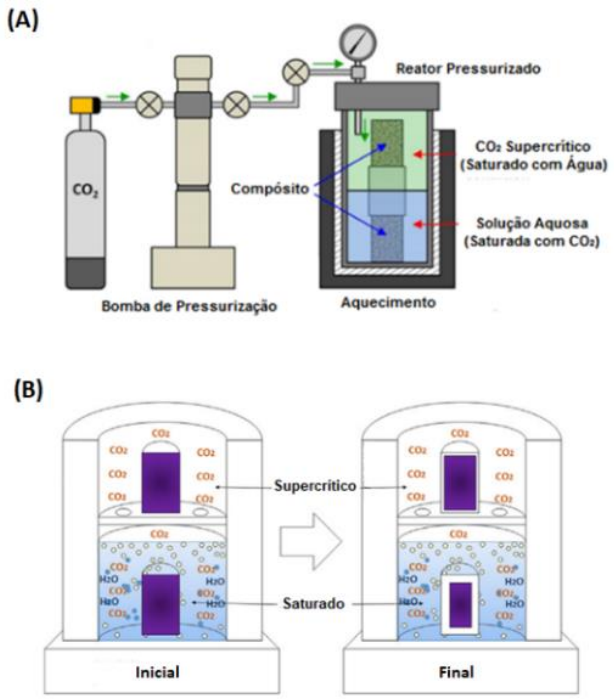

Figura 3-10. Sistema reacional estático utilizado nos estudos de carbonatação da pasta de cimento: (A) reator e sistema de pressurização (NAKANO *et al.*, 2016) e (B) efeito da carbonatação na pasta de cimento (DE SENA COSTA *et al.*, 2018)

O processo de degradação é o resultado da interação entre o CO_2 e os materiais cimentícios. Na carbonatação, as espécies de carbono inorgânico dissolvido

(DIC - H_2CO_3, HCO_3^- e/ou CO_3^{2-}) atacam os componentes hidratados reativos da pasta de cimento e reduzem o pH da matriz cimentícia (AJAYI; GUPTA, 2019; LOREK; LABUS; BUJOK, 2016). Com base na literatura, as principais reações de degradação consomem as fases de silicato de cálcio hidratado (C-S-H) e portlandita (CH) e produzem diferentes polimorfos de carbonato de cálcio ($CaCO_3$) (carbonato amorfo, calcita, aragonita e vaterita) e derivados silicosos (C-S-H descalcificado e sílica amorfa) (KOUKOUZAS *et al.*, 2017; TIONG; GHOLAMI; RAHMAN, 2019). Além disso, as frações não hidratadas de cimento (C_3S e C_2S) também podem ser consumidas pelo processo de degradação e produzir $CaCO_3$ e produtos siliciosos. Essas reações são representadas pelas Equações 3.7 a 3.14 (BAI *et al.*, 2015a; CAREY *et al.*, 2007; DUGUID; RADONJIC; SCHERER, 2011).

$$C_3S_{(s)} + 3CO_{2(aq)} + nH_2O_{(l)} \rightarrow SiO_2.nH_2O_{(s)} + 3CaCO_{3(s)} \quad (3.7)$$

$$C_2S_{(s)} + 3CO_{2(aq)} + nH_2O_{(l)} \rightarrow SiO_2.nH_2O_{(s)} + 3CaCO_{3(s)} \quad (3.8)$$

$$Ca(OH)_{2(s)} + CO_3^{2-}{}_{(aq)} + 2H^+{}_{(aq)} \rightarrow CaCO_{3(s)} + 2H_2O_{(l)} \quad (3.9)$$

$$Ca(OH)_{2(s)} + HCO_3^-{}_{(aq)} + H^+{}_{(aq)} \rightarrow CaCO_{3(s)} + 2H_2O_{(l)} \quad (3.10)$$

$$\mathrm{C-S-H}_{(s)} + CO_3^{2-}{}_{(aq)} + 2H^+{}_{(aq)} \rightarrow CaCO_{3(s)} + SiO_xOH_{x(s)} \quad (3.11)$$

$$\mathrm{C-S-H}_{(s)} + HCO_3^-{}_{(aq)} + H^+{}_{(aq)} \rightarrow CaCO_{3(s)} + SiO_xOH_{x(s)} \quad (3.12)$$

$$CaCO_{3\,(s)} + CO_{2\,(g)} + H_2O_{(l)} \leftrightarrow Ca^{2+}{}_{(aq)} + HCO_3^-{}_{(aq)} \quad (3.13)$$

$$CaCO_{3\,(s)} + 2H^+{}_{(aq)} \leftrightarrow CO_{2\,(g)} + H_2O_{(l)} + Ca^{2+}{}_{(aq)} \quad (3.14)$$

A principal consequência do ataque do CO_2 à matriz da pasta de cimento é a perda potencial da integridade do material (ABID *et al.*, 2018), que pode ser mais acelerado se o CO_2 encontrar-se no estado supercrítico (PARK *et al.*, 2021). Neste cenário, alguns fatores podem influenciar a taxa de degradação da pasta de cimento, incluindo: (*i*) condições de cura do material, (*ii*) tipo de cimento (composição química), (*iii*) presença de aditivos e (*iv*) a relação água/cimento (*water-to-cement ratio*) da pasta (AJAYI; GUPTA, 2019). Na Figura 3-11, é apresentado a evolução das principais fases da pasta de cimento ao longo da degradação do material.

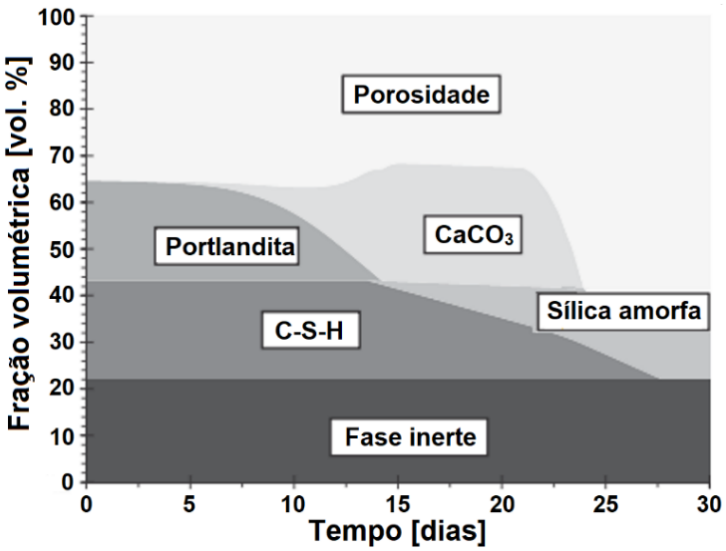

Figura 3-11. Evolução das fases hidratadas e da porosidade da pasta de cimento ao longo do tempo de exposição ao CO_2**.** Adaptado de Liaudat *et al.*, (2018)

Ao longo do processo de degradação, o CO_2 consome inicialmente a reserva alcalina de portlandita (CH), produzindo carbonato de cálcio ($CaCO_3$) e reduzindo a porosidade da pasta de cimento a partir do preenchimento dos poros com $CaCO_3$ (BAGHERI; SHARIATIPOUR; GANJIAN, 2018; GU *et al.*, 2017; TIONG; GHOLAMI; RAHMAN, 2019). À medida que o pH do meio reduz, o processo de bicarbonatação começa a dissolver o carbonato de cálcio ($CaCO_3$), resultando na descalcificação da matriz cimentícia, na lixiviação de íons cálcio (Ca^{2+}) pelo íon bicarbonato (HCO_3^-) e no aumento da porosidade da pasta de cimento (BAGHERI; SHARIATIPOUR; GANJIAN, 2018; TIONG; GHOLAMI; RAHMAN, 2019). Por fim, a perda de integridade

da pasta de cimento segue a partir do consumo do silicato de cálcio hidratado (C-S-H), o que resulta na produção de $CaCO_3$, C-S-H descalcificado e sílica amorfa (BAGHERI; SHARIATIPOUR; GANJIAN, 2018; GU *et al.*, 2017; TIONG; GHOLAMI; RAHMAN, 2019). Assim, ao longo do processo de degradação da pasta de cimento por CO_2, vários fenômenos de transformação podem levar a formação de fraturas, microfissuras, estrutura porosa e falhas de interface (cimento-aço e formação-cimento), resultando em uma série de caminhos preferenciais para a fuga de fluidos (AJAYI; GUPTA, 2019; BAGHERI; SHARIATIPOUR; GANJIAN, 2018; CARROLL *et al.*, 2016; KIRAN *et al.*, 2017).

3.4. Monitoramento da carbonatação da pasta de cimento

Os principais componentes dos materiais cimentícios (CH e C-S-H) são sensíveis à ação do CO_2 em meio aquoso e estão sujeitos ao processo de carbonatação (LIU *et al.*, 2021b; MOON; CHOI, 2019). A partir da reação de carbonatação, carbonato de cálcio ($CaCO_3$) e sílica amorfa são produzidos, entre outros compostos minoritários (ŠAVIJA; LUKOVIĆ, 2016). Devido à complexidade dos materiais cimentícios, é necessário empregar várias técnicas analíticas complementares para caracterizar o material (BJØRGE *et al.*, 2019; HORGNIES; CHEN; BOUILLON, 2013). Além disso, quando o processo de carbonatação é considerado, muitas dificuldades e incertezas são adicionadas aos projetos de pesquisa e desenvolvimento (WU; YE, 2019). Neste contexto, é essencial: (*i*) quantificar os produtos da reação de carbonatação, (*ii*) controlar o processo de carbonatação e (*iii*) compreender os seus efeitos na integridade e propriedades da pasta de cimento. Assim, técnicas como o teste de fenolftaleína, a fluorescência de Raios-X (XRF), a difração de Raios-X (DRX), a microscopia eletrônica de transmissão (TEM), a microscopia eletrônica de varredura (MEV), a microtomografia de Raios-X (MicroCT), a análise termogravimétrica (TGA), a espectroscopia de ressonância magnética nuclear (NMR) e a espectroscopia na região do infravermelho (FTIR), são aplicadas para caracterizar materiais cimentícios (BALDISSERA *et al.*, 2017a, 2017b; DUGGAN *et al.*, 2017; GASTALDI *et al.*, 2010; HORGNIES; CHEN; BOUILLON, 2013;

KUPWADE-PATIL *et al.*, 2018; LEDESMA *et al.*, 2020; MORAES; COSTA, 2022; REBOUÇAS; ROHWEDDER; PASQUINI, 2018; SCHÜTZ *et al.*, 2019, 2018).

Dentre os métodos de caracterização, a análise do $CaCO_3$ em materiais cimentícios pode ser realizada da seguinte forma: (*i*) qualitativa, por meio dos métodos de fenolftaleína, TEM e MEV, (*ii*) semiquantitativa, utilizando os métodos de FTIR, MicroCT, DRX e XRF e (*iii*) quantitativos, por meio da análise de TGA (DUGGAN *et al.*, 2017; HENRY; WATSON; JOHN, 2017; HIGL *et al.*, 2021; KUPWADE-PATIL *et al.*, 2018; LIU *et al.*, 2019). Além disso, o DRX, o MEV, o FTIR e o TGA, podem ser aplicados, com suas respectivas limitações, para identificar a presença de diferentes polimorfos de $CaCO_3$ (carbonato amorfo, vaterita, aragonita e calcita) (CHANG *et al.*, 2017; PARK *et al.*, 2021; VANCE *et al.*, 2015). Por outro lado, o NMR é aplicado apenas para analisar as fases silicosas (^{29}Si NMR) e de aluminato (^{27}Al NMR) da pasta de cimento; no entanto, geralmente não é aplicado para analisar o $CaCO_3$ por ^{13}C NMR (HIGL *et al.*, 2021; LIU *et al.*, 2019; SAILLIO *et al.*, 2021).

3.4.1. Espectroscopia na região do infravermelho

O FTIR é um método rápido, preciso e amplamente disponível em universidades e laboratórios de pesquisa e de serviços (HIGL *et al.*, 2021; REBOUÇAS; ROHWEDDER; PASQUINI, 2018; SHI *et al.*, 2019). O FTIR varre a amostra com uma faixa especificada do espectro da radiação eletromagnética no comprimento de onda do infravermelho médio (WITKOWSKI; KONIORCZYK, 2018). Os espectros de FTIR são usados para caracterizar grupos funcionais moleculares dos materiais a partir do perfil espectral registrado pelo equipamento como transmitância (% T) ou absorbância (% A) versus comprimento de onda (cm^{-1}) (OMOSEBI *et al.*, 2016; RANJAN; KUMAR; MOHAN, 2018). Uma vez que a energia vibracional molecular é quantizada, cada pico no espectro de FTIR denota a presença de um grupo funcional molecular específico, enquanto a intensidade relativa da radiação absorvida (ou seja, a altura do pico no espectro) pode ser diretamente relacionada à concentração do componente químico (OMOSEBI *et al.*, 2015, 2016).

Aplicações de FTIR foram propostas na literatura para qualificar ou quantificar componentes minerais em rochas, sedimentos, solo e pasta de cimento ou para estudar processos de transformação (ou seja, hidratação, degradação, carbonatação, etc.) em materiais cimentícios (HENRY; WATSON; JOHN, 2017; HIGL *et al.*, 2021; JOSE *et al.*, 2020; VALLIANT *et al.*, 2016). Nesse contexto, o uso do acessório de Refletância Total Atenuada (*Atenuated Total Reflectance* - ATR) é especialmente interessante para análise de FTIR, uma vez que é possível eliminar e simplificar as etapas de preparo de amostras e favorecer a reprodutibilidade e a sensibilidade da análise (HENRY; WATSON; JOHN, 2017; HIGL *et al.*, 2021; HORGNIES; CHEN; BOUILLON, 2013; VALLIANT *et al.*, 2016; VEERASINGAM; VENKATACHALAPATHY, 2014). Assim, a análise ATR-FTIR apresenta todos os requisitos para aplicação em estudos de materiais cimentícios, subsidiando o desenvolvimento de métodos qualitativos e quantitativos e possibilitando avaliações rápidas e confiáveis de processos de transformação da pasta de cimento, como a carbonatação. Na Figura 3-12, é apresentado um espectro de FTIR característico da pasta de cimento hidratada.

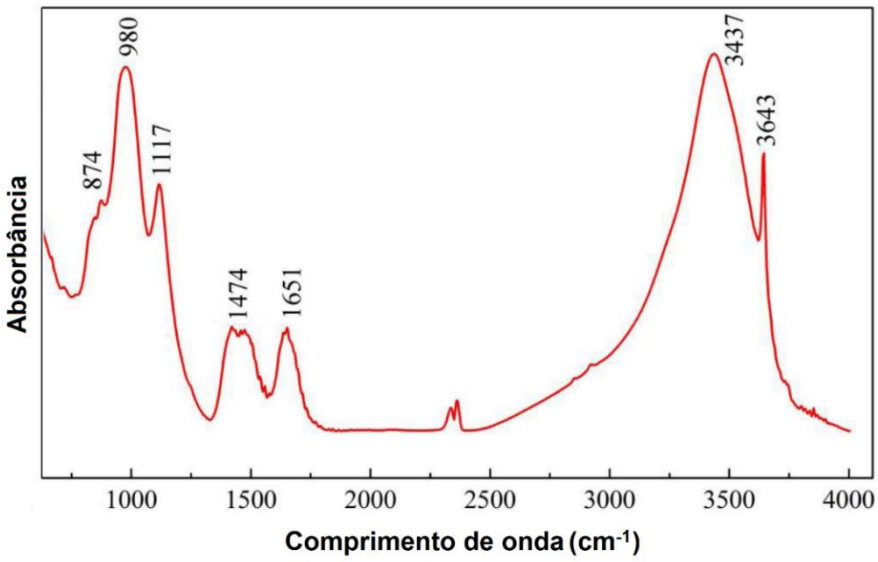

Figura 3-12. Espectro de FTIR de pasta de cimento hidratada. Adaptado de Shi *et al*., (2019)

A partir do perfil espectral do FTIR da pasta de cimento hidratada, é possível descrever as seguintes características: (*i*) a presença do pico relacionado ao alongamento OH da portlandita (CH) em 3643 cm^{-1}, (*ii*) uma banda larga na faixa de 3600-3100 cm^{-1}, atribuída ao alongamento OH da água associado à matriz de cimento, (*iii*) um pequeno pico em 1640 cm^{-1}, atribuído à vibração molecular da água associada aos sulfatos, (*iv*) os picos de carbonato (CO_3^{2-}) em 1474 cm^{-1} (estiramento assimétrico de C-O) e 874 cm^{-1} (vibração fora do plano), associado com a calcita (polimorfo de $CaCO_3$) e (*v*) uma banda larga (800-1200 cm^{-1}), centrada em 1117 cm^{-1} e 980 cm^{-1}, associado ao estiramento assimétrico do Si-O (υ_3) das espécies de silicato de cálcio hidratado (C-S-H) (HIDALGO *et al.*, 2008; HIGL *et al.*, 2021; SKOCEK; ZAJAC; BEN HAHA, 2020; TU; SHI; FARZADNIA, 2018; WU; YE, 2019; ZHAN *et al.*, 2018).

A análise quantitativa de $CaCO_3$ na matriz cimentícia é um dos pontos centrais em todos os estudos que envolvem o processo de carbonatação. No entanto, os métodos de caracterização sofrem de uma ou mais restrições relacionadas a: (*i*) disponibilidade de equipamentos, (*ii*) sensibilidade e especificidade do método, (*iii*) falta de recursos humanos especializados, (*iv*) custo de análise e/ou (*v*) procedimentos demorados para preparação e análise de amostras (HENRY; WATSON; JOHN, 2017; REBOUÇAS; ROHWEDDER; PASQUINI, 2018; SCHNEIDER DOS SANTOS; ROLIM; HEPP PULGATI, 2015). Assim, é necessário o desenvolvimento de novas soluções que permitam a quantificação rápida, econômica e confiável do teor de $CaCO_3$ na matriz cimentícia. Nesse contexto, identifica-se que a espectroscopia no infravermelho com transformada de Fourier (FTIR) é uma técnica que atende a todos os requisitos listados. O FTIR está amplamente disponível em laboratórios de análises, é simples e fácil de operar, realiza análises rápidas e não destrutivas, requer pequenas quantidades de amostra (0,1 g), apresenta poucas etapas de preparo da amostra, é versátil e capaz de avaliar matrizes amorfas e cristalinas, apresenta custo acessível de operação e de manutenção e gera quantidades substanciais de dados (espectros) (HIGL *et al.*, 2021; JOSE *et al.*, 2020; NASRAZADANI; SPRINGFIELD, 2014; OTSUKA *et al.*, 2015; ROSÉN *et al.*, 2010; SHI *et al.*, 2019; VEERASINGAM; VENKATACHALAPATHY, 2014).

Anteriormente, o FTIR foi aplicado para análise quantitativa de $CaCO_3$ em: (*i*) rocha carbonática (HENRY; WATSON; JOHN, 2017), (*ii*) minério de diatomita (GUATAME-GARCIA; BUXTON, 2018), (*iii*) sedimentos (LIU *et al.*, 2013; LUZINOVA *et al.*, 2011; MECOZZI *et al.*, 2001; ROSÉN *et al.*, 2010; VEERASINGAM; VENKATACHALAPATHY, 2014), (*iv*) solos (TATZBER *et al.*, 2007) e (*v*) materiais cimentícios (HUGHES *et al.*, 1995; LEGODI; DE WAAL; POTGIETER, 2001). No estudo de materiais à base de cimento, o FTIR é normalmente aplicado como uma ferramenta analítica complementar para avaliar produtos de hidratação ou carbonatação em nível qualitativo ou semiquantitativo (ASHRAF, 2016; HIGL *et al.*, 2021; JOSE *et al.*, 2020; SHI *et al.*, 2019). No entanto, para fins quantitativos, o FTIR pode ser acoplado à análise multivariada (MVA) para aumentar a sensibilidade e especificidade dos métodos.

3.5. Geoquímica isotópica

Isótopos são átomos cujos núcleos contêm o mesmo número de prótons, mas um número diferente de nêutrons. Trata-se de um termo utilizado para agrupar elementos químicos na mesma posição da tabela periódica, mas cujas propriedades físico-químicas apresentem diferenças discretas (HOEFS, 2004). Os isótopos podem ser divididos em dois tipos fundamentais, as espécies estáveis e instáveis (radioativas). Enquanto os radioisótopos sofrem alterações de identidade química e na sua composição isotópica devido a ocorrência de processos naturais e espontâneos de emissões radioativas (α, β e γ), os isótopos estáveis não sofrem alterações detectáveis ao longo do tempo (HOEFS, 2004). Nesse contexto, as medições das abundâncias isotópicas requerem instrumentos especializados, como o espectrômetro de massas com multicoletor, também conhecido como espectrometria de massas com razão isotópica (IRMS) (MUCCIO; JACKSON, 2009).

A análise das diferenças que ocorrem naturalmente na composição de isótopos estáveis é parte importante de muitos ramos das ciências naturais, que incluem:

geologia, química, agricultura, ecologia e microbiologia (HOEFS, 2004). Embora a razão isotópica média de cada elemento tenha sido fixada no momento da formação da Terra, ocorrem variações localizadas na composição dos isótopos estáveis com base em uma série de processos físico-químicos ou biológicos, que resultam no enriquecimento/empobrecimento seletivo dos isótopos mais pesados em relação aos valores médios locais (MUCCIO; JACKSON, 2009). Assim, os processos que alteram as abundâncias de isótopos estáveis são denominados como “fracionamento isotópico” e compreendem reações que são sensíveis às pequenas diferenças químicas e físicas que existem entre os isótopos de um elemento (HOEFS, 2004).

As mudanças nas propriedades químicas e físicas associados às variações de massa atômica de um dado elemento são chamadas de "efeitos isotópicos" (HOEFS, 2004). Essas alterações nas características físico-químicas dos isótopos são explicadas pela mecânica quântica, compreendendo as mudanças nas propriedades nucleares, massa atômica e mudanças discretas nos níveis energéticos dos orbitais moleculares (HOEFS, 2004; LEAVITT, 2009; MUCCIO; JACKSON, 2009). Assim, o processo de fracionamento isotópico, que pode ser de natureza cinética ou termodinâmica, estão associados a estas mudanças de propriedades dos isótopos (LEAVITT, 2009). Em particular, as diferenças de massa são mais pronunciadas entre os elementos mais leves, que podem sofrer processos de fracionamento isotópico mais evidentes (HOEFS, 2004). Dessa forma, as razões isotópicas do carbono ($\delta^{13}C$), hidrogênio (δD), oxigênio ($\delta^{18}O$) e nitrogênio ($\delta^{15}N$) podem se tornar localmente enriquecidas ou empobrecidas como resultado de uma variedade de fatores cinéticos e/ou termodinâmicos (HOEFS, 2004; MUCCIO; JACKSON, 2009).

O fenômeno de partição de isótopos entre duas fases ou materiais com diferentes proporções de isótopos é chamada de "fracionamento isotópico” (HOEFS, 2004; LEAVITT, 2009). O fracionamento termodinâmico, ou distribuição isotópica de equilíbrio, compreende uma série de transformações em equilíbrio químico que, para uma dada condição reacional (*e.g.*, temperatura, pressão e pH), resultam na modificação da razão isotópica original das espécies químicas envolvidas (HOEFS,

2004). Normalmente, é possível obter uma constante de equilíbrio “K” do processo de fracionamento isotópico termodinâmico (frequentemente substituída pelo fator de fracionamento - *α*). Assim, os produtos de processos que ocorrem sob maior influência de parâmetros termodinâmicos de fracionamento guardam relação com o material de origem (fonte) e tendem a ocorrer em reações com tempos longos de equilíbrio químico, como os estudados pela geoquímica (HOEFS, 2004; LEAVITT, 2009).

O fracionamento isotópico cinético está associado, principalmente, às diferenças nas taxas de reação dos isotopólogos (*e.g.*, $^{12}CO_2$ e $^{13}CO_2$) presentes no sistema reacional (HOEFS, 2004). Os efeitos cinéticos de fracionamento são resultantes da ocorrência de processos químicos com taxas elevadas de transformação, o que resultam em um fluxo unidirecional e preferencial de um isotopólogo. Além disso, a presença de aceleradores de reação (e.g., catalisadores, enzimas, pH elevado) e a ocorrência de fenômenos dependentes da massa (como a taxa de difusão), somados às condições de processo (temperatura e pressão), resultam em fracionamentos isotópicos pronunciados e em produtos que mantem uma menor relação isotópica com a matéria-prima (HOEFS, 2004; LEAVITT, 2009). Com relação a taxa diferencial de reação dos diferentes isótopos, a diferença de força de ligação química formada pelos isótopos (leve e pesado), que estão associados aos efeitos da mecânica quântica nuclear, resultam em um fluxo unidirecional de um isótopo, normalmente o mais leve, para o produto da reação (HOEFS, 2004).

O carbono tem dois isótopos estáveis (não radioativos), sendo a razão $^{13}C/^{12}C$ ($\delta^{13}C$) dos materiais medidos pelo IRMS. Na natureza, o isótopo ^{12}C compreende 98,89% de todo o carbono e o ^{13}C compõe os 1,11% restantes (LEAVITT, 2009). O carbono ocorre em uma ampla variedade de compostos na Terra, desde compostos orgânicos reduzidos, como o metano, até compostos inorgânicos oxidados, como CO_2 e carbonatos (LEAVITT, 2009). Nesse contexto, os isótopos de carbono são preservados e expressos na composição de diferentes componentes orgânicos, inorgânicos e abiogênicos do ciclo biogeoquímico do carbono, compreendendo materiais como o ar atmosférico, minerais, compostos dissolvidos (orgânicos e

inorgânicos), solos, sedimentos, biomassa e combustíveis, entre outros tantos (HOEFS, 2004; LEAVITT, 2009). O amplo espectro de estados de oxidação do carbono, diversidade das condições de reação e uma série de fatores bióticos (enzimas) e abióticos (e.g., pressão, temperatura e pH), favorecem aos processos de fracionamento naturais dos isótopos estáveis de carbono (HOEFS, 2004; LEAVITT, 2009). Dessa forma, a faixa de $\delta^{13}C$ é muito ampla, variando de valores negativos, em metano biogênico (-80‰), até valores positivos, em CO_2 metamórfico (+10‰). Na Figura 3-13, é apresentada a faixa natural de assinatura isotópica de carbono.

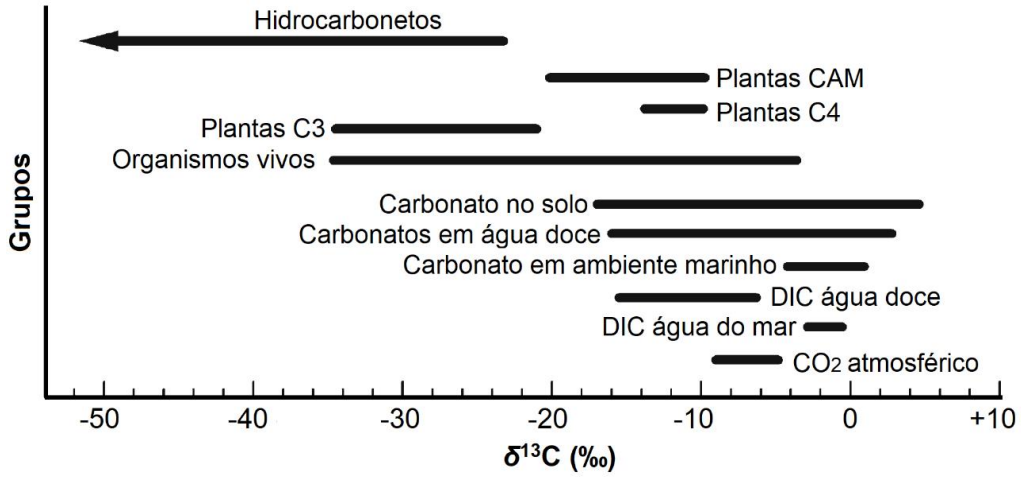

Figura 3-13. Faixa natural de assinatura isotópica identificados em diferentes materiais do ciclo biogeoquímico do carbono. Adaptado de Leavitt, (2009)

3.5.1. Espectrometria de massas com razão isotópica (IRMS)

A espectrometria de massas com razão isotópica (IRMS) é uma técnica especializada usada para fornecer informações sobre a composição de isótopos estáveis de carbono ($^{13}C/^{12}C$); hidrogênio (D/H), oxigênio ($^{18}O/^{16}O$), nitrogênio ($^{15}N/^{14}N$) e enxofre ($^{36}S/^{34}S$) de diferentes materiais, com o objetivo de identificar suas origens geográficas, químicas e biológicas (MUCCIO; JACKSON, 2009). Como as razões isotópicas de elementos leves, como carbono, hidrogênio, oxigênio, enxofre e nitrogênio, podem se tornar localmente enriquecidas ou empobrecidas, como resultado de uma variedade de fatores cinéticos e termodinâmicos, a medição das

razões isotópicas pode ser usada para diferenciar a origem de amostras que, de outra forma, não poderiam ser discriminadas (HOEFS, 2004; MUCCIO; JACKSON, 2009). Conforme representados na Figura 3-14, existem cinco seções principais de um IRMS: (*i*) um sistema de introdução de amostra, (*ii*) uma fonte de ionização de elétrons, (*iii*) um analisador de setor magnético, (*iv*) um conjunto de detectores coletores de Faraday e (*v*) um sistema de aquisição de dados controlado por computador.

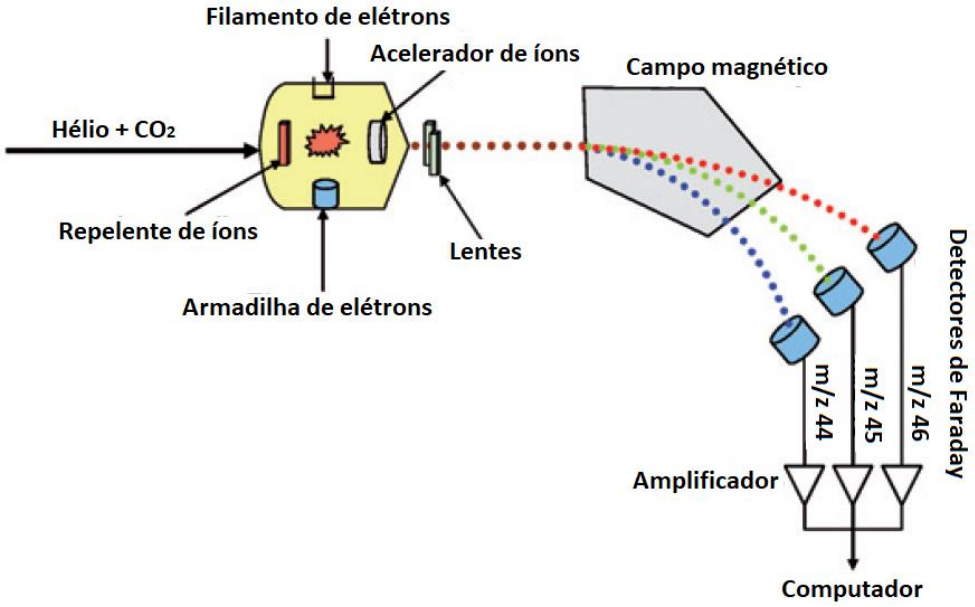

Figura 3-14. Esquema representativo do sistema/interface de introdução de amostras no espectrômetro de massas com razão isotópica (IRMS). Adaptado de Muccio e Jackson, (2009)

Os métodos de espectrometria de massa são os meios mais eficazes de medir a abundância de isótopos estáveis. O IRMS realiza as medidas a partir da análise individual dos elementos com base na relação específica massa/carga (m/z) dos diferentes isotopólogos e de um padrão certificado (HOEFS, 2004). Ao longo do processo de análise, a fonte de íons serve para ionizar as moléculas de amostras gasosas que foram inseridas no equipamento (MUCCIO; JACKSON, 2009). O processo de bombardeamento das moléculas com elétrons ocorre sob vácuo e na presença de campo eletromagnético para otimizar o processo de geração de íons (HOEFS, 2004). Após, os íons gerados são focalizados e acelerados em direção ao detector, passando por um campo magnético. No campo magnético, os diferentes

isotopólogos são separados em razão das diferentes relações massa/carga (m/z) dos compostos, sendo cada um dos elementos analisados individualmente no sistema multicoletor de Faraday (HOEFS, 2004; MUCCIO; JACKSON, 2009). Por fim, o estímulo do feixe de íons é convertido em sinal eletrônico no detector e em resultados numéricos pelo sistema computacional (MUCCIO; JACKSON, 2009).

Os resultados de isótopos estáveis ($\delta^{13}C$) são expressos na unidade per mil (‰) e configuram-se como uma razão (R) entre o isótopo mais pesado (menos abundante) sobre o isótopo mais leve (mais abundante), conforme a Equação 3.15. As amostras que estabelecem os valores “R” do padrão são geralmente selecionadas porque representam um material estável que é altamente enriquecido em isótopos pesados (menos abundantes), enquanto os padrões de trabalho (*working standards*) compreendem materiais com assinaturas isotópicas intermediárias dentro da faixa de aplicação do laboratório de análise (MUCCIO; JACKSON, 2009).

$$Razão\ isotópica\ (R) = \frac{Abundância\ do\ isótopo\ mais\ pesado}{Abundância\ do\ isótopo\ mais\ leve} \tag{3.15}$$

Para fins de aplicação prática, a assinatura isotópica é medida em relação a um padrão internacional com valor certificado de isótopos estáveis, conforme apresentado na Equação 3.16 (HA *et al.*, 2020). Assim, os dados de $\delta^{13}C$ são apresentados como valores relativos ao padrão internacional VPDB (*Vienna Pee Dee Belemnite*), sendo calculados a partir da Equação 3.17 ($\delta^{13}C$) (HANSEN; GARDELER; MATTHIESSEN, 2013; KUMAR *et al.*, 2006; LI *et al.*, 2007; MUSTAPHA *et al.*, 2013; WANG; WEN; LI, 2017; ZHOU *et al.*, 2015).

$$\delta_{amostra} = \frac{\mathrm{R}_{amostra} - \mathrm{R}_{\,padrão}}{\mathrm{R}_{\,padrão}} \times 1000 \tag{3.16}$$

$$\delta^{13}C_{amostra} = \frac{(^{13}C/^{12}C)_{amostra} - (^{13}C/^{12}C)_{\,padrão}}{(^{13}C/^{12}C)_{\,padrão}} \times 1000 \tag{3.17}$$

As análises de isótopos estáveis das espécies de carbono ($\delta^{13}C$) são realizados por espectrômetro de massa com razão isotópica (IRMS), sendo o esquema representado na Figura 3-15. Antes da análise, os frascos de amostragem passam por um processo de *flush* de hélio para remover o ar atmosférico. Após a purga, o CO_2 do carbonato de cálcio e/ou das amostras de DIC são liberados a partir da reação das amostras com o ácido fosfórico (H_3PO_4 - 99%) em um bloco de digestão aquecido (ENGELMANN *et al.*, 2018; WANG; WEN; LI, 2017; ZHOU *et al.*, 2015). Após a reação química e equilíbrio do CO_2 com o *headspace* do amostrador, a amostra é injetada no IRMS e a razão isotópica medida.

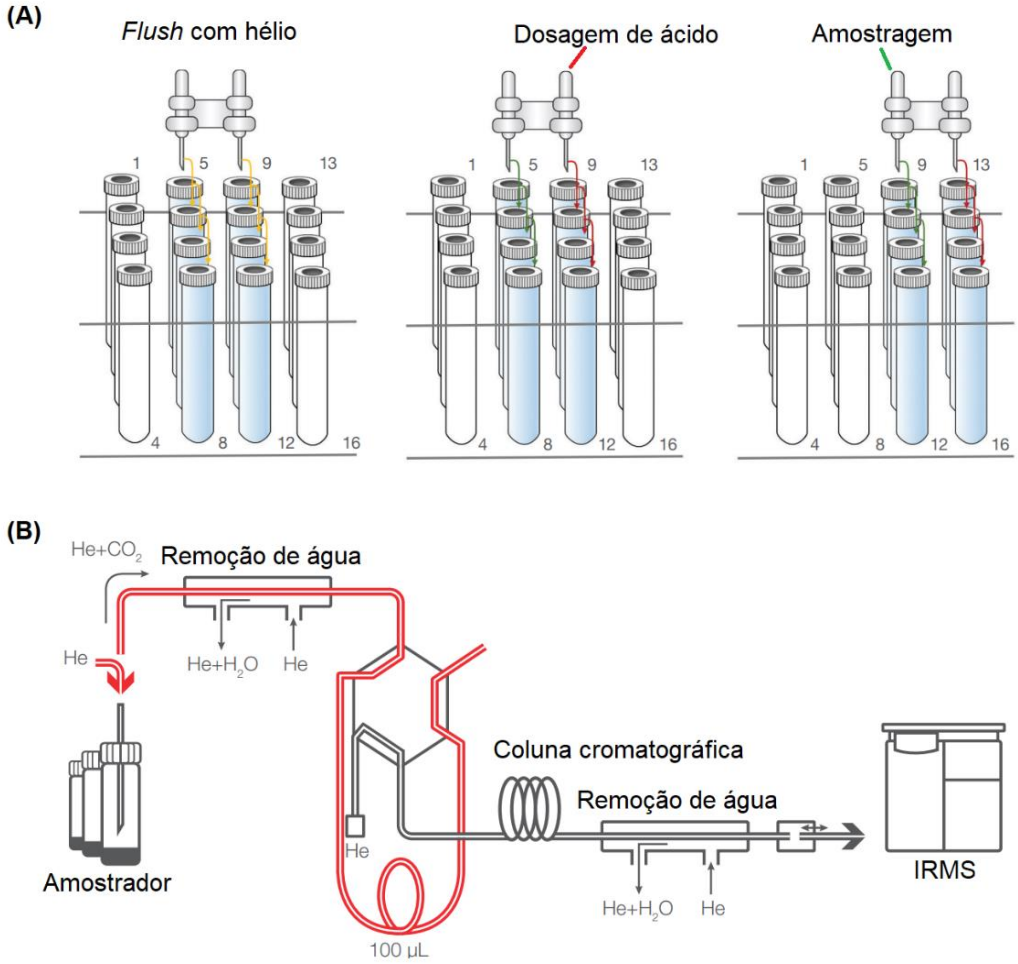

Figura 3-15. Esquema representativo do sistema de preparo de amostras para a análise isotópica de $\delta^{13}C$ de carbonato ($CaCO_3$) e de DIC. Adaptado da Thermo Fisher Scientific (2022)

Além da assinatura isotópica, os parâmetros de fracionamento isotópico (ε), também conhecido como fator de enriquecimento isotópico, podem ser estimados para avaliar as alterações de assinatura isotópicas entre diferentes fases de um mesmo sistema químico (HOEFS, 2004). Assim, os fatores de enriquecimento isotópico (ε) de carbono ($\delta^{13}C$), que resultam do fracionamento isotópico entre as frações gasosas (CO_2), líquidas (carbono inorgânico dissolvido – DIC) e sólidas ($CaCO_3$), podem ser medidas a partir da Equação 3.18 (KAROLYTĖ *et al.*, 2017).

$$\ln \alpha \times 10^3 \approx \varepsilon_{produto-reagente} = \delta_{produto} - \delta_{reagente} \quad (3.18)$$

3.5.2. Aplicação de isótopos no monitoramento poços

Assegurar a integridade dos poços de produção e injeção ao longo de todo o ciclo de vida do empreendimento (perfuração, exploração, produção, monitoramento, injeção e/ou abandono) é essencial para garantir a segurança das operações de exploração de O&G e de armazenamento de CO_2. Porém, conforme comentado anteriormente, é amplamente relatado pela literatura que os materiais utilizados pela indústria de O&G para a cimentação dos poços (pasta de cimento e aço) passam por processos de degradação em meios ricos em CO_2. Nesse contexto, o poço constitui-se como um ponto de fragilidade significativo, uma vez que pode configurar-se como o caminho de menor resistência para a migração CO_2. Ainda, é importante ressaltar que a concentração de CO_2 no entorno do poço é sempre elevada, o que agrava ainda mais os processos de perda de integridade dos materiais. Assim, se houver alguma falha na interface da pasta de cimento/formação, uma série de processos podem resultar na perda da integridade da estrutura e na formação de caminhos preferenciais para a migração de fluidos (BAGHERI; SHARIATIPOUR; GANJIAN, 2018; CONDE SILVA; MILESTONE, 2018a; XIAO *et al.*, 2017). Na Figura 3-16, é esquematizado o processo de injeção de CO_2 em reservatório de CCS (Figura 3-16A), enquanto na Figura 3-16B é representado como que o CO_2 pode interagir os elementos do poço.

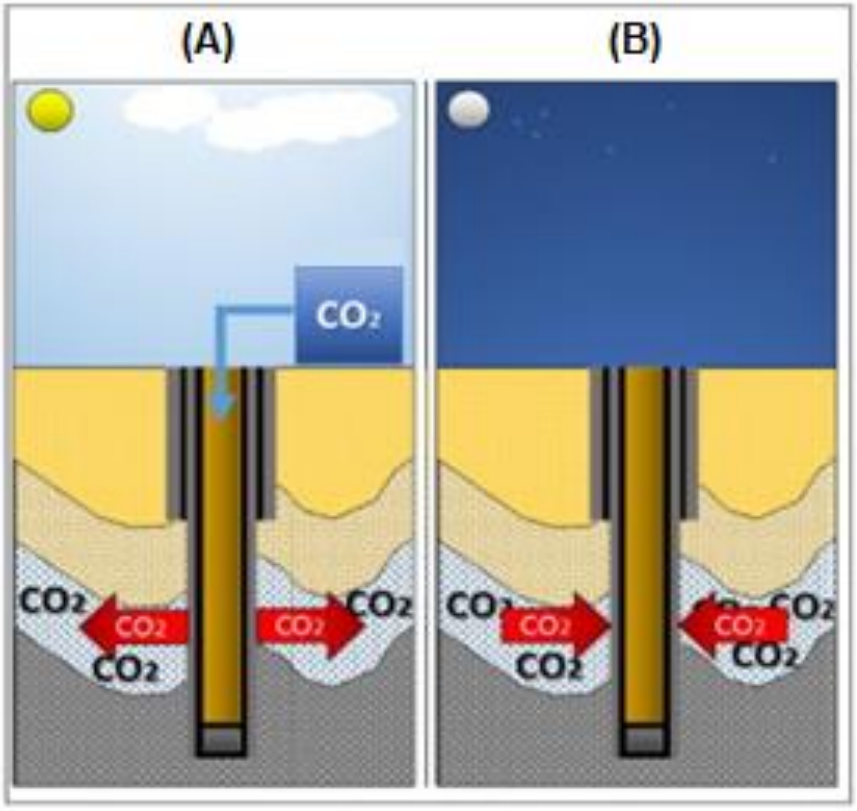

Figura 3-16. Injeção de CO_2 em reservatório de CCS: (A) operação de injeção de CO_2 e (B) interação do CO_2 com os componentes do poço. Adaptado de Costa *et al.*, (2018)

Mesmo que o CCS já seja uma tecnologia validada e comprovada em operações de grande escala, ainda há necessidade de realizar o desenvolvimento de novos métodos e ferramentas para rastrear e monitorar o CO_2 durante e após a injeção (IGLESIAS *et al.*, 2019). As tecnologias atuais de monitoramento de CO_2 vão desde as medições diretas e indiretas focadas no reservatório, até o monitoramento ambiental das seções próximas à superfície (VERMEUL *et al.*, 2016). Nesse contexto, as assinaturas isotópicas das espécies de carbono ($\delta^{13}C$) já foram utilizados como traçadores químicos para monitorar o processo de injeção de CO_2 em reservatórios de Captura e Armazenamento de Carbono (CCS) e para estudar a dinâmica do transporte reativo ao longo da percolação da pluma de gás no reservatório (BARTH *et al.*, 2015; MAYER *et al.*, 2015; WIESE *et al.*, 2013; ZIMMER *et al.*, 2018). Assim, o valor de $\delta^{13}C$ do CO_2 pode ser utilizado para: (*i*) identificar o vazamento de CO_2 injetado, (*ii*) estudar a distribuição subsuperficial da pluma de CO_2 e (*iii*) avaliar a

proporção de CO_2 injetado versus o gás originário do reservatório (BARTH *et al.*, 2015; JOHNSON *et al.*, 2011; MAYER *et al.*, 2015). Para que os métodos de isótopos estáveis possam atingir seus objetivos, é essencial que exista diferenças na composição isotópica entre os fluidos injetados e os “nativos” (VERMEUL *et al.*, 2016).

Tradicionalmente, a aplicação de isótopos estáveis em projetos de Captura e Armazenamento de Carbono (CCS) tem se concentrado em utilizar os valores $\delta^{13}C$ do CO_2 para rastrear a migração de CO_2 injetado na subsuperfície (JOHNSON; MAYER, 2011; WELCH *et al.*, 2019). Ainda, a assinatura isotópica ($\delta^{13}C$) de CO_2 foi sugerida como uma ferramenta eficaz para monitorar o vazamento de fluidos para seções geológicas mais superficiais (HA *et al.*, 2020; SHIN *et al.*, 2020; ZHANG *et al.*, 2021). Por outro lado, há um número limitado de estudos que realizaram a análise isotópica da pasta de cimento de poços carbonatados (CAREY *et al.*, 2007; GABOREAU *et al.*, 2012; MANCEAU *et al.*, 2016), sendo que nenhum dos autores se aprofundou sobre a importância e aplicabilidade desses resultados. Assim, ainda existem na literatura questões importantes não resolvidas relacionadas à dinâmica do processo de carbonatação dos materiais cimentícios em meios ricos em CO_2, tais como a capacidade de identificar a origem do gás que induziu o processo de degradação e descrever a influência da reatividade da pasta de cimento na composição isotópica dos fluidos ácidos.

Recentemente, um dos desafios enfrentados pela indústria de O&G é a presença substancial de CO_2 em formações geológicas (COSTA *et al.*, 2019). Observa-se na literatura que a maioria dos vazamentos associados à pasta de cimento podem ser atribuídos à perda ocasional da integridade do material (ABID *et al.*, 2018). Nesse contexto, a formação de caminhos preferenciais (microfraturas e espaço microanular) resultam do processo de degradação da pasta de cimento exposta à pluma de CO_2. Recentemente, estudos no poço piloto em Ketzin (Alemanha) utilizaram o conteúdo de CO_2 e sua assinatura de isótopos ($\delta^{13}C$) para estudar a distribuição vertical da pluma de CO_2 ao longo das seções externas adjacentes ao poço, sendo os resultados apresentados na Figura 3-17 (BARTH *et al.*, 2015).

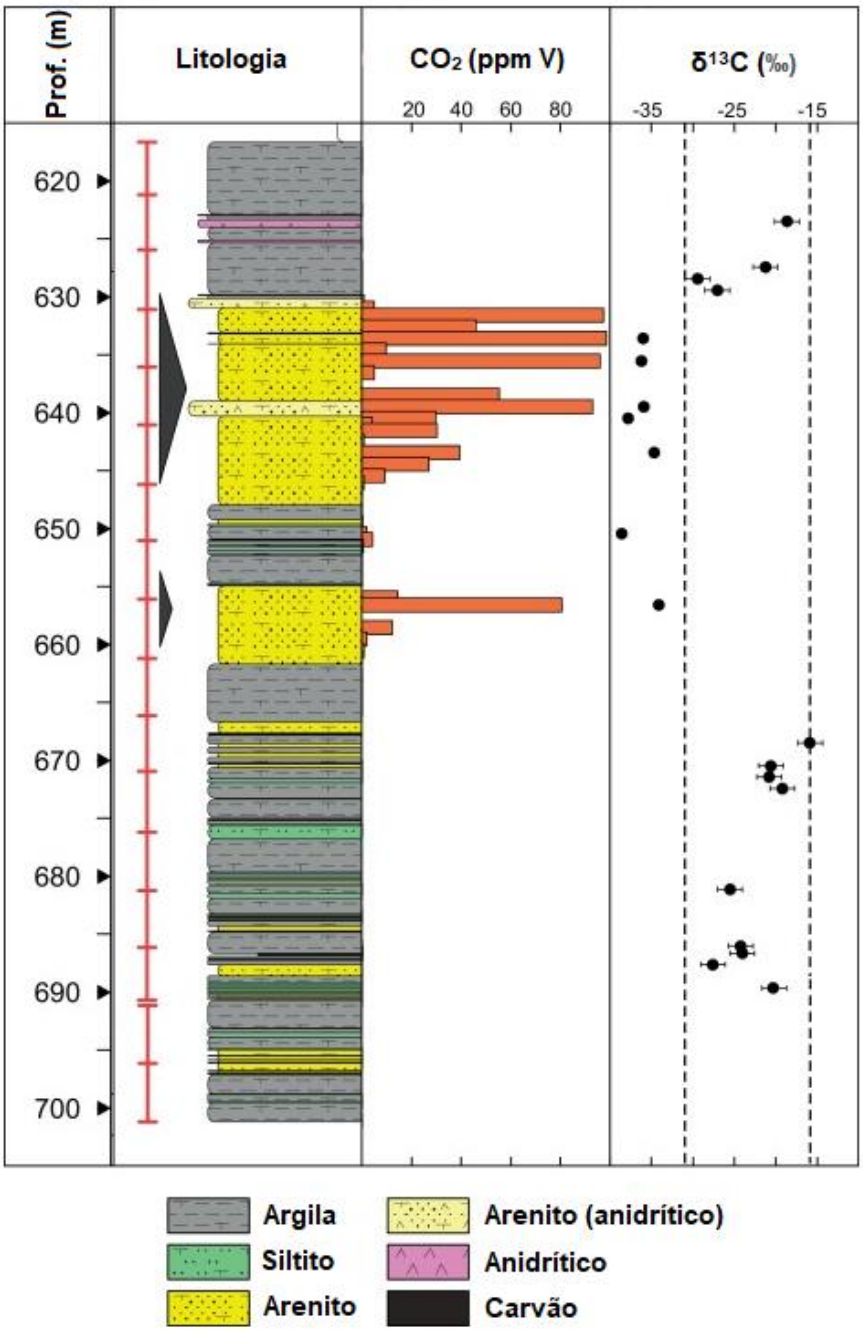

Figura 3-17. Perfil litológico e dados medidos de conteúdo de CO_2 e sua respectiva assinatura de isótopos de carbono ($\delta^{13}C$) no poço piloto em Ketzin, Alemanha. Adaptado de Barth *et al.*, (2015)

A partir do trabalho de Barth *et al*., (2015), é possível observar que o aumento de concentração de CO_2 na fração externa do poço é acompanhada por uma mudança

de nível da assinatura isotópica do gás. Uma vez que o CO_2 do reservatório (“nativo”) e o injetado apresentam diferentes impressões digitais isotópicas, foi possível identificar que o gás presente ao longo da seção vertical do poço é oriundo da injeção. Assim, estes resultados indicam a presença de alguma falha de interface ou fratura no reservatório que permitiu que a pluma de CO_2 alcançasse seções geológicas mais superficiais. Considerando que qualquer gás ácido (CO_2 ou H_2S) que venha a interagir com a bainha de cimento vai desencadear o processo de degradação do material, há de se supor que os processos de perda de integridade das estruturas já estivessem em ação nos poços de Ketzin (Alemanha), o que não foi abordado pelos autores. Essa preocupação mostra-se pertinente, uma vez que é de amplo conhecimento os relatos de ocorrência de processos de degradação em seções intermediárias de poços, como os relatados por Carey *et al.*, (2007) (Figura 3-18), em que materiais cimentícios degradados foram amostradas e estudadas a partir das seções intermediárias de poços em operação há 30 anos na unidade de SACROC, Texas (EUA).

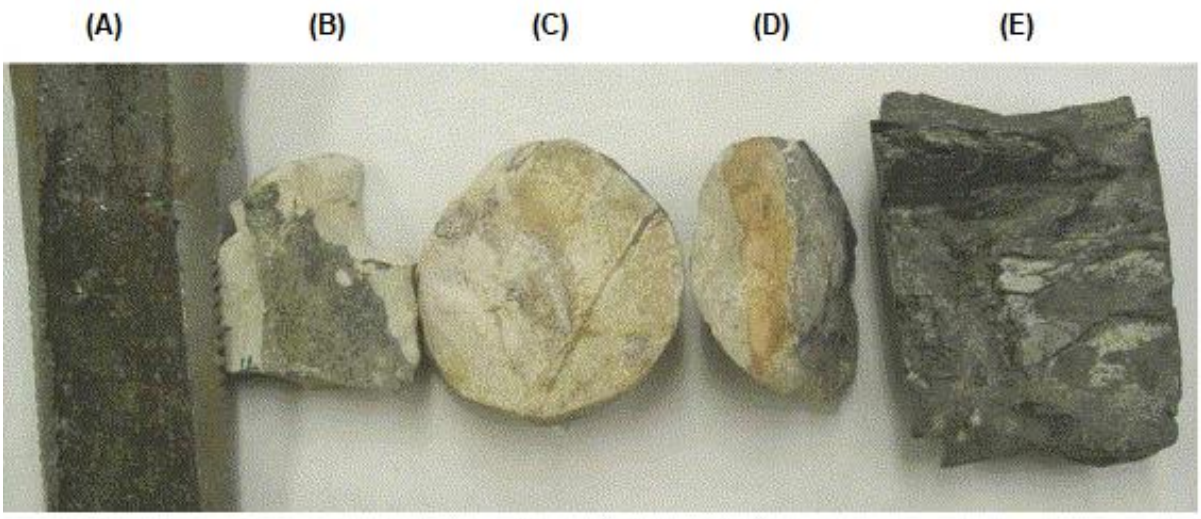

Figura 3-18. Amostras da bainha de cimento carbonatado retiradas de poços em operação há 30 anos na unidade de SACROC, Texas – EUA: (A) tubo de aço, (B) interface cimento-aço, (C) cimento preservado, (D) interface cimento-rocha e (E) folhelho. Adaptado de Carey *et al.*, (2007)

A partir da Figura 3-18, é possível observar a presença de vários componentes da estrutura do poço, entre elas: a tubulação de aço (Figura 3-18A), a interface

cimento-aço (Figura 3-18B), o cimento preservado (Figura 3-18C), a interface cimento-rocha (Figura 3-18D) e o folhelho oriundo da formação geológica adjacente (Figura 3-18E). Conforme Carey *et al.*, (2007), foram identificados sinais de carbonatação em intensidades diferentes em ambas as interfaces (cimento-aço e cimento-rocha). A fim de avaliar as características dos carbonatos identificados, foi realizado o estudo preliminar de assinatura isotópica dos materiais, apresentados na Figura 3-19.

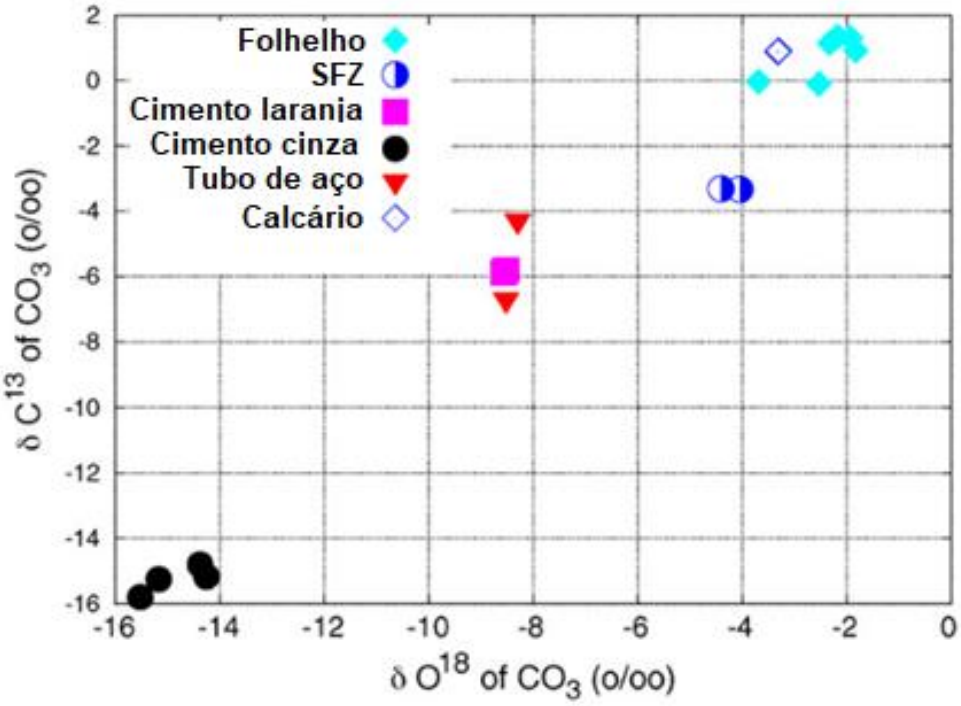

Figura 3-19. Medições de isótopos de carbono e oxigênio dos carbonatos identificados nos poços em operação há 30 anos na unidade de SACROC, EUA. Adaptado de Carey *et al.*, (2007)

Assim, a partir dos resultados da Figura 3-19, foi possível discriminar a assinatura isotópica dos carbonatos presentes em cada uma das fases do sistema. A partir de caracterizações complementares, os autores conseguiram identificar que os carbonatos da porção preservada da pasta de cimento foram formados em meio com baixa concentração de CO_2, enquanto a degradação severa da pasta de cimento nas interfaces cimento-aço e cimento-rocha, indicam exposições elevada dos materiais a fluidos ácidos. Como resultado, os autores sugeriram que o CO_2 que promoveu a degradação dos materiais ao longo das zonas interfaciais (cimento-aço e cimento-

rocha) é oriundo do processo de armazenamento geológico de carbono e que a pluma de gás permeou pelas falhas de interfaces (CAREY *et al.*, 2007). Porém, a falta de maiores informações sobre a assinatura isotópica dos gases (gás injetado e CO_2 do reservatório), bem como sobre os processos de fracionamento isotópico presentes no sistema estudado, não permitiu que os autores chegassem a nenhuma hipótese forte para identificar a origem do CO_2 que foi responsável pela degradação dos materiais do poço. Dessa forma, ficou evidente que as ações de monitoramento baseadas nas ferramentas de análise isotópica necessitam de informações confiáveis sobre as impressões digitais de todos os elementos do sistema estudado, bem como avaliar qualquer alteração temporal do $\delta^{13}C$ ao longo da injeção de CO_2 (FLUDE *et al.*, 2017; ŚLIWIŃSKI *et al.*, 2017).

Até o momento, é possível observar que os métodos de isótopos estáveis são ferramentas importantes para identificar a migração e destino do CO_2 injetado ao longo do armazenamento geológico e para realizar o monitoramento da eficiência do processo de mineralização do CO_2 (MYERS *et al.*, 2019). Nesse contexto, as técnicas de isótopos podem ajudar a melhorar nossa compreensão sobre os processos químicos subsuperficiais que ocorrem ao longo a injeção de CO_2 e aumentar a eficiência dos programas de monitoramento de vazamento (VAN GELDERN *et al.*, 2014). Porém, a partir da revisão bibliográfica, foi possível observar que ainda há espaço para desenvolvimentos técnicos importantes sobre as potencialidades dos métodos de análise isotópica para monitorar o deslocamento vertical da pluma de CO_2, especialmente em áreas adjacentes aos poços ou a partir dos produtos de degradação dos componentes dos poços (pasta de cimento e aço). Esses estudos devem levar em conta que o CO_2 promoverá processos reativos em contato com os materiais dos poços, em especial a pasta de cimento, sendo necessário avaliar todos os fenômenos e produtos do sistema.

4. PROCEDIMENTO EXPERIMENTAL E RESULTADOS

Os resultados da presente tese dividem-se em dois tópicos, compreendendo: (4.1) o desenvolvimento de método quantitativo para o monitoramento do processo de carbonatação de materiais cimentícios e (4.2) a avaliação do potencial dos métodos de geoquímica isotópica para aprofundar os conhecimentos sobre o processo de carbonatação da pasta de cimento em ambientes ricos em CO_2. Nesta seção, os procedimentos experimentais e resultados dos respectivos tópicos são apresentados no formato de artigo científico, sendo brevemente detalhados abaixo:

Método de monitoramento: A Seção 4.1 apresenta os resultados do desenvolvimento de método quantitativo para o monitoramento do processo de carbonatação de materiais cimentícios. O artigo, sob o título de "*Application of Fourier Transform infrared spectroscopy (FTIR) coupled with multivariate regression for calcium carbonate ($CaCO_3$) quantification in cement*" (DOI: 10.1016/j.conbuildmat.2021.125413), foi publicado no ano de 2021 no periódico *"Construction and Building Materials"* (ISSN: 0950-0618) (SANTOS *et al.*, 2021).

Geoquímica isotópica: A Seção 4.2 apresenta os resultados do estudo do potencial dos métodos de geoquímica isotópica para aprofundar os conhecimentos sobre o processo de carbonatação da pasta de cimento em ambientes ricos em CO_2. O manuscrito, sob o título inicial de "*Evaluation of the potential of stable isotope methods to study the cement carbonation process in Carbon Capture and Storage wells*", será submetido em periódico internacional indexado.

4.1. Desenvolvimento de método quantitativo

Construction and Building Materials 313 (2021) 125413

Contents lists available at ScienceDirect

Construction and Building Materials

journal homepage: www.elsevier.com/locate/conbuildmat

Application of Fourier Transform infrared spectroscopy (FTIR) coupled with multivariate regression for calcium carbonate ($CaCO_3$) quantification in cement

Victor Hugo Jacks Mendes dos Santos [a,b], Darlan Pontin [a], Gabriela Gonçalves Dias Ponzi [a,b], Amanda Sofia de Guimarães e Stepanha [a,b], Renan Bordulis Martel [a], Marta Kerber Schütz [a,c], Sandra Mara Oliveira Einloft [a,b,c], Felipe Dalla Vecchia [a,b,c,*]

[a] Pontifical Catholic University of Rio Grande do Sul, PUCRS. Institute of Petroleum and Natural Resources, Avenida Ipiranga, 6681, – TECNOPUC, Building 96J, 90619-900, Porto Alegre, Brazil
[b] Pontifical Catholic University of Rio Grande do Sul, PUCRS, Graduate Program in Materials Engineering and Technology, Avenida Ipiranga, 6681– Building 32, 90619-900, Porto Alegre, Brazil
[c] Pontifical Catholic University of Rio Grande do Sul, PUCRS, School of Technology, Avenida Ipiranga, 6681 – Building 30, 90619-900, Porto Alegre, Brazil

ARTICLE INFO

Keywords:
Accelerated carbonation
Carbon capture and storage
Natural carbonation
Carbonation curing
Chemometrics
Multivariate analysis

ABSTRACT

Partial least squares (PLS) regression models were developed to quantify $CaCO_3$ in cement and to study the CO_2 effect on the material matrix. PLS results presented good correlation coefficient (R^2 = 0.9995) and low estimation error (RMSEP = 3.61 mg $CaCO_3$/g cement). From the results, it was observed that the portlandite consumption, the increase in $CaCO_3$ content and the C-S-H decalcification-polymerization are the most relevant cement chemical transformations. Thus, it was concluded that: *i*) it is possible to obtain fast, low-cost, and reliable models to quantify $CaCO_3$ by FTIR and *ii*) the method is applicable to study carbonated cement-based materials.

1. Introduction

Greenhouse gases (GHG) influence on the environment is one of the humanity's greatest concerns in the 21st century. Emissions of greenhouse gases, such as methane (CH_4) and carbon dioxide (CO_2), are among the main drivers of global warming [1–3]. Currently, the main sources of GHG emissions are related to: (*i*) energy from fossil fuels, (*ii*) land use change and deforestation and (*iii*) decomposition of minerals (carbonates) [1,4–5]. In this context, the largest emission source from carbonate decomposition comes from cement production chain, representing about 5 to 7% of the global emissions budget [6–7].

Cement is one of the most important materials in civil construction and is applied as a binding agent in structural foundations or as a protective element [8]. Within this context, cement and CO_2 are two topics of interest to the academic community and are often closely related. Although the environmental issue is predominant, with attention focused on mitigating the impacts associated with the cement production chain, there are key issues under discussion about the influence of CO_2 on the performance or integrity of cementitious materials. All cement-based material undergoes a certain level of carbonation throughout its life cycle due to its chemical composition [9–10]. Thus, carbonation is a topic of great interest in several economic segments [10–11]. While the research topics: (*i*) natural carbonation (atmospheric carbonation), (*ii*) accelerated carbonation and (*iii*) well cement carbonation, focus on material integrity issues [6,12–15], the fields of study: (*iv*) carbonation curing (accelerated curing) and (*v*) CO_2 mineralization (mineral sequestration), evaluate cement-based materials in the context of Carbon Capture, Utilization, and Storage (CCUS) [13,16–17].

Portland cement is a dominant class of cementitious materials. It is composed of four main compounds: tricalcium silicate (C_3S - Ca_3SiO_5 - alite), dicalcium silicate (C_2S - Ca_2SiO_4 - belite), tricalcium aluminate (C_3A - $Ca_3Al_2O_6$ - celite) and tetracalcium aluminoferrates (C_4AF - $Ca_4Al_2Fe_2O_{10}$ - brownmillerite) [18–21]. These compounds are hydrated during the cement curing process, that takes place over several days and gives the necessary mechanical and chemical characteristics to the

* Corresponding author at: Pontifical Catholic University of Rio Grande do Sul, PUCRS. Institute of Petroleum and Natural Resources, Avenida Ipiranga, 6681, – TECNOPUC, Building 96J, 90619-900, Porto Alegre, Brazil.
E-mail addresses: victor.santos@pucrs.br (V.H.J.M. Santos), felipe.vecchia@pucrs.br (F. Dalla Vecchia).

https://doi.org/10.1016/j.conbuildmat.2021.125413
Received 18 June 2021; Received in revised form 4 October 2021; Accepted 25 October 2021
Available online 12 November 2021

material for several application [18,22–25]. The main hydration products are calcium silicate hydrate (C-S-H), a semi-amorphous phase responsible for the cement mechanical properties, and portlandite [CH - calcium hydroxide - $Ca(OH)_2$], which serves as an alkaline reserve of the material and is characterized by having a crystalline structure [19,26–28].

The main components of cementitious materials are sensitive to the CO_2 action and are subject to the carbonation process [3,29]. These chemical processes produce calcium carbonate ($CaCO_3$) and amorphous silica, among other minority compounds, which induce several changes in the chemical composition, mechanical strength, and pore size distribution of the cement matrix [30]. The main consequence of CO_2 attack on the cement matrix is a potential loss of material's integrity [27], which can be accelerated by exposure to supercritical CO_2 [31]. In this context, some factors can influence the carbonation rate of cement, including: (*i*) curing conditions of the material, (*ii*) type of cement (chemical composition), (*iii*) presence of additives and (*iv*) water-to-cement ratio [65]. Thus, it is of great importance to develop methods that can be used to evaluate the extent of the carbonation process of cementitious materials.

Because of the complexity of cementitious materials, it is necessary to employ several complementary analytical techniques to comprehensively characterize such materials [32–33]. Furthermore, when the carbonation process is considered, many difficulties and uncertainties are added to research and development projects [34]. In this context, it is essential to: (*i*) quantify the carbonation reaction products, (*ii*) control the carbonation process and (*iii*) understand its effects on the cement integrity and properties. Thus, techniques such as phenolphthalein test, X-ray florescence (XRF), X-ray diffraction (XRD), transmission electron microscopy (TEM), scanning electron microscopy (SEM), X-ray microtomography (MicroCT), thermogravimetric analysis (TGA), nuclear magnetic resonance (NMR) spectroscopy and infrared (IR) spectroscopy are widely applied in the literature to characterize carbonated cementitious materials and their composites [32,35–38]. Among the characterization methods, the analysis of $CaCO_3$ in cementitious materials can be performed in the following way: (*i*) qualitative, by means of phenolphthalein, TEM and SEM methods, (*ii*) semi-quantitative, using the IR, MicroCT, XRD and XRF instruments and (*iii*) quantitative, through TGA analysis [11,35–36,39–40]. In addition, XRD, SEM, IR and TGA can be applied, with their respective limitations, to identify the presence of different $CaCO_3$ polymorphs (amorphous carbonate, vaterite, aragonite and calcite) [31,41–42]. Otherwise, NMR is applied only to analyze the siliceous (^{29}Si NMR) and aluminate (^{27}Al NMR) cement phases; however, it is not usually applied to analyze $CaCO_3$ from ^{13}C NMR [11,39,43].

The quantitative analysis of $CaCO_3$ in the cementitious matrix is one of the central points in all studies involving the carbonation process. However, the characterization methods suffer from one or more restrictions related to: (*i*) equipment availability, (*ii*) sensitivity and specificity of the method, (*iii*) lack of specialized human resources, (*iv*) analysis cost and/or (*v*) time-consuming procedures for sample preparation and analysis [38,40,44]. Thus, developing new solutions that allow fast, low-cost, and reliable quantification of $CaCO_3$ content in cementitious matrix is necessary. In this context, it was identified that Fourier Transform Infrared Spectroscopy (FTIR) is a technique that meets all the listed requirements. FTIR is widely available in analysis laboratories, is simple and easy to operate, performs fast and non-destructive analysis, requires small amounts of sample (0.1 g), presents few sample preparation steps, is versatile and capable of evaluating both amorphous and crystalline matrices, presents low operation and maintenance cost, and generates substantial amounts of data (spectra) [8,39,45–49]. In the study of cement-based materials, FTIR is normally applied as a complementary analytical tool to evaluate hydration or carbonation products at qualitative or semi-quantitative level [8–9,39,46]. However, for quantitative purposes, FTIR could be coupled with multivariate analysis (MVA) to increase the sensitivity and specificity of the method.

Previously, FTIR was applied for quantitative analysis of $CaCO_3$ in: (*i*) carbonate rock [40], (*ii*) diatomite ore [50], (*iii*) sediments [45,49,51–53], (*iv*) soil [54] and (*v*) cement [55–56]. Among the studies involving the $CaCO_3$ quantification in cement, it was observed that Hughes et al. [56] applied the Diffuse Reflectance Mid-Infrared Fourier Transform Spectroscopy (DRIFTS) coupled with multivariate analysis to estimate the $CaCO_3$ content in API well cements with known elemental composition and varied origin. However, despite presenting partial least squares (PLS) regression with a good correlation coefficient (R^2 = 0.9950), the model's application range was limited to 0 to 2 wt.% of $CaCO_3$. On the other hand, Legodi et al. [55] applied the FTIR to calibrate a quantitative model to estimate the $CaCO_3$ content in limestone and neat cement mixtures, covering the range of 0 to 100% by weight. The best model was obtained from the integrated area of the carbonate peak (CO_3^{2-}) at 876 cm^{-1} presenting a good correlation coefficient (R^2 = 0.9990). However, none of these studies considered the effect of the carbonation reaction on the cement. Thus, it was not possible to assess whether there is a matrix effect resulting from other products of the carbonation reaction as well as the influence of these transformations in the FTIR spectrum and in the predictive capacity of quantitative models. In addition, both works applied KBr to perform sample preparation [55–56], which adds an additional analysis procedure step and a new source of possible measurement errors. To our knowledge, since Legodi et al. [55], there was no research proposing methods to quantify $CaCO_3$ in cement by FTIR.

In this context, it was proposed in this work to use the Fourier Transform Infrared Spectroscopy (FTIR) and multivariate calibration as a fast, low-cost, and reliable solution to obtain quantitative models to analyze $CaCO_3$ content in cement. The analyzes were performed using the Attenuated Total Reflectance (ATR) accessory, which requires a reduced number of preparation steps [32,40]. API class G cement was used as reference and the material was submitted to carbonation process with supercritical CO_2. Previously, no study considered the effect of the carbonation reaction on the cement matrix to develop quantitative models. It should be emphasized that carbonation reaction influence on the cement properties (chemical and physical). Thus, it is necessary to study the effect of chemical transformations resulting from the exposure of cement to supercritical CO_2 on the quality of predictive models. In this way, the multivariate calibration model was developed with a carbonated cementitious material. It is noteworthy that the application of CO_2 curing and/or CO_2 mineralization (mineral sequestration) to mitigate environmental impacts is beyond the scope of this study.

2. Materials and methods

2.1. Materials

Calcium oxide (Êxodo, 95%), calcium carbonate (calcite $CaCO_3$, Merck – 99.9%), phosphoric acid (Sigma-Aldrich, 85%), carbon dioxide – CO_2 (Air Products, 99.99%) and phenolphthalein (Química Moderna, analytical grade) were used without further purification and its basic properties are detailed in Table S1 (Supplementary Material). The cement applied in this study was an API class G cement (Lafarge Holcim)

Table 1
Chemical composition of API Class G cement.

Chemical composition	Percentage [%]
SiO_2	29.25
Al_2O_3	3.95
Fe_2O_3	4.57
CaO	65.07
MgO	2.32
SO_3	2.27
Na_2O	0.25
K_2O	0.33

and its chemical composition is shown in Table 1.

2.2. Sample preparation

Class G cement paste (cement anhydrous + water) was prepared following the recommendations of American Petroleum Institute specification 10A [57]. The cement paste was prepared with no additives using 0.44 water-to-cement ratio. The detailed procedure for preparing the cement paste using a Chandler Engineering mixer (model 3260) is: (*i*) initially, water is added to the mixing vessel, (*ii*) the cement powder is added over a 15 s mixing cycle at 4,000 rpm and (*iii*) the final mixing is carried out through a second mixing cycle of 35 s at 12,000 rpm. Then, the cement paste is poured into 16 PVC molds (Figure S1 - Supplementary Material), the molds are closed and cured in a thermostatic bath at 65 °C and at atmospheric pressure for 14 days. After curing, cylindrical cement specimens were demolded, and their dimensions were adjusted to 22 mm in diameter and 44 mm in height with a low-speed cutter (Isomet).

2.2.1. Preparation of non-carbonated cement powder

Cured cement specimens were ground in a ball mill (De Leo 0907) to obtain the non-carbonated cement powder (C1 - non-carbonated). Half (8) of the class G cement specimens were ground in a cylindrical vessel (17.8 cm in height and 17.8 cm in diameter) under 150 rpm for 12 h, while the other half (8) were used to study the carbonation process of cylindrical cement specimens. The load of the grinding steel balls was: Ø50 mm balls (5 units), Ø40 mm balls (5 units), Ø32 mm balls (5 units), Ø15 mm balls (5 units), Ø25 mm balls (24 units), Ø19 mm balls (15 units) and Ø10 mm balls (21 units). After grinding, the cement powder was manually sieved through #270 mesh sieve and stored in a desiccator.

2.3. Carbonation with supercritical CO_2

Cement carbonation experiments (cylindrical specimens and powders) were conducted in an HPHT (high pressure-high temperature) pressure vessel under CO_2 supercritical environment, as shown in Fig. 1. The supercritical state is a special condition in which fluids acquire unique properties, being reached by CO_2 at pressures greater than 7.39 MPa and temperatures above 31.1 °C [30,58]. Eight cylindrical cement specimens were exposed to a supercritical CO_2-ultrapure water system at 65 °C and 15 MPa for 7 days (wet carbonation). Such reaction conditions simulate environments compatible with the application of cement in Carbon Capture and Storage (CCS) wells. The quasi-static reaction environment is reported as the most appropriate model to simulate the well dynamics [22,59], since continuous and extensive failures are not frequent in geological formations [60]. The experiment with cylindrical specimens was carried out to evaluate the behavior of the cement material when exposed to supercritical CO_2. After the carbonation experiments, the cylindrical cement specimens were evaluated by the phenolphthalein test, SEM-EDS microscopy and MicroCT analysis.

The experiment with the cement powder was carried out to accelerate the carbonation processes from the exposure of the material to supercritical CO_2 [31]. C1 sample (non-carbonated cement) was exposed to a supercritical CO_2-ultrapure water system at 65 °C and 15 MPa for 7 days. After the reaction with CO_2, both solid and liquid fractions from the HPHT pressure vessel were dried together in an oven at 60 °C for 24 h, obtaining a homogeneous solid fraction with a whitish color. After the carbonation experiments, the non-carbonated (C1) and carbonated (C11) cement powders were evaluated by the XRD diffraction, SEM-EDS microscopy, gas chromatography analysis and FTIR spectroscopy.

2.3.1. Cement carbonation reactions

In the present work, the carbonation process in an aqueous medium

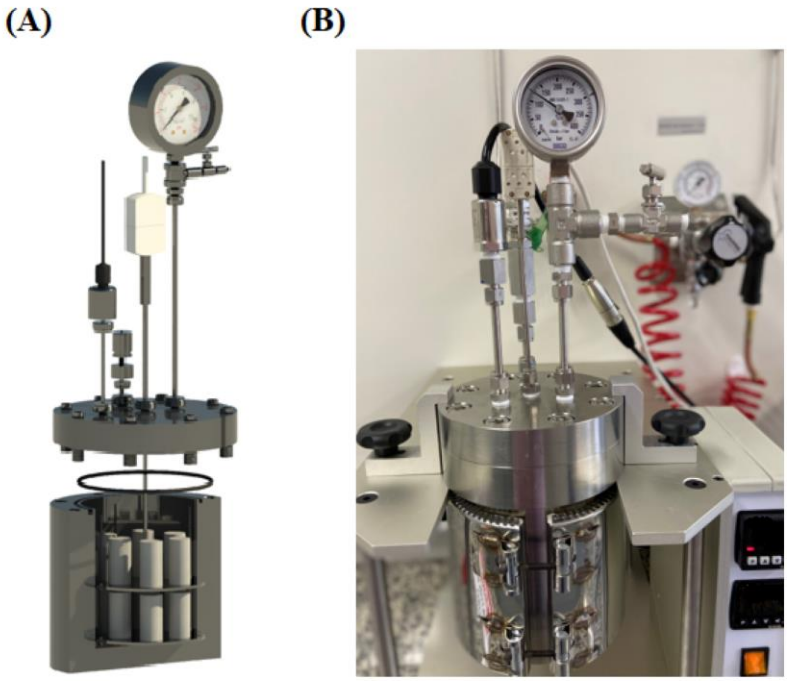

Fig. 1. Experimental arrangement to perform cement specimen's carbonation experiments with supercritical CO_2: (A) conceptual design and (B) high pressure-high temperature (HPHT) pressure vessel.

(wet carbonation) was carried out to simulate the conditions of CCS reservoirs. Based on the literature, the main carbonation reactions consume the calcium silicate hydrate (C-S-H) and portlandite (CH) phases, producing different calcium carbonate ($CaCO_3$) polymorphs (amorphous, calcite, aragonite and vaterite) and amorphous silica [24,61]. In addition, non-hydrated cement fractions (C_3S and C_2S) are also consumed by the carbonation process and produce $CaCO_3$ and siliceous products. These reactions are represented by Equations 1–8 [12–13,22].

$$C_3S_{(s)} + 3CO_{2(aq)} + nH_2O_{(l)} \rightarrow SiO_2.nH_2O_{(s)} + 3CaCO_{3(s)} \quad (1)$$

$$C_2S_{(s)} + 3CO_{2(aq)} + nH_2O_{(l)} \rightarrow SiO_2.nH_2O_{(s)} + 3CaCO_{3(s)} \quad (2)$$

$$Ca(OH)_{2(s)} + CO^{2-}_{3(aq)} + 2H^{+}_{(aq)} \rightarrow CaCO_{3(s)} + 2H_2O_{(l)} \quad (3)$$

$$Ca(OH)_{2(s)} + HCO^{-}_{3(aq)} + H^{+}_{(aq)} \rightarrow CaCO_{3(s)} + 2H_2O_{(l)} \quad (4)$$

$$C-S-H_{(s)} + CO^{2-}_{3(aq)} + 2H^{+}_{(aq)} \rightarrow CaCO_{3(s)} + SiO_xOH_{x(s)} \quad (5)$$

$$C-S-H_{(s)} + HCO^{-}_{3(aq)} + H^{+}_{(aq)} \rightarrow CaCO_{3(s)} + SiO_xOH_{x(s)} \quad (6)$$

$$CaCO_{3(s)} + CO_{2(g)} + H_2O_{(l)} \leftrightarrow Ca^{2+}_{(aq)} + HCO^{-}_{3(aq)} \quad (7)$$

$$CaCO_{3(s)} + 2H^{+}_{(aq)} \leftrightarrow CO_{2(g)} + H_2O_{(l)} + Ca^{2+}_{(aq)} \quad (8)$$

2.4. Sample characterization

In the present work, the following characterizations methods were performed to analyze the non-carbonated and carbonated cement samples: (*i*) phenolphthalein test, (*ii*) X-ray microtomography analysis (MicroCT), (*iii*) scanning electron microscopy (SEM), (*iv*) X-ray diffraction analysis (XRD), (*v*) gas chromatography to estimate carbonation degree of cement powder, and (*iv*) Fourier Transform Infrared Spectroscopy (FTIR). The experimental procedures and analytical methods are detailed below.

2.4.1. Phenolphthalein test

The phenolphthalein test is one of the most used methods to evaluate the carbonation of cementitious materials [9,62]. In this test, the cylindrical cement specimens were cut longitudinally, and a solution of phenolphthalein (2%) in ethyl alcohol-water (48:50 v%) was sprayed on the surface of the material to highlight the boundaries of non-carbonated (pink colored) and carbonated (grey colored) cement phases.

2.4.2. X-ray microtomography analysis (MicroCT)

X-ray microtomography (MicroCT) analysis was performed on the Skyscan 1173 X-Ray Microtomograph (Bruker) following the manufacturer's recommendations. The cylindrical cement specimens were analyzed by MicroCT before and after the carbonation process to evaluate the effect of supercritical CO_2 on the microstructure of the material using a non-destructive method.

2.4.3. Scanning electron microscopy (SEM)

The analysis of cement by scanning electron microscopy with energy dispersive X-ray spectroscopy (SEM-EDS) was performed using the Inspect F50 - FEI microscope to: (*i*) characterize the structure of the cement, (*ii*) analyze the elementary profile of cement specimens after the carbonation process (elemental mapping) and (*iii*) characterize the morphological structure of the cement powder before and after the carbonation process.

2.4.4. X-ray diffraction analysis (XRD)

Mineral composition analyzes were performed using an XRD diffractometer D8 Advance A25 (Bruker) at a voltage of 40 kV, a current of 30 mA with Cu-Kα radiation and a scanning step size 0.02° in the θ-2θ ranging from 2 to 80°. The mineral composition of the cement powder was analyzed by XRD before and after the carbonation process.

2.4.5. Carbonation degree of cement powder

Before developing the $CaCO_3$ quantification method in cement by FTIR, it was necessary to estimate the $CaCO_3$ content of the samples in an appropriate unit of measurement. In the present work, mg $CaCO_3$/g cement was proposed as the appropriate unit of measurement. A detailed description of the sample preparation, characterization procedures and the results of analysis are presented in the Supplementary Material (Table S2 and Figure S2) [9,63–64]. Thus, the calcium carbonate content of the non-carbonated (C1 – 45.80 mg $CaCO_3$/g cement) and carbonated (C11 – 468.20 mg $CaCO_3$/g cement) samples were estimated from the experimental analysis, while the carbonation degree of the non-carbonated (C1 – 3.80%) and carbonated (C11 – 38.82%) samples were estimated from Equation (9) and (10).

$$Max CO_2 uptake\,(\%) = 0.785(CaO - 0.7SO_3) + 1.091MgO + 1.420Na_2O + 0.935K_2O \quad (9)$$

$$Carbonation\ degree\ (\%) = 100x\frac{CO_2\ uptake}{max\ CO_2\ uptake} \quad (10)$$

From the results, it was observed that the non-carbonated cement powder (C1) underwent a partial process of natural carbonation, while the carbonated cement powder (C11) was considerably transformed from the reaction with supercritical CO_2. Thus, this information is essential for the FTIR-based method and was considered throughout the quantitative model development to estimate the $CaCO_3$ content in cement.

2.4.6. Fourier transform infrared spectroscopy (FTIR)

Fourier transform infrared (FTIR) spectra were obtained using a PerkinElmer Spectrum 100 instrument with a Universal Attenuated Total Reflectance (ATR) accessory. The ATR consists of diamond/ZnSe crystal (1 reflection), top plate and pressure arm with force indicator. FTIR spectra were recorded in the range of 4000 to 650 cm^{-1}, resolution of 4 cm^{-1}, 16 scans and triplicate analysis. Clean ATR diamond/ZnSe crystal was used to record the background spectra.

2.4.7. Preparation of cement powder mixtures

The samples for calibration (C1-C11) and validation (V1-V10) of the FTIR-based method for $CaCO_3$ quantification were prepared from a physical mixture between non-carbonated (C1 – 45.80 mg $CaCO_3$/g cement) and carbonated (C11 – 468.20 mg $CaCO_3$/g cement) samples. All mixtures are detailed in Table 2. The application domain of the multivariate model covers the range of 45.80 to 468.20 mg $CaCO_3$/g cement. For model calibration, triplicates of non-carbonated (C1) and carbonated (C11) samples were obtained from the homogenized sample quartering. In addition, triplicate was prepared for each calibration mixture (C2-C10), while a duplicate was prepared for each point in the validation set (V1-V10). Thus, 33 samples and 99 FTIR spectra comprise the calibration set, while 20 samples and 60 FTIR spectra compose the validation set.

2.5. Data analysis

The data analysis was performed by means of partial least squares (PLS) regression in the software Solo + MIA (Eigenvector Research). Thus, PLS regression was applied to develop the model to quantify $CaCO_3$ in cement. The method is briefly detailed below.

2.5.1. Partial least squares (PLS) regression

Partial least squares (PLS) regression is the multivariate method applied to develop quantitative models. Thus, PLS aims to evaluate the

Table 2
Cement powder calibration and validation sets applied in the multivariate model.

Calibration set		Validation set	
Sample	mg $CaCO_3$/g cement	Sample	mg $CaCO_3$/g cement
C1_1	45.80	V1_1	67.17
C1_2	45.80	V1_2	69.92
C1_3	45.80	V2_1	110.96
C2_1	88.73	V2_2	110.69
C2_2	88.60	V3_1	152.11
C2_3	88.39	V3_2	152.38
C3_1	132.68	V4_1	193.25
C3_2	131.98	V4_2	193.81
C3_3	130.68	V5_1	235.74
C4_1	173.74	V5_2	236.46
C4_2	173.56	V6_1	276.66
C4_3	171.82	V6_2	278.50
C5_1	214.56	V7_1	319.58
C5_2	215.60	V7_2	319.65
C5_3	216.08	V8_1	360.40
C6_1	256.50	V8_2	360.45
C6_2	257.48	V9_1	403.45
C6_3	258.13	V9_2	404.29
C7_1	298.13	V10_1	445.33
C7_2	298.43	V10_2	445.92
C7_3	298.65		
C8_1	339.80		
C8_2	340.57		
C8_3	341.35		
C9_1	380.95		
C9_2	381.09		
C9_3	382.80		
C10_1	422.69		
C10_2	425.26		
C10_3	425.62		
C11_1	468.20		
C11_2	468.20		
C11_3	468.20		

relationship between predictive variables (X) and response properties (Y) through latent variables (factors) and load weights, optimizing the covariance relationship (X/Y) and establishing a regression. In the present work, the pre-processing of the FTIR spectra was carried out through the mean centering (MC), baseline correction (BC), standard normal variate (SNV) normalization and first derivative (1st Der).

3. Results and discussion

The results and discussions of the present work were divided between: (*i*) the carbonation reaction of the cylindrical cement specimens by supercritical CO_2, (*ii*) the carbonation reaction of the cement powder (C1) by supercritical CO_2 and (*iii*) the development of the multivariate analysis models based on FTIR spectra of non-carbonated (C1) and carbonated (C11) cement mixtures. For brevity purposes, the results of the carbonation study of cylindrical cement specimens are presented in Supplementary Material (Pages S12-S17).

3.1. Carbonation of cement powder

After evaluating the effect of supercritical CO_2 on cylindrical cement specimens (Supplementary Material), the carbonation process was accelerated from the reaction of CO_2 with powdered cement. The high surface area of the powdered cement reduces the time required for the carbonation process to achieve high conversions of the CH and C-S-H phases and produce a large amount of $CaCO_3$ and siliceous products [31]. Thus, the non-carbonated cement powder (C1) was obtained from the grinding of class G cement specimens, while the carbonated cement powder (C11) was obtained from the reaction of sample C1 with supercritical CO_2. Then, both samples (C1 and C11) were extensively characterized by XRD diffraction, SEM microscopy and FTIR spectroscopy.

3.1.1. Cement powder XRD analysis

Initially, non-carbonated (C1) and carbonated (C11) cement powders were analyzed by XRD diffraction. XRD was applied to identify the cement crystalline mineral components, although there is considerable amorphous fraction in the material [9,43,65]. Fig. 2 shows the XRD diffraction pattern, and the Supplementary Material (Table S3) presents the estimated mineral content of the crystalline fraction.

From the XRD pattern (Fig. 2A and Table S3) of the non-carbonated cement powder (C1), it was possible to observe that cement presents a greater diversity of crystalline components, characterized by: (*i*) unhydrated cement phases, composed of C_3S (Ca_3SiO_5 - Alite) and calcium aluminum iron oxide ($Ca_2Fe_{1.5}Al_{0.5}O_5$), (*ii*) cement hydration products, from the presence of portlandite (CH) and ettringite [$Ca_6Al_2(SO_4)_3(OH)_{12}{\cdot}26H_2O$] and (*iii*) a small fraction of calcite ($CaCO_3$ polymorph), resulting from the process of natural carbonation by atmospheric CO_2 throughout the sample preparation. No other $CaCO_3$ polymorph (amorphous, vaterite or aragonite) was identified. The observed profile is commonly described in the literature since a complete cure is unlikely and CH and ettringite are expected products of API class G cement hydration [3,10,19,66]. In addition, a small content of $CaCO_3$ is expected since it is unlikely to prevent the occurrence of natural carbonation [6,14,30]. Natural carbonation is explained by the reactivity of $Ca(OH)_2$ with atmospheric CO_2 and the difficulty of carrying out all sample preparation procedures (cement curing, grinding, sieving and storage) in inert environments. Furthermore, the calcium carbonate content for C1 (non-carbonated cement powder) was estimated as 45.80 mg $CaCO_3$/g cement, corresponding to 2.01 wt.% of CO_2 and 3.80% of carbonation degree.

On the other hand, from the XRD pattern (Fig. 2B and Table S3) of the carbonated cement powder (C11), it was confirmed that the sample undergoes a high degree of chemical transformation. It was observed that the crystalline fraction of C11 (carbonated cement powder) is basically composed of calcite ($CaCO_3$ polymorph). In addition, trace fractions of C_3S (Ca_3SiO_5 - Alite), calcium aluminum iron oxide ($Ca_2Fe_{1.5}Al_{0.5}O_5$) and quartz (SiO_2) are still identified, although they are not very representative in the composition of carbonated cement (C11). The carbonation process completely consumed portlandite (CH), being not identified in the C11 sample. The observed profile is commonly described in the literature since most carbonation products have amorphous characteristics [39,66–68]. In addition, from the XRD results, the $CaCO_3$ content of the C11 sample (carbonated cement) is significantly greater than what would be obtained from the single conversion of portlandite (CH). Thus, it was concluded that there is a high conversion of calcium silicate hydrate (C-S-H) to calcium carbonate and that both phases (CH and C-S-H) carbonation resulted in the formation of calcite polymorph. The preferential precipitation of the $CaCO_3$ polymorphs (calcite, aragonite and vaterite) is influenced by the reaction time, the carbonation degree and the other chemicals presence [11,41]. However, calcite is the most stable polymorph of calcium carbonate [69]. In this context, it is expected that in advanced stages of cement carbonation calcite will be the predominant $CaCO_3$ polymorph, being produced by precipitation and transformation processes of other calcium carbonate compounds (amorphous, vaterite and aragonite) [30,42–43]. Furthermore, the calcium carbonate content for C11 (carbonated cement powder) was estimated as 468.20 mg $CaCO_3$/g cement, corresponding to 20.59 wt.% of CO_2 and 38.82% of carbonation degree (approximately 10 times greater than in the C1 sample). Thus, these values found for C1 and C11 samples should be considered to develop a quantitative model based on FTIR.

3.1.2. Cement powder SEM microscopy

After characterizing the mineral composition of the non-carbonated (C1) and carbonated (C11) cement powders, SEM was applied to perform the materials morphological analysis (see Fig. 3).

From the non-carbonated cement (C1) SEM images (Fig. 3A and 3B), only pulverized calcium silicate hydrate was identified. Although C-S-H

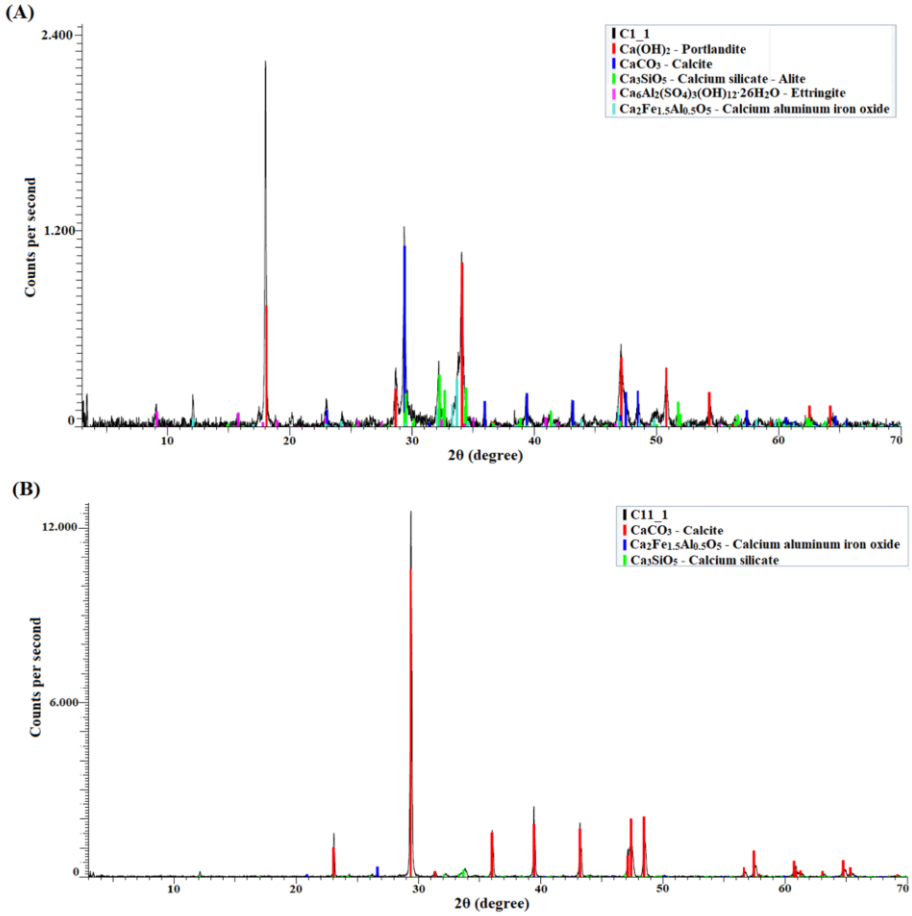

Fig. 2. XRD diffraction pattern of non-carbonated (C1) and carbonated (C11) cement powders.

gel is the major responsible for the development of mechanical strength of the cement [46,70], due to its low crystallinity and absence of preferential plans for cleavage of the mineral [19,67], the ball milling process results in a powder fraction containing particles with irregular shapes and different sizes. In addition, no additional components (CH, C_3S and $CaCO_3$), as identified by XRD diffraction (Fig. 2 and Table S3), could be observed in the analyzed fraction. On the other hand, from the carbonated cement (C11) SEM images (Fig. 3C and 3D), it was possible to observe some decalcified C-S-H and amorphous silica grains that were covered by poorly-crystalline calcite ($CaCO_3$) [42,71]. Calcite, identified in the XRD pattern, is characterized by its crystalline morphological structure. However, it requires long reaction times and slow precipitation processes to achieve its regular crystalline structure [71]. In addition, as observed in carbonated cylindrical cement specimens (Supplementary Material), $CaCO_3$ precipitates around the silica-rich phase (decalcified C-S-H and amorphous silica) were evidenced, resulting in a delay in the leaching process due to the passivation conferred by $CaCO_3$ covering the unreacted C-S-H [30,41,68].

3.1.3. Cement powder FTIR analysis

Fourier Transform Infrared Spectroscopy (FTIR) is a fast, low-cost, accurate and widely available method in universities and service and research laboratories [8,38–39]. FTIR scans the sample with a specified range of the electromagnetic radiation spectrum at the mid-infrared wavelength [72]. The profile of the IR spectra, recorded by the equipment as percentage of transmittance (% T) or percentage of absorbance (% A) versus wavenumber (cm^{-1}), is used to characterize molecular functional groups of the materials [19,62]. Since the molecular vibrational energy is quantized, each peak in the IR spectrum denotes the presence of a specific molecular functional group, while the relative intensity of the absorbed radiation (*i.e.*, height of the infrared peak) can be directly related to its concentration [19,73].

Several applications of FTIR were proposed in the literature to qualify or quantify minerals components in rocks, sediments, soil, and cement or to study transformation processes (*i.e.*, hydration, degradation, carbonation, etc.) in cementitious materials [39–40,46,74]. In this context, the use of Attenuated Total Reflectance (ATR) accessory is especially interesting for FTIR analysis, eliminating and simplifying sample preparations steps, favoring the analysis reproducibility, and increasing the method sensitivity [32,39–40,49,74]. Thus, the ATR-FTIR analysis presents all requirements for application in studies of cementitious materials, supporting the development of qualitative and quantitative methods, enabling quick, reliable, and low-cost evaluations of transformation processes, such as carbonation.

The present work proposes to use ATR-FTIR to: (*i*) study the carbonation process of cement by supercritical CO_2, (*ii*) evaluate changes in the IR spectral profile in mixtures of non-carbonated cement (C1) and carbonated (C11) cement powders and (*iii*) develop a

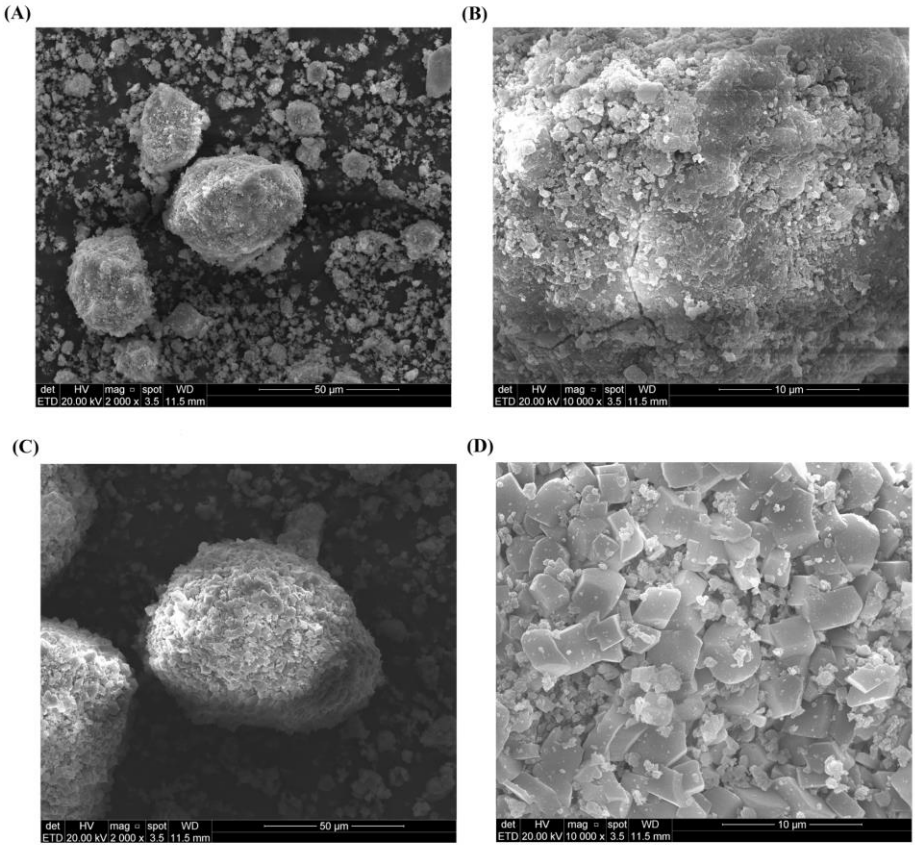

Fig. 3. SEM image of the non-carbonated (C1) and carbonated (C11) cement powders. Magnification of the cement powders: (A) C1 at 2000x, (B) C1 at 10000x, (C) C11 at 2000x and (D) C11 at 10000x.

quantitative method for $CaCO_3$ analysis in cement. Thus, API class G cement was used as reference material. The reference material was cured as recommended by the American Petroleum Institute (API) specification 10A [57], and then subjected to the carbonation process with supercritical CO_2 (at 65 °C, 15 MPa and 7 days). Fig. 4 shows the FTIR spectra of non-carbonated (C1) and carbonated (C11) cement powders.

From the FTIR spectral profile of the non-carbonated sample (C1), it

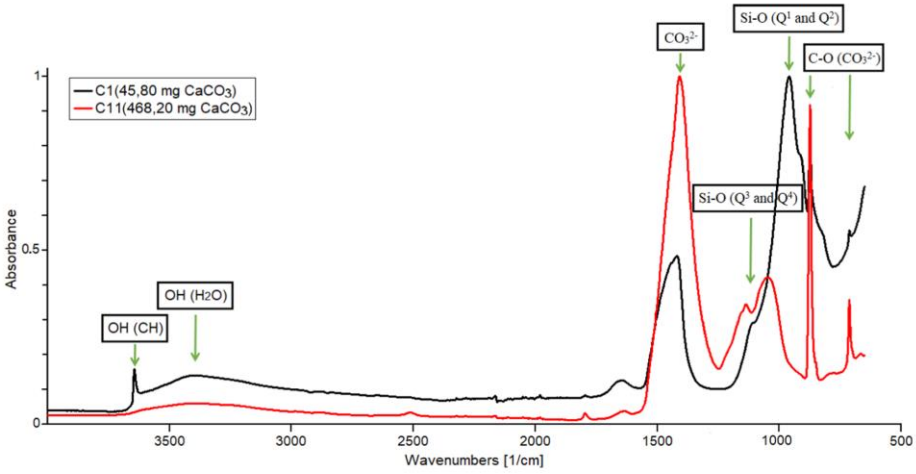

Fig. 4. FTIR spectra of non-carbonated (C1) and carbonated (C11) cement powders.

was possible to describe the following characteristics: (*i*) the presence of the peak related to the OH stretching of portlandite (CH) at 3640 cm^{-1}, (*ii*) a broadband at the 3600–3100 cm^{-1} range, attributed to the OH stretching of the water associated with the cement matrix, (*iii*) a small peak at 1640 cm^{-1}, attributed to bending vibration of water in sulfates, (*iv*) the carbonate (CO_3^{2-}) peaks at 1410 cm^{-1} (asymmetric C-O stretching), 873 cm^{-1} (out-of-plane vibration) and 713 cm^{-1} (in-plane vibration), associated with calcite ($CaCO_3$ polymorph) and (*v*) a broadband (800–1200 cm^{-1}), centered at 960 cm^{-1}, assigned to the Si-O asymmetric stretching (υ_3) of Q^1 and Q^2 species of calcium silicate hydrate (C-S-H) [34,39,65,70,75–76]. Thus, all the characteristics expected for API class G cement after curing was identified in the FTIR spectrum of the non-carbonated sample (C1). In addition, the result reinforces the occurrence of the natural carbonation process and confirms that the ATR-FTIR is sensitive to identify low contents of $CaCO_3$ (C1 – 45.80 mg $CaCO_3$/g cement) in cementitious material.

In contrast, from the FTIR spectral profile of the carbonated cement (C11), it was possible to highlight the following characteristics: (*i*) a broadband at the 3600–3100 cm^{-1} range, attributed to the OH stretching of the water associated with the cement matrix, (*ii*) a small peak at 1640 cm^{-1}, attributed to bending vibration of water in sulfates, (*iii*) the carbonate (CO_3^{2-}) peaks at 1410 cm^{-1} (asymmetric C-O stretching), 873 cm^{-1} (out-of-plane vibration) and 713 cm^{-1} (in-plane vibration), associated with calcite ($CaCO_3$ polymorph), in addition to weak peaks observed around 1790 cm^{-1} and 2518 cm^{-1} and (*iv*) a broadband (1250–900 cm^{-1}), centered at 1140 cm^{-1} and 1050 cm^{-1}, assigned to the Si-O asymmetric stretching (υ_3) of the decalcified C-S-H (Q^3 at 1050 cm^{-1}) and polymerized silica (Q^4 at 1140 cm^{-1}) phases [39,43,46,65,70,75,77]. Thus, the FTIR spectrum of the carbonated sample (C11) confirms the XRD data (Fig. 2 and Table S3) and indicates the total consumption of CH by the disappearance of the OH elongation at 3640 cm^{-1}, with the production of calcite, from the increase in the carbonate (CO_3^{2-}) peaks at 1410 cm^{-1} (asymmetric C-O stretching), 873 cm^{-1} (out-of-plane vibration) and 713 cm^{-1} (in-plane vibration). In addition, the position and intensity shift of the Si-O asymmetric stretching (υ_3) was observed from the non-carbonated sample (C1), centered at 960 cm^{-1}, to the carbonated sample (C11), centered at 1140 cm^{-1} and 1050 cm^{-1} [75]. These changes indicate the consumption of Q^1 and Q^2 species of calcium silicate hydrate (C-S-H) of non-carbonated cement powder by the carbonation process, resulting in a decalcification-polymerization process of C-S-H (Q^1 and Q^2) and leading to the production of decalcified C-S-H (Q^3) and polymerized silica (Q^4) phases [9,11,43]. Q^3 species are characterized by C-S-H with a lower Ca/Si ratio and cross-linked silicate tetrahedra, while Q^4 species are defined as amorphous silica with a highly condensed network of silicate tetrahedrons [9,34,43,65].

After the initial assessment of non-carbonated (C1) and carbonated (C11) cement powders, several intermediate mixtures were prepared from the mixture of C1 and C11, as detailed in Table 2. From the FTIR results (Fig. 4), it was observed that the spectral range (1700 to 650 cm^{-1}) comprises the main transformations of the cement matrix induced by the carbonation process. Thus, the ATR-FTIR sequential analyzes, representative of the calibration samples (C1-C11), are shown in Fig. 5.

In Fig. 5, the evolution of the FTIR spectrum profile is observed as the carbonated (C11) fraction of the mixture increases. Thus, the following most relevant characteristics are observed: (*i*) the increase in the carbonate (CO_3^{2-}) peaks at 1410 cm^{-1} (asymmetric C-O stretching), 873 cm^{-1} (out-of-plane vibration) and 713 cm^{-1} (in-plane vibration) of the calcite, (*ii*) decalcification-polymerization of the C-S-H chain, leading to a shift in the broadband attributed to Si-O asymmetric stretching from 800 to 1200 cm^{-1} (Q^1 and Q^2 species) to a higher wavenumber range 1250–900 cm^{-1} (Q^3 and Q^4 species), (*iii*) reduction of the relative intensities of the Si-O asymmetric stretching due to the polymerization process of the silicate phases [34,46,75], and (*iv*) reduction in the detection interference of the carbonate peaks (873 cm^{-1} and 713 cm^{-1}) due to the overlapping effect caused by C-S-H (Q^1 and Q^2 species). Thus,

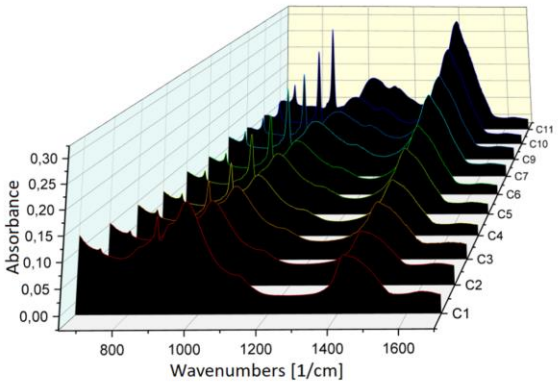

Fig. 5. Sequential modification of FTIR spectra of cement powder mixtures.

the increase in the intensity of specific $CaCO_3$ bands and the reduction of interference from other cement components indicate that it was possible to develop methods to quantify $CaCO_3$ in cement by ATR-FTIR.

From the analysis of non-carbonated cement (C1), carbonated cement (C11), and its mixtures (C2-C10), it was possible to: (*i*) evaluate the changes resulting from the carbonation process with supercritical CO_2, (*ii*) identify the spectral profile of non-carbonated (C1) and carbonated (C11) cement, (*iii*) confirm the potential of ATR-FTIR to analyze cementitious materials, (*iv*) perform a clear identification of $CaCO_3$ and (*v*) relate the intensity of the absorbed radiation to the cement components concentration. In addition, complementing the previous information provided by MicroCT (Figure S4), SEM-EDS (Figure S5 and Fig. 3) and XRD (Fig. 2 and Table S3), ATR-FTIR was able to identify changes in the siliceous fraction of cement, usually studied by the expensive ^{29}Si NMR.

3.2. Multivariate analysis

Based on the IR results, ATR-FTIR shows to be an adequate method to develop fast, reliable, and low-cost quantitative models for the characterization of cementitious materials. Continuous variables, such as FTIR spectra, are incredibly informative and compatible with multivariate analysis tools. Thus, applying the MVA methods, it was possible to identify the IR spectrum regions that best fit to the intended response. In this context, to obtain reliable quantitative models, special attention is required to pre-process the FTIR spectra and the calibration and validation procedures. Thus, the development of a predictive model to quantify $CaCO_3$ in cement was evaluated from the application of partial least squares (PLS) regression. To develop the MVA models, the pre-processing of the FTIR spectra were performed through the mean centering (MC), baseline correction (BC), standard normal variate (SNV) normalization and first derivative (1st Der). Therefore, three PLS models were developed evaluating different combinations of pre-processing of the infrared spectra, which are: (Model 1) mean centering (MC) and baseline correction (BC), (Model 2) MC, BC, and standard normal variate (SNV) normalization and (Model 3) MC, BC, SNV and first derivative (1st Der). Thus, the PLS models were calibrated (C1 to C11) and evaluated with an independent validation set (V1-V10). From the validation set, consisting of samples not included in the calibration, it was possible to: (*i*) avoid an optimum evaluation of the results, (*ii*) confirm the predictive capacity of the model and (*iii*) guarantee the transferability of experimental procedures to characterize carbonated cement by ATR-FTIR. Thus, the PLS models (calibration and validation) to quantify $CaCO_3$ in cement are shown in Table 3. At the same time, the reference and predicted values are presented in the Supplementary Material (Table S4).

From Table 3, it was observed that all developed PLS models used 6

Table 3
Parameters obtained for PLS regression models.

Parameters	PLS		
	Model 1	Model 2	Model 3
Pre-processing	MC; BC	MC; BC; SNV	MC; BC; SNV; 1st Der
Factors	6	6	6
EV% (X/y)	99.96	99.82	99.59
R^2 Calibration	0.9981	0.9996	0.9997
R^2 Prediction	0.9975	0.9993	0.9995
RMSEC	5.85	2.81	2.41
RMSEP	11.85	4.13	3.61
Calibration Bias	0.00	0.00	0.00
Prediction Bias	8.79	2.50	2.37

EV - Explained variance; RMSEC - Root Mean Square Error of Calibration; RMSEP - Root Mean Square Error of Prediction; MC - mean centered; BC - baseline correction; SVN - standard normal variate; 1st Der - first derivative transformation.

factors (LV) for the calibration, resulting in a total of 99.96% (Model 1), 99.82% (Model 2), and 99.59% (Model 3) of explained variance. From the calibration set, good correlation coefficients (R^2) were obtained for Model 1 (R^2 = 0.9981), Model 2 (R^2 = 0.9996) and Model 3 (R^2 = 0.9997). In addition, regression modeling resulted in low root mean square error of calibration (RMSEC) for Model 1 (RMSEC = 5.85 mg $CaCO_3$/g cement), Model 2 (RMSEC = 2.81 mg $CaCO_3$/g cement) and Model 3 (RMSEC = 2.41 mg $CaCO_3$/g cement) and bias close to 0. However, the final evaluation of multivariate regression models must be performed based on an independent validation set. Thus, from Table 3, it was observed that the correlation coefficients (R^2) were obtained from the application of Model 1 (R^2 = 0.9975), Model 2 (R^2 = 0.9993) and Model 3 (R^2 = 0.9995) also showed good regression adjustment. From the validation set, low root mean square errors of prediction (RMSEP) and good bias values were obtained for Model 1 (RMSEP = 11.85 mg $CaCO_3$/g cement; bias = 8.79 mg $CaCO_3$/g cement), Model 2 (RMSEP = 4.13 mg $CaCO_3$/g cement; bias = 2.50 mg $CaCO_3$/g cement) and Model 3 (RMSEP = 3.61 mg $CaCO_3$/g cement; bias = 2.37 mg $CaCO_3$/g cement). Thus, it was concluded that it is possible to calibrate PLS regressions with minimum requirements to quantify $CaCO_3$ in cement using ATR-FTIR, which are: (*i*) correlation coefficients (R^2) close to 1, (*ii*) low estimation errors (RMSEC and RMSEP) and (*iii*) low bias values (calibration bias and prediction bias). Thus, after the initial assessment, Model 3 was selected for a more comprehensive interpretation, as it presents the best PLS regression outputs. The results are shown in Fig. 6.

From Fig. 6A, it was possible to observe the good correlation coefficient (R^2 = 0.9995) from the "predicted vs. reference" plot of PLS (Model 3). The "residual plot" (Fig. 6B) shows the difference between the predicted and the reference values. No systematic error can be observed, with the values being distributed randomly around 0. Furthermore, from the PLS loading (Fig. 6C and 6D), it was possible to identify the most important regions of the FTIR spectrum to quantify

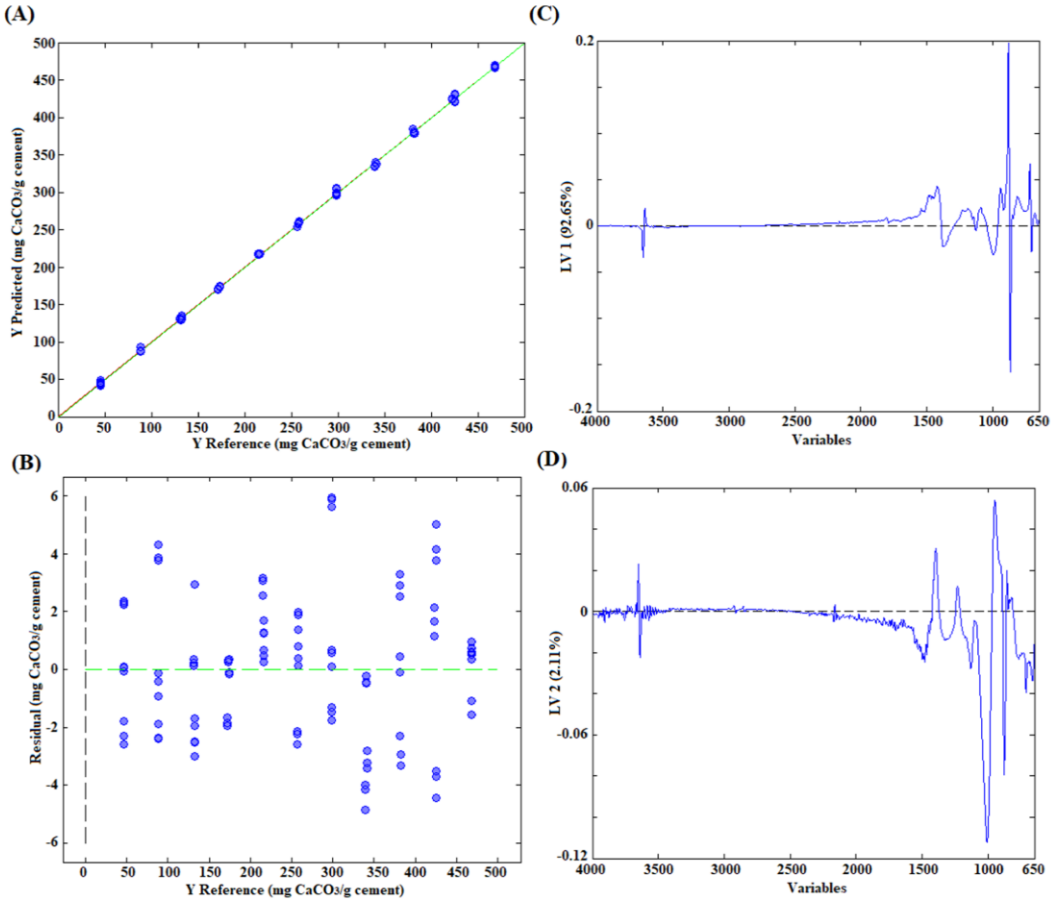

Fig. 6. PLS regression analysis from FTIR spectra of cement powders to quantify $CaCO_3$: (A) predicted vs. reference plot, (B) residual plot, (C) PLS loading (LV 1) and (D) PLS loading (LV 2).

$CaCO_3$ in cement. The spectral regions and characteristics most relevant to the PLS regression are: (*i*) the consumption of portlandite (CH), with the reduction in OH stretching at 3640 cm^{-1}, (*ii*) the increase in the carbonate (CO_3^{2-}) peaks at 1410 cm^{-1} (asymmetric C-O stretching), 873 cm^{-1} (out-of-plane vibration) and 713 cm^{-1} (in-plane vibration) and (*iii*) the displacement of the Si-O asymmetric stretching from 800 to 1200 cm^{-1} (Q^1 and Q^2 species) to 1250–900 cm^{-1} (Q^3 and Q^4 species) due to the decalcification-polymerization of the calcium silicate hydrate (C-S-H) chain throughout the carbonation process.

It was concluded that it is possible to develop reliable PLS models to quantify $CaCO_3$ in cement by ATR-FTIR. The experimental advantages of ATR-FTIR cement powder analysis are: (*i*) eliminate sample preparation steps, (*ii*) reduce the analysis time, (*iii*) eliminate the KBR use, (*iv*) reduce the analysis costs, (*v*) improve the reproducibility of the method and (*vi*) mitigate the occurrence of operator errors. In addition, the analysis time of the ATR-FTIR (a few minutes) is significantly shorter than the TGA (a few hours) and the average percentage of Model 3 prediction error (±2.75%) is lower than that obtained by thermogravimetric analysis (±5%) [41,43]. Furthermore, from the interpretation of the PLS, it was observed that it is necessary to consider the global effect of the carbonation process in the cement matrix to obtain reliable models, since the chemical transformations significantly change the profile of the infrared spectra. The most important processes are: (*i*) the consumption of portlandite (CH), (*ii*) the decalcification-polymerization process of calcium silicate hydrate (C-S-H) and (*iii*) the increase in the $CaCO_3$ content.

4. Conclusions

Partial least squares (PLS) regression models were developed to quantify $CaCO_3$ in cement and to study the CO_2 effect on the material matrix. PLS models were calibrated and validated, and the regression results presented good correlation coefficient ($R^2 = 0.9995$) and low estimation error (RMSEP = 3.61 mg $CaCO_3$/g cement). From the results, it was observed that the portlandite (CH) consumption, the increase in $CaCO_3$ content and the C-S-H decalcification-polymerization are the most relevant chemical transformations of cement throughout the carbonation process. Thus, it was concluded that: *i*) it is possible to obtain fast, low-cost, and reliable models to quantify $CaCO_3$ by FTIR and *ii*) the method is applicable to study carbonated cement-based materials.

The results of the present work show that it is necessary to consider the physical and chemical transformations induced by the carbonation process in the cement matrix to develop reliable quantitative models to estimate the $CaCO_3$ content in the material. To expand the scope of application of the FTIR-based method for the analysis of carbonated cementitious materials, future studies should: (*i*) reproduce the experimental procedure with other types of cement, (*ii*) evaluate the influence of the carbonation type (natural, accelerated, or supercritical) or the exposure stage (carbonation cure or cement degradation) on the model and (*iii*) study the effect of other $CaCO_3$ polymorphs on the performance of the method.

CRediT authorship contribution statement

Victor Hugo Jacks Mendes dos Santos: Conceptualization, Methodology, Software, Validation, Formal analysis, Investigation, Data curation, Writing – original draft, Writing – review & editing, Visualization. **Darlan Pontin:** Methodology, Formal analysis, Investigation, Writing – review & editing. **Gabriela Gonçalves Dias Ponzi:** Methodology, Formal analysis, Investigation, Writing – review & editing. **Amanda Sofia de Guimarães e Stepanha:** Methodology, Formal analysis, Investigation, Writing – review & editing. **Renan Bordulis Martel:** Methodology, Formal analysis, Investigation, Writing – review & editing. **Marta Kerber Schütz:** Conceptualization, Validation, Formal analysis, Investigation, Writing – review & editing, Visualization. **Sandra Mara Oliveira Einloft:** Conceptualization, Validation, Formal analysis, Investigation, Writing – review & editing, Visualization. **Felipe Dalla Vecchia:** Conceptualization, Methodology, Validation, Formal analysis, Investigation, Resources, Writing – review & editing, Visualization, Supervision, Project administration, Funding acquisition.

Declaration of Competing Interest

The authors declare that they have no known competing financial interests or personal relationships that could have appeared to influence the work reported in this paper.

Acknowledgments

The authors would like to thank the Institute of Petroleum and Natural Resource (IPR) of the Pontifical Catholic University of Rio Grande do Sul for the infrastructure, Dra. Rosalia Barili da Cunha for help with the XRD diffraction analyzes interpretation and Lafarge Holcim for the donation of the cement. This study was financed in part by the Coordenação de Aperfeiçoamento de Pessoal de Nível Superior – Brasil (CAPES) – Finance Code 001. In addition, this work was supported by Petrobras (grant numbers: 2017/00742-8 and 2018/00235-1) and by ANP (Brazil's National Oil, Natural Gas and Biofuels Agency), through the R&D levy regulation.

Appendix A. Supplementary material

Supplementary data to this article can be found online at https://doi.org/10.1016/j.conbuildmat.2021.125413.

References

[1] T. Wilberforce, A.G. Olabi, E.T. Sayed, K. Elsaid, M.A. Abdelkareem, Progress in carbon capture technologies, Sci. Total Environ. 761 (2021) 143203, https://doi.org/10.1016/j.scitotenv.2020.143203.
[2] M. Bai, J. Sun, K. Song, K.M. Reinicke, C. Teodoriu, Evaluation of mechanical well integrity during CO_2 underground storage, Environ, Earth Sci. 73 (11) (2015) 6815–6825, https://doi.org/10.1007/s12665-015-4157-5.
[3] L. Liu, Y. Ji, F. Gao, L.i. Zhang, Z. Zhang, XiangYu Liu, Study on high-efficiency CO_2 absorption by fresh cement paste, Constr. Build. Mater. 270 (2021) 121364, https://doi.org/10.1016/j.conbuildmat.2020.121364.
[4] R.M. Andrew, Global CO_2 emissions from cement production, Earth Syst. Sci. Data. 10 (2018) 195–217, https://doi.org/10.5194/essd-10-195-2018.
[5] B. Metz, O. Davidson, H. De Coninck, M. Loos, L. Meyer. IPCC special report on carbon dioxide capture and storage, Working Group III of the Intergovernmental Panel on Climate Change, Cambridge University Press, Cambridge, United Kingdom and New York, NY, USA, 2005, pp. 442–pp.
[6] E. Benhelal, E. Shamsaei, M.I. Rashid, Challenges against CO_2 abatement strategies in cement industry: A review, J. Environ. Sci. 104 (2021) 84–101, https://doi.org/10.1016/j.jes.2020.11.020.
[7] L. Mazurana, P.R.S. Bittencourt, F.R. Scremin, A. Neves Junior, E. Possan, Determination of CO_2 capture in rendering mortars produced with recycled construction and demolition waste by thermogravimetry, J. Therm. Anal. Calorim. (2021), https://doi.org/10.1007/s10973-020-10436-0.
[8] T. Shi, Y. Gao, D.J. Corr, S.P. Shah, FTIR study on early-age hydration of carbon nanotubes-modified cement-based materials, Adv. Cem. Res. 31 (8) (2019) 353–361, https://doi.org/10.1680/jadcr.16.00167.
[9] W. Ashraf, Carbonation of cement-based materials: Challenges and opportunities, Constr. Build. Mater. 120 (2016) 558–570, https://doi.org/10.1016/j.conbuildmat.2016.05.080.
[10] B.L.d.S. Costa, J.C.d.O. Freitas, D.M.d.A. Melo, R.G.d.S. Araujo, Y.H.d. Oliveira, C. A. Simão, Evaluation of density influence on resistance to carbonation process in oil well cement slurries, Constr. Build. Mater. 197 (2019) 331–338, https://doi.org/10.1016/j.conbuildmat.2018.11.232.
[11] W. Liu, Y.-Q. Li, L.-P. Tang, Z.-J. Dong, XRD and ^{29}Si MAS NMR study on carbonated cement paste under accelerated carbonation using different concentration of CO_2, Mater. Today Commun. 19 (2019) 464–470, https://doi.org/10.1016/j.mtcomm.2019.05.007.
[12] F. Dalla Vecchia, V.H.J.M. dos Santos, M.K. Schütz, G.G.D. Ponzi, A.S.d.G. e. Stepanha, C.d.F. Malfatti, E.M.d. Costa, Wellbore integrity in a saline aquifer: Experimental steel-cement interface degradation under supercritical CO_2 conditions representative of Brazil's Parana basin, Int. J. Greenh. Gas Control. 98 (2020) 103077, https://doi.org/10.1016/j.ijggc.2020.103077.
[13] B. Liu, J. Qin, J. Shi, J. Jiang, X. Wu, Z. He, New perspectives on utilization of CO_2 sequestration technologies in cement-based materials, Constr. Build. Mater. 272 (2021), 121660, https://doi.org/10.1016/j.conbuildmat.2020.121660.

[14] S.O. Ekolu, A review on effects of curing, sheltering, and CO_2 concentration upon natural carbonation of concrete, Constr. Build. Mater. 127 (2016) 306–320, https://doi.org/10.1016/j.conbuildmat.2016.09.056.
[15] G.G.D. Ponzi, V.H.J.M.D. Santos, R.B. Martel, D. Pontin, A.S.d.G.e. Stepanha, M. K. Schütz, S.C. Menezes, S.M.O. Einloft, F.D. Vecchia, Basalt powder as a supplementary cementitious material in cement paste for CCS wells: chemical and mechanical resistance of cement formulations for CO_2 geological storage sites, Int. J. Greenh. Gas Control. 109 (2021) 103337, https://doi.org/10.1016/j.ijggc.2021.103337.
[16] S. Yadav, A. Mehra, A review on ex situ mineral carbonation, Environ. Sci. Pollut. Res. 28 (10) (2021) 12202–12231, https://doi.org/10.1007/s11356-020-12049-4.
[17] D. Zhang, Z. Ghouleh, Y. Shao, Review on carbonation curing of cement-based materials, J. CO_2 Util. 21 (2017) 119–131, https://doi.org/10.1016/j.jcou.2017.07.003.
[18] S. Salehi, J. Khattak, F.K. Saleh, S. Igbojekwe, Investigation of mix design and properties of geopolymers for application as wellbore cement, J. Pet. Sci. Eng. 178 (2019) 133–139, https://doi.org/10.1016/j.petrol.2019.03.031.
[19] O. Omosebi, H. Maheshwari, R. Ahmed, S. Shah, S. Osisanya, S. Hassani, G. DeBruijn, W. Cornell, D. Simon, Degradation of well cement in HPHT acidic environment: Effects of CO_2 concentration and pressure, Cem. Concr. Compos. 74 (2016) 54–70, https://doi.org/10.1016/j.cemconcomp.2016.09.006.
[20] J.M. Paris, J.G. Roessler, C.C. Ferraro, H.D. DeFord, T.G. Townsend, A review of waste products utilized as supplements to Portland cement in concrete, J. Clean. Prod. 121 (2016) 1–18, https://doi.org/10.1016/j.jclepro.2016.02.013.
[21] P. Šiler, I. Kolářová, T. Sehnal, R. Snop, T. Opravil, F. Šoukal, The Influence of Particle Size of Cement and Different Additives on the Properties of Portland Cement Pastes, Mater. Sci. Forum. 851 (2016) 104–109, https://doi.org/10.4028/www.scientific.net/MSF.851.104.
[22] M. Bagheri, S.M. Shariatipour, E. Ganjian, A review of oil well cement alteration in CO_2-rich environments, Constr. Build. Mater. 186 (2018) 946–968, https://doi.org/10.1016/j.conbuildmat.2018.07.250.
[23] A. Deshpande, R. Patil, Applications of Nanotechnology in Oilwell Cementing, in: SPE Middle East Oil Gas Show Conf., Society of Petroleum Engineers, 2017: pp. 6–9. doi:10.2118/183727-MS.
[24] M. Tiong, R. Gholami, M.E. Rahman, Cement degradation in CO_2 storage sites: a review on potential applications of nanomaterials, J. Pet. Explor. Prod. Technol. 9 (1) (2019) 329–340, https://doi.org/10.1007/s13202-018-0490-z.
[25] J. Hwang, R. Ahmed, S. Tale, S. Shah, Shear bond strength of oil well cement in carbonic acid environment, J. CO_2 Util. 27 (2018) 60–72, https://doi.org/10.1016/j.jcou.2018.07.001.
[26] T. Gu, X. Guo, Z. Li, X. Cheng, X. Fan, A. Korayem, W.H. Duan, Coupled effect of CO_2 attack and tensile stress on well cement under CO_2 storage conditions, Constr. Build. Mater. 130 (2017) 92–102, https://doi.org/10.1016/j.conbuildmat.2016.10.117.
[27] K. Abid, R. Gholami, H. Elochukwu, M. Mostofi, C.H. Bing, G. Muktadir, A methodology to improve nanosilica based cements used in CO_2 sequestration sites, Petroleum. 4 (2) (2018) 198–208, https://doi.org/10.1016/j.petlm.2017.10.005.
[28] S. Al Wakeel, J. Němeček, L. Li, Y. Xi, M. Hubler, The effect of introducing nanoparticles on the fracture toughness of well cement paste, Int. J. Greenh. Gas Control. 84 (2019) 147–153, https://doi.org/10.1016/j.ijggc.2019.03.009.
[29] E.-J. Moon, Y.C. Choi, Carbon dioxide fixation via accelerated carbonation of cement-based materials: Potential for construction materials applications, Constr. Build. Mater. 199 (2019) 676–687, https://doi.org/10.1016/j.conbuildmat.2018.12.078.
[30] B. Savija, M. Luković, Carbonation of cement paste: Understanding, challenges, and opportunities, Constr. Build. Mater. 117 (2016) 285–301, https://doi.org/10.1016/j.conbuildmat.2016.04.138.
[31] S. Park, H. Moon, J.-H. Kim, M. Lee, C.-W. Chung, Reaction of hydrated cement paste with supercritical carbon dioxide, Constr. Build. Mater. 281 (2021) 122615, https://doi.org/10.1016/j.conbuildmat.2021.122615.
[32] M. Horgnies, J.J. Chen, C. Bouillon, Overview about the use of Fourier Transform Infrared spectroscopy to study cementitious materials, in, WIT Trans. Eng. Sci. (2013) 251–262, https://doi.org/10.2495/MC130221.
[33] R. Bjørge, K. Gawel, E.A. Chavez Panduro, M. Torsæter, Carbonation of silica cement at high-temperature well conditions, Int. J. Greenh. Gas Control. 82 (2019) 261–268, https://doi.org/10.1016/j.ijggc.2019.01.011.
[34] B. Wu, G. Ye, Study of carbonation rate of synthetic C-S-H by XRD, NMR and FTIR, Heron. 64 (2019) 21–38.
[35] K. Kupwade-Patil, S.D. Palkovic, A. Bumajdad, C. Soriano, O. Büyüköztürk, Use of silica fume and natural volcanic ash as a replacement to Portland cement: Micro and pore structural investigation using NMR, XRD, FTIR and X-ray microtomography, Constr. Build. Mater. 158 (2018) 574–590, https://doi.org/10.1016/j.conbuildmat.2017.09.165.
[36] A.R. Duggan, J. Goggins, E. Clifford, B.A. McCabe, The Use of Carbonation Depth Techniques on Stabilized Peat, Geotech. Test. J. 40 (6) (2017) 20160223, https://doi.org/10.1520/GTJ20160223.
[37] D. Gastaldi, F. Canonico, S. Irico, D. Pellerej, M.C. Paganini, Near-infrared spectroscopy investigation on the hydration degree of a cement paste, J. Mater. Sci. 45 (12) (2010) 3169–3174, https://doi.org/10.1007/s10853-010-4323-9.
[38] J.P. Rebouças, J.J.R. Rohwedder, C. Pasquini, Near infrared emission spectroscopy for rapid compositional analysis of Portland cements, Anal. Chim. Acta. 1024 (2018) 136–144, https://doi.org/10.1016/j.aca.2018.03.035.
[39] J. Higl, D. Hinder, C. Rathgeber, B. Ramming, M. Lindén, Detailed in situ ATR-FTIR spectroscopy study of the early stages of C-S-H formation during hydration of monoclinic C_3S, Cem. Concr. Res. 142 (2021) 106367, https://doi.org/10.1016/j.cemconres.2021.106367.
[40] D.G. Henry, J.S. Watson, C.M. John, Assessing and calibrating the ATR-FTIR approach as a carbonate rock characterization tool, Sediment. Geol. 347 (2017) 36–52, https://doi.org/10.1016/j.sedgeo.2016.07.003.
[41] K. Vance, G. Falzone, I. Pignatelli, M. Bauchy, M. Balonis, G. Sant, Direct Carbonation of Ca(OH)2 Using Liquid and Supercritical CO2: Implications for Carbon-Neutral Cementation, Ind. Eng. Chem. Res. 54 (2015) 8908–8918, https://doi.org/10.1021/acs.iecr.5b02356.
[42] R. Chang, S. Kim, S. Lee, S. Choi, M. Kim, Y. Park, Calcium Carbonate Precipitation for CO_2 Storage and Utilization: A Review of the Carbonate Crystallization and Polymorphism, Front. Energy Res. 5 (2017) 1–12, https://doi.org/10.3389/fenrg.2017.00017.
[43] M. Saillio, V. Baroghel-Bouny, S. Pradelle, M. Bertin, J. Vincent, J.-B. d'Espinose de Lacaillerie, Effect of supplementary cementitious materials on carbonation of cement pastes, Cem. Concr. Res. 142 (2021) 106358, https://doi.org/10.1016/j.cemconres.2021.106358.
[44] R. Schneider dos Santos, S.B.A. Rolim, F. Hepp Pulgati, Application of visible and near infrared spectroscopy in non-destructive evaluation of cement materials, Int. J. Remote Sens. 36 (3) (2015) 917–938, https://doi.org/10.1080/01431161.2014.1001083.
[45] P. Rosén, H. Vogel, L. Cunningham, N. Reuss, D.J. Conley, P. Persson, Fourier transform infrared spectroscopy, a new method for rapid determination of total organic and inorganic carbon and biogenic silica concentration in lake sediments, J. Paleolimnol. 43 (2) (2010) 247–259, https://doi.org/10.1007/s10933-009-9329-4.
[46] A. Jose, M.R. Nivitha, J.M. Krishnan, R.G. Robinson, Characterization of cement stabilized pond ash using FTIR spectroscopy, Constr. Build. Mater. 263 (2020) 120136, https://doi.org/10.1016/j.conbuildmat.2020.120136.
[47] Y. Otsuka, M. Takeuchi, M. Otsuka, B. Ben-Nissan, D. Grossin, H. Tanaka, Effect of carbon dioxide on self-setting apatite cement formation from tetracalcium phosphate and dicalcium phosphate dihydrate; ATR-IR and chemoinformatics analysis, Colloid Polym. Sci. 293 (10) (2015) 2781–2788, https://doi.org/10.1007/s00396-015-3616-6.
[48] S. Nasrazadani, T. Springfield, Application of Fourier transform infrared spectroscopy in cement Alkali quantification, Mater. Struct. 47 (10) (2014) 1607–1615, https://doi.org/10.1617/s11527-013-0140-3.
[49] S. Veerasingam, R. Venkatachalapathy, Estimation of carbonate concentration and characterization of marine sediments by Fourier Transform Infrared Spectroscopy, Infrared Phys. Technol. 66 (2014) 136–140, https://doi.org/10.1016/j.infrared.2014.06.005.
[50] A. Guatame-Garcia, M. Buxton, The Use of Infrared Spectroscopy to Determine the Quality of Carbonate-Rich Diatomite Ores, Minerals. 8 (2018) 120, https://doi.org/10.3390/min8030120.
[51] X. Liu, S.M. Colman, E.T. Brown, E.C. Minor, H. Li, Estimation of carbonate, total organic carbon, and biogenic silica content by FTIR and XRF techniques in lacustrine sediments, J. Paleolimnol. 50 (3) (2013) 387–398, https://doi.org/10.1007/s10933-013-9733-7.
[52] Y. Luzinova, G.T. Dobbs, L. Lapham, J.P. Chanton, B. Mizaikoff, Detection of cold seep derived authigenic carbonates with infrared spectroscopy, Mar. Chem. 125 (1-4) (2011) 8–18, https://doi.org/10.1016/j.marchem.2011.01.006.
[53] M. Mecozzi, E. Pietrantonio, M. Amici, G. Romanelli, Determination of carbonate in marine solid samples by FTIR-ATR spectroscopy, Analyst. 126 (2001) 144–146, https://doi.org/10.1039/b009031j.
[54] M. Tatzber, M. Stemmer, H. Spiegel, C. Katzlberger, G. Haberhauer, M. H. Gerzabek, An alternative method to measure carbonate in soils by FT-IR spectroscopy, Environ. Chem. Lett. 5 (1) (2007) 9–12, https://doi.org/10.1007/s10311-006-0079-5.
[55] M.A. Legodi, D. De Waal, J.H. Potgieter, Quantitative Determination of $CaCO_3$ in Cement Blends by FT-IR, Appl. Spectrosc. 55 (3) (2001) 361–365, https://doi.org/10.1366/0003702011951786.
[56] T.L. Hughes, C.M. Methven, T.G.J. Jones, S.E. Pelham, P. Fletcher, C. Hall, Determining cement composition by Fourier transform infrared spectroscopy, Adv. Cem. Based Mater. 2 (3) (1995) 91–104, https://doi.org/10.1016/1065-7355(94)00031-X.
[57] A.P.I. Specification, API 10A - Specification for Cements and Materials for Well Cementing, Am. Pet. Inst. 2009 (2010) 50, https://doi.org/10.1002/jcc.
[58] M.A. Celia, S. Bachu, J.M. Nordbotten, K.W. Bandilla, Status of CO_2 storage in deep saline aquifers with emphasis on modeling approaches and practical simulations, Water Resour. Res. 51 (9) (2015) 6846–6892, https://doi.org/10.1002/2015WR017609.
[59] C. Teodoriu, O. Bello, A review of cement testing apparatus and methods under CO_2 environment and their impact on well integrity prediction – Where do we stand? J. Pet. Sci. Eng. 187 (2020) 106736, https://doi.org/10.1016/j.petrol.2019.106736.
[60] A. Lavrov, Stiff cement, soft cement: Nonlinearity, arching effect, hysteresis, and irreversibility in CO_2-well integrity and near-well geomechanics, Int. J. Greenh. Gas Control. 70 (2018) 236–242, https://doi.org/10.1016/j.ijggc.2017.11.012.
[61] N. Koukouzas, Z. Kypritidou, C. Vasilatos, N. Tsoukalas, C.A. Rochelle, G. Purser, Geochemical modeling of carbonation of hydrated oil well cement exposed to CO_2-saturated brine solution, Appl. Geochemistry. 85 (2017) 35–48, https://doi.org/10.1016/j.apgeochem.2017.08.002.
[62] A. Ranjan, R. Kumar, D. Mohan, Comparative analysis of phenolphthalein indicator, XRDA and FTIR methods for measurement of carbonation depth of concrete, Int. J. Civ. Eng. Technol. 9 (2018) 315–320.

[63] T. Chen, M. Bai, X. Gao, Carbonation curing of cement mortars incorporating carbonated fly ash for performance improvement and CO_2 sequestration, J. CO_2 Util. 51 (2021) 101633, https://doi.org/10.1016/j.jcou.2021.101633.
[64] H.H. Steinour, Some effects of carbon dioxide on mortars and concrete-discussion, J. Am. Concr. Inst. 30 (1959) 905–907.
[65] J. Skocek, M. Zajac, M. Ben Haha, Carbon Capture and Utilization by mineralization of cement pastes derived from recycled concrete, Sci. Rep. 10 (2020) 5614, https://doi.org/10.1038/s41598-020-62503-z.
[66] L. Li, M.H. Hubler, Y. Xi, Theoretical modeling on chemical composition and mechanical properties of well cement under carbonation reactions, J. Clean. Prod. 276 (2020) 124270, https://doi.org/10.1016/j.jclepro.2020.124270.
[67] A.E. Morandeau, C.E. White, In situ X-ray pair distribution function analysis of accelerated carbonation of a synthetic calcium–silicate–hydrate gel, J. Mater. Chem. A. 3 (16) (2015) 8597–8605, https://doi.org/10.1039/C5TA00348B.
[68] V. Shah, K. Scrivener, B. Bhattacharjee, S. Bishnoi, Changes in microstructure characteristics of cement paste on carbonation, Cem. Concr. Res. 109 (2018) 184–197, https://doi.org/10.1016/j.cemconres.2018.04.016.
[69] M. Bagheri, S.M. Shariatipour, E. Ganjian, A methodology for reactive transport modelling and geomechanical investigation of wellbores in CO_2 storage sites, Constr. Build. Mater. 268 (2021) 121100, https://doi.org/10.1016/j.conbuildmat.2020.121100.
[70] B.J. Zhan, D.X. Xuan, C.S. Poon, C.J. Shi, S.C. Kou, Characterization of C-S–H formed in coupled CO_2–water cured Portland cement pastes, Mater. Struct. 51 (2018) 92, https://doi.org/10.1617/s11527-018-1211-2.
[71] D. Wang, Y. Fang, Y. Zhang, J. Chang, Changes in mineral composition, growth of calcite crystal, and promotion of physico-chemical properties induced by carbonation of β-C_2S, J. CO_2 Util. 34 (2019) 149–162, https://doi.org/10.1016/j.jcou.2019.06.005.
[72] H. Witkowski, M. Koniorczyk, New sampling method to improve the reliability of FTIR analysis for Self-Compacting Concrete, Constr. Build. Mater. 172 (2018) 196–203, https://doi.org/10.1016/j.conbuildmat.2018.03.216.
[73] O. Omosebi, H. Maheshwari, R. Ahmed, S. Shah, S. Osisanya, A. Santra, A. Saasen, Investigating temperature effect on degradation of well cement in HPHT carbonic acid environment, J. Nat. Gas Sci. Eng. 26 (2015) 1344–1362, https://doi.org/10.1016/j.jngse.2015.08.018.
[74] E.M. Valliant, B.T. Dickey, R. Price, D. Boyd, M.J. Filiaggi, Fourier transform infrared spectroscopy as a tool to study the setting reaction in glass-ionomer cements, Mater. Lett. 185 (2016) 256–259, https://doi.org/10.1016/j.matlet.2016.08.131.
[75] A. Hidalgo, C. Domingo, C. Garcia, S. Petit, C. Andrade, C. Alonso, Microstructural changes induced in Portland cement-based materials due to natural and supercritical carbonation, J. Mater. Sci. 43 (9) (2008) 3101–3111, https://doi.org/10.1007/s10853-008-2521-5.
[76] Z. Tu, C. Shi, N. Farzadnia, Effect of Limestone Powder Content on the Early-Age Properties of CO_2-Cured Concrete, J. Mater. Civ. Eng. 30 (8) (2018) 04018164, https://doi.org/10.1061/(ASCE)MT.1943-5533.0002232.
[77] E.N. Kani, H. Mehdizadeh, Investigating Gel Molecular Structure and Its Relation with Mechanical Strength in Geopolymer Cement Based on Natural Pozzolan Using In Situ ATR-FTIR Spectroscopy, J. Mater. Civ. Eng. 29 (2017) 04017078. doi: 10.1061/(ASCE)MT.1943-5533.0001917.

4.1.1. Material suplementar do desenvolvimento método quantitativo

Supplementary Material

Application of Fourier Transform Infrared Spectroscopy (FTIR) coupled with multivariate regression for calcium carbonate ($CaCO_3$) quantification in cement

Victor Hugo Jacks Mendes dos Santos [a,b], Darlan Pontin [a], Gabriela Gonçalves Dias Ponzi [a,b], Amanda Sofia de Guimarães e Stepanha [a,b], Renan Bordulis Martel [a], Marta Kerber Schütz [a,c], Sandra M. O. Einloft [a,b,c] and Felipe Dalla Vecchia [a,b,c]*

[a] Pontifical Catholic University of Rio Grande do Sul, PUCRS. Institute of Petroleum and Natural Resources, Avenida Ipiranga, 6681, – TECNOPUC, Building 96J, 90619-900, Porto Alegre, Brazil.

[b] Pontifical Catholic University of Rio Grande do Sul, PUCRS, Graduate Program in Materials Engineering and Technology, Avenida Ipiranga, 6681– Building 32, 90619-900, Porto Alegre, Brazil.

[c] Pontifical Catholic University of Rio Grande do Sul, PUCRS, School of Technology, Avenida Ipiranga, 6681 – Building 30, 90619-900, Porto Alegre, Brazil.

AUTHOR INFORMATION

Corresponding Author

***E-mail:** felipe.vecchia@pucrs.br;

Tel: +55 51 3320-3689

Submitted to: Construction and Building Materials Journal

Table S1. Basic properties of materials and chemicals

Material/chemicals	Supplier	Purity	Description
Calcium oxide	Êxodo	95.00%	**CAS:** 1305 - 78 - 8 **Formula:** CaO **Molecular weight:** 56.08 g·mol^{-1} **Impurity:** Insoluble in HCl: Max. 0.5%; Loss on ignition: Max. 3%; Iron (Fe): Max. 0.1%; Heavy metals (Pb): Max. 0.005%; Chloride (Cl): Max. 0.05% and Sulfate (SO_4): Max. 0.5%
Calcium carbonate	Merck	99.95%	**CAS:** 471-34-1 **Formula:** $CaCO_3$ **Molecular weight:** 100.09 g·mol^{-1} **Impurity:** Chloride (Cl): ≤ 5 ppm; Phosphate (PO_4): ≤ 10 ppm; Sulfate (SO_4): ≤ 20 ppm; Iron (Fe): ≤ 0.100 ppm; Aluminum (Al): ≤ 0.20 ppm; Barium (Ba): ≤ 2.0 ppm; Potassium (K): ≤ 2.0 ppm; Magnesium (Mg): ≤ 5.0 ppm; Sodium (Na): ≤ 3.0 ppm; Lead (Pb): ≤ 0.050 ppm; Rubidium (Rb): ≤ 20 ppm and Strontium (Sr): ≤ 100 ppm
Phosphoric acid	Sigma-Aldrich	85.00%	**CAS:** 7664-38-2 **Formula:** H_3PO_4 **Molecular weight:** 98.00 g·mol^{-1} **Impurity:** Assay (acidimetric): ≥ 85.0 %; Chloride (Cl): ≤ 500 ppb; Nitrate (NO_3): ≤ 500 ppb; Sulphate (SO_4): ≤ 10 ppm; Iron (Fe): ≤ 200 ppb; Aluminum (Al): ≤ 20 ppb; Barium (Ba): ≤ 20 ppb; Potassium (K): ≤ 50 ppb; Magnesium (Mg): ≤ 20 ppb; Sodium (Na): ≤ 100 ppb; Lead (Pb): ≤ 20 ppb and Strontium (Sr): ≤ 50ppb
Carbon dioxide	Air Products	99.99%	**CAS:** 124-38-9 **Formula:** CO_2 **Molecular weight:** 44.01 g·mol^{-1} **Impurity:** Oxygen (O_2) ≤ 10 ppm; nitrogen (N_2) ≤ 25 ppm; carbon monoxide (CO) ≤ 2 ppm; total hydrocarbon (THC) ≤ 5 ppm and water (H_2O) ≤ 7 ppm
Phenolphthalein	Química Moderna	98.00%	**CAS:** 77-09-8 **Formula:** $C_{20}H_{14}O_4$ **Molecular weight:** 318,33 g·mol^{-1} **Description:** Meets ACS requirements; Appearance (color) white to off-white; Appearance (form) powder; pH 8.0 colorless; pH 8.2 pale pink; pH 8.6 pink and pH 10.0 red

Table S2. $CaCO_3$ content in cement obtained by gas chromatography analysis

Sample	Predicted (mg $CaCO_3$/g cement)	Calibration (mg $CaCO_3$/g cement)	N.A	Sample mass (g)	CO_2 (U.A)	N_2 (U.A)
C1	45.80	NC	76368.3	0.0029	2177518	9832.2
M-2.5	-	NC+25.90	146793.2	0.0026	2258562	5917.7
M-5	-	NC+50.00	151339.3	0.0027	2872530	7029.9
M-10	-	NC+100.10	258512.0	0.0030	3870622	4990.9
M-20	-	NC+202.60	349083.4	0.0030	5607292	5354.3
M-75	-	NC+748.60	1108751.0	0.0027	13345891	4458.1
M-100	1000.00	1000.00	1561632.4	0.0028	16289575	3725.4
C11	468.20	-	780262.4	0.0028	10707166	4900.9

NC – Naturally carbonated; U.A - unit of area; N.A – normalized unit of area = [CO_2 U.A/(sample mass * N_2 U.A)]

Table S3. Mineral composition of non-carbonated (C1) and carbonated (C11) cement powders

XRD Mineral Composition	Abbreviation	[a]C1	[a]C11
Calcite [wt.%]	CC	40.66	90.75
Portlandite [wt.%]	CH	34.14	ND
Alite [wt.%]	C_3S	NQ	ND
Ettringite [wt.%]	AFt	3.78	ND
Calcium Aluminum Iron Oxide [wt. %]	C_2FA	21.42	6.81
Quartz [wt.%]	Qtz	ND	2.44

[a] Mass percentage of crystalline fraction of cement powder; non-carbonated cement (C1); carbonated cement (C11); NQ - not quantified; ND - not detected.

Table S4. Reference, predicted and error values of $CaCO_3$ content in cement powders estimated for the validation set

Validation set		Model 2		Model 3	
Sample	**Reference (mg $CaCO_3$/g cement)**	**Predicted (mg $CaCO_3$/g cement)**	**Error (mg $CaCO_3$/g cement)**	**Predicted (mg $CaCO_3$/g cement)**	**Error (mg $CaCO_3$/g cement)**
V1_1 1	67.17	75.90	8.73	72.76	5.59
V1_1 2	67.17	75.20	8.03	71.78	4.61
V1_1 3	67.17	75.09	7.92	72.38	5.20
V1_2 1	69.92	74.50	4.58	75.52	5.60
V1_2 2	69.92	73.93	4.01	75.51	5.59
V1_2 3	69.92	73.68	3.76	75.32	5.40
V2_1 1	110.96	112.60	1.64	115.01	4.05
V2_1 2	110.96	112.15	1.19	115.00	4.04
V2_1 3	110.96	111.82	0.86	115.19	4.23
V2_2 1	110.69	112.47	1.77	114.98	4.28
V2_2 2	110.69	111.98	1.29	115.14	4.45
V2_2 3	110.69	111.68	0.99	115.04	4.35
V3_1 1	152.11	152.06	-0.05	152.79	0.67
V3_1 2	152.11	151.78	-0.33	153.18	1.06
V3_1 3	152.11	151.58	-0.53	153.25	1.14
V3_2 1	152.38	149.83	-2.55	151.55	-0.83
V3_2 2	152.38	149.22	-3.16	151.34	-1.05
V3_2 3	152.38	149.21	-3.18	150.92	-1.46
V4_1 1	193.25	199.12	5.87	196.99	3.73
V4_1 2	193.25	198.74	5.48	197.08	3.83
V4_1 3	193.25	198.73	5.48	197.23	3.98
V4_2 1	193.81	196.43	2.62	195.46	1.65

Table S4. (Continued)

Validation set		Model 2		Model 3	
Sample	**Reference (mg $CaCO_3$/g cement)**	**Predicted (mg $CaCO_3$/g cement)**	**Error (mg $CaCO_3$/g cement)**	**Predicted (mg $CaCO_3$/g cement)**	**Error (mg $CaCO_3$/g cement)**
V4_2 2	193.81	196.10	2.29	195.28	1.47
V4_2 3	193.81	195.92	2.11	195.66	1.85
V5_1 1	235.74	244.78	9.04	239.71	3.97
V5_1 2	235.74	244.38	8.65	239.81	4.07
V5_1 3	235.74	244.37	8.63	240.05	4.31
V5_2 1	236.46	238.76	2.31	236.43	-0.03
V5_2 2	236.46	238.66	2.21	236.67	0.21
V5_2 3	236.46	238.62	2.16	236.87	0.41
V6_1 1	276.66	282.38	5.72	279.43	2.77
V6_1 2	276.66	281.97	5.31	279.70	3.04
V6_1 3	276.66	281.64	4.98	279.68	3.02
V6_2 1	278.50	282.23	3.73	278.54	0.05
V6_2 2	278.50	281.40	2.90	277.98	-0.51
V6_2 3	278.50	281.06	2.56	278.19	-0.31
V7_1 1	319.58	325.62	6.04	326.85	7.27
V7_1 2	319.58	325.47	5.89	327.25	7.67
V7_1 3	319.58	325.48	5.90	327.44	7.86
V7_2 1	319.65	316.47	-3.18	314.82	-4.83
V7_2 2	319.65	316.13	-3.52	314.93	-4.71
V7_2 3	319.65	316.07	-3.58	315.03	-4.62
V8_1 1	360.40	359.14	-1.26	360.11	-0.29
V8_1 2	360.40	359.02	-1.39	360.48	0.08

Table S4. (Continued)

Validation set		Model 2		Model 3	
Sample	**Reference (mg $CaCO_3$/g cement)**	**Predicted (mg $CaCO_3$/g cement)**	**Error (mg $CaCO_3$/g cement)**	**Predicted (mg $CaCO_3$/g cement)**	**Error (mg $CaCO_3$/g cement)**
V8_1 3	360.40	358.87	-1.53	361.04	0.63
V8_2 1	360.45	358.86	-1.59	360.28	-0.17
V8_2 2	360.45	359.02	-1.43	360.38	-0.07
V8_2 3	360.45	358.93	-1.52	361.01	0.56
V9_1 1	403.45	406.95	3.50	406.53	3.08
V9_1 2	403.45	406.93	3.47	407.08	3.63
V9_1 3	403.45	406.76	3.31	407.71	4.25
V9_2 1	404.29	406.62	2.33	407.01	2.72
V9_2 2	404.29	406.41	2.12	407.42	3.13
V9_2 3	404.29	406.38	2.09	407.88	3.59
V10_1 1	445.33	447.31	1.98	448.49	3.16
V10_1 2	445.33	447.36	2.03	448.86	3.54
V10_1 3	445.33	447.30	1.98	449.17	3.84
V10_2 1	445.92	449.82	3.90	447.90	1.98
V10_2 2	445.92	449.82	3.89	448.46	2.54
V10_2 3	445.92	449.66	3.73	448.55	2.63

Model 2 - Pre-processing (MC; BC; SNV), Model 3 - Pre-processing (MC; BC; SNV; 1st Der), MC – mean centered; BC – baseline correction; SVN - standard normal variate; 1st Der - first derivative transformation

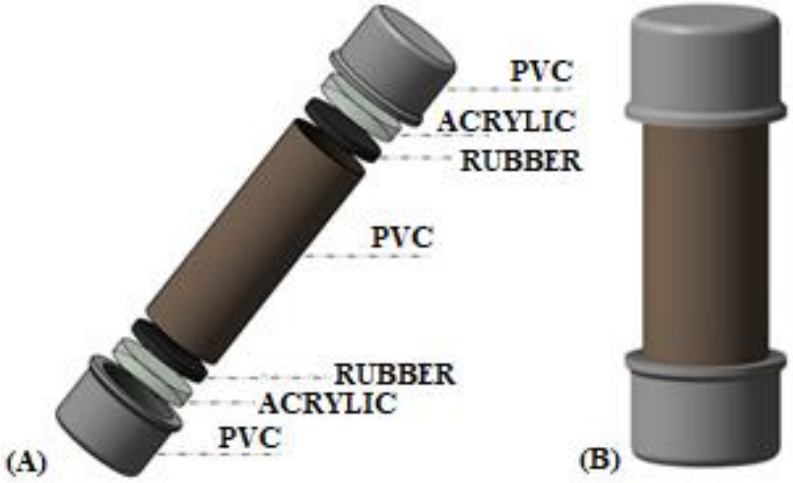

Figure S1. Cylindrical mold used to prepare the cement paste specimens

Carbonation degree of cement powder

Before developing the $CaCO_3$ quantification method in cement by FTIR, it was necessary to estimate the $CaCO_3$ content of the samples in an appropriate unit of measurement. In this context, mg $CaCO_3$/g cement was proposed as the appropriate unit of measurement. Thus, the $CaCO_3$ content of the samples was estimated using gas chromatography (GC) analysis. For the measurement, a calibration curve was prepared from the mixture of calcium carbonate ($CaCO_3$) with the non-carbonated cement powder (C1), the procedure is detailed below.

Initially, a calibration curve was prepared mixing 0 wt.% (C1), 2.5 wt.% (M-2.5), 5 wt.% (M-5), 10 wt.% (M-10), 20 wt.% (M-20), 75 wt.% (M-75) and 100 wt.% (M-100) of calcium carbonate (calcite $CaCO_3$ - 99.99%) with non-carbonated cement powder (C1). Then, a small amount (0.0027 to 0.0030 g) of each mixture was added to a vial sealed with butyl rubber stoppers and a septum lid. Thus, the sampling vials undergo a helium flush process for 5 minutes ($100mL \cdot min^{-1}$) to remove the atmospheric air. After purging, CO_2 from calcium carbonate was released from the reaction of $CaCO_3$ with phosphoric acid (H_3PO_4 - 85%) for 1 hour at 72 °C in a digestion block. The sample preparation method used in the present work is the same applied in studies of stable carbon isotope analysis ($\delta^{13}C$), which guarantees the complete and quantitative

conversion of the carbonate mineral fraction of the samples to CO_2 gas [1–4]. After preparation, the samples are immediately analyzed by gas chromatography (GC). The GC analysis was conducted in a GC-2014 (Shimadzu) equipped with a Carboxen Plot 1006 capillary column (30 m length, 0.53 mm ID), thermal conductivity detector (TCD), flame ionization detector (FID) and a 100-µL sampling loop. From the chromatographic analysis, the units of area (U.A) of CO_2, N_2 and O_2 were estimated. Nitrogen (N_2) and oxygen (O_2) were measured to normalize any differences in the efficiency of the helium flush step.

For the construction of the calibration curve the regression forced to cross the origin, the normalized unit of area (N.A) of CO_2 was used as the predictor variable (X) and the equivalent of mg $CaCO_3$/g cement as a response (Y). While the use of N.A allows to attenuate the differences in sample mass and in the efficiency of the helium flush, the regression crossing by origin allows to estimate the fraction of C1 that reacted with atmospheric CO_2 (natural carbonation). In this context, normalization was performed from Equation S1.

$$CO_2(N.A) = \frac{CO_2(U.A)}{\text{Sample mass (g)} \times N_2(U.A)} \quad (S1)$$

The description of the prepared samples and the results of the chromatographic analysis are presented in the Supplementary Material (Table S1 and Figure S2) and the calibration curve was obtained with an appropriate fit (R^2 = 0.9904). Thus, the calcium carbonate content of the non-carbonated (C1 - 45.80 mg $CaCO_3$/g cement) and carbonated (C11 - 468.20 mg $CaCO_3$/g cement) samples was estimated from linear regression. In addition, the theoretical maximum CO_2 uptake of cement can be estimated from its chemical composition (Table 1) and Equation S2 [5–7]. The mass percentage of CO_2 was calculated from the fraction of CaO, SO_3, MgO, Na_2O, and K_2O oxides and the maximum potential of API Class G cement (Table 1) is 53.03 wt.% of the material. Then, the carbonation degree of the non-carbonated (C1 - 45.80 mg $CaCO_3$/g cement) and carbonated (C11 - 468.20 mg $CaCO_3$/g cement) samples were

estimated from Equation S3, as a ratio between the estimated CO_2 uptake compared to the theoretical maximum. A fraction of 2.01 wt.% of CO_2 was estimated in C1 sample (non-carbonated), representing 3.80% of carbonation degree, while the carbonated cement powder sample (C11) presented 20.59 wt.% of CO_2 uptake and 38.82% of carbonation degree.

$$Max\ CO_2\ uptake\ (\%) = 0.785(CaO - 0.7SO_3) + 1.091MgO + 1.420Na_2O + 0.935K_2O \quad (S2)$$

$$Carbonation\ degree\ (\%) = 100\ x\ \frac{CO_2\ uptake}{max\ CO_2\ uptake} \quad (S3)$$

From the results, it was observed that the non-carbonated cement powder (C1) underwent a partial process of natural carbonation, while the carbonated cement powder (C11) was considerably transformed from the reaction with supercritical CO_2. Thus, this information is essential for the FTIR-based method and was considered throughout the quantitative model development to estimate the $CaCO_3$ content in cement.

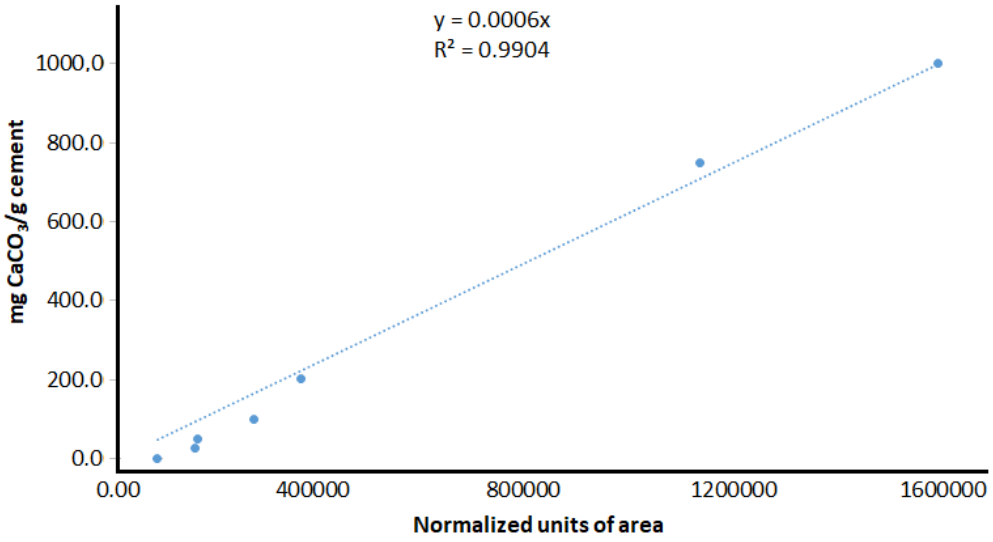

Figure S2. Regression between calcium carbonate ($CaCO_3$) content in cement and gas chromatography data (normalized unit of area)

Carbonation of cylindrical cement specimens

Initially, the carbonation process of cylindrical cement specimens by supercritical CO_2 was evaluated to identify the patterns of the transformation processes and to reproduce the results of the previous literature. Thus, the API class G cement specimens were exposed to a reaction medium (65 °C and 150 bar) compatible with the conditions found in CCS wells. Figure S3 shows the result of the phenolphthalein test of a longitudinal section of the cement specimen after exposure to supercritical CO_2.

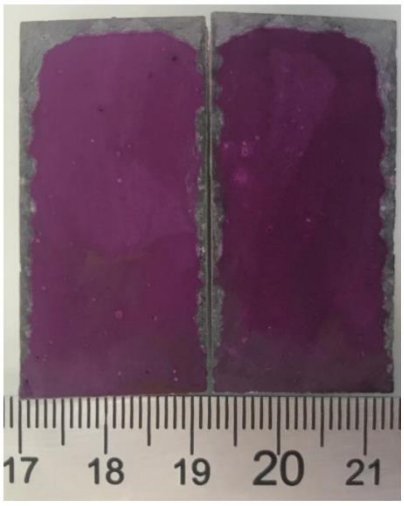

Figure S3. API class G cement after carbonation process with supercritical CO_2

From Figure S3, it was observed that supercritical CO_2 permeated into the cement matrix and reacted with the material. As Portland cement has an alkaline reserve of portlandite (CH), phenolphthalein highlights in pink the preserved portion of the material (pH above 9), while the carbonated fraction remains unpigmented (grey) [8, 9]. Thus, it was possible to observe a significant non-pigmented area (carbonated cement) in the boundaries of the cement specimen with 1.25 mm (± 0.58 mm) depth average. In the non-pigmented fraction, it can be concluded that the portlandite (CH) fraction was completely depleted. However, the carbonation process continues from the consumption of other cement compounds sensitive to CO_2, such as calcium silicate

hydrate (C-S-H). In this context, CO_2 reactions with portlandite (CH), calcium silicate hydrate (C-S-H) and non-hydrated cement (C_2S and C_3S), result in the production of $CaCO_3$, amorphous silica and other degradation products. On the other hand, the pink highlighted area in the center of the cement sample preserved significant fraction of the alkaline reserve and kept the pH of the material high. This means that supercritical CO_2 did not reach the area or only partially reacted with the cement matrix.

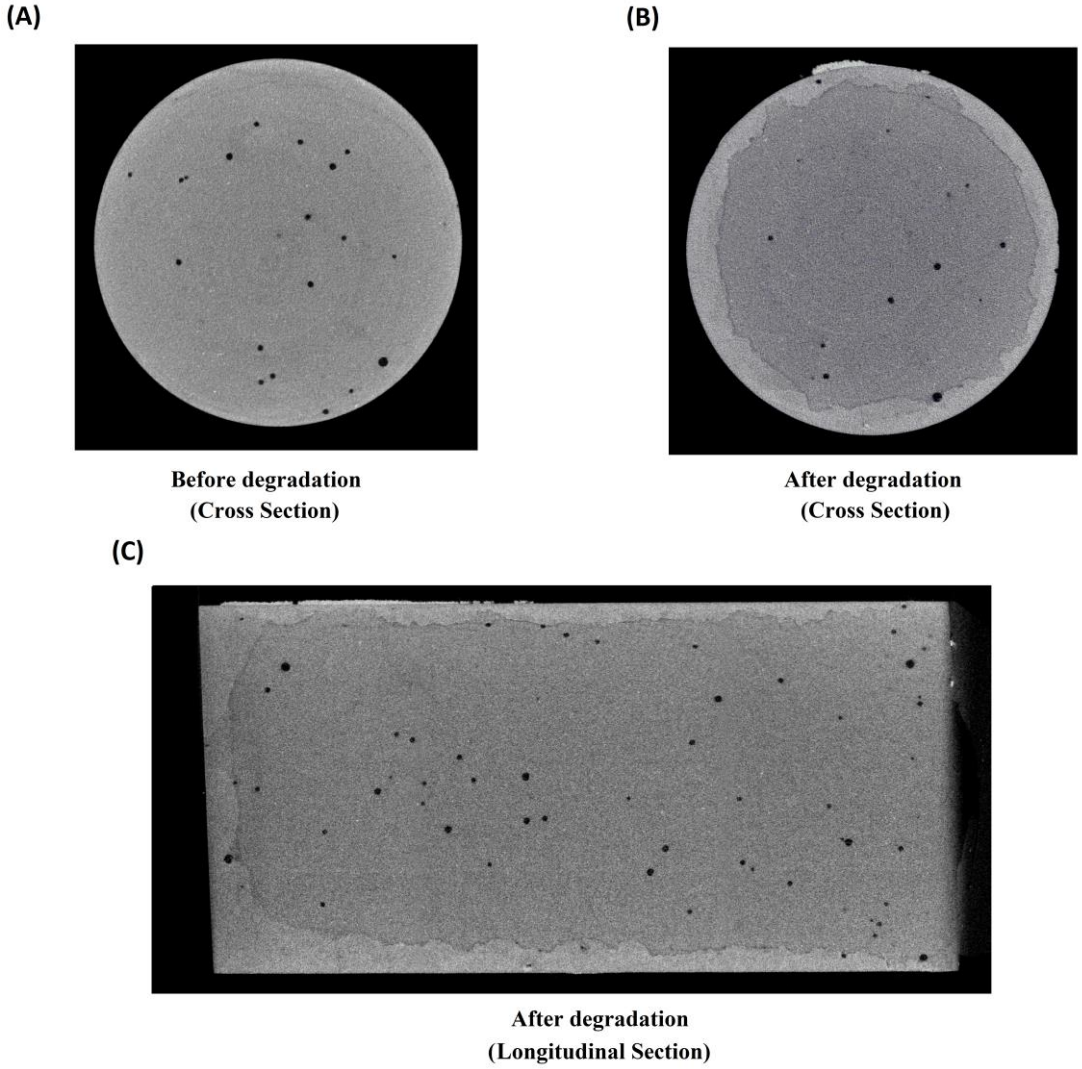

Figure S4. MicroCT images of cement specimen's: (A) cross-section before carbonation tests, (B) cross-section after carbonation tests and (C) longitudinal section after carbonation tests

Although it is a fast and low-cost method, the phenolphthalein test provides no information on the carbonation process step or quantitative data on the content of $CaCO_3$. Because it is a qualitative colorimetric method, the phenolphthalein test underestimates the extent of the carbonation process when compared to classic methods such as XRD diffraction [9]. Furthermore, from the pH indicator, it was not possible to identify whether the decalcification process starts at the edges of the cement specimens. Thus, to deepen the study of the carbonation process, the cement specimens were evaluated by X-ray microtomography (MicroCT). From the MicroCT, it was possible to: (*i*) study the structural changes of the cement specimens exposed to CO_2 and (*ii*) evaluate the changes in the density and porosity of the material [10–12]. For that, the same cement specimen was evaluated before and after exposure to supercritical CO_2 and the results are shown in Figure S4.

From Figure S4, it was possible to observe the transformations that occur in the same cement specimen before and after the reaction with CO_2. Denser mineral phases, such as $CaCO_3$, was identified as brighter spots, while the lighter microconstituents, such as aqueous solution and porosity, were represented as darker areas [13]. From Figure S4A, it was observed that the cement specimen after the curing process has a homogeneous structure characterized by the isochromatic pigmentation of the matrix. In addition, the presence of small dark spots on the material indicates the presence of macropores filled with solution or gases. On the other hand, in Figures S4B and S4C, the bright gray area at the edge of the cement specimen (not seen in Figure S4A) results from the reaction between CO_2 and cement minerals and indicates the formation of a denser carbonated layer. According to Han *et al.* [13], the higher density area (bright gray) is the result of the $CaCO_3$ precipitation process produced from CO_2 and cement matrix reactions, consuming portlandite (CH) and C-S-H fractions and resulting in pore filling and reducing material permeability. From MicroCT results (Figures S4B and S4C), it was estimated that the carbonated volume of the material is approximately 20.40%, significantly higher than that obtained by the phenolphthalein test (11.36 ± 5.28%). In addition to the carbonated volume, it was possible to estimate the macroporosity of the cement specimen before (Figure S4A)

and after (Figures S4B and S4C) its exposure to supercritical CO_2. From the analysis of image data, reduction in the macroporosity from 0.49% (before) to 0.40% (after) was identified. Thus, the results indicate that cement carbonation process is in its first stages, in which the $CaCO_3$ precipitation step and pore filling effect are more significant than decalcification and Ca^{2+} leaching processes from the material matrix.

After identifying that the carbonation process consumed the cement alkaline reserve (Figure S3), resulting in the precipitation of $CaCO_3$ and in reducing the porosity of the material (Figure S4), it was necessary to further characterize the material to evaluate changes in the material's microstructure. Thus, scanning electron microscopy (SEM) coupled with elemental mapping by energy-dispersive X-ray spectroscopy (EDS) was applied to study the morphological and microstructural changes of cement specimens after supercritical CO_2 exposure. The results of microscopy and elemental mapping analyses of calcium (Ca) and silicon (Si) are shown in Figure S5.

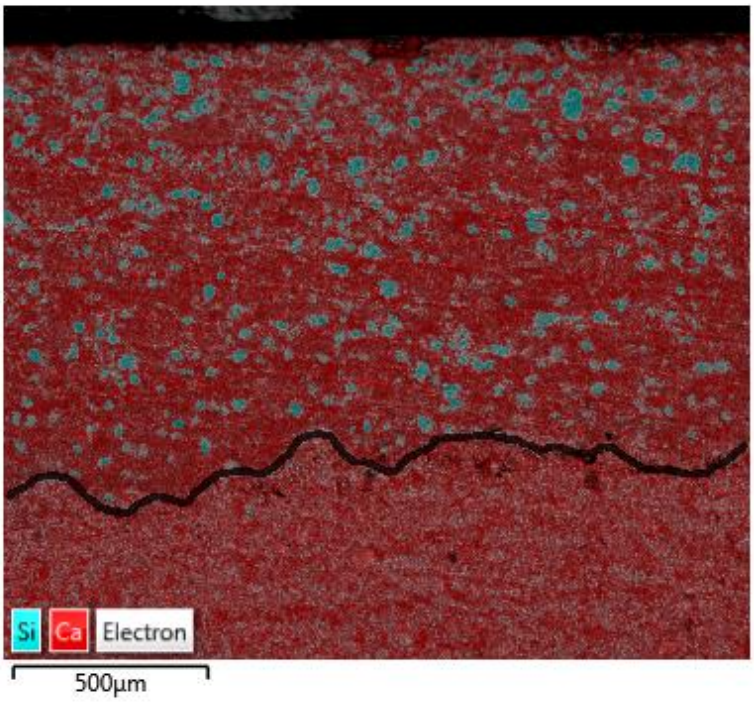

Figure S5. Ca and Si elemental distribution in the non-carbonated and carbonated phases of the cement specimen

From Figure S5, it was possible to identify a clear boundary line between the carbonated and non-carbonated phases and delimiting the carbonation front in the cement specimen. While the non-carbonated phase in the center of the material keeps its microstructure cohesive, the carbonated cement specimen edge shows a reduction in porosity and an increase in the heterogeneity of the cement matrix. Thus, the formation of calcium-rich (with a high $CaCO_3$ concentration) and silicon-rich (with high content of amorphous silica) phases in the carbonated zone are highlighted in the elementary mapping by SEM-EDS (Figure S5). This microstructure profile for the carbonated cement zone was previously reported in the literature, in which $CaCO_3$ precipitation occurs between and around the decalcified C-S-H and amorphous silica phases [14–16]. From a structural point of view, this modification results in material integrity loss [17], while for CO_2 capture and mineralization, it leads to a delay in the weathering process due to the passivation conferred by $CaCO_3$ covering the unreacted cement grains [15].

After the study and comprehensive characterization of the cement specimen exposed to supercritical CO_2, it was possible to observe a series of characteristics that must be considered in the development of methods to quantify $CaCO_3$ in carbonated cementitious materials, either by: (*i*) natural carbonation, (*ii*) carbonation curing, (*iii*) accelerated carbonation (with exposure to supercritical CO_2) or (*iv*) mineral sequestration. Cement matrix undergoes certain physical and chemical transformations that mainly result in the portlandite (CH) consumption and the calcium silicate hydrate (C-S-H) decalcification with the production of $CaCO_3$ and siliceous products. Thus, it was expected that these significant material changes will be reflected in the FTIR spectrum profile, and their effects must be considered in the quantification of $CaCO_3$ in cementitious materials to increase the method reliability.

References (Supplementary Material)

[1] S.F.M. Breitenbach, S.M. Bernasconi, Carbon and oxygen isotope analysis of small carbonate samples (20 to 100 µg) with a GasBench II preparation device, Rapid Commun. Mass Spectrom. 25 (**2011**) 1910–1914. doi:10.1002/rcm.5052.

[2] D. Paul, G. Skrzypek, Assessment of carbonate-phosphoric acid analytical technique performed using GasBench II in continuous flow isotope ratio mass spectrometry, Int. J. Mass Spectrom. 262 (**2007**) 180–186. doi:10.1016/j.ijms.2006.11.006.

[3] G. Skrzypek, D. Paul, $\delta^{13}C$ analyses of calcium carbonate: comparison between the GasBench and elemental analyzer techniques, Rapid Commun. Mass Spectrom. 20 (**2006**) 2915–2920. doi:10.1002/rcm.2688.

[4] D. Paul, G. Skrzypek, Flushing time and storage effects on the accuracy and precision of carbon and oxygen isotope ratios of sample using the Gasbench II technique, Rapid Commun. Mass Spectrom. 20 (**2006**) 2033–2040. doi:10.1002/rcm.2559.

[5] T. Chen, M. Bai, X. Gao, Carbonation curing of cement mortars incorporating carbonated fly ash for performance improvement and CO_2 sequestration, J. CO_2 Util. 51 (**2021**) 101633. doi:10.1016/j.jcou.2021.101633.

[6] W. Ashraf, Carbonation of cement-based materials: challenges and opportunities, Constr. Build. Mater. 120 (**2016**) 558–570. doi:10.1016/j.conbuildmat.2016.05.080.

[7] H.H. Steinour, Some effects of carbon dioxide on mortars and concrete-discussion, J. Am. Concr. Inst. 30 (**1959**) 905–907.

[8] A.R. Duggan, J. Goggins, E. Clifford, B.A. McCabe, The use of carbonation depth techniques on stabilized peat, Geotech. Test. J. 40 (**2017**) 20160223. Doi: 10.1520/GTJ20160223.

[9] A. Ranjan, R. Kumar, D. Mohan, Comparative analysis of phenolphthalein indicator, XRDA and FTIR methods for measurement of carbonation depth of concrete, Int. J. Civ. Eng. Technol. 9 (**2018**) 315–320.

[10] L.W. Zhang, X.X. Miao, Y. Wang, X.W. Cheng, K. Ellett, M.G. Gan, X.J. Fu, S.N. Liu, X.C. Li, A novel index to evaluate CO_2-induced wellbore cement degradation in CO_2 rich environment, IOP Conf. Ser. Earth Environ. Sci. 570 (**2020**) 062017. doi:10.1088/1755-1315/570/6/062017.

[11] E.A. Chavez Panduro, M. Torsæter, K. Gawel, R. Bjørge, A. Gibaud, Y. Yang, S. Bruns, Y. Zheng, H.O. Sørensen, D.W. Breiby, In-situ X-ray tomography study of cement exposed to CO_2 saturated brine, Environ. Sci. Technol. 51 (**2017**) 9344–9351. doi:10.1021/acs.est.6b06534.

[12] E.A. Chavez Panduro, B. Cordonnier, K. Gawel, I. Børve, J. Iyer, S.A. Carroll, L. Michels, M. Rogowska, J.A. McBeck, H.O. Sørensen, S.D.C. Walsh, F. Renard, A. Gibaud, M. Torsæter, D.W. Breiby, Real time 3D observations of Portland cement carbonation at CO_2 storage conditions, Environ. Sci. Technol. 54 (**2020**) 8323–8332. doi:10.1021/acs.est.0c00578.

[13] J. Han, W. Sun, G. Pan, X-ray microtomography of the carbonation front shape evolution of cement mortar and modeling of accelerated carbonation reaction, J. Wuhan Univ. Technol. Sci. Ed. 28 (**2013**) 303–308. Doi: 10.1007/s11595-013-0683-8.

[14] V. Shah, K. Scrivener, B. Bhattacharjee, S. Bishnoi, Changes in microstructure characteristics of cement paste on carbonation, Cem. Concr. Res. 109 (**2018**) 184–197. doi:10.1016/j.cemconres.2018.04.016.

[15] B. Šavija, M. Luković, Carbonation of cement paste: understanding, challenges, and opportunities, Constr. Build. Mater. 117 (**2016**) 285–301. doi:10.1016/j.conbuildmat.2016.04.138.

[16] K. Vance, G. Falzone, I. Pignatelli, M. Bauchy, M. Balonis, G. Sant, Direct carbonation of $Ca(OH)_2$ using liquid and supercritical CO_2: implications for carbon-neutral cementation, Ind. Eng. Chem. Res. 54 (**2015**) 8908–8918. doi:10.1021/acs.iecr.5b02356.

[17] L. Li, M.H. Hubler, Y. Xi, Theoretical modeling on chemical composition and mechanical properties of well cement under carbonation reactions, J. Clean. Prod. 276 (**2020**) 124270. doi:10.1016/j.jclepro.2020.124270.

4.2. Geoquímica isotópica

Evaluation of the potential of stable isotope methods to study the cement carbonation process in Carbon Capture and Storage wells

Abstract

The potential of stable isotope ($\delta^{13}C$) methods to study the carbonation of cementitious materials (cement, portlandite [CH] and calcium silicate hydrate [C-S-H]) were studied. From the results, it was identified that the solution pH and the mineral phases (CH and C-S-H) solubility and pH influenced the kinetic and thermodynamic factors and the equilibrium/distribution of carbon isotopes throughout the system. From data analysis, it is suggested that the CO_2 pressure acts on the pH of the medium and on the activity of DIC species. However, have a small influence on the isotopic signature ($\delta^{13}C$) and isotopic enrichment factors (ε), while temperature was not identified to be a significant parameter. In addition, the following conclusions were reached: *i*) enriched $\delta^{13}C$-DIC and higher $\varepsilon_{DIC\text{-}CO2}$ are related to solutions with higher pH, *ii*) enriched $\delta^{13}C$-$CaCO_3$ and higher $\varepsilon_{CaCO3\text{-}DIC}$ indicate the $CaCO_3$ precipitation under a higher thermodynamic equilibrium and were associated with solutions with higher DIC content, higher electrical conductivity (EC) and lower pH, *iii*) mineral carbonate generated from carbonation of cement, CH, and C-S-H preserves the isotopic signature of the $\delta^{13}C$-CO_2 source with a small or insignificant isotopic fractionation ($\varepsilon_{CaCO3\text{-}CO2}$) and *iv*) the $\varepsilon_{CaCO3\text{-}DIC}$ regulates the overall isotopic fractionation of the carbonation process ($\varepsilon_{CaCO3\text{-}CO2}$).

Keywords: Wellbore integrity; degradation by CO_2; cement carbonation; isotope geochemistry; stable isotope

1. Introduction

Emissions of greenhouse gases (GHG), especially carbon dioxide (CO_2), are among the main modern environmental concerns. CO_2 has been identified as one of the main drivers of global warming, comprehensively affecting the entire ecosystem of planet Earth and causing harmful effects to the environment (*et al.*, 2005; Zhang *et al.*, 2021). Thus, global efforts have been made to propose solutions to mitigate the impacts associated with GHG emissions and develop technologies with better environmental performance, without significant changes to technical and economic requirements. In this context, Carbon Capture and Storage (CCS) technologies were identified as one of the most important solutions to support the transition to a low carbon economy (Bai *et al.*, 2016; Tiong *et al.*, 2019).

CCS technologies involve the processes of CO_2 capture, transport, and long-term geological storage. The CO_2 geological storage must consider: (*i*) selection of the target reservoir, normally depleted oil and gas reservoirs, unexplored coal seams and/or deep saline aquifers, (*ii*) well drilling and cementation in order to access deep geological sections, (*iii*) CO_2 injection plant operation, (*iv*) study of reservoir CO_2 dynamics, (*v*) monitoring of potential leaks and (*vi*) permanent and safe abandonment of structures (Schulz *et al.*, 2012; Zimmer *et al.*, 2018). CCS sensitive issues, such as cement degradation/integrity processes in CO_2-rich environments and the dynamics and monitoring of CO_2 injected into the geological reservoir, have been addressed in recent literature. Despite this, other points related to the identity of the gas in different extensions of the reservoir and the origin of CO_2 involved in well cement degradation processes has not been studied extensively and require a combined approach between the topics of well integrity and CCS operation monitoring.

Portland cement is the most common type of cementitious material and about 95% of well drilling projects use API class G cement (L. Li *et al.*, 2020). Portland cement

is mostly composed of four main constituents, which are: tricalcium silicate (C_3S - Ca_3SiO_5 - alite), dicalcium silicate (C_2S - Ca_2SiO_4 - belite,), tricalcium aluminate (C_3A - $Ca_3Al_2O_6$ - celite) and tetracalcium aluminoferrates (C_4AF - $Ca_4Al_2Fe_2O_{10}$ - brownmillerite) (Omosebi *et al.*, 2016; Paris *et al.*, 2016). Cement cure involves the hydration of these compounds, resulting in the production of calcium silicate hydrate (C-S-H), a semi-amorphous phase, and portlandite [CH - calcium hydroxide - $Ca(OH)_2$], a crystalline alkaline mineral (Abid *et al.*, 2018; Gu *et al.*, 2017). While C-S-H acts as a bonding agent and comprises about 70% of the mass fraction of cement, CH serves as an alkaline reserve of the material and represents 15-20% of the cement weight (Gu *et al.*, 2017; Wakeel *et al.*, 2019). Both cement phases (CH and C-S-H) are sensitive to CO_2, whose reactive processes results in the production of calcium carbonate ($CaCO_3$) polymorphs, siliceous derivatives, and loss of material integrity (Park *et al.*, 2021; Šavija and Luković, 2016). This degradation process has been extensively documented in experimental studies (Ponzi *et al.*, 2021; Teodoriu and Bello, 2020), and in full-scale CCS wells (Carey *et al.*, 2007; Crow *et al.*, 2010; Duguid *et al.*, 2017, 2014).

Throughout the operation process of a CCS well, a series of operational issues, physical, chemical and/or mechanical processes, can compromise material integrity and produce preferential paths (*e.g.*, fractures, microannuli, mud channels and gaps) for the leakage of injected CO_2 (Lu *et al.*, 2011; Wiese *et al.*, 2013). However, based on the methods currently used to monitor the carbonation process, it is not possible to identify the origin of the CO_2 (injection gas or endogenous fluids from the geological formation) that induced cement degradation processes. Thus, it is not possible to guide the best mitigation strategy for an eventual partial or catastrophic failure, either through well cementation (corrective or *plug* and permanent abandonment) or through the recovery of CCS reservoir failures.

Studying the dynamics of injected CO_2 in the reservoir and monitoring its displacement throughout the geological storage site is a subject of great interest for

CCS projects. Even though CCS is already a proven technology, there is still a need to carry out the development of new methods and tools to track and monitor CO_2 during and after injection (Iglesias *et al.*, 2019). Current CO_2 monitoring technologies range from direct and indirect measurements focused on the CCS reservoir, to environmental monitoring of sections close to the surface (shallower geological sections) or to assess the occurrence of CO_2 leaks to the atmosphere (Van Geldern *et al.*, 2014; Vermeul *et al.*, 2016). Thus, stable isotope methods are important tools to identify the migration and fate of injected CO_2 along the geological storage site and to monitor the efficiency of the CO_2 mineralization process. However, there are still gaps in the potential of isotopic analysis methods to monitor the cement degradation process and assess the vertical displacement of the CO_2 plume, especially in areas adjacent to wells and through the structural interfaces (formation-cement and cement-casing).

In this context, carbon isotope signatures ($\delta^{13}C$) have already been used as a chemical tracer to monitor the CO_2 injection process in CCS reservoirs and to study the dynamics of reactive transport along the percolation of the CO_2 plume through the geological storage site (Barth *et al.*, 2015; Mayer *et al.*, 2015; Wiese *et al.*, 2013; Zimmer *et al.*, 2018). $\delta^{13}C$-CO_2 value can be used to: (*i*) identify injected CO_2 leakage, (*ii*) verify the subsurface distribution of the CO_2 plume and (*iii*) evaluate the proportion of injected CO_2 versus original gases from the reservoir (endogenous gas) (Barth *et al.*, 2015; Johnson *et al.*, 2011; Mayer *et al.*, 2015). However, the differences in isotopic composition between injected and "native" fluids are essential to stable isotope methods achieve their goals (Vermeul *et al.*, 2016).

Cement carbonation and CO_2 monitoring in the reservoir are topics widely documented in the scientific literature. The carbonation of cement can cause integrity loss of CCS wells and lead to financial losses of millions of dollars, resulting in a reduction or shutdown in the CO_2 injection process, reservoir fluid leakages and incalculable environmental damages. Thus, the development of tools able to differentiate injected CO_2 from the endogenous fluids of the storage site can reduce

the time and allocation of financial resources involved in monitoring processes, investigating the cause of engineering failures and developing quick and accurate corrective actions. However, there is a lack of studies that assess the origin of the gas involved in the process of well integrity loss and that monitor any vertical displacements of the CO_2 plume along well vicinity and through its interfaces (formation-cement and cement-casing).

Recently, studies in a pilot well in Ketzin (Germany) used the CO_2 content and its isotope signature ($\delta^{13}C$-CO_2) to understand the vertical distribution of the CO_2 plume along the outer section of the well (around the cement sheath) and discriminate its origin (Barth *et al.*, 2015). From this study, it was possible to identify that the CO_2 in the adjoining section to the well had a signature compatible with the injected gas due to failures at the well interface or reservoir fractures that allowed the migration of the CO_2 plume to shallower geological sections. However, issues related to the integrity of well materials were not evaluated by the authors (Barth *et al.*, 2015). Furthermore, there are a limited number of studies that performed cement isotopic analysis from carbonated wells (Carey *et al.*, 2007; Gaboreau *et al.*, 2012; Manceau *et al.*, 2016), and none of the authors discussed in a comprehensive way the importance and applicability of these results. Among previous results of wells cement isotope analysis, Carey *et al.* (2007) reported clear signs of cement carbonation in intermediate sections of a 30 years operation at SACROC Unit, Texas (USA). In this work, different intensities of carbonation signs were identified at the interfaces (cement-steel and cement-rock) and the isotopic analysis method was used to discriminate the origin of the gas that induced the degradation process. Based on the results, the authors suggested that carbonates were generated in environments with different degrees of CO_2 exposure. However, the lack of information on the isotopic signature of the gases (injected CO_2 and endogenous gas from the reservoir), as well as on the isotopic fractionation processes of the studied system, did not allow them to obtain any strong hypothesis to identify the origin of the CO_2 that degraded the well materials (Carey *et al.*, 2007).

So far, it was observed that stable isotope methods are important tools to identify the migration and fate of injected CO_2 along the geological storage site and to monitor the efficiency of the CO_2 mineralization process (Myers *et al.*, 2019). Within this framework, isotope techniques can help to improve understanding of the subsurface chemical processes as well as increase the efficiency of monitoring programs (Van Geldern *et al.*, 2014). In the literature, it has been noted that well monitoring based on isotopic analysis tools requires reliable fingerprint information for all elements of the studied system, as well as data on any temporal changes in $\delta^{13}C$ during CO_2 injection (Flude *et al.*, 2017; Śliwiński *et al.*, 2017). Therefore, it was observed that there are still gaps about the potential of isotopic analysis methods to monitor CO_2 plume vertical displacement, especially in areas adjacent to wells and through the structural interfaces (formation-cement and cement-casing). To contribute to the well integrity and CCS research topics, the present work proposes to evaluate the use of isotopic geochemistry methods to study cement carbonation process of wells exposed to CO_2-rich environments. The potential of stable isotopic methods ($\delta^{13}C$) to identify the origin of CO_2 consumed in cementitious material carbonation was studied and the occurrence of isotopic fractionation processes among the phases (gas, liquid and solid) of the reaction system was evaluated.

2. Materials and Methods

2.1. Materials

Calcium oxide (95%), calcium carbonate (99.9%), sodium carbonate (99%), silicon oxide (Neon - 95%), phosphoric acid (85%) and phosphoric acid (99%) were used without further purification. The gases used were: (*i*) carbon dioxide - CO_2 (99.5%) for carbonation reactions, (*ii*) carbon dioxide - CO_2 (Air Products - 99.99%) for isotopic analysis and (*iii*) Helium - He (Air Products - 99.999%) as carrier gas and sample preparation. For isotopic analysis, the following standards were applied: (*i*) the reference material NIST® RM 8543 (NBS18 - $CaCO_3$) with a carbon ($\delta^{13}C$-$CaCO_3$) isotopic signature of -5.01 ± 0.07 ‰ and (*ii*) the CM-1 in-house $CaCO_3$ standard with

a carbon ($\delta^{13}C$-$CaCO_3$) isotopic signature of +2.12 ± 0.20 ‰ (1SD - standard deviation from routine control chart). Both isotopic values ($\delta^{13}C$) are given using a Vienna Peedee Belemnite (VPDB) standard. The chemical composition of the API class G cement (Lafarge Holcim) applied in this study is shown in Table 1.

Table 1. API Class G cement composition

Chemical composition	Percentage [%]
SiO_2	29.25
Al_2O_3	3.95
Fe_2O_3	4.57
CaO	65.07
MgO	2.32
SO_3	2.27
Na_2O	0.25
K_2O	0.33

2.2. Sample preparation

2.2.1. Preparation of cement paste powder

Class G cement paste was prepared following the API 10A procedures from American Petroleum Institute (API Specification, 2010). The hydrated cement specimens were prepared with no additives, 0.44 water-to-cement ratio and using cylindrical molds (Supplementary Material - Figure S1). The cement paste curing process was performed in a thermostatic bath at 65°C for 14 days. Class G hydrated cement powder were obtained from the ball milling process with a grinding steel ball loading of: Ø50 mm balls (5 units), Ø40 mm balls (5 units), Ø32 mm balls (5 units), Ø15 mm balls (5 units), Ø25 mm balls (24 units), Ø19 mm balls (15 units) and Ø10 mm balls (21 units). The non-carbonated hydrated cement powder comprises the fraction of the material passing through the #270 mesh sieve and was stored in a desiccator until the carbonation experiments.

2.2.2. Preparation of Portlandite (CH)

Synthetic portlandite (CH) was prepared by hydrating calcium oxide with a water-to-solid ratio of 10:1 and stirring overnight. Then, the synthetic CH was filtered, and oven dried at 80°C for 24h.

2.2.3. Preparation of synthetic calcium silicate hydrate (C-S-H)

Calcium silicate hydrate (C-S-H) is a Portland cement hydration product and the most representative phase of cementitious materials. The ratio between calcium/silicon (C/S) in the C-S-H of Portland cement has an average of 1.75, ranging from 1.3 to 2.1 (Tajuelo *et al.*, 2017). In the present work, synthetic hydrated calcium silicate was prepared using the hydrothermal procedure by mixing the CaO slurry with amorphous SiO_2 in an autoclave. The synthesis was carried out with a Ca/Si molar ratio of 1.7:1, a water-to-solid ratio of 10:1, a temperature of 95 °C and mixing for 72h with a stirring speed of 400 rpm (Falzone *et al.*, 2021; Y. Li *et al.*, 2020). Then, the synthetic C-S-H was filtered, and oven dried at 80°C for 24h. The actual measure of the Ca/Si ratio of synthetic C-S-H was subsequently characterized by XRD.

2.3. Carbonation of cementitious materials

Carbonation of cementitious materials experiments (class G cement powders, CH, and C-S-H) were conducted in a high pressure-high temperature (HPHT) pressure vessel (Figure S2) under CO_2-rich environment. The experimental setup used aims to simulate the environment of the Carbon Capture and Storage (CCS) wells. Reactions with powdered materials were applied to accelerate reaction processes and material flow between the phases (gas/liquid/solid) and the quasi-static reaction medium adopted as the most representative of the geological well system (Park *et al.*, 2021; Teodoriu and Bello, 2020).

2.3.1. Cement paste samples

For the study of cement powder carbonation, a factorial design was applied varying the temperature (30 °C, 65 °C and 100 °C) and pressure (50 bar, 100 bar, 150 bar) of the reaction medium, resulting in a total of 9 experiments detailed in Table 2. Thus, Experiments 1-3 were conducted in a subcritical CO_2 medium, while Experiments 4-9 were performed in a supercritical CO_2 environment (CO_2 pressures greater than 73.9 bar and temperatures above 31.1 °C) (Celia *et al.*, 2015; Šavija and Luković, 2016). The reactions were developed in the HPHT reactor with a water-to-solid ratio of 10:1, ultrapure water, and CO_2-rich environment for 7 days. After the carbonation reaction, the carbonated cement powders were filtered, oven dried at 80°C for 24h and characterized. In addition, the liquid fraction of the reaction medium was reserved for the analysis of pH, electrical conductivity (EC), DIC content and isotopic signature. In the present work, it is understood as "liquid fraction" the filtered solution resulting from the depressurization process of the HPHT reactors followed by 24h of liquid equilibrium with the sampling vial headspace. The initial isotopic signature of the CO_2 cylinder was analyzed, and the final isotopic gas analysis was performed to evaluate the isotopic fractionation process.

Table 2. Description of cement powder carbonation experiments

Experiments	Sample	Pressure (bar)	Temperature (°C)	Time (days)
1	C50_30	50	30	7
2	C50_65	50	65	7
3	C50_100	50	100	7
4	C100_30	100	30	7
5	C100_65	100	65	7
6	C100_100	100	100	7
7	C150_30	150	30	7
8	C150_65	150	65	7
9	C150_100	150	100	7

2.3.2. Synthetic C-S-H and CH samples

The carbonation study of synthetic C-S-H and CH were conducted under fixed reaction conditions. Thus, a duplicate carbonation reaction of portlandite (CH_R1 and CH_R2) and calcium silicate hydrate (C-S-H_R1 and C-S-H_R2) was performed at 65 °C and 150 bar in the HPHT reactor with a water-to-solid ratio of 10:1, ultrapure water, and CO_2-rich environment for 7 days. After the carbonation reaction, the carbonated portlandite (CH_R1 and CH_R2) and degraded calcium silicate hydrate (C-S-H_R1 and C-S-H_R2) was filtered, oven dried at 80 °C for 24 h and characterized. In addition, the liquid fraction of the reaction medium was reserved for the analysis of pH, electrical conductivity, DIC content and isotopic signature. The handling and storage of the liquid fraction was conducted as previously described. The initial isotopic signature of the CO_2 cylinder was analyzed to evaluate the isotopic fractionation process related to carbonation of synthetic C-S-H and CH .

2.3.3. Cementitious material carbonation reactions

In the present work, the carbonation process was performed in an aqueous medium to simulate the environment of the Carbon Capture and Storage (CCS) wells. The carbonation process modifies the chemical structure of non-hydrated cement fractions (C_3S and C_2S) and the hydrated portlandite (CH) and calcium silicate hydrate (C-S-H) phases of the cement, resulting in the production of calcium carbonate ($CaCO_3$) polymorphs (amorphous, calcite and aragonite) and siliceous fractions, mostly amorphous silica (Koukouzas *et al.*, 2017; Tiong *et al.*, 2019). Thus, the most representative reactions of cementitious material carbonation processes are presented by Equations 1-8 (Carey *et al.*, 2007; Crow *et al.*, 2010; Duguid *et al.*, 2017, 2014).

$$C_2S_{(s)} + 3CO_{2(aq)} + nH_2O_{(l)} \rightarrow SiO_2.nH_2O_{(s)} + 3CaCO_{3(s)} \quad (1)$$

$$C_3S_{(s)} + 3CO_{2(aq)} + nH_2O_{(l)} \rightarrow SiO_2.nH_2O_{(s)} + 3CaCO_{3(s)} \quad (2)$$

$$Ca(OH)_{2(s)} + HCO_3^-{}_{(aq)} + H^+{}_{(aq)} \rightarrow CaCO_{3(s)} + 2H_2O_{(l)} \quad (3)$$

$$Ca(OH)_{2(s)} + CO_3^{2-}{}_{(aq)} + 2H^+{}_{(aq)} \rightarrow CaCO_{3(s)} + 2H_2O_{(l)} \quad (4)$$

$$\mathrm{C-S-H}_{(s)} + HCO_3^-{}_{(aq)} + H^+{}_{(aq)} \rightarrow CaCO_{3(s)} + SiO_xOH_{x(s)} \quad (5)$$

$$\mathrm{C-S-H}_{(s)} + CO_3^{2-}{}_{(aq)} + 2H^+{}_{(aq)} \rightarrow CaCO_{3(s)} + SiO_xOH_{x(s)} \quad (6)$$

$$CaCO_{3(s)} + 2H^+{}_{(aq)} \leftrightarrow CO_{2(g)} + H_2O_{(l)} + Ca^{2+}{}_{(aq)} \quad (7)$$

$$CaCO_{3(s)} + CO_{2(g)} + H_2O_{(l)} \leftrightarrow Ca^{2+}{}_{(aq)} + HCO_3^-{}_{(aq)} \quad (8)$$

2.4. Sample characterization

This work used the following characterization methods: (*i*) electrical conductivity and pH analysis, (*ii*) Fourier transform infrared spectroscopy (FTIR), (*iii*) X-ray diffraction analysis (XRD), (*iv*) scanning electron microscopy (SEM), (*v*) determination of $CaCO_3$ content in cement from the FTIR-based PLS model, (*vi*) analysis of dissolved inorganic carbon (DIC) content and (*vii*) stable isotope analysis of CO_2 (δ^{13}C-CO_2), DIC (δ^{13}C-DIC) and $CaCO_3$ (δ^{13}C- $CaCO_3$). The experimental procedures are detailed below.

2.4.1. Electrical conductivity and pH analysis.

The pH and electrical conductivity measurements were performed on the resulting liquid fraction after the cementitious material carbonation process. The samples were analyzed at room temperature using a Metrohm bench pH meter and electrical conductivity meter.

2.4.2. Fourier transform infrared spectroscopy (FTIR)

FTIR spectra were acquired through a PerkinElmer Spectrum 100 instrument with a Universal Attenuated Total Reflectance (ATR) accessory. Infrared spectra were recorded in the range of 4000 to 650 cm^{-1}, resolution of 4 cm^{-1}, 16 scans and analysis in triplicate. ATR's clean diamond/ZnSe crystal was used to record the background spectra.

2.4.3. X-ray diffraction analysis (XRD)

The mineral profile of the cementitious materials was obtained from the XRD diffractometer D8 Advance A25 (Bruker). The scan was performed at 40 kV and 30 mA with Cu-Kα radiation and scanning step size of 0.02° in the θ-2θ ranging from 2 to 80°. The mineral composition of the cementitious materials was evaluated before and after the carbonation process using PDF4+ database.

2.4.4. Scanning electron microscopy (SEM)

Scanning electron microscopy topography images were obtained using the Inspect F50 - FEI microscope to characterize the cementitious materials structure before and after the carbonation process. The samples were oven dried at 80 °C overnight, kept in a dry box under vacuum, and subjected to gold sputtering coatings.

2.4.5. Determination of $CaCO_3$ content in cement

The $CaCO_3$ determination in cement was performed using a Partial Least Squares (PLS) regression model developed based on FTIR spectra. Thus, calibration and validation cement powder samples (Table S1) were prepared from physical mixture of non-carbonated (C1 - 45.80 mg $CaCO_3$/g cement) and carbonated (C11 - 468.20 mg $CaCO_3$/g cement) cement samples, presented in the Figure S3 (Supplementary Material). For the development of the PLS model, 33 calibration mixtures (99 spectra) and 20 validation mixtures (60 spectra) were used. Thus, Partial least squares (PLS) regression models were developed to quantify $CaCO_3$ in cement

and the results are detailed in the Supplementary Material (Figure S4 and Table S2). PLS model presented good correlation coefficient (R^2 = 0.9993) and low estimation error (RMSEP = 4.13 mg $CaCO_3$/g cement) and was applied to estimate the $CaCO_3$ content in cement powders samples resulting from the carbonation experiments (Table 2). The detailed procedure was described in previous publication (Santos *et al.*, 2021).

2.4.6. Analysis of dissolved inorganic carbon (DIC) content

Dissolved inorganic carbon (DIC) refers to the sum of all inorganic carbon species [$CO_{2(aq)}$, H_2CO_3, HCO_3^- and/or CO_3^{2-}] dissolved in aqueous solution (Herath *et al.*, 2020). For DIC content analysis, an aliquot of the aqueous solution is added to a 12 mL screw cap vial with butyl rubber septum. Then, the samples underwent a flush process with helium (100 mL·min^{-1}) for 5 min to remove atmospheric gases and other interferences from the vial headspace. After flushing, 100 µL of concentrated phosphoric acid (H_3PO_4 – 85%) was added to the aqueous solution and allowed to react for 1 h at room temperature to promote the release of CO_2 gas from the DIC and allow the saturation and equilibration of the vial headspace fluids. Quantification of DIC content by gas chromatograph was performed using a calibration curve from sodium carbonate solutions (Na_2CO_3) (Hansen *et al.*, 2013; Li *et al.*, 2007). For quantification purposes, the primary standard of Na_2CO_3 was used for its purity, stability, and solubility in aqueous solution and the DIC content results were expressed in sodium carbonate equivalents (Na_2CO_3-eq ppm). The detailed procedure was described in previous publication (Engelmann *et al.*, 2018).

2.4.7. Stable isotope analysis ($\delta^{13}C$)

The stable carbon isotope analyzes ($\delta^{13}C$) were performed in the GasBench II (GB) device, connected to a Delta V Plus isotope ratio mass spectrometer (IRMS) from Thermo Fisher Scientific. For isotopic analysis, the following standards were used: (*i*) the reference material NIST® RM 8543(NBS18 - $CaCO_3$) with a carbon ($\delta^{13}C$-$CaCO_3$) isotopic signature of -5.01 ± 0.07 ‰ and (*ii*) the CM-1 in-house $CaCO_3$ standard with

a carbon (δ^{13}C-$CaCO_3$) isotopic signature of +2.12 ± 0.20 ‰ (1SD - standard deviation from routine control chart). The results of stable isotopes (δ^{13}C) are expressed in the per mil unit (‰) as a ratio (R) between the heavier (least abundant) and lighter (more abundant) isotope, as shown in the Equation 9.

$$Isotopic\ ratio\ \ (R) = \frac{Abundance\ of\ heavier\ isotope}{Abundance\ of\ lighter\ isotope} \tag{9}$$

For practical purposes, the isotope signatures of an analyte were measured against an international standard with a certified stable isotope value (δ^{13}C) from Equations 10. Thus, the δ^{13}C values were presented as relative results to the VPDB international standard (*Vienna Pee Dee Belemnite*) (Wang *et al.*, 2017; Zhou *et al.*, 2015).

$$\delta^{13}C_{sample} = \frac{(^{13}C/^{12}C)_{sample} - (^{13}C/^{12}C)_{\ standard}}{(^{13}C/^{12}C)_{\ standard}} \times 1000 \tag{10}$$

In addition to the isotopic signature, the parameters of isotopic fractionation (ε) of carbon (δ^{13}C) between gaseous (δ^{13}C-CO_2), liquid (dissolved inorganic carbon - δ^{13}C-DIC) and solid (δ^{13}C-$CaCO_3$) phases of the cementitious material carbonation system were evaluated from Equation 11 (Karolytė *et al.*, 2017).

$$\ln \alpha \times 10^3 \ \approx\ \varepsilon_{product-reagent} = \delta_{product} - \delta_{reagent} \tag{11}$$

For isotopic analysis of calcium carbonate (δ^{13}C-$CaCO_3$) and DIC (δ^{13}C-DIC), samples are added to the 12 mL screw cap vial with butyl rubber septum. Then, the samples underwent a flush process with helium (100 mL·min^{-1}) for 5 min, to remove atmospheric gases and other interferences from the vial headspace. After the flush, 100 µL of concentrated phosphoric acid (H_3PO_4 – 99%) was added to the vial and allowed to react for 1 h at 72 °C to promote the release of CO_2 gas from $CaCO_3$ or DIC species and allow the saturation and equilibrium of the vial headspace fluids. For

isotopic analysis of CO_2 cylinder ($\delta^{13}C$-CO_2), the 12 mL screw cap vial also underwent a flush process with helium. However, the sample was introduced into the vial after the flush. Thus, 100 µL of concentrated CO_2 (cylinder or HPHT reactor) was added to the vial and allowed to equilibrate with the vial headspace fluids. After preparing the samples, the analysis in IRMS proceeds as described above and the detailed procedure can be found described in previous publications (Engelmann *et al.*, 2018).

2.5. Data analysis

Univariate statistical methods are limited for evaluating data from complex and multifactorial systems, such as carbonation of CCS well cement in CO_2 rich environments. Thus, multivariate tools were applied for a simultaneous assessment of multiple parameters. In the present work, partial least squares regression (PLS) was applied to quantify $CaCO_3$ in cement from the FTIR analysis and Principal Component Analysis (PCA) and Correlation Analysis (CA) methods were applied to perform the exploratory analysis of chemical and isotopic data.

2.5.1. Geochemical modeling (PHREEQC)

PhreeqC is a computer program developed by the USGS (*United States Geological Survey*) to perform speciation, geochemical calculations, identification of reaction routes and reactive transport simulation. Thus, the PhreeqC version 3.0 geochemistry program was used to identify the reaction conditions of the equilibrium of HPHT pressurized reactor systems (Table 2), to calculate the activities of dissolved inorganic carbon species (DIC) and to predict the balance of CO_2 with water in a pressurized (pCO_2) and heated environment (Parkhurst and Appelo, 2013). The thermodynamic database used was the PITZER.DAT incorporated into the program since its last update. For the simulation, temperature, partial pressure of CO_2 (pCO_2), pH (experimental after carbonation reactions) and DIC content were considered. As a result of the geochemical simulation, the theoretical parameters [pH (initial), $CO_{2(aq)}$

(mol/L), CO_3^{2-} (mol/L), HCO_3^- (mol/L), $\alpha CO_{2(aq)}$, αCO_3^{2-}, αHCO_3^-, αH_2O] were incorporated into the data analysis.

3. Results and Discussion

The present work evaluated the prospect of using stable isotope methods to study the cement carbonation process in Carbon Capture and Storage (CCS) wells. Thus, the results and discussions were divided into: (*i*) carbonation and stable isotope ($\delta^{13}C$) analysis of cement powder and (*ii*) carbonation and stable isotope ($\delta^{13}C$) analysis of portlandite (CH) and calcium silicate hydrate (C-S-H).

3.1. Carbonation of cement powder

Before the carbonation experiments, the raw non-carbonated hydrated class G cement powder was prepared and characterized by X-ray diffraction (XRD), infrared spectroscopy (FTIR) and scanning electron microscopy (SEM). The results of XRD and FTIR are presented in Figure 1, while the SEM image is presented in the Supplementary Material (Figure S5). From the XRD pattern (Figure 1A), it was identified that non-carbonated hydrated cement powder is composed of the crystalline components: (*i*) unhydrated C_3S (Ca_3SiO_5 - Alite) and calcium aluminum iron oxide ($Ca_2Fe_{1.5}Al_{0.5}O_5$) cement phases, (*ii*) portlandite (CH) and ettringite [$Ca_6Al_2(SO_4)_3(OH)_{12}\cdot 26H_2O$] hydration products and (*iii*) calcite ($CaCO_3$ polymorph), resulting from the natural carbonation process of cement with atmospheric CO_2 during sample handling. All characterized components are expected in class G hydrated cement paste (L. Li *et al.*, 2020; L. Liu *et al.*, 2021), and the $CaCO_3$ content in non-carbonated hydrated cement powder was estimated at 45.80 mg $CaCO_3$/g cement. Furthermore, the main cement characteristics identified from the FTIR spectral profile (Figure 1B) were: (*i*) the peak related to the OH stretching of portlandite (CH) at 3640 cm^{-1}, (*ii*) a broadband attributed to the OH stretching of water (3600–3100 cm^{-1}), (*iii*) the carbonate (CO_3^{2-}) peaks of calcite ($CaCO_3$ polymorph) at 1410 cm^{-1} (asymmetric C-O stretching), 873 cm^{-1} (out-of-plane vibration) and 713 cm^{-1} (in-plane vibration) and

(*iv*) a broadband (800-1200 cm^{-1}) attributed to asymmetric Si-O stretching (υ_3) of Q^1 and Q^2 calcium silicate hydrate (C-S-H) species (Higl *et al.*, 2021; Skocek *et al.*, 2020).

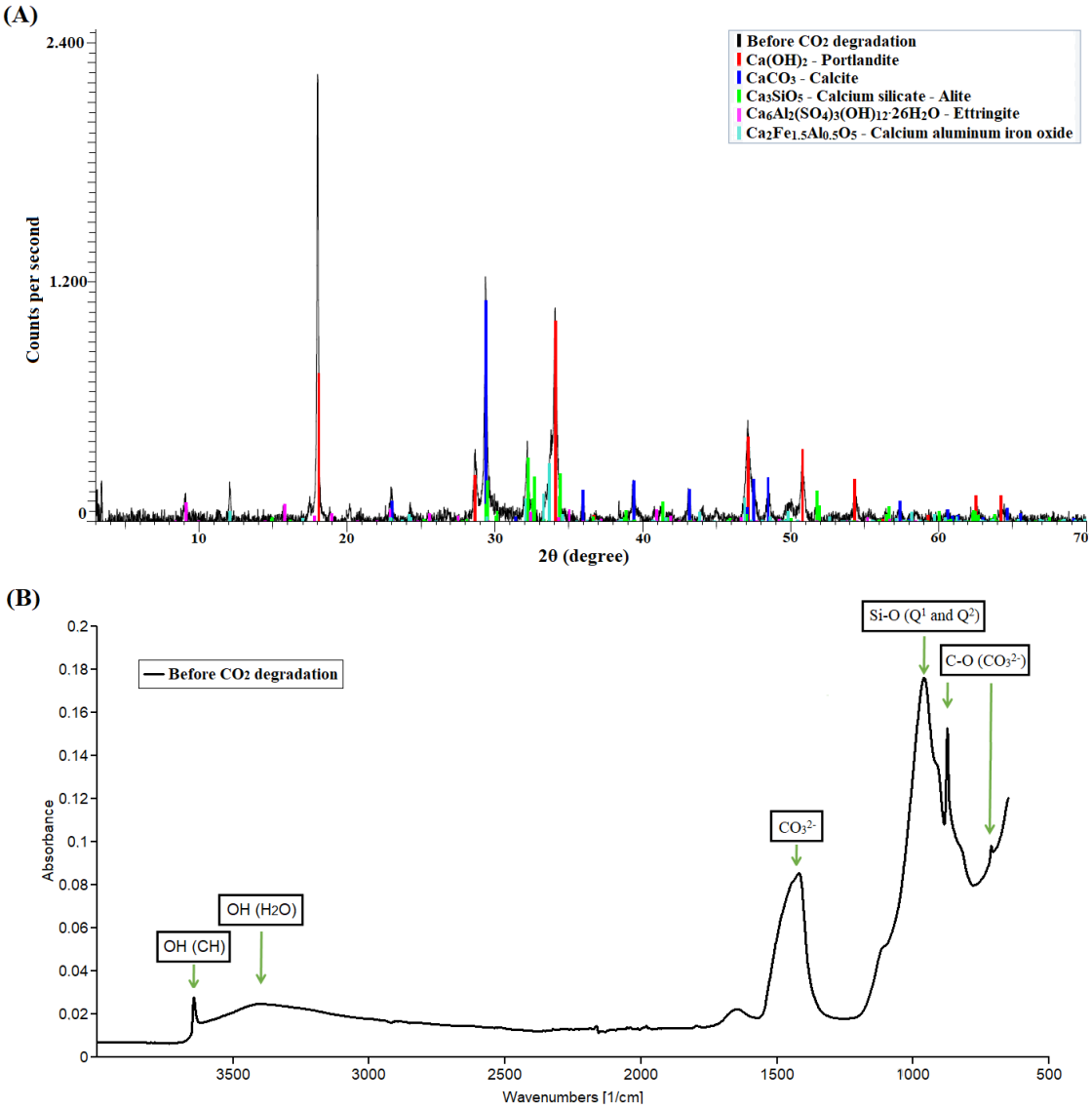

Figure 1. Non-carbonated hydrated cement powder characterization: (A) X-ray diffraction evidencing portlandite (CH), calcite ($CaCO_3$), alite, ettringite and calcium aluminum iron oxide and (B) infrared spectrum showing characteristic FTIR peaks of water (OH), portlandite (CH), calcium silicate hydrate (C-S-H) and calcite ($CaCO_3$)

After characterizing the non-carbonated hydrated cement powder, the carbonation experiments detailed in Table 2 were performed. Thus, the

characterization results of the liquid phase (pH, electrical conductivity and DIC content) and the $CaCO_3$ content in the carbonated cement powder are presented in Table 3. Additionally, the detailed results of the DIC (Table S3) and $CaCO_3$ (Table S4) content, as well as X-ray diffractograms (Figure S6-S11), FTIR spectra (Figure S12-17) and SEM images (Figure S18-23) of the carbonated cement powders from Experiments 1-6 (Table 2) are presented in the Supplementary Material.

Table 3. Results of the characterizations of cement powder carbonation experiments

Sample	pH	Electrical conductivity ($\mu s.cm^{-1}$)	[a]DIC (ppm)	$CaCO_3$ content (mg $CaCO_3$/g cement)
C50_30	6.99	3123.0	7281.4 ± 552.3	355.1 ± 0.7
C50_65	6.57	2529.7	6444.8 ± 564.9	390.4 ± 0.8
C50_100	7.05	2480.0	6547.0 ± 28.8	381.5 ± 0.7
C100_30	6.80	1630.0	5287.3 ± 490.2	386.5 ± 0.2
C100_65	6.89	1465.0	4069.1 ± 823.4	364.0 ± 0.6
C100_100	6.77	1652.0	5074.6 ± 62.4	396.1 ± 0.6
C150_30	6.94	1480.4	4994.2 ± 511.4	345.0 ± 0.4
C150_65	6.93	1555.0	6444.8 ± 60.0	385.1 ± 0.8
C150_100	6.87	1508.3	5256.2 ± 484.0	367.9 ± 0.8

[a] Expressed as Na_2CO_3-eq ppm

The pH of the solutions presented values close to neutrality ranging from 6.57 to 7.05 (Table 3). The ions in solution come from the solubilization process of hydrated cement components (CH and C-S-H) and from the dissolution of carbonate minerals, especially $CaCO_3$, producing alkalinity and buffering fluids pH (Huerta *et al.*, 2016; Zuo and Bennett, 2021). Furthermore, the electrical conductivity ranged from 1465.0 to 3123.0 $\mu s.cm^{-1}$ and the dissolved inorganic carbon (DIC) content from 4069.1 to 7281.4 ppm. Based on unhydrated (Table 1) and hydrated (Figure 1) class G cement composition, it was suggested that the solutions are enriched in cations, especially calcium (Ca^{2+}), resulting in the formation of the carbonate buffering system (Shelton *et al.*, 2014; Zhang *et al.*, 2014). This medium indicates the formation of a reactive

environment in which the CO_2, CH and C-S-H dissolutions are followed by the cement degradation process and by the decalcification/leaching of carbonated minerals (Dalla Vecchia *et al.*, 2020). While portlandite (CH) undergoes dissolution and regulates the pH of the medium to values above 12.5, C-S-H control the pH of the environment between 12.5 to 10 through dissolution, decalcification, and lixiviation of ions as the CO_2 interacts with the cement matrix (Gaboreau *et al.*, 2012). Considering that the pH of the solution saturated with CO_2 presents acidic characteristics, the results suggest that the ions of the medium results in a buffering effect that balances the pH of the solutions independent of the experimental conditions of the carbonation reactions. Thus, at first, it was not possible to identify a clear effect of the temperature and pressure of the carbonation experiments on the results of the solution parameters.

The carbonation process takes place in solution, involving a complex system of dissolution and diffusion of CO_2 and ions, comprising a series of precipitation, leaching, reprecipitation and polymerization processes of different minerals in the reaction system. Although the processes occur in a dispersed way, the carbonation reactions are intensified around the cement grains (Šavija and Luković, 2016; Shah *et al.*, 2018; Vance *et al.*, 2015), in which the mineral phases of the cement significantly influence the surrounding pH and the local concentration of calcium ions (Ca^{2+}) (Letolle *et al.*, 1990; Mayer *et al.*, 2015). Thus, the carbonated minerals, especially $CaCO_3$, form around the degraded cement grains, delaying the extension of the carbonation process. From the calibrated PLS regression, the $CaCO_3$ content in cement was estimated (Table 3), resulting in a range of 355.1 to 396.1 mg $CaCO_3$/g cement throughout the carbonation experiments. The value obtained is significantly higher than non-carbonated hydrated cement (45.80 mg $CaCO_3$/g cement) and is within the calibrated range for the PLS model (45.80 to 468.20 mg $CaCO_3$/g cement. At first, it was not possible to identify a clear effect of the temperature and pressure of the carbonation experiments on the $CaCO_3$ content of carbonated cement powders. After the initial characterizations, the XRD results of Experiments 7-9 (Table 2), representing the series of carbonation reactions conducted at 150 bar, are presented in Figure 2,

while the other diffractograms (Experiments 1-6) are presented in the Supplementary Material (Figure S6-S11).

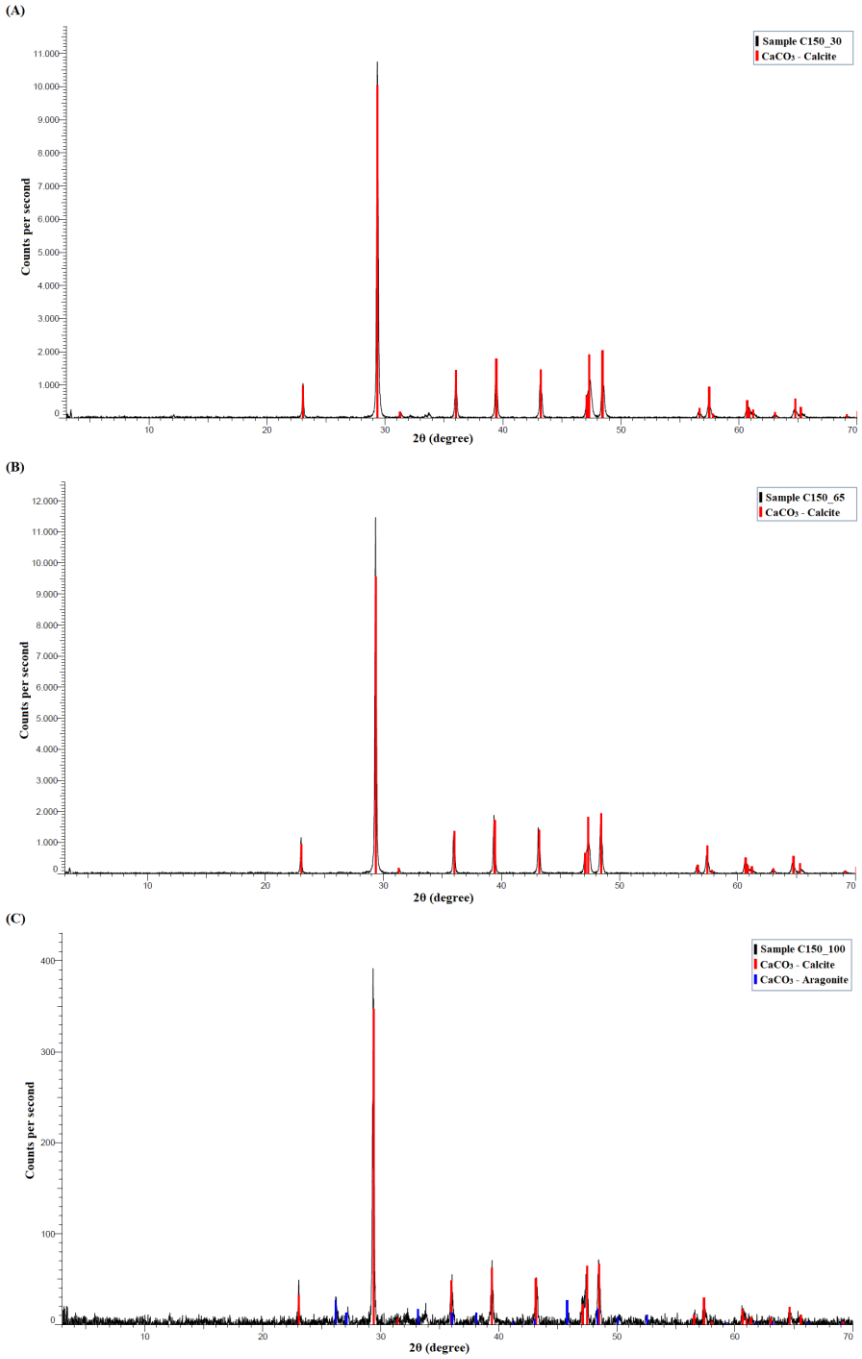

Figure 2. X-ray diffraction pattern of carbonated cement powder samples: (A) C150_30 (calcite $CaCO_3$ polymorph), (B) C150_65 (calcite $CaCO_3$ polymorph) and (C) C150_100 (calcite and aragonite $CaCO_3$ polymorphs)

The $CaCO_3$ polymorphs (calcite and aragonite) formed during the carbonation process is influenced by parameters such as reaction time, CO_2 pressure, pH, Ca/Mg solution ratio, carbonation degree and presence of other chemicals (Liu *et al.*, 2019; Vance *et al.*, 2015). Thus, it was expected that calcite will be the predominant $CaCO_3$ polymorph in advanced stages of cement carbonation, being produced by transformation of other $CaCO_3$ polymorphs (amorphous and aragonite) and precipitation/reprecipitation processes (Chang *et al.*, 2017; Saillio *et al.*, 2021; Šavija and Luković, 2016). From XRD pattern (Figure 2 and Figure S6-S11), it was identified that the cement powder samples underwent a high degree of chemical transformation. In Figure 2, it was observed that the carbonation process completely consumed the CH fraction, due to its disappearance in the diffractogram, and it is suggested that the C-S-H phase of the cement was significantly degraded, considering the intensity of the signals attributed to calcium carbonate ($CaCO_3$). In addition, it was observed that the crystalline fraction of the degraded cement is composed of $CaCO_3$ polymorphs. Thus, carbonated samples at temperatures of 30 °C and 65 °C are exclusively composed of calcite (Figure 2A and 2B), however the samples carbonated at a temperature of 100 °C (Figure 2C) also present a small fraction of aragonite. While calcite is the most stable $CaCO_3$ polymorph in mild reaction conditions and after long reaction periods(Christensen *et al.*, 2021; Sade *et al.*, 2020; Yan *et al.*, 2020), aragonite is identified more frequently in geothermal environments and its formation may be influenced by other factors in the cement carbonation reaction system at 100 °C (Figure 2C, Figure S8 and Figure S11), such as CO_2 pressure, pH, Ca/Mg solution ratio and the presence of other chemicals (Liu *et al.*, 2019; Vance *et al.*, 2015). In the cement carbonation reaction system, the temperature of the medium was identified as being more influential than the CO_2 pressure for the formation of $CaCO_3$ polymorphs. Since many carbonation products do not have crystalline characteristics (Higl *et al.*, 2021; L. Li *et al.*, 2020; Morandeau and White, 2015; Shah *et al.*, 2018), the degradation products were also characterized by FTIR. Thus, the infrared results of Experiments 7-9 (Table 2), representing the series of carbonation reactions conducted at 150 bar,

are presented in Figure 3, while the other FTIR spectra (Experiments 1-6) are presented in the Supplementary Material (Figure S12-S17).

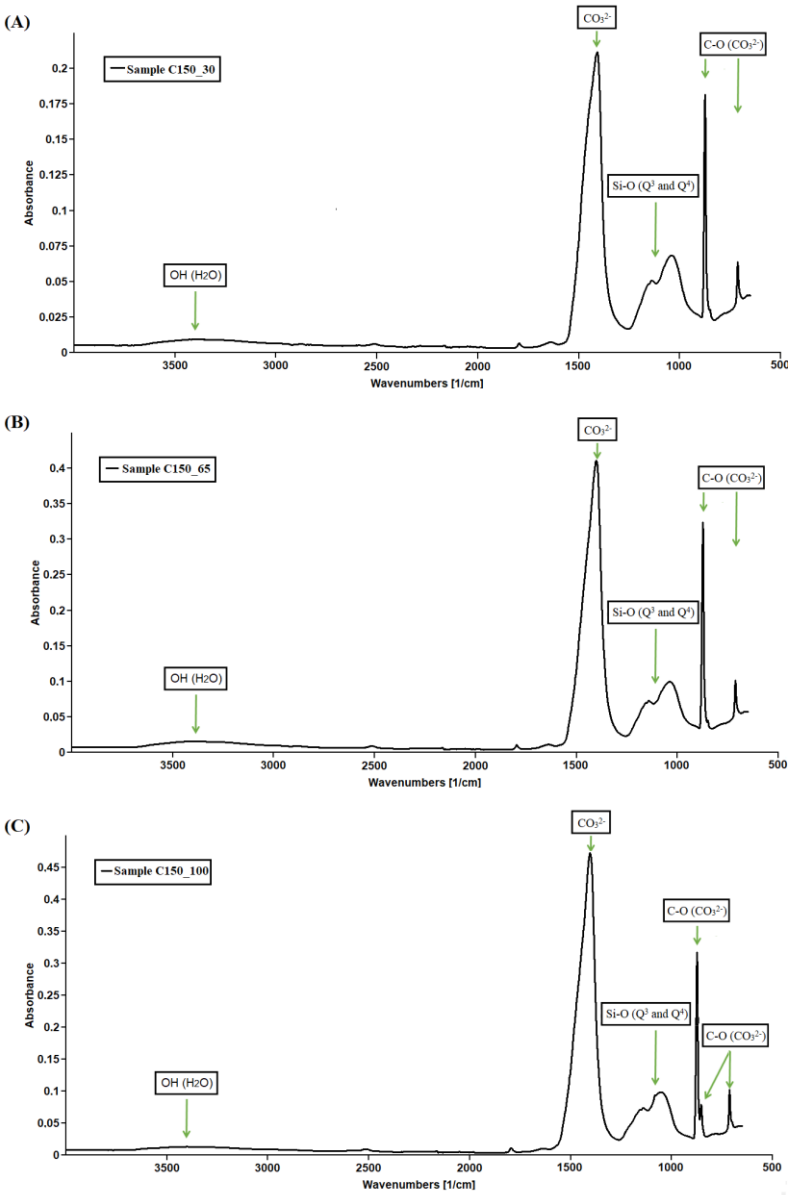

Figure 3. Infrared spectrum of carbonated cement powder samples: (A) C150_30 (FTIR peaks of water, CH, decalcified C-S-H, and calcite $CaCO_3$ polymorph), (B) C150_65 (FTIR peaks of water, CH, decalcified C-S-H, and calcite $CaCO_3$ polymorph) and (C) C150_100 (FTIR peaks of water, CH, decalcified C-S-H and calcite and aragonite $CaCO_3$ polymorphs)

Corroborating the XRD results, FTIR spectra (Figure 3 and Figure S12-S17) indicate the consumption of portlandite (CH), due to the absence of the characteristic peak at 3640 cm^{-1}, and the significant increase in $CaCO_3$ FTIR characteristic bands in the cement powder. From infrared data (Figure 3A, 3B and 3C), the following characteristics were identified: (*i*) a broadband attributed to the OH stretching of water (3600–3100 cm^{-1}), (*ii*) the carbonate (CO_3^{2-}) peaks of calcite ($CaCO_3$ polymorph) at 1410 cm^{-1} (asymmetric C-O stretching), 873 cm^{-1} (out-of-plane vibration) and 713 cm^{-1} (in-plane vibration) and (*iii*) a broadband (1250-900 cm^{-1}) attributed to asymmetric Si-O stretching (υ_3) of the decalcified C-S-H (Q^3 at 1050 cm^{-1}) and polymerized silica (Q^4 at 1140 cm^{-1}) phases (Higl *et al.*, 2021; Skocek *et al.*, 2020). The presence of aragonite in the samples (Figure 3C, Figure S14 and Figure S17), resulting from carbonation reactions at 100 °C, was indicated by the presence of specific carbonate peaks (850 cm^{-1}) (Park *et al.*, 2021). Thus, the FTIR analysis indicates the consumption of CH and the decalcification-polymerization process of C-S-H (Q^1 and Q^2), leading to the production of $CaCO_3$ polymorphs, decalcified C-S-H (Q^3) and polymerized silica (Q^4) phases (Liu *et al.*, 2019; Saillio *et al.*, 2021). In addition to the speciation of the carbonation reaction products, it is necessary to evaluate the morphology of the carbonated cement. Thus, the SEM images from Experiments 7-9 (Table 2), representing the series of carbonation reactions performed at 150 bar, are presented in Figure 4, while the other SEM images (Experiments 1-6) are presented in the Supplementary Material (Figure S18-S23).

From SEM images (Figures 4 and Figure S18-S23), it was observed that the decalcified C-S-H and amorphous silica grains were covered by crystalline $CaCO_3$ polymorphs (Chang *et al.*, 2017; Wang *et al.*, 2019). While the calcite observed in all SEM images present characteristics of typical rhombohedral crystals, the aragonite identified in cement powders from carbonation reactions at 100 °C (Figure 4C, Figure S20 and Figure S23) presented a needle-like structure (Chang *et al.*, 2017; Christensen *et al.*, 2021). The carbonation process is intensified around the cement grains (Šavija and Luković, 2016; Shah *et al.*, 2018; Vance *et al.*, 2015), in which the mineral phases of the cement significantly influence the surrounding pH and the local

calcium ions concentration (Ca^{2+}) (Letolle *et al.*, 1990; Mayer *et al.*, 2015). Thus, considering the quasi-static environment, $CaCO_3$ precipitates preferentially nearby the silica-rich phase (decalcified C-S-H and amorphous silica), resulting in the C-S-H grain passivation due to the protection provided by the carbonate “coating” and in a delay in the cement decalcification/leaching processes (Šavija and Luković, 2016; Shah *et al.*, 2018; Vance *et al.*, 2015).

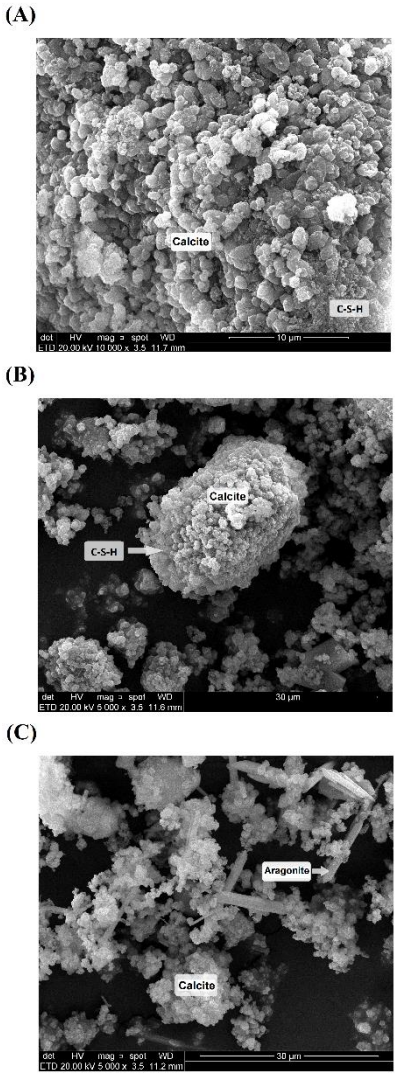

Figure 4. SEM images of carbonated cement powder samples: (A) C150_30 (decalcified C-S-H covered by calcite $CaCO_3$ - mag: 10000 X), (B) C150_65 (decalcified C-S-H covered by calcite $CaCO_3$ - mag: 5000 X) and (C) C150_100 (decalcified C-S-H covered by calcite and aragonite $CaCO_3$ - mag: 5000 X)

3.1.1 Stable isotope ($\delta^{13}C$) analysis of carbonated cement

The isotopic phases composition (gas, liquid and solid) of the reaction system were characterized and the occurrence of isotopic fractionation processes among the components of the reaction medium was studied. To evaluate the application of the stable carbon isotopes method to discriminate the origin of the CO_2 that promoted the cement carbonation process it is necessary to evaluate the isotopic parameters of the system, as well as the isotope enrichment factors (ε) among all the components of the reaction system. Thus, the results of the isotopic characterizations are presented in Table 4, while the detailed results of $\delta^{13}C$-CO_2 (Table S5), $\delta^{13}C$-DIC (Table S6) and $\delta^{13}C$-$CaCO_3$ (Table S7) analyzes are presented in the Supplementary Material.

The cement carbonation is a dynamic process that occurs in a short time horizon if compared to geological mineralization processes in reservoirs. The carbonation process is a complex system of dissolution and diffusion of CO_2 and ions, comprising a series of precipitation, leaching, reprecipitation and polymerization processes of different minerals in the reaction system. In geological environments compatible with CCS wells, parameters such as temperature, pressure, CO_2 pressure, pH of the medium and the chemical speciation of the components in the reaction system (gas/liquids/cement) are expected to influence on the isotope fractionation processes due to slightly different equilibrium constants for each carbon isotope (^{12}C and ^{13}C) (Becker *et al.*, 2011; Ha *et al.*, 2020; Mayer *et al.*, 2015). Thus, for the stable isotope method to be applicable, it is necessary to know the distribution of isotopes and the influence of the parameters on isotopic fractionation related with the well cement carbonation process (Ha *et al.*, 2020; Zhang *et al.*, 2021). In addition, due to the pH of the cement matrix (> 12.5) and the chemical reactivity of CH and C-S-H against the CO_2, it must be considered that the reaction processes involved are proceeding in non-equilibrium and that $\delta^{13}C$ data will be influenced by kinetic and thermodynamic factors.

Table 4. Stable isotope analysis and isotopic fractionation between phases of the cement powder carbonation reactions systems

Sample	δ^{13}C-DIC (‰)	$\varepsilon_{DIC\text{-}CO2}$ (δ^{13}C ‰)	δ^{13}C-$CaCO_3$ (‰)	$\varepsilon_{CaCO3\text{-}DIC}$ (δ^{13}C ‰)	$\varepsilon_{CaCO3\text{-}CO2}$ (δ^{13}C ‰)
C50_30	-30.50 ± 0.00	11.4	-38.36 ± 0.06	-7.9	3.5
C50_65	-30.71 ± 0.21	11.2	-38.16 ± 0.10	-7.5	3.7
C50_100	-29.23 ± 0.14	12.6	-38.88 ± 0.05	-9.6	3.0
C100_30	-29.78 ± 0.11	12.1	-42.70 ± 0.12	-12.9	-0.8
C100_65	-30.35 ± 0.38	11.5	-41.01 ± 0.02	-10.7	0.8
C100_100	-30.22 ± 0.14	11.6	-40.67 ± 0.05	-10.5	1.2
C150_30	-29.99 ± 0.33	11.9	-38.30 ± 0.19	-8.3	3.6
C150_65	-29.52 ± 0.52	12.3	-42.31 ± 0.12	-12.8	-0.5
C150_100	-31.13 ± 0.30	10.7	-41.25 ± 0.12	-10.1	0.6

* $CO_{2(Cylinder)}$ δ^{13}C = -41.86 ± 0.12 ‰; ** $CO_{2(post\ reactor)}$ δ^{13}C = -42.30 ± 0.00 ‰

The $\delta^{13}C\text{-}CO_2$ from the gas cylinder used to pressurize the reactors throughout the carbonation experiments (Table 2) has an isotopic signature of $\delta^{13}C$ = -41.86 ‰ (±0.12 ‰) and, from the initial CO_2 data ($\delta^{13}C\text{-}CO_2$), the isotope enrichment factors (ε) were estimated along the components of the reaction system. From Table 4, it was observed that the isotopic signatures of DIC ($\delta^{13}C$-DIC) are in the range of -31.13 to -29.23 ‰, while the isotope enrichment factor between $\delta^{13}C\text{-}CO_2$ and $\delta^{13}C$-DIC ($\varepsilon_{DIC\text{-}CO2}$) is in the range of 10.7 to 12.6 ‰. From the results of $\delta^{13}C$-DIC, whose values are enriched in ^{13}C in relation to the source $\delta^{13}C\text{-}CO_2$, it was suggested that the dissolution process of CO_2 and the formation of reactional medium alkalinity is occurring in a high pH environment and were in non-equilibrium state (Becker *et al.*, 2011). Thus, the solubilization of portlandite (CH) and C-S-H, influencing the increase in the pH of the medium, related with the dissolution process of CO_2 and its dissociation to DIC species (H_2CO_3, HCO_3^- and CO_3^{2-}), resulted in a significant carbon isotope fractionation (Eshel and Singer, 2016; Mayer *et al.*, 2013). The values obtained for the isotope enrichment factor (ε) between $\delta^{13}C\text{-}CO_2$ and $\delta^{13}C$-DIC ($\varepsilon_{DIC\text{-}CO2}$ = 10.7 to 12.6 ‰) are within the range described in the literature as expected for similar reaction conditions (temperature/pressure/pH) (Eshel and Singer, 2016; Welch *et al.*, 2019; Yan *et al.*, 2021). In addition, the post reactor $\delta^{13}C\text{-}CO_2$ has an isotopic signature of $\delta^{13}C$ = -42.30 ‰ (±0.00 ‰), detailed in the Table S5, and slightly depleted relative to cylinder $\delta^{13}C\text{-}CO_2$ ($\delta^{13}C$ = -41.86 ‰). This result reflects the more intense relative flow of ^{13}C from the gas phase to the enriched $\delta^{13}C$-DIC pool that occurs due to the pH of the solution, the kinetic and thermodynamic factors of the process, and the non-equilibrium state of the reaction system (Barth *et al.*, 2015).

Furthermore, it was observed that the isotopic signatures of carbonate minerals ($\delta^{13}C\text{-}CaCO_3$) are in the range of -42.70 to -38.16 ‰, while the isotope enrichment factor between $\delta^{13}C$-DIC and $\delta^{13}C\text{-}CaCO_3$ ($\varepsilon_{CaCO3\text{-}DIC}$) is in the range of -12.9 to -7.5 ‰. From $\delta^{13}C\text{-}CaCO_3$ results, whose value are depleted in ^{13}C in relation to the respective DIC isotopic signatures ($\delta^{13}C$-DIC) of the reaction media, it was suggested that the process of cement carbonation and $CaCO_3$ precipitation is occurring in a high

pH environment and were in non-equilibrium state (Dietzel *et al.*, 2016; Hansen *et al.*, 2019; Krishnamurthy *et al.*, 2003; Shevalier *et al.*, 2014). As previously discussed, the carbonation process is intensified around the cement grains (Šavija and Luković, 2016; Shah *et al.*, 2018; Vance *et al.*, 2015), in which the mineral phases of the cement significantly influence the surrounding pH and the local concentration of calcium ions (Ca^{2+}) (Letolle *et al.*, 1990; Létolle *et al.*, 1992; Mayer *et al.*, 2015). Thus, the presence of alkaline minerals (CH and C-S-H) in the reactional system results in the: (*i*) calcite precipitation in non-equilibrium with the δ^{13}C-DIC pool (Mayer *et al.*, 2015; Rafai *et al.*, 1991; Shevalier *et al.*, 2014), (*ii*) isotope enrichment factor between δ^{13}C-DIC and δ^{13}C-$CaCO_3$ with negative values ($\varepsilon_{CaCO3\text{-}DIC}$ = -12.9 to -7.5 ‰) (Dietzel *et al.*, 2016, 1992; Hansen *et al.*, 2019; Krishnamurthy *et al.*, 2003), and (*iii*) an additional influencing factor on DIC isotopic (δ^{13}C-DIC) fractionation in solution due to the more significant flow of ^{12}C to the mineral carbonate (Dotsika *et al.*, 2009; Yan *et al.*, 2021, 2020). In addition, the values obtained for the isotope enrichment factor (ε) between δ^{13}C-DIC and δ^{13}C-$CaCO_3$ ($\varepsilon_{CaCO3\text{-}DIC}$ = -12.9 to -7.5 ‰) are within the range described in the literature as expected for similar reaction conditions (temperature/pressure/pH) (Dietzel *et al.*, 2016; Hansen *et al.*, 2019; Yan *et al.*, 2021, 2020). The origin of CO_2 involved in the cement carbonation process in CCS well environment can be natural (endogenous) or artificial (Costa *et al.*, 2019). Previously, the isotopic fractionation value between δ^{13}C-CO_2 and δ^{13}C-$CaCO_3$ under reservoir conditions was described as close to 3 ‰ (Györe *et al.*, 2017), like those observed for the enrichment factor isotope between δ^{13}C-CO_2 and δ^{13}C-$CaCO_3$ ($\varepsilon_{CaCO3\text{-}CO2}$ = -0.8 to 3.7 ‰). Thus, it was suggested that global isotopic enrichment factor ($\varepsilon_{CaCO3\text{-}CO2}$) of the entire cement carbonation reaction system, comprising the sum of the fractionation between δ^{13}C-CO_2 and δ^{13}C-DIC ($\varepsilon_{DIC\text{-}CO2}$) and between δ^{13}C-DIC and δ^{13}C-$CaCO_3$ ($\varepsilon_{CaCO3\text{-}DIC}$), results in mineral carbonate that preserves the isotopic identity of the CO_2 source (δ^{13}C-CO_2) (Dreybrodt, 2008).

The global dynamics of CO_2 in the geological storage environment and adjoining sections of engineering elements, including the CCS well, will depend on the pH evolution of the environment over time (Becker *et al.*, 2011; Iglesias *et al.*, 2018; Yan

et al., 2021). From the results obtained, the same interpretation applies to the flow of different carbon isotopes (^{12}C and ^{13}C) along with the phases (gas/liquid/solid) of the cement carbonation in the reaction system. Thus, it was initially suggested that the pH of the environment regulates more significantly the kinetic and thermodynamic factors of chemical reactions (equilibrium/non-equilibrium) and the carbon isotopic fractionation than the pressure and temperature parameters of the process. At first, it was not possible to identify a clear effect of the temperature and pressure of the carbonation experiments on the stable isotope results. In agreement with the literature, the state of CO_2 (subcritical or supercritical) does not significantly influence the carbon isotopic signature of the chemical species in the system (Becker *et al.*, 2015). From the analysis of variance (ANOVA) of the results obtained from the factorial design of the carbonation experiments (Table 2), it was not possible to identify significant effect of pressure and temperature on the isotopic signature of DIC (δ^{13}C-DIC) and $CaCO_3$ (δ^{13}C-$CaCO_3$), as well as on the isotopic enrichment factors (ε). The ANOVA tables (Table S8-S12) and the factorial effect graph of the parameters on the results (Figure S24) are presented in the Supplementary Material.

3.1.2 Data analysis of cement carbonation experiments

After the initial analysis of the isotope ratio results, the global data analysis of the cement carbonation experiments was performed from the Correlation Analysis (CA) and Principal Components Analysis (PCA) based on (*i*) chemical characterization data (Table 3), (*ii*) isotopic signature data (Table 4) and (*iii*) geochemical modeling parameters estimated by PHREEQC (Supplementary Material - Table S13). To keep the discussion concise, only the clearest and most significant relationships were discussed, and the data analysis results are shown in Figure 5. The numerical values of the correlation matrix (Table S14), as well as the PCA scores (Figure S25) and PCA loadings (Figure S26) graphs, were made available in the Supplementary Material. Initially, the linear relationship between pairs of variables was evaluated from the correlation coefficient (R^2).

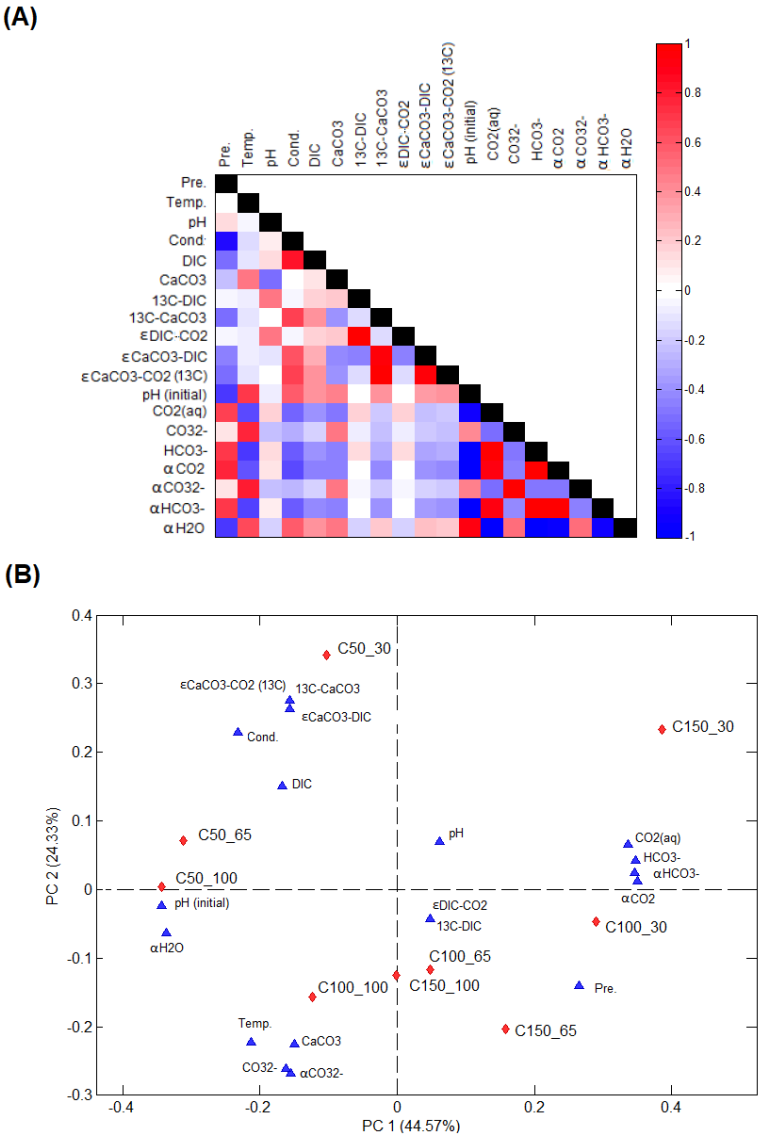

Figure 5. Data analysis of cement powder carbonation experiments: (A) correlation analysis, in which the red color indicates a direct relationship, the blue color indicates inverse relationships, the white color indicates that there is no apparent linear correlation between the parameters, and the analysis shade bar denotes the degree of relationship between the variables and (B) PCA analysis, in which red prisms represent sample scores, while blue triangles indicate parameter loadings.

Thus, it is possible to evaluate the degree (high correlation $R^2 > 0.7$, moderate correlation $0.7 > R^2 > 0.5$ and weak correlation $R^2 < 0.5$) and the type (direct [+] or inverse [-]) of the relationship between the evaluated parameters. On the correlation

map (Figure 5A), white color indicates no linear correlation, blue tones indicate inverse correlation and red tones indicate direct correlation between the variables. From CA, the following patterns were recognized:

(*i*) Pressure presents direct relationship with the dissolution of CO_2 and with the concentration and activity of $CO_{2(aq)}$ ($CO_{2(aq)}$ – R^2 = 0.68; αCO_2 - R^2 = 0.77) and HCO_3^- (HCO_3^- - R = 0.69; αHCO_3^- - R^2 = 0.71) in solution. Furthermore, pressure shows an inverse relationship with electrical conductivity (R^2 = -0.85), $pH_{initial}$ (R^2 = -0.70), DIC content (R^2 = -0.51), δ^{13}C-$CaCO_3$ isotopic signature (R^2 = -0.52) and with $\varepsilon_{CaCO3\text{-}DIC}$ (R^2 = -0.46) and $\varepsilon_{CaCO3\text{-}CO2}$ (R^2 = -0.52) isotopic enrichment factor;

(*ii*) Temperature shows direct relationship with the $CaCO_3$ content in cement (R^2 = 0.49), $pH_{initial}$ (R^2 = 0.69) and with concentration and activity of CO_3^{2-} (αCO_3^{2-} – R^2 = 0.78; αCO_3^{2-} - R^2 = 0.79). Moreover, temperature presents an inverse relationship with the dissolution of CO_2 and with the concentration and activity of $CO_{2(aq)}$ ($CO_{2(aq)}$ – R^2 = -0.63; αCO_2 - R^2 = -0.61) and HCO_3^- (HCO_3^- - R = -0.69; αHCO_3^- - R^2 = -0.68) in solution;

(*iii*) The final pH of the reactor solution is directly related to δ^{13}C-DIC isotopic signature (R^2 = 0.47) and with $\varepsilon_{CaCO3\text{-}DIC}$ isotopic enrichment factor (R^2 = 0.47), while is inverse related to $CaCO_3$ content in cement (R^2 = -0.53). In addition, the electrical conductivity of the solutions is directly related to DIC content (R^2 = 0.82), δ^{13}C-$CaCO_3$ isotopic signature (R^2 = 0.66) and with $\varepsilon_{CaCO3\text{-}DIC}$ (R^2 = 0.62) and $\varepsilon_{CaCO3\text{-}CO2}$ (R^2 = 0.66) isotopic enrichment factor, while is inversely related to the $CO_{2(aq)}$ (R^2 = -0.56);

(*iv*) δ^{13}C-DIC isotopic signature is directly related to the final pH of the reactor solution (R^2 = 0.47), while is inversely related with $\varepsilon_{CaCO3\text{-}DIC}$ isotopic enrichment factor (R^2 = -0.44). On the other hand, δ^{13}C-$CaCO_3$ isotopic signature is directly related to electrical conductivity (R^2 = 0.66), DIC content (R^2 = 0.40) and with $\varepsilon_{CaCO3\text{-}DIC}$ isotopic enrichment factor (R^2 = 0.95), while it has an inverse relationship with pressure (R^2 = -0.52) and $CaCO_3$ content (R^2 = -0.39);

(*v*) The $\varepsilon_{DIC\text{-}CO2}$ isotopic enrichment factor is directly related to the final pH of the reactor solution (R^2 = 0.47). The $\varepsilon_{CaCO3\text{-}DIC}$ isotopic enrichment factor is directly related to electrical conductivity (R^2 = 0.62) and δ^{13}C-$CaCO_3$ (R^2 = 0.95), while it has an inverse relationship with pressure (R^2 = -0.46), $CaCO_3$ content (R^2 = -0.42) and δ^{13}C-DIC isotope signature (R^2 = -0.44). Lastly, the global $\varepsilon_{CaCO3\text{-}CO2}$ isotopic enrichment factor is directly related to electrical conductivity (R^2 = 0.66), δ^{13}C-$CaCO_3$ (R^2 = 0.95), DIC content (R^2 = 0.40) and $\varepsilon_{CaCO3\text{-}DIC}$ isotopic enrichment factor (R^2 = 0.95), while it has an inverse relationship with pressure (R^2 = -0.52), $CaCO_3$ content (R^2 = -0.39), $\alpha CO_{2(aq)}$ (R^2 = -0.41) and αHCO_3^- (R^2 = -0.38).

Previously, from the ANOVA on the results of the factorial design, a significant effect of temperature and pressure on the isotope ratio data (δ^{13}C-DIC and δ^{13}C-$CaCO_3$) and with the isotopic enrichment factors (ε) was not identified. However, from the CA, there is a series of indirect relationships influenced by the reaction parameters (temperature and pressure) that help to clarify the processes involved and isotope flow (^{12}C and ^{13}C) throughout the cement carbonation reaction system. Thus, the CA data were analyzed with the PCA (Figure 5B) to assess the multivariate relationship between the parameters. For the PCA analysis, the data were auto-scaled and mean centered, with the graph of PC-1 (44.57% of explained variance) versus PC-2 (24.33% of explained variance) being plotted in Figure 5B. From the data analysis (CA and PCA), it was suggested that:

(*i*) The amount of dissolved CO_2 influences the solution's capacity to solubilize and/or leach ions from the cement (carbonated and non-carbonated), regulate the solution's electrical conductivity and produce alkalinity (DIC). From the results, it was identified that the increase in pressure is directly related to the amount of dissolved CO_2, but inversely related to the alkalinity (DIC) of the solution. Regarding the isotopic signature of δ^{13}C-DIC, it was suggested that higher values of final pH are related to δ^{13}C-DIC pool enriched in ^{13}C and with higher isotopic enrichment factor ($\varepsilon_{DIC\text{-}CO2}$) as a result of a modification of the kinetic parameters (non-equilibrium) of the system,

reinforcing the previous literature results (Becker *et al.*, 2011; Mayer *et al.*, 2015). On the other hand, no direct relationships were identified between the isotopic signature of δ^{13}C-DIC and the $\varepsilon_{DIC\text{-}CO2}$ with the temperature and pressure of the reaction system;

(*ii*) Temperature reduces the solution's capacity to dissolve CO_2 and increases the concentration and activity of carbonate ions (CO_3^{2-}) and $CaCO_3$ content in cement. From the literature, it was observed that $CaCO_3$ precipitation comes exclusively from carbonate ions (CO_3^{2-}) in solution (Devriendt *et al.*, 2017). Regarding the isotopic signature of δ^{13}C-$CaCO_3$ and $\varepsilon_{CaCO3\text{-}DIC}$ isotopic enrichment factor, it was suggested that higher values of DIC content and solution electrical conductivity results in enriched δ^{13}C-$CaCO_3$ and larger $\varepsilon_{CaCO3\text{-}DIC}$ isotope fractionation, while higher pressurized reactional system results in carbonated cement with lower content of $CaCO_3$, depleted δ^{13}C-$CaCO_3$ isotopic signatures and less pronounced $\varepsilon_{CaCO3\text{-}DIC}$ isotopic fractionation. These results are explained by a set of factors that act simultaneously, so that the less acidic environment (lower CO_2 pressure and higher initial pH) and with higher alkalinity and Ca^{2+} saturation in solution (DIC content and electrical conductivity) results in $CaCO_3$ precipitation with greater thermodynamic equilibrium (DIC-$CaCO_3$) and under less pronounced isotopic kinetic effect (Christensen *et al.*, 2021; Hansen *et al.*, 2019; Higgs *et al.*, 2015). Due to the high ion (Ca^{2+}) reserve and the thermodynamic conditions of carbonate precipitation, while the carbonate ions (CO_3^{2-}) are consumed to form $CaCO_3$, the reaction medium quickly deprotonates HCO_3^- to replenish the CO_3^{2-} content without a significant isotopic fractionation concerning the δ^{13}C-DIC pool (Christensen *et al.*, 2021; Devriendt *et al.*, 2017; Mayer *et al.*, 2015). Thus, it was observed that, under milder reaction conditions and greater thermodynamic equilibrium, the δ^{13}C-$CaCO_3$ isotopic signature is enriched in ^{13}C and better preserves the δ^{13}C-DIC isotopic ratio (Hansen *et al.*, 2019; Krishnamurthy *et al.*, 2003; Rafai *et al.*, 1991; Yan *et al.*, 2021). Conversely, more aggressive reaction conditions (higher CO_2 pressure and lower initial pH) and lower ion reserve and medium alkalinity (DIC and electrical conductivity) results in a greater kinetic effect (non-equilibrium) in the carbonate precipitation process and the formation of δ^{13}C-$CaCO_3$ more depleted in ^{13}C (Dreybrodt, 2008; Yan *et al.*, 2021). This profile is explicitly observed in the almost

linear relationship (R^2 = 0.95) between the value of $\delta^{13}C\text{-}CaCO_3$ and the $\varepsilon_{CaCO3\text{-}DIC}$ isotopic enrichment factor. Furthermore, these results reinforce the assertion that the fractionation between $\delta^{13}C\text{-}CaCO_3$ and the $\delta^{13}C$-DIC pool ($\varepsilon_{CaCO3\text{-}DIC}$) remains almost constant throughout the precipitation process even with local changes in the chemical profile of the solution, precipitation rate and temperature (Yan *et al.*, 2021);

(*iii*) Mineral carbonate ($\delta^{13}C\text{-}CaCO_3$) generated from cement carbonation preserves the isotopic signature of the $\delta^{13}C\text{-}CO_2$ source. Thus, it was indicated that isotopic enrichment factor ($\varepsilon_{CaCO3\text{-}CO2}$) of the entire cement carbonation reaction system, comprising the sum of the fractionation between $\delta^{13}C\text{-}CO_2$ and $\delta^{13}C$-DIC ($\varepsilon_{DIC\text{-}CO2}$) and between $\delta^{13}C$-DIC and $\delta^{13}C\text{-}CaCO_3$ ($\varepsilon_{CaCO3\text{-}DIC}$), results in a small or insignificant isotopic fractionation ($\varepsilon_{CaCO3\text{-}CO2}$). From the data analysis (CA and PCA), it was observed that the $\varepsilon_{CaCO3\text{-}DIC}$ isotopic enrichment factor regulates the overall isotopic fractionation of the carbonation process ($\varepsilon_{CaCO3\text{-}CO2}$) with an almost linear direct correlation coefficient (R^2 = 0.95), while the $\varepsilon_{DIC\text{-}CO2}$ isotopic enrichment factor has an insignificant correlation coefficient (R^2 = -0.15) concerning the global cement carbonation process ($\varepsilon_{CaCO3\text{-}CO2}$). Thus, similarly to the $\varepsilon_{CaCO3\text{-}DIC}$ isotopic enrichment factor, the kinetic and thermodynamic factors of chemical reactions (equilibrium/non-equilibrium) and the global carbon isotopic fractionation ($\varepsilon_{CaCO3\text{-}CO2}$) of the cement carbonation process is regulated by the set of factors involving the CO_2 pressure, initial and final pH of the reactional system and alkalinity (DIC) and electrical conductivity of the solution. Furthermore, the isolated effect of temperature and pressure were not identified as capable of significantly influencing the isotopic fractionation processes of the cement carbonation reaction system under the experimental conditions evaluated. Thus, from the obtained results, it was possible to clarify the fractionation of the different carbon isotopes (^{12}C and ^{13}C) along with the phases (gas/liquid/solid) of the CCS well cement carbonation reaction system.

3.2. Carbonation of CH and C-S-H

Initially, CH and synthetic C-S-H were characterized using XRD and FTIR. From the XRD (Figure S27) and FTIR (Figure S28) of portlandite (CH), it was identified that the CH prepared from laboratory present the expected characteristics. However, it also shows low calcite content because of the unavoidable natural carbonation of the mineral during its processing, handling, and storage. Furthermore, from the XRD (Figure S29) and FTIR (Figure S30) of the synthetic calcium silicate hydrate (C-S-H), it was observed that the preparation procedure resulted in a C-S-H with Ca/Si ratio of 1.5 and no signs of natural carbonation during processing, handling, and storage. Thus, duplicate carbonation reaction of portlandite (CH_R1 and CH_R2) and calcium silicate hydrate (C-S-H_R1 and C-S-H_R2) was performed and chemical characterizations results are shown in Table 5, while the detailed DIC content results are presented in the Table S15 (Supplementary Material).

From Table 5, it was observed that the pH of both reaction systems (CH and C-S-H) present values close to neutrality. While the average pH of the solutions after carbonation of portlandite (CH) was 7.57, the average pH value of the C-S-H reaction media was 7.44. The ions in solution come from the solubilization process of hydrated cement components (CH and C-S-H) and from the dissolution of carbonate minerals, especially $CaCO_3$, buffering the pH of fluids and producing alkalinity (Huerta *et al.*, 2016; Kampman *et al.*, 2014; Zuo and Bennett, 2021). Furthermore, the carbonation processes of portlandite (CH) resulted in solutions with average electrical conductivity values of 1065 $\mu s.cm^{-1}$ and DIC of 1741.3 ppm, while the reactions involving C-S-H presented average electrical conductivity values of 1304 $\mu s.cm^{-1}$ and DIC of 1831.2 ppm. Based on CH and C-S-H chemical composition, it was assumed that the solutions are enriched in cations, especially calcium (Ca^{2+}), resulting in the formation of the carbonate buffering system (Shelton *et al.*, 2014; Zhang *et al.*, 2014). This medium indicates the formation of a reactive environment in which the CO_2, CH and C-S-H dissolutions are followed by the cement degradation process and by the decalcification/leaching of carbonate minerals (Dalla Vecchia *et al.*, 2020). After the initial characterizations, the XRD results of carbonated portlandite (CH), and carbonated calcium silicate hydrate (C-S-H) are presented in Figure 6.

Table 5. Results of the characterizations of carbonation experiments of portlandite (CH) and synthetic calcium silicate hydrate (C-S-H)

Sample	pH	Electrical conductivity ($\mu s.cm^{-1}$)	[a]DIC (ppm)
CH_R1	7.77	1005.0	2011.9 ± 205.1
CH_R2	7.36	1125.0	1470.7 ± 48.4
$CH_{(average)}$	7.57 ± 0.29	1065 ± 85	1741.3 ± 382.7
C-S-H_R1	7.29	1483.0	1983.1 ± 95.5
C-S-H_R2	7.58	1125.0	1679.3 ± 522.4
$C\text{-}S\text{-}H_{(average)}$	7.44 ± 0.21	1304 ± 253	1831.2 ± 214.8

[a] Expressed as Na_2CO_3-eq ppm

From XRD pattern (Figure 6), it was identified that both cement phases (CH and C-S-H) underwent high degree of chemical transformation. In Figure 6A, it was observed that the carbonation process completely consumed the CH fraction and resulted in the production of calcium magnesium carbonate ($Ca_{0.845}Mg_{0.155}CO_3$) and aragonite ($CaCO_3$). Furthermore, from Figure 6B, it was identified that synthetic C-S-H was consumed to produce calcium magnesium carbonate ($Ca_{0.845}Mg_{0.155}CO_3$) as a carbonation product. Both calcium magnesium carbonate and aragonite were formed under reaction conditions (65 °C, 150 bar and 7days) due to the presence of MgO impurities in the CaO reagent used in synthetic procedures (Christensen *et al.*, 2021).

Corroborating the XRD results, the FTIR spectra (Figure S31 – Supplementary Material) showed the absence of portlandite (CH) and the significant increase in carbonate minerals after carbonation of CH (Figure S31A). In addition, in the carbonated C-S-H sample (Figure S31B), the following characteristics were identified: (*i*) the carbonate (CO_3^{2-}) peaks at 1410 cm^{-1} (asymmetric C-O stretching), 873 cm^{-1} (out-of-plane vibration) and 713 cm^{-1} (in-plane vibration) (*ii*) a broadband (1250-900 cm^{-1}) attributed to asymmetric Si-O stretching (υ_3) of the decalcified C-S-H (Q^3 at 1050 cm^{-1}) and polymerized silica (Q^4 at 1140 cm^{-1}) phases, and (*iii*) a broadband (800-1200

cm^{-1}) attributed to asymmetric Si-O stretching (u_3) of Q^1 and Q^2 calcium silicate hydrate (C-S-H) species (Higl *et al.*, 2021; Skocek *et al.*, 2020).

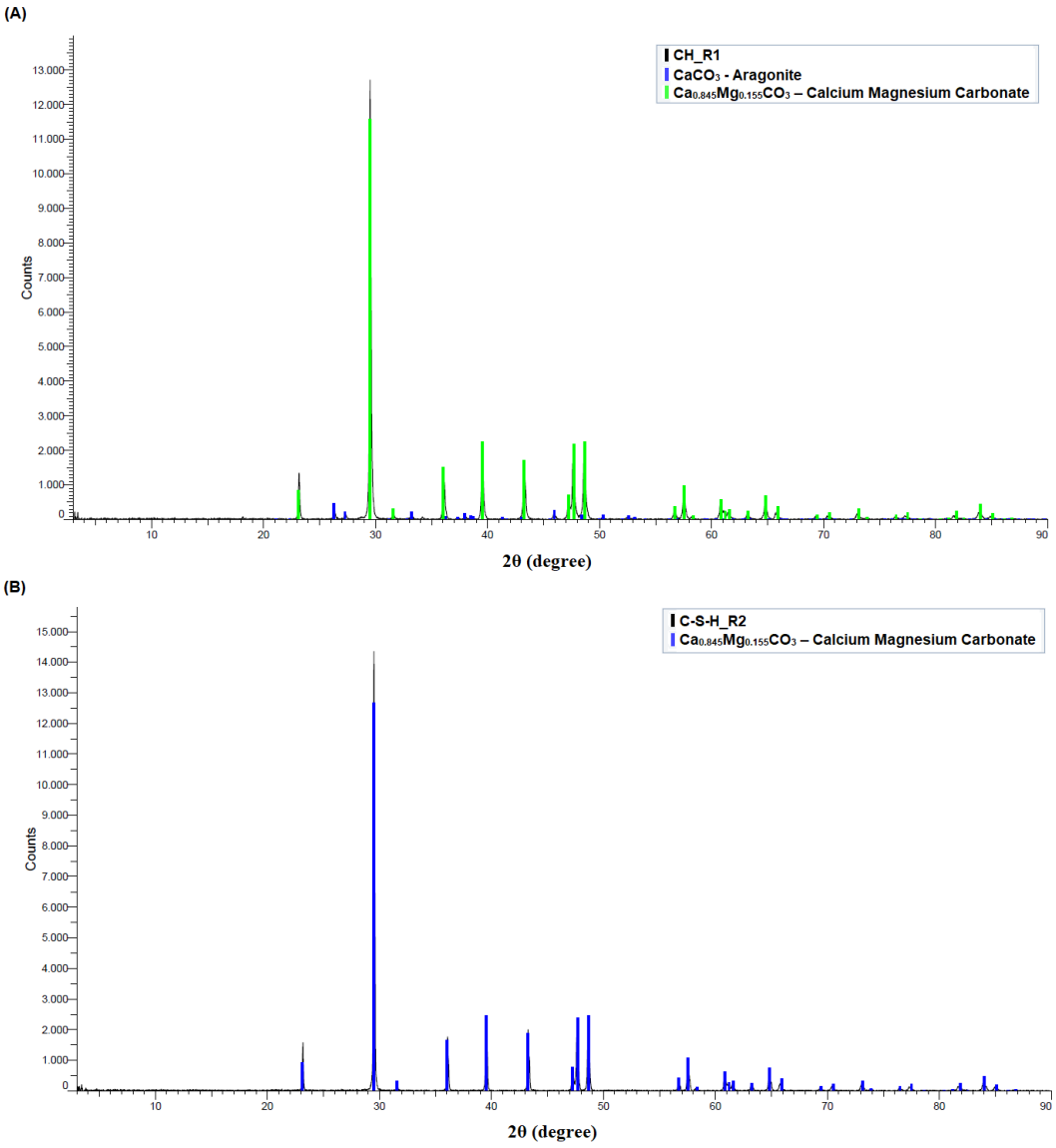

Figure 6. X-ray diffraction pattern of the cement phase carbonation experiment: (A) carbonated portlandite (CH), evidencing aragonite $CaCO_3$ polymorph and calcium magnesium carbonate, and (B) carbonated calcium silicate hydrate (C-S-H), showing calcium magnesium carbonate

In addition, SEM images of the portlandite (CH) and synthetic calcium silicate hydrate (non-carbonated and carbonated) samples are shown in Figure 7. Thus, it was

possible to observe the characteristics of portlandite (CH) crystal plates and a small content of crystalline $CaCO_3$ polymorphs (Figure 7A), while calcium magnesium carbonate crystals and the needle-like structure of aragonite were identified in the carbonated CH (Figure 7B). Furthermore, from Figure 7C, it was possible to visualize the synthetic calcium silicate hydrate amorphous gel, while the decalcified C-S-H covered with calcium magnesium carbonate was observed in Figure 7D.

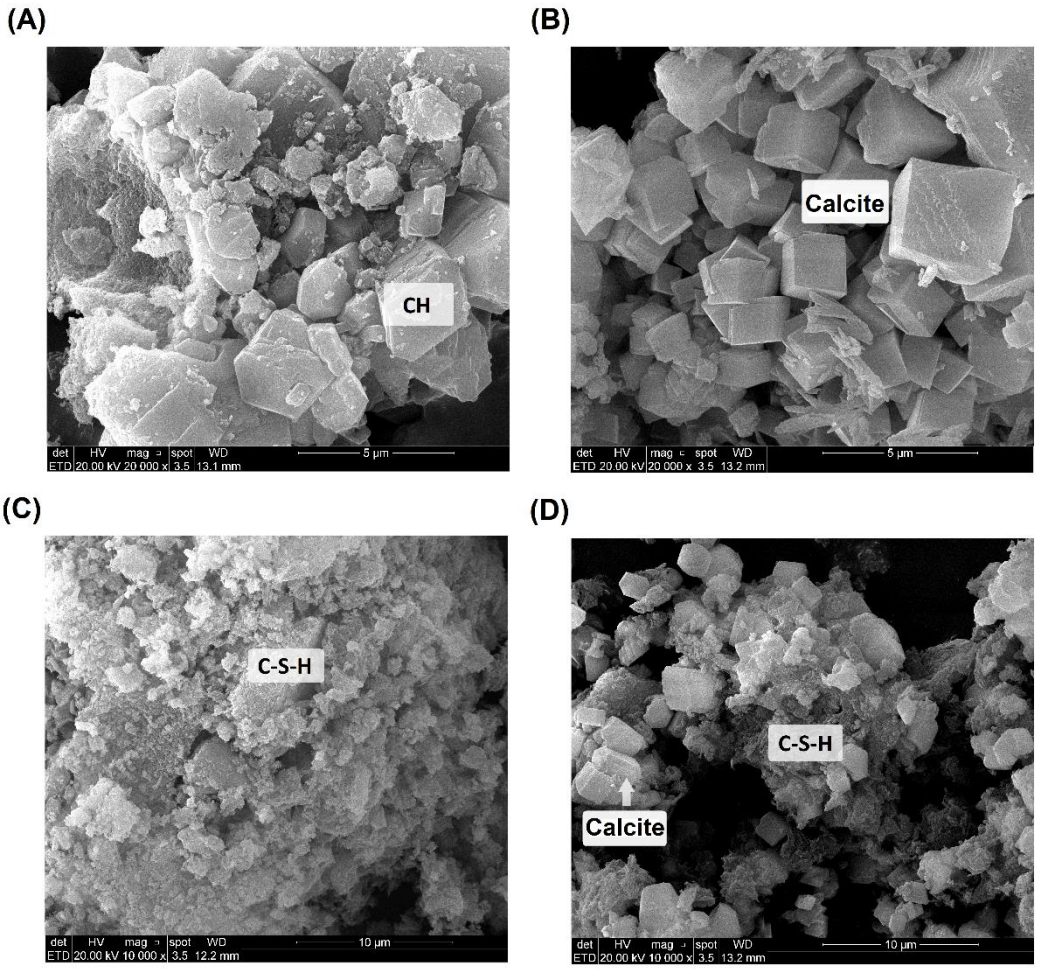

Figure 7. CH and C-S-H carbonation experiment: (A) synthetic portlandite (mag: 20000 X), (B) carbonated portlandite (mag: 20000 X), (C) synthetic calcium silicate hydrate (mag: 10000 X) and (D) carbonated calcium silicate hydrate (mag: 10000 X)

3.2.1. Stable isotope ($\delta^{13}C$) analysis of carbonated CH and C-S-H

The stable carbon isotope ($\delta^{13}C$) analysis method was applied to evaluate the isotopic signature and to study the isotopic fractionation processes of the specific carbonation processes of CH and synthetic C-S-H. Thus, the results of the isotopic results are presented in Table 6, while the detailed results of $\delta^{13}C$-CO_2 (Table S16), $\delta^{13}C$-DIC (Table S17) and $\delta^{13}C$-$CaCO_3$ (Table S18) analyzes are presented in the Supplementary Material.

The $\delta^{13}C$-CO_2 from the gas cylinder used to pressurize the reactors throughout the carbonation of portlandite (CH) and synthetic hydrated calcium silicate (C-S-H) has an isotopic signature of $\delta^{13}C$ = -36.69 ‰ (±0.06 ‰) and, from the initial CO_2 data ($\delta^{13}C$-CO_2), the isotope enrichment factors (ε) were estimated along with the components of the reaction system. The isotopic signatures of DIC ($\delta^{13}C$-DIC) from the CH carbonation system (Table 6) presented an average $\delta^{13}C$-DIC of -22.85 ‰ (± 0.16 ‰), resulting in an isotope enrichment factor between $\delta^{13}C$-CO_2 and $\delta^{13}C$-DIC ($\varepsilon_{DIC\text{-}CO2}$) of 13.9 ‰ (± 0.2 ‰). In addition, $\delta^{13}C$-DIC of the C-S-H reactional system had an average isotopic signature of -24.96 ‰ (± 0.91 ‰) and the isotope enrichment factor between $\delta^{13}C$-CO_2 and $\delta^{13}C$-DIC ($\varepsilon_{DIC\text{-}CO2}$) of 11.8 ‰ (± 0.9 ‰). From the results of $\delta^{13}C$-DIC, whose values are enriched in ^{13}C in relation to the source $\delta^{13}C$-CO_2, it was identified that the process of dissolution of CO_2 and formation of alkalinity of the reactional medium is occurring in an environment with high pH and were a non-equilibrium state (Becker *et al.*, 2011). Thus, a significant carbon isotopic fractionation occurs associated with the solubilization of portlandite (CH) and C-S-H, influencing the increase in the pH of the medium, together with the dissolution process of CO_2 and its dissociation to DIC species (H_2CO_3, HCO_3^- and CO_3^{2-}) (Eshel and Singer, 2016; Mayer *et al.*, 2013). The difference in the mean values of $\delta^{13}C$-DIC and isotopic fractionation ($\varepsilon_{DIC\text{-}CO2}$) after carbonation of CH and C-S-H is explained by the greater solubility and capacity of portlandite (CH) to increase the pH of the solution (Gaboreau *et al.*, 2012). This influence results in a large kinetic isotope fractionation of the reaction system and a greater enrichment of the $\delta^{13}C$-DIC pool of reactions involving CH (Krishnamurthy *et al.*, 2003; Shevalier *et al.*, 2014).

Table 6. Isotopic fractionation between the phases of the carbonation of portlandite (CH) and synthetic hydrated calcium silicate (C-S-H) reactions systems

Sample	δ^{13}C-DIC (‰)	$\varepsilon_{DIC\text{-}CO2}$ (δ^{13}C ‰)	δ^{13}C-$CaCO_3$ (‰)	$\varepsilon_{CaCO3\text{-}DIC}$ (δ^{13}C ‰)	$\varepsilon_{CaCO3\text{-}CO2}$ (δ^{13}C ‰)
CH_R1	-22.74 ± 0.24	14.0	-36.45 ± 0.20	-13.7	0.2
CH_R2	-22.96 ± 0.60	13.7	-36.91 ± 0.21	-14.0	-0.2
CH$_{(average)}$	-22.85 ± 0.16	13.9 ± 0.2	-36.68 ± 0.33	-13.9 ± 0.2	0.0 ± 0.3
C-S-H_R1	-25.60 ± 0.92	11.1	-34.24 ± 0.22	-8.6	2.5
C-S-H_R2	-24.32 ± 0.62	12.4	-33.83 ± 0.08	-9.5	2.9
C-S-H$_{(average)}$	-24.96 ± 0.91	11.8 ± 0.9	-34.04 ± 0.29	-9.1 ± 0.6	2.7 ± 0.3

* $CO_{2(Cylinder)}$ δ^{13}C = -36.69 ± 0.06 ‰

Furthermore, it was also observed that the isotopic signatures of $CaCO_3$ polymorphs ($\delta^{13}C$-$CaCO_3$) from the CH carbonation system presented an average $\delta^{13}C$-$CaCO_3$ of -36.68 ‰ (± 0.33 ‰), resulting in an isotope enrichment factor between $\delta^{13}C$-DIC and $\delta^{13}C$-$CaCO_3$ ($\varepsilon_{CaCO3\text{-}DIC}$) of -13.9 ‰ (± 0.2 ‰). In addition, $\delta^{13}C$-$CaCO_3$ of the C-S-H reactional system shows an average isotopic signature of -34.04 ‰ (± 0.29 ‰) and the isotope enrichment factor between $\delta^{13}C$-DIC and $\delta^{13}C$-$CaCO_3$ ($\varepsilon_{CaCO3\text{-}DIC}$) of -9.1 ‰ (± 0.6 ‰). From the results of $\delta^{13}C$-$CaCO_3$, whose value are depleted in ^{13}C with the respective DIC isotopic signatures ($\delta^{13}C$-DIC) of the reaction media, it was indicated that the process of cement carbonation and $CaCO_3$ precipitation is occurring in an environment with high pH and were in non-equilibrium state (Dietzel *et al.*, 2016; Hansen *et al.*, 2019; Krishnamurthy *et al.*, 2003; Shevalier *et al.*, 2014). As previously discussed, the carbonation process being intensified around the solid phase grains (Šavija and Luković, 2016; Shah *et al.*, 2018; Vance *et al.*, 2015), in which the mineral phases of the cement significantly influence the surrounding pH and the local concentration of calcium ions (Ca^{2+}) (Letolle *et al.*, 1990; Létolle *et al.*, 1992; Mayer *et al.*, 2015). The difference in the mean values of $\delta^{13}C$-$CaCO_3$ and isotopic fractionation ($\varepsilon_{CaCO3\text{-}DIC}$) after carbonation of CH and C-S-H is explained due to the higher pH around the portlandite grains, whose dissolution regulates the pH at values greater than 12.5, while the dissolution of the C-S-H gel is within the range of 12.5 to 10 (Gaboreau *et al.*, 2012). This influence results in a large kinetic isotope fractionation, precipitation in non-equilibrium isotopic conditions, and in carbonated fraction depleted in $\delta^{13}C$-$CaCO_3$ from CH carbonation system (Rafai *et al.*, 1991; Yan *et al.*, 2021).

The isotopic fractionation value between $\delta^{13}C$-CO_2 and $\delta^{13}C$-$CaCO_3$ under reservoir conditions was described as close to 3 ‰ (Györe *et al.*, 2017), like those observed for the enrichment factor isotope between $\delta^{13}C$-CO_2 and $\delta^{13}C$-$CaCO_3$ of the C-S-H reactional system ($\varepsilon_{CaCO3\text{-}CO2}$ = 2.7 ± 0.3 ‰) and greater than that obtained for the carbonation of portlandite ($\varepsilon_{CaCO3\text{-}CO2}$ = 0.0 ± 0.3 ‰). Thus, it was identified that isotopic enrichment factor ($\varepsilon_{CaCO3\text{-}CO2}$) of the cementitious materials carbonation reaction system, comprising the sum of the fractionation between $\delta^{13}C$-CO_2 and $\delta^{13}C$-DIC ($\varepsilon_{DIC\text{-}CO2}$) and between $\delta^{13}C$-DIC and $\delta^{13}C$-$CaCO_3$ ($\varepsilon_{CaCO3\text{-}DIC}$), resulted in a mineral

carbonate that preserves the isotopic identity of the $\delta^{13}C\text{-}CO_2$ source (Dreybrodt, 2008). The global dynamics of CO_2 in the geological storage environment and in adjoining sections of engineering elements, including the CCS well, will depend largely on the pH evolution of the environment over time (Becker *et al.*, 2011; Iglesias *et al.*, 2018; Yan *et al.*, 2021).

The same interpretation applies to the flow of different carbon isotopes (^{12}C and ^{13}C) along with the phases (gas/liquid/solid) of the reaction system. In the same way as obtained for the cement carbonation experiments, the pH of the environment presents high impact on the kinetic and thermodynamic factors of chemical reactions (equilibrium/non-equilibrium) and the carbon isotopic fractionation throughout the cementitious materials carbonation. For the PCA analysis (Figure 8), the data were auto-scaled and mean centered, with the graph of PC-1 (70.89% of explained variance) versus PC-2 (18.49% of explained variance).

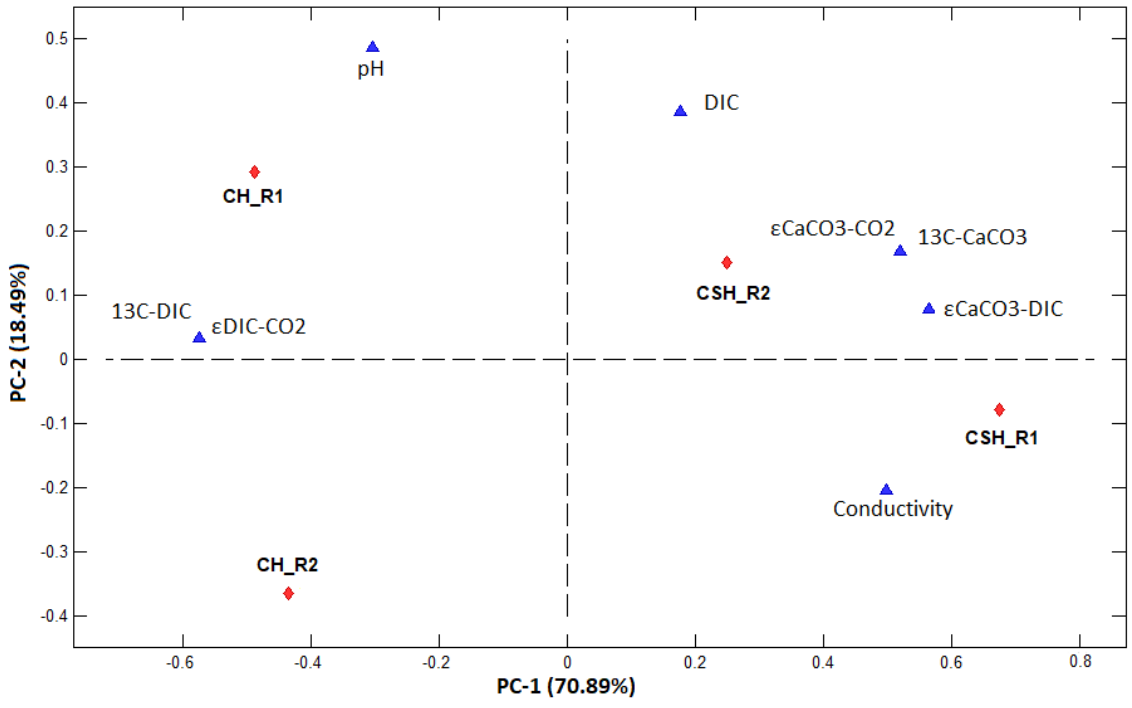

Figure 8. Principal component analysis (PCA) of carbonation experiments of portlandite (CH) and synthetic calcium silicate hydrate (C-S-H). Red prisms represent sample scores, while blue triangles indicate parameter loadings

The samples derived from CH carbonation showed: (*i*) higher post-reaction pH, (*ii*) enriched δ^{13}C-DIC and (*iii*) higher values of $\varepsilon_{DIC\text{-}CO2}$ isotopic enrichment factor. In addition, samples derived from C-S-H carbonation presented: higher alkalinity (DIC) and electrical conductivity, enriched δ^{13}C-$CaCO_3$ and higher values of $\varepsilon_{CaCO3\text{-}DIC}$ and $\varepsilon_{CaCO3\text{-}CO2}$ isotopic enrichment factors. Thus, it was identified that the cementitious materials carbonation reaction system presented the same essential data profile as previously obtained for the cement carbonation experiments (Figure 5). In summary to the previously discussed results, it was reinforced that:

(*i*) Regarding the isotopic signature of δ^{13}C-DIC, it was identified that higher values of final pH are related to δ^{13}C-DIC pool enriched in ^{13}C and with higher $\varepsilon_{DIC\text{-}CO2}$ isotopic enrichment factor because of a modification of the kinetic parameters (non-equilibrium) of the system. The difference in the δ^{13}C-DIC and isotopic fractionation ($\varepsilon_{DIC\text{-}CO2}$) after carbonation of CH and C-S-H is explained by the greater solubility and capacity of portlandite (CH) to increase the pH of the solution (Gaboreau *et al.*, 2012). This influence results in a large kinetic isotope fractionation of the reaction system and a greater enrichment of the δ^{13}C-DIC pool of reactions involving CH (Krishnamurthy *et al.*, 2003; Shevalier *et al.*, 2014).

(*ii*) Carbonation of C-S-H resulted in higher values of $\varepsilon_{CaCO3\text{-}DIC}$ and $\varepsilon_{CaCO3\text{-}CO2}$ isotopic enrichment factors. These results are explained by a set of factors that act simultaneously, so that the higher alkalinity and Ca^{2+} saturation in solution (DIC and electrical conductivity) and lower pH of C-S-H grains results in a precipitation of $CaCO_3$ with a greater thermodynamic equilibrium (DIC-$CaCO_3$) and under a less pronounced kinetic effect (Christensen *et al.*, 2021; Hansen *et al.*, 2019; Higgs *et al.*, 2015). Thus, the highest thermodynamic equilibrium resulted in the precipitation of carbonate minerals with the isotopic signature (δ^{13}C-$CaCO_3$) enriched in ^{13}C and which better preserves the δ^{13}C-DIC isotope ratio (Hansen *et al.*, 2019; Krishnamurthy *et al.*, 2003; Rafai *et al.*, 1991; Yan *et al.*, 2021). This profile is explicitly observed due to the high

correlation between δ^{13}C-$CaCO_3$ and the $\varepsilon_{CaCO3\text{-}DIC}$ isotopic enrichment factor PCA loadings.

(*iii*) Mineral carbonate (δ^{13}C-$CaCO_3$) generated from carbonation of cementitious materials (CH and C-S-H) preserves the isotopic signature of the δ^{13}C-CO_2 source. The global isotopic enrichment factor ($\varepsilon_{CaCO3\text{-}CO2}$) of the cementitious materials carbonation system, comprising the sum of the fractionation between δ^{13}C-CO_2 and δ^{13}C-DIC ($\varepsilon_{DIC\text{-}CO2}$) and between δ^{13}C-DIC and δ^{13}C-$CaCO_3$ ($\varepsilon_{CaCO3\text{-}DIC}$), results in a small or insignificant isotopic fractionation ($\varepsilon_{CaCO3\text{-}CO2}$). From the PCA loadings, it was observed that the $\varepsilon_{CaCO3\text{-}DIC}$ isotopic enrichment factor regulates the overall isotopic fractionation of the carbonation process ($\varepsilon_{CaCO3\text{-}CO2}$) with an almost direct correlation. Thus, from the obtained results, it was possible to clarify the fractionation of the different carbon isotopes (^{12}C and ^{13}C) along the CH and C-S-H cement phases and between the fractions (gas/liquid/solid) of the CCS well cement carbonation reaction system.

4. Conclusions

Stable isotope methods are important tools to identify the migration and fate of injected CO_2 along with the CCS geological storage site and monitor the efficiency of the CO_2 mineralization process. In the present work, the potential of the stable carbon isotope (δ^{13}C) technique to identify the origin of the CO_2 consumed in the carbonation of cementitious materials (class G cement, portlandite [CH] and calcium silicate hydrate [C-S-H]) was studied. Thus, the δ^{13}C analysis was applied to evaluate the isotopic signature of different phases participating in the reaction system (gas/liquid/solid) and to study the isotopic fractionation along with the carbonation process. Thus, a comprehensive study involving the chemical and isotopic characterization of the carbonation process products and extensive data analysis were conducted. From the results, the main conclusions obtained were:

(*i*) Kinetic and thermodynamic factors regulate the isotopic signature and isotopic fractionation (*ε*) among the phases (gas/liquid/solid) of the cementitious materials carbonation reaction system. From the results, it was identified that the isolated effect of temperature and pressure did not significantly change the parameters of the isotope ratio data (δ^{13}C-DIC and δ^{13}C-$CaCO_3$) and the isotopic enrichment factors (*ε*). From the data analysis, it was identified that the pH of the solution and the solubility and pH of the mineral phases (CH and C-S-H) influenced the kinetic and thermodynamic factors and the equilibrium/distribution of carbon isotopes (^{12}C and ^{13}C) throughout the system reaction. To a lesser extent, the pressure of CO_2 acts on the pH of the medium and on the activity of DIC species ($CO_{2(aq)}$, HCO_3^- and CO_3^{2-}) and have a small influence on the isotopic signature and isotopic fractionation (*ε*) of the process, while temperature was not shown to be a significant parameter throughout the study;

(*ii*) Regarding the isotopic signature of δ^{13}C-DIC, it was identified that higher values of final pH are related to δ^{13}C-DIC pool enriched in ^{13}C and with higher $\varepsilon_{DIC\text{-}CO2}$ isotopic enrichment factor because of a modification of the kinetic parameters (non-equilibrium) of the system. The difference in the δ^{13}C-DIC and isotopic fractionation ($\varepsilon_{DIC\text{-}CO2}$) after carbonation of CH and C-S-H is explained by the greater solubility and capacity of portlandite (CH) to increase the pH of the solution. This influence results in a large kinetic isotope fractionation of the reaction system and a greater enrichment of the δ^{13}C-DIC pool of reactions involving CH;

(*iii*) Regarding the isotopic signature of δ^{13}C-$CaCO_3$ and $\varepsilon_{CaCO3\text{-}DIC}$ isotopic enrichment factor, it was identified that higher values of DIC content, solution electrical conductivity and lower pH results in enriched δ^{13}C-$CaCO_3$ and larger $\varepsilon_{CaCO3\text{-}DIC}$ isotope fractionation. These results are explained by a set of factors that act simultaneously, so that the higher alkalinity and Ca^{2+} saturation in solution (DIC and electrical conductivity) and lower pH results in a precipitation of $CaCO_3$ with a greater thermodynamic equilibrium (DIC-$CaCO_3$) and under a less pronounced kinetic effect. Thus, the highest thermodynamic equilibrium resulted in the precipitation of carbonate

minerals with the isotopic signature (δ^{13}C-$CaCO_3$) enriched in ^{13}C and which better preserves the δ^{13}C-DIC isotope ratio;

iv) Mineral carbonate (δ^{13}C-$CaCO_3$) generated from carbonation of cementitious materials (class G cement, CH, and C-S-H) preserves the isotopic signature of the δ^{13}C-CO_2 source. The global isotopic enrichment factor ($\varepsilon_{CaCO3\text{-}CO2}$) of the cementitious materials carbonation system, comprising the sum of the fractionation between δ^{13}C-CO_2 and δ^{13}C-DIC ($\varepsilon_{DIC\text{-}CO2}$) and between δ^{13}C-DIC and δ^{13}C-$CaCO_3$ ($\varepsilon_{CaCO3\text{-}DIC}$), results in a small or insignificant isotopic fractionation ($\varepsilon_{CaCO3\text{-}CO2}$). From the data analysis, it was observed that the $\varepsilon_{CaCO3\text{-}DIC}$ isotopic enrichment factor regulates the overall isotopic fractionation of the carbonation process ($\varepsilon_{CaCO3\text{-}CO2}$) with an almost direct correlation;

v) Stable isotope methods are applicable to evaluate and monitor the cement carbonation process in Carbon Capture and Storage (CCS) wells, especially when the objective is to discriminate the origin of the CO_2 (injected or endogenous) that induced the degradation process of material.

Acknowledgments

The authors would like to thank the Institute of Petroleum and Natural Resource (IPR) of the Pontifical Catholic University of Rio Grande do Sul for the infrastructure and Lafarge Holcim for the donation of the cement. This work was supported by Petrobras (grant numbers: 2017/00742-8 and 2018/00235-1) and by ANP (Brazil's National Oil, Natural Gas and Biofuels Agency), through the R&D levy regulation.

Conflict of Interest

The authors declare that they have no known competing financial interests or personal relationships that could have appeared to influence the work reported in this paper.

Supporting information available

This work presents supplementary material detailing the: PLS calibration and validation sets to quantify $CaCO_3$ in cement (Table S1), parameters obtained for PLS regression models (Table S2), DIC quantification from cement powder carbonation experiments (Table S3), $CaCO_3$ quantification in cement powder (Table S4), stable carbon isotope analysis of cylinder CO_2 and post-carbonation gas (Table S5), DIC stable carbon isotope signature from cement powder carbonation experiments (Table S6), stable carbon isotope analysis of the cement powder carbonation experiments (Table S7), ANOVA of the effect of parameters on the DIC stable carbon isotope signature (Table S8), ANOVA of the effect of parameters on $CaCO_3$ stable carbon isotope signature (Table S9), ANOVA of the effect of parameters on the isotopic fractionation between CO_2 and DIC (Table S10), ANOVA of the effect of parameters on the isotopic fractionation between DIC and $CaCO_3$ (Table S11), ANOVA of the effect of parameters on the isotopic fractionation between CO_2 and $CaCO_3$ (Table S12), PHREEQC geochemical parameters (Table S13), correlation index between the variables (Table S14), DIC quantification from the portlandite (CH) and calcium silicate hydrate (C-S-H) carbonation experiments (Table S15), CO_2 isotopic signature used in the portlandite (CH) and calcium silicate hydrate (C-S-H) carbonation experiments (Table S16), DIC isotopic signatures from the portlandite (CH) and calcium silicate hydrate (C-S-H) carbonation experiments (Table S17) and $CaCO_3$ isotopic signatures from the portlandite (CH) and calcium silicate hydrate (C-S-H) carbonation experiments (Table S18). In addition, are also represented the: mold for preparing cement paste samples (Figure S1), scheme of carbonation experiments (Figure S2), SEM images of non-carbonated and carbonated cement powders (Figure S3), PLS regression results (Figure S4), hydrated class G cement powder (Figure S5), X-ray diffraction pattern of C50_30 carbonated cement powder sample (Figure S6), X-ray diffraction pattern of C50_65 carbonated cement powder sample (Figure S7), X-ray diffraction pattern of C50_100 carbonated cement powder sample (Figure S8), X-ray diffraction pattern of C100_30 carbonated cement powder sample (Figure S9), X-ray

diffraction pattern of C100_65 carbonated cement powder sample (Figure S10), X-ray diffraction pattern of C100_100 carbonated cement powder sample (Figure S11), Infrared spectrum of C50_30 carbonated cement powder sample (Figure S12), Infrared spectrum of C50_65 carbonated cement powder sample (Figure S13), Infrared spectrum of C50_100 carbonated cement powder sample (Figure S14), Infrared spectrum of C100_30 carbonated cement powder sample (Figure S15), Infrared spectrum of C100_65 carbonated cement powder sample (Figure S16), Infrared spectrum of C100_100 carbonated cement powder sample (Figure S17), SEM image of C50_30 carbonated cement powder sample (Figure S18), SEM image of C50_65 carbonated cement powder sample (Figure S19), SEM image of C50_100 carbonated cement powder sample (Figure S20), SEM image of C100_30 carbonated cement powder sample (Figure S21), SEM image of C100_65 carbonated cement powder sample (Figure S22), SEM image of C100_100 carbonated cement powder sample (Figure S23), temperature and pressure effect factorial plot (Figure S24), Principal component analysis (PCA) scores (Figure S25), Principal component analysis (PCA) loadings (Figure S26), X-ray diffraction pattern of synthetic portlandite (CH) (Figure S27), Infrared spectrum of synthetic portlandite (CH) (Figure S28), X-ray diffraction pattern of synthetic calcium silicate hydrate (C-S-H) (Figure S29), Infrared spectrum of synthetic calcium silicate hydrate (C-S-H) (Figure S30) and the infrared spectrum of carbonated portlandite (CH) and carbonated calcium silicate hydrate (C-S-H) (Figure S31).

References

Abid, K., Gholami, R., Elochukwu, H., Mostofi, M., Bing, C.H., Muktadir, G., **2018**. A methodology to improve nanosilica based cements used in CO_2 sequestration sites. Petroleum 4, 198–208. https://doi.org/10.1016/j.petlm.2017.10.005

API Specification, **2010**. API 10A - Specification for cements and materials for well cementing. Am. Pet. Inst. 2009, 50.

Bai, M., Zhang, Z., Fu, X., **2016**. A review on well integrity issues for CO_2 geological storage and enhanced gas recovery. Renew. Sustain. Energy Rev. 59, 920–926. https://doi.org/10.1016/j.rser.2016.01.043

Barth, J.A.C., Nowak, M.E., Zimmer, M., Norden, B., Van Geldern, R., **2015**. Monitoring of cap-rock integrity during CCS from field data at the Ketzin pilot site (Germany): evidence from gas composition and stable carbon isotopes. Int. J. Greenh. Gas Control 43, 133–140. https://doi.org/10.1016/j.ijggc.2015.10.017

Becker, V., Myrttinen, A., Blum, P., Van Geldern, R., Barth, J.A.C., **2011**. Predicting δ^{13}C-DIC dynamics in CCS: a scheme based on a review of inorganic carbon chemistry under elevated pressures and temperatures. Int. J. Greenh. Gas Control 5, 1250–1258. https://doi.org/10.1016/j.ijggc.2011.05.001

Becker, V., Myrttinen, A., Nightingale, M., Shevalier, M., Rock, L., Mayer, B., Barth, J.A.C., **2015**. Stable carbon and oxygen equilibrium isotope fractionation of supercritical and subcritical CO_2 with DIC and H_2O in saline reservoir fluids. Int. J. Greenh. Gas Control 39, 215–224. https://doi.org/10.1016/j.ijggc.2015.05.020

Carey, J.W., Wigand, M., Chipera, S.J., WoldeGabriel, G., Pawar, R., Lichtner, P.C., Wehner, S.C., Raines, M.A., Guthrie, G.D., **2007**. Analysis and performance of oil well cement with 30 years of CO_2 exposure from the SACROC Unit, West Texas, USA. Int. J. Greenh. Gas Control 1, 75–85. https://doi.org/10.1016/S1750-5836(06)00004-1

Celia, M.A., Bachu, S., Nordbotten, J.M., Bandilla, K.W., **2015**. Status of CO_2 storage in deep saline aquifers with emphasis on modeling approaches and practical simulations. Water Resour. Res. 51, 6846–6892. https://doi.org/10.1002/2015WR017609

Chang, R., Kim, S., Lee, S., Choi, S., Kim, M., Park, Y., **2017**. Calcium carbonate precipitation for CO_2 storage and utilization: a review of the carbonate crystallization and polymorphism. Front. Energy Res. 5, 1–12. https://doi.org/10.3389/fenrg.2017.00017

Christensen, J.N., Watkins, J.M., Devriendt, L.S., DePaolo, D.J., Conrad, M.E., Voltolini, M., Yang, W., Dong, W., **2021**. Isotopic fractionation accompanying CO_2 hydroxylation and carbonate precipitation from high pH waters at The Cedars, California, USA. Geochim. Cosmochim. Acta 301, 91–115. https://doi.org/10.1016/j.gca.2021.01.003

Costa, B.L. de S., Freitas, J.C. de O., Melo, D.M. de A., Araujo, R.G. da S., Oliveira, Y.H. de, Simão, C.A., **2019**. Evaluation of density influence on resistance to carbonation process in oil well cement slurries. Constr. Build. Mater. 197, 331–338. https://doi.org/10.1016/j.conbuildmat.2018.11.232

Crow, W., Carey, J.W., Gasda, S., Brian Williams, D., Celia, M., **2010**. Wellbore integrity analysis of a natural CO_2 producer. Int. J. Greenh. Gas Control 4, 186–197. https://doi.org/10.1016/j.ijggc.2009.10.010

Dalla Vecchia, F., dos Santos, V.H.J.M., Schütz, M.K., Ponzi, G.G.D., Stepanha, A.S. de G. e., Malfatti, C. de F., Costa, E.M. da, **2020**. Wellbore integrity in a saline aquifer: experimental steel-cement interface degradation under supercritical CO_2 conditions representative of Brazil's Parana basin. Int. J. Greenh. Gas Control 98, 103077. https://doi.org/10.1016/j.ijggc.2020.103077

Devriendt, L.S., Watkins, J.M., McGregor, H. V., **2017**. Oxygen isotope fractionation in the $CaCO_3$-DIC-H_2O system. Geochim. Cosmochim. Acta 214, 115–142. https://doi.org/10.1016/j.gca.2017.06.022

Dietzel, M., Schön, F., Heinrichs, J., Deditius, A.P., Leis, A., **2016**. Tracing formation and durability of calcite in a Punic–Roman cistern mortar (Pantelleria Island, Italy). Isotopes Environ. Health Stud. 52, 112–127. https://doi.org/10.1080/10256016.2015.1016430

Dietzel, M., Usdowski, E., Hoefs, J., **1992**. Chemical and $^{13}C/^{12}C$- and $^{18}O/^{16}O$-isotope evolution of alkaline drainage waters and the precipitation of calcite. Appl. Geochemistry 7, 177–184. https://doi.org/10.1016/0883-2927(92)90035-2

Dotsika, E., Psomiadis, D., Poutoukis, D., Raco, B., Gamaletsos, P., **2009**. Isotopic analysis for degradation diagnosis of calcite matrix in mortar. Anal. Bioanal. Chem. 395, 2227–2234. https://doi.org/10.1007/s00216-009-3135-8

Dreybrodt, W., **2008**. Evolution of the isotopic composition of carbon and oxygen in a calcite precipitating $H_2O–CO_2–CaCO_3$ solution and the related isotopic composition of calcite in stalagmites. Geochim. Cosmochim. Acta 72, 4712–4724. https://doi.org/10.1016/j.gca.2008.07.022

Duguid, A., Carey, J.W., Butsch, R., **2014**. Well integrity assessment of a 68 year old well at a CO_2 injection project. Energy Procedia 63, 5691–5706. https://doi.org/10.1016/j.egypro.2014.11.602

Duguid, A., Guo, B., Nygaard, R., **2017**. Well integrity assessment of monitoring wells at an active CO_2-EOR flood. Energy Procedia 114, 5118–5138. https://doi.org/10.1016/j.egypro.2017.03.1667

Engelmann, P. de M., Santos, V.H.J.M. dos, Barbieri, C.B., Augustin, A.H., Ketzer, J.M.M., Rodrigues, L.F., **2018**. Environmental monitoring of a landfill area through the application of carbon stable isotopes, chemical parameters and multivariate analysis. Waste Manag. 76, 591–605. https://doi.org/10.1016/j.wasman.2018.02.027

Eshel, G., Singer, M.J., **2016**. Inorganic carbon transformations between phases and its impact on its isotopic signature under open conditions. Geoderma 273, 20–24. https://doi.org/10.1016/j.geoderma.2016.03.014

Falzone, G., Mehdipour, I., Neithalath, N., Bauchy, M., Simonetti, D., Sant, G., **2021**. New insights into the mechanisms of carbon dioxide mineralization by portlandite. AIChE J. 67. https://doi.org/10.1002/aic.17160

Flude, S., Györe, D., Stuart, F.M., Zurakowska, M., Boyce, A.J., Haszeldine, R.S., Chalaturnyk, R., Gilfillan, S.M.V., **2017**. The inherent tracer fingerprint of captured CO_2. Int. J. Greenh. Gas Control 65, 40–54. https://doi.org/10.1016/j.ijggc.2017.08.010

Gaboreau, S., Lerouge, C., Dewonck, S., Linard, Y., Bourbon, X., Fialips, C.I., Mazurier, A., Pret, D., Borschneck, D., Montouillout, V., Gaucher, E.C., Claret, F., **2012**. In-situ interaction of cement paste and shotcrete with claystones in a deep disposal context. Am. J. Sci. 312, 314–356. https://doi.org/10.2475/03.2012.03

Gu, T., Guo, X., Li, Z., Cheng, X., Fan, X., Korayem, A., Duan, W.H., **2017**. Coupled effect of CO_2 attack and tensile stress on well cement under CO_2 storage conditions. Constr. Build. Mater. 130, 92–102. https://doi.org/10.1016/j.conbuildmat.2016.10.117

Györe, D., Gilfillan, S.M.V., Stuart, F.M., **2017**. Tracking the interaction between injected CO_2 and reservoir fluids using noble gas isotopes in an analogue of large-scale carbon capture and storage. Appl. Geochemistry 78, 116–128. https://doi.org/10.1016/j.apgeochem.2016.12.012

Ha, J.H., Jeen, S.-W., Hwang, H.-T., Lee, K.-K., **2020**. Changes in geochemical and carbon isotopic compositions during reactions of CO_2-saturated groundwater with aquifer materials. Int. J. Greenh. Gas Control 95, 102961. https://doi.org/10.1016/j.ijggc.2020.102961

Hansen, M., Scholz, D., Schöne, B.R., Spötl, C., **2019**. Simulating speleothem growth in the laboratory: Determination of the stable isotope fractionation ($\delta^{13}C$ and $\delta^{18}O$) between H_2O, DIC and $CaCO_3$. Chem. Geol. 509, 20–44. https://doi.org/10.1016/j.chemgeo.2018.12.012

Hansen, T., Gardeler, B., Matthiessen, B., **2013**. Technical note: precise quantitative measurements of total dissolved inorganic carbon from small amounts of seawater using a gas chromatographic system. Biogeosciences 10, 6601–6608. https://doi.org/10.5194/bg-10-6601-2013

Herath, I.K., Wu, S., Ma, M., Huang, P., **2020**. Reservoir CO_2 evasion flux and controlling factors of carbon species traced by $\delta^{13}C$-DIC at different regulating phases of a hydro-power dam. Sci. Total Environ. 698, 134184. https://doi.org/10.1016/j.scitotenv.2019.134184

Higgs, K.E., Haese, R.R., Golding, S.D., Schacht, U., Watson, M.N., **2015**. The Pretty Hill Formation as a natural analogue for CO_2 storage: an investigation of mineralogical and isotopic changes associated with sandstones exposed to low, intermediate and high CO_2 concentrations over geological time. Chem. Geol. 399, 36–64. https://doi.org/10.1016/j.chemgeo.2014.10.019

Higl, J., Hinder, D., Rathgeber, C., Ramming, B., Lindén, M., **2021**. Detailed in situ ATR-FTIR spectroscopy study of the early stages of C-S-H formation during hydration of monoclinic C_3S. Cem. Concr. Res. 142, 106367. https://doi.org/10.1016/j.cemconres.2021.106367

Huerta, N.J., Hesse, M.A., Bryant, S.L., Strazisar, B.R., Lopano, C., **2016**. Reactive transport of CO_2-saturated water in a cement fracture: application to wellbore leakage during geologic CO_2 storage. Int. J. Greenh. Gas Control 44, 276–289. https://doi.org/10.1016/j.ijggc.2015.02.006

Iglesias, R.S., Ketzer, J.M., Maraschin, A.J., Sbrissa, G., **2018**. Characterization and modeling of CO_2-water-rock interactions in Hygiene Sandstones (Upper Cretaceous), Denver Basin, aimed for carbon dioxide geological storage. Greenh. Gases Sci. Technol. 8, 781–795. https://doi.org/10.1002/ghg.1788

Iglesias, R.S., Romio, C., Melo, C.L., Musse, A.P.S., do Rosário, F., Oldenburg, C.M., **2019**. Modeling CO_2 flow in support of a shallow subsurface controlled leakage field test. Greenh. Gases Sci. Technol. 9, 1027–1042. https://doi.org/10.1002/ghg.1917

Johnson, G., Mayer, B., Shevalier, M., Nightingale, M., Hutcheon, I., **2011**. Tracing the movement of CO_2 injected into a mature oilfield using carbon isotope abundance ratios: the example of the Pembina Cardium CO_2 Monitoring project. Int. J. Greenh. Gas Control 5, 933–941. https://doi.org/10.1016/j.ijggc.2011.02.003

Kampman, N., Bickle, M., Wigley, M., Dubacq, B., **2014**. Fluid flow and CO_2–fluid–mineral interactions during CO_2-storage in sedimentary basins. Chem. Geol. 369, 22–50. https://doi.org/10.1016/j.chemgeo.2013.11.012

Karolytė, R., Serno, S., Johnson, G., Gilfillan, S.M.V., **2017**. The influence of oxygen isotope exchange between CO_2 and H_2O in natural CO_2-rich spring waters: Implications for geothermometry. Appl. Geochemistry 84, 173–186. https://doi.org/10.1016/j.apgeochem.2017.06.012

Koukouzas, N., Kypritidou, Z., Vasilatos, C., Tsoukalas, N., Rochelle, C.A., Purser, G., **2017**. Geochemical modeling of carbonation of hydrated oil well cement

exposed to CO_2-saturated brine solution. Appl. Geochemistry 85, 35–48. https://doi.org/10.1016/j.apgeochem.2017.08.002

Krishnamurthy, R.V., Schmitt, D., Atekwana, E.A., Baskaran, M., **2003**. Isotopic investigations of carbonate growth on concrete structures. Appl. Geochemistry 18, 435–444. https://doi.org/10.1016/S0883-2927(02)00089-6

Letolle, R., Gegout, P., Moranville-Regourd, M., Gaveau, B., **1990**. Carbon-13 and Oxygen-18 mass spectrometry as a potential tool for the study of carbonate phases in concretes. J. Am. Ceram. Soc. 73, 3617–3625. https://doi.org/10.1111/j.1151-2916.1990.tb04267.x

Létolle, R., Gégout, P., Rafai, N., Revertegat, E., **1992**. Stable isotopes of carbon and oxygen for the study of carbonation/decarbonation processes in concretes. Cem. Concr. Res. 22, 235–240. https://doi.org/10.1016/0008-8846(92)90061-Y

Li, L., Hubler, M.H., Xi, Y., **2020**. Theoretical modeling on chemical composition and mechanical properties of well cement under carbonation reactions. J. Clean. Prod. 276, 124270. https://doi.org/10.1016/j.jclepro.2020.124270

Li, Y., Liu, W., Xing, F., Wang, S., Tang, L., Lin, S., Dong, Z., **2020**. Carbonation of the synthetic calcium silicate hydrate (C-S-H) under different concentrations of CO_2: Chemical phases analysis and kinetics. J. CO_2 Util. 35, 303–313. https://doi.org/10.1016/j.jcou.2019.10.001

Li, Z.-P., Tao, M.-X., Li, L.-W., Wang, Z.-D., Du, L., Zhang, M.-F., **2007**. Determination of isotope composition of dissolved inorganic carbon by gas chromatography-conventional isotope-ratio mass spectrometry. Chinese J. Anal. Chem. 35, 1455–1458. https://doi.org/10.1016/S1872-2040(07)60089-9

Liu, B., Qin, J., Shi, J., Jiang, J., Wu, X., He, Z., **2021**. New perspectives on utilization of CO_2 sequestration technologies in cement-based materials. Constr. Build. Mater. 272, 121660. https://doi.org/10.1016/j.conbuildmat.2020.121660

Liu, L., Ji, Y., Gao, F., Zhang, L., Zhang, Z., Liu, X., **2021**. Study on high-efficiency CO_2 absorption by fresh cement paste. Constr. Build. Mater. 270, 121364. https://doi.org/10.1016/j.conbuildmat.2020.121364

Liu, W., Li, Y.-Q.Q., Tang, L.-P.P., Dong, Z.-J.J., **2019**. XRD and ^{29}Si MAS NMR study on carbonated cement paste under accelerated carbonation using different concentration of CO_2. Mater. Today Commun. 19, 464–470. https://doi.org/10.1016/j.mtcomm.2019.05.007

Lu, J., Wilkinson, M., Haszeldine, R.S., Boyce, A.J., **2011**. Carbonate cements in Miller field of the UK North Sea: a natural analog for mineral trapping in CO_2 geological storage. Environ. Earth Sci. 62, 507–517. https://doi.org/10.1007/s12665-010-0543-1

Manceau, J.C.C., Tremosa, J., Lerouge, C., Gherardi, F., Nussbaum, C., Wasch, L.J.J., Alberic, P., Audigane, P., Claret, F., **2016**. Well integrity assessment by a 1:1 scale wellbore experiment: exposition to dissolved CO_2 and overcoring. Int. J. Greenh. Gas Control 54, 258–271. https://doi.org/10.1016/j.ijggc.2016.09.012

Mayer, B., Humez, P., Becker, V., Dalkhaa, C., Rock, L., Myrttinen, A., Barth, J.A.C., **2015**. Assessing the usefulness of the isotopic composition of CO_2 for leakage monitoring at CO_2 storage sites: a review. Int. J. Greenh. Gas Control 37, 46–60. https://doi.org/10.1016/j.ijggc.2015.02.021

Mayer, B., Shevalier, M., Nightingale, M., Kwon, J.-S., Johnson, G., Raistrick, M., Hutcheon, I., Perkins, E., **2013**. Tracing the movement and the fate of injected

CO_2 at the IEA GHG Weyburn-Midale CO_2 monitoring and storage project (Saskatchewan, Canada) using carbon isotope ratios. Int. J. Greenh. Gas Control 16, S177–S184. https://doi.org/10.1016/j.ijggc.2013.01.035

Metz, B., Davidson, O., De Coninck, H., Loos, M., Meyer, L., **2005**. IPCC special report on carbon dioxide capture and storage, Working Group III of the Intergovernmental Panel on Climate Change, Cambridge University Press, Cambridge, United Kingdom and New York, NY, USA, 2005.

Morandeau, A.E., White, C.E., **2015**. In situ X-ray pair distribution function analysis of accelerated carbonation of a synthetic calcium–silicate–hydrate gel. J. Mater. Chem. A 3, 8597–8605. https://doi.org/10.1039/C5TA00348B

Myers, M.B., Roberts, J.J., White, C., Stalker, L., **2019**. An experimental investigation into quantifying CO_2 leakage in aqueous environments using chemical tracers. Chem. Geol. 511, 91–99. https://doi.org/10.1016/j.chemgeo.2019.02.033

Omosebi, O., Maheshwari, H., Ahmed, R., Shah, S., Osisanya, S., Hassani, S., DeBruijn, G., Cornell, W., Simon, D., **2016**. Degradation of well cement in HPHT acidic environment: effects of CO_2 concentration and pressure. Cem. Concr. Compos. 74, 54–70. https://doi.org/10.1016/j.cemconcomp.2016.09.006

Paris, J.M., Roessler, J.G., Ferraro, C.C., DeFord, H.D., Townsend, T.G., **2016**. A review of waste products utilized as supplements to Portland cement in concrete. J. Clean. Prod. 121, 1–18. https://doi.org/10.1016/j.jclepro.2016.02.013

Park, S., Moon, H., Kim, J.-H., Lee, M., Chung, C.-W., **2021**. Reaction of hydrated cement paste with supercritical carbon dioxide. Constr. Build. Mater. 281, 122615. https://doi.org/10.1016/j.conbuildmat.2021.122615

Parkhurst, D.L., Appelo, C.A.J., **2013**. Description of Input and Examples for PHREEQC Version 3 — A Computer Program for Speciation, Batch-Reaction , One-Dimensional Transport , and Inverse Geochemical Calculations, U.S. Geological Survey Techniques and Methods, book 6, chapter A43. U.S. Geological Survey, Denver. https://doi.org/10.1016/0029-6554(94)90020-5

Ponzi, G.G.D., Santos, V.H.J.M. dos, Martel, R.B., Pontin, D., Stepanha, A.S. de G. e, Schütz, M.K., Menezes, S.C., Einloft, S.M.O., Vecchia, F.D., **2021**. Basalt powder as a supplementary cementitious material in cement paste for CCS wells: chemical and mechanical resistance of cement formulations for CO_2 geological storage sites. Int. J. Greenh. Gas Control 109, 103337. https://doi.org/10.1016/j.ijggc.2021.103337

Rafai, N., Letolle, R., Blanc, P., Person, A., Gegout, P., **1991**. Isotope geochemistry (^{13}C, ^{18}O) of carbonation processes in concretes. Cem. Concr. Res. 21, 368–377. https://doi.org/10.1016/0008-8846(91)90018-D

Sade, Z., Yam, R., Shemesh, A., Halevy, I., **2020**. Kinetic fractionation of carbon and oxygen isotopes during $BaCO_3$ precipitation. Geochim. Cosmochim. Acta 280, 395–422. https://doi.org/10.1016/j.gca.2020.04.025

Saillio, M., Baroghel-Bouny, V., Pradelle, S., Bertin, M., Vincent, J., d'Espinose de Lacaillerie, J.-B., **2021**. Effect of supplementary cementitious materials on carbonation of cement pastes. Cem. Concr. Res. 142, 106358. https://doi.org/10.1016/j.cemconres.2021.106358

Santos, V.H.J.M. dos, Pontin, D., Ponzi, G.G.D., Stepanha, A.S. de G. e., Martel, R.B., Schütz, M.K., Einloft, S.M.O., Dalla Vecchia, F., **2021**. Application of Fourier transform infrared spectroscopy (FTIR) coupled with multivariate regression for calcium carbonate ($CaCO_3$) quantification in cement. Constr. Build. Mater. 313, 125413. https://doi.org/10.1016/j.conbuildmat.2021.125413

Šavija, B., Luković, M., **2016**. Carbonation of cement paste: understanding, challenges, and opportunities. Constr. Build. Mater. 117, 285–301. https://doi.org/10.1016/j.conbuildmat.2016.04.138

Schulz, A., Vogt, C., Lamert, H., Peter, A., Heinrich, B., Dahmke, A., Richnow, H.-H., **2012**. Monitoring of a simulated CO_2 leakage in a shallow aquifer using stable carbon isotopes. Environ. Sci. Technol. 46, 11243–11250. https://doi.org/10.1021/es3026837

Shah, V., Scrivener, K., Bhattacharjee, B., Bishnoi, S., **2018**. Changes in microstructure characteristics of cement paste on carbonation. Cem. Concr. Res. 109, 184–197. https://doi.org/10.1016/j.cemconres.2018.04.016

Shelton, J.L., McIntosh, J.C., Warwick, P.D., Yi, A.L.Z., **2014**. Fate of injected CO_2 in the Wilcox Group, Louisiana, Gulf Coast Basin: chemical and isotopic tracers of microbial–brine–rock–CO_2 interactions. Appl. Geochemistry 51, 155–169. https://doi.org/10.1016/j.apgeochem.2014.09.015

Shevalier, M., Dalkhaa, C., Humez, P., Mayer, B., Becker, V., Nightingale, M., Rock, L., Zhang, G., **2014**. Coupling of TOUGHREACT-geochemist workbench (GWB) for modeling changes in the isotopic composition of CO_2 leaking from a CCS storage reservoir. Energy Procedia 63, 3751–3760. https://doi.org/10.1016/j.egypro.2014.11.404

Skocek, J., Zajac, M., Ben Haha, M., **2020**. Carbon capture and utilization by mineralization of cement pastes derived from recycled concrete. Sci. Rep. 10, 5614. https://doi.org/10.1038/s41598-020-62503-z

Śliwiński, M.G., Kitajima, K., Kozdon, R., Spicuzza, M.J., Denny, A., Valley, J.W., **2017**. In situ $\delta^{13}C$ and $\delta^{18}O$ microanalysis by SIMS: a method for characterizing the

carbonate components of natural and engineered CO_2-reservoirs. Int. J. Greenh. Gas Control 57, 116–133. https://doi.org/10.1016/j.ijggc.2016.12.013

Tajuelo, E., Garbev, K., Merz, D., Black, L., Richardson, I.G., **201**7. Thermal stability of C-S-H phases and applicability of Richardson and Groves' and Richardson C-(A)-S-H (I) models to synthetic C-S-H. Cem. Concr. Res. 93, 45–56. https://doi.org/10.1016/j.cemconres.2016.12.005

Teodoriu, C., Bello, O., **2020**. A review of cement testing apparatus and methods under CO_2 environment and their impact on well integrity prediction – where do we stand? J. Pet. Sci. Eng. 187, 106736. https://doi.org/10.1016/j.petrol.2019.106736

Tiong, M., Gholami, R., Rahman, M.E., **2019**. Cement degradation in CO_2 storage sites: a review on potential applications of nanomaterials. J. Pet. Explor. Prod. Technol. 9, 329–340. https://doi.org/10.1007/s13202-018-0490-z

Van Geldern, R., Nowak, M.E., Zimmer, M., Szizybalski, A., Myrttinen, A., Barth, J.A.C., Jost, H.-J., **2014**. Field-based stable isotope analysis of carbon dioxide by mid-infrared laser spectroscopy for carbon capture and storage monitoring. Anal. Chem. 86, 12191–12198. https://doi.org/10.1021/ac5031732

Vance, K., Falzone, G., Pignatelli, I., Bauchy, M., Balonis, M., Sant, G., **2015**. Direct carbonation of $Ca(OH)_2$ using liquid and supercritical CO_2: implications for carbon-neutral cementation. Ind. Eng. Chem. Res. 54, 8908–8918. https://doi.org/10.1021/acs.iecr.5b02356

Vermeul, V.R., Amonette, J.E., Strickland, C.E., Williams, M.D., Bonneville, A., **2016**. An overview of the monitoring program design for the FutureGen 2.0 CO_2 storage site. Int. J. Greenh. Gas Control 51, 193–206. https://doi.org/10.1016/j.ijggc.2016.05.023

Wakeel, S. Al, Němeček, J., Li, L., Xi, Y., Hubler, M., **2019**. The effect of introducing nanoparticles on the fracture toughness of well cement paste. Int. J. Greenh. Gas Control 84, 147–153. https://doi.org/10.1016/j.ijggc.2019.03.009

Wang, D., Fang, Y., Zhang, Y., Chang, J., **2019**. Changes in mineral composition, growth of calcite crystal, and promotion of physico-chemical properties induced by carbonation of β-C_2S. J. CO_2 Util. 34, 149–162. https://doi.org/10.1016/j.jcou.2019.06.005

Wang, J., Wen, X., Li, S., **2017**. Differentiated correction on the signal intensity dependence of GasBench II-IRMS from blank effect and instrument nonlinear effect. Int. J. Mass Spectrom. 422, 80–87. https://doi.org/10.1016/j.ijms.2017.08.012

Welch, S.A., Sheets, J.M., Place, M.C., Saltzman, M.R., Edwards, C.T., Gupta, N., Cole, D.R., **2019**. Assessing geochemical reactions during CO_2 injection into an oil-bearing reef in the Northern Michigan basin. Appl. Geochemistry 100, 380–392. https://doi.org/10.1016/j.apgeochem.2018.12.008

Wiese, B., Zimmer, M., Nowak, M., Pellizzari, L., Pilz, P., **2013**. Well-based hydraulic and geochemical monitoring of the above zone of the CO_2 reservoir at Ketzin, Germany. Environ. Earth Sci. 70, 3709–3726. https://doi.org/10.1007/s12665-013-2744-x

Yan, H., Dreybrodt, W., Bao, H., Peng, Y., Wei, Y., Ma, S., Mo, B., Sun, H., Liu, Z., **2021**. The influence of hydrodynamics on the carbon isotope composition of inorganically precipitated calcite. Earth Planet. Sci. Lett. 565, 116932. https://doi.org/10.1016/j.epsl.2021.116932

Yan, H., Liu, Z., Sun, H., **2020**. Large degrees of carbon isotope disequilibrium during precipitation-associated degassing of CO_2 in a mountain stream. Geochim. Cosmochim. Acta 273, 244–256. https://doi.org/10.1016/j.gca.2020.01.012

Zhang, L., Huang, H., Wang, Y., Ren, B., Ren, S., Chen, G., Zhang, H., **2014**. CO_2 storage safety and leakage monitoring in the CCS demonstration project of Jilin oilfield, China. Greenh. Gases Sci. Technol. 4, 425–439. https://doi.org/10.1002/ghg.1411

Zhang, T., Zhang, W., Yang, R., Liu, Y., Jafari, M., **2021**. CO_2 capture and storage monitoring based on remote sensing techniques: a review. J. Clean. Prod. 281, 124409. https://doi.org/10.1016/j.jclepro.2020.124409

Zhou, Y., Guo, H., Lu, H., Mao, R., Zheng, H., Wang, J., **2015**. Analytical methods and application of stable isotopes in dissolved organic carbon and inorganic carbon in groundwater. Rapid Commun. Mass Spectrom. 29, 1827–1835. https://doi.org/10.1002/rcm.7280

Zimmer, M., Szizybalski, A., Norden, B., Vieth-Hillebrand, A., Liebscher, A., **2018**. Monitoring of the gas composition and stable carbon isotopes during side track drilling in Ktzi 203 at the Ketzin CO_2 storage pilot site, Germany. Adv. Geosci. 45, 7–11. https://doi.org/10.5194/adgeo-45-7-2018

Zuo, Z.-C.C., Bennett, T., **2021**. The chemical and mechanical effects of calcium carbonate precipitation for cement-based materials exposed to carbonated brine. Int. J. Greenh. Gas Control 104, 103221. https://doi.org/10.1016/j.ijggc.2020.103221

4.2.1. Material suplementar do estudo de geoquímica isotópica

Table S1. Calibration and validation sets applied in the multivariate model for quantification of $CaCO_3$ in cement

Calibration set		Validation set	
Sample	**mg $CaCO_3$/g cement**	**Sample**	**mg $CaCO_3$/g cement**
C1_1	45.80	**V1_1**	67.17
C1_2	45.80	**V1_2**	69.92
C1_3	45.80	**V2_1**	110.96
C2_1	88.73	**V2_2**	110.69
C2_2	88.60	**V3_1**	152.11
C2_3	88.39	**V3_2**	152.38
C3_1	132.68	**V4_1**	193.25
C3_2	131.98	**V4_2**	193.81
C3_3	130.68	**V5_1**	235.74
C4_1	173.74	**V5_2**	236.46
C4_2	173.56	**V6_1**	276.66
C4_3	171.82	**V6_2**	278.50
C5_1	214.56	**V7_1**	319.58
C5_2	215.60	**V7_2**	319.65
C5_3	216.08	**V8_1**	360.40
C6_1	256.50	**V8_2**	360.45
C6_2	257.48	**V9_1**	403.45
C6_3	258.13	**V9_2**	404.29
C7_1	298.13	**V10_1**	445.33
C7_2	298.43	**V10_2**	445.92
C7_3	298.65		
C8_1	339.80		
C8_2	340.57		
C8_3	341.35		
C9_1	380.95		
C9_2	381.09		
C9_3	382.80		
C10_1	422.69		
C10_2	425.26		
C10_3	425.62		
C11_1	468.20		
C11_2	468.20		
C11_3	468.20		

Table S2. Parameters obtained for PLS regression models for quantification of $CaCO_3$ in cement

Parameters	PLS-R
Pre-processing	MC; BC; SNV
Factors	6
EV% (X/y)	99.82
R^2 Calibration	0.9996
R^2 Prediction	0.9993
RMSEC	2.81
RMSEP	4.13
Bias	0.00
P Bias	2.50

EV - Explained variance; RMSEC - Root Mean Square Error of Calibration; RMSEP - Root Mean Square Error of Prediction; MC - mean centered; BC - baseline correction; SVN - standard normal variate

Table S3. Results of inorganic carbon dissolve (DIC) quantification from cement powder carbonation experiments

Sample		DIC	
		Concentration (Na_2CO_3-eq ppm)	**Average concentration (Na_2CO_3-eq ppm)**
C50_30	1	7671.9	7281.4 ± 552.3
	2	6890.8	
C50_65	1	6844.2	6444.8 ± 564.9
	2	6045.3	
C50_100	1	6567.3	6547.0 ± 28.8
	2	6526.6	
C100_30	1	4940.7	5287.3 ± 490.2
	2	5633.9	
C100_65	1	4651.4	4069.1 ± 823.4
	2	3486.9	
C100_100	1	5030.5	5074.6 ± 62.4
	2	5118.7	
C150_30	1	4632.6	4994.2 ± 511.4
	2	5355.8	
C150_65	1	6487.3	6444.8 ± 60.0
	2	6402.4	
C150_100	1	5598.4	5256.2 ± 484.0
	2	4914.0	

Table S4. Results of $CaCO_3$ quantification in cement powder

Samples	$CaCO_3$ content (mg $CaCO_3$/g cement)	Error (mg $CaCO_3$/g cement)	Average (mg $CaCO_3$/g cement)
C50_30 (1)	354.3	9.5	
C50_30 (2)	355.3	9.4	355.13 ± 0.74
C50_30 (3)	355.8	9.3	
C50_65 (1)	389.5	8.6	
C50_65 (2)	390.5	8.6	390.36 ± 0.83
C50_65 (3)	391.1	8.5	
C50_100 (1)	380.8	9.7	
C50_100 (2)	381.8	9.6	381.53 ± 0.66
C50_100 (3)	382.0	9.6	
C100_30 (1)	386.3	8.8	
C100_30 (2)	386.6	8.8	386.49 ± 0.21
C100_30 (3)	386.6	8.8	
C100_65 (1)	363.2	10.3	
C100_65 (2)	364.2	10.2	363.97 ± 0.65
C100_65 (3)	364.5	10.2	
C100_100 (1)	395.4	9.0	
C100_100 (2)	396.4	9.0	396.10 ± 0.58
C100_100 (3)	396.5	9.0	
C150_30 (1)	344.6	10.1	
C150_30 (2)	345.0	10.0	344.96 ± 0.37
C150_30 (3)	345.3	10.0	
C150_65 (1)	384.3	8.3	
C150_65 (2)	385.3	8.3	385.13 ± 0.76
C150_65 (3)	385.8	8.2	
C150_100 (1)	367.0	11.4	
C150_100 (2)	368.1	11.3	367.90 ± 0.78
C150_100 (3)	368.5	11.3	

Table S5. Results of stable carbon isotope analysis of cylinder CO_2 and post-carbonation gas

Sample		$\delta^{13}C$ (‰)	Average (‰)
CO_2 (Cylinder)	**1**	-41.98	-41.86 ± 0.12
	2	-41.85	
	3	-41.75	
CO_2 (Post reactor)	**1**	-42.31	-42.30 ± 0.00
	2	-42.30	

Table S6. Results of DIC stable carbon isotope signature from cement powder carbonation experiments

Sample	$\delta^{13}C$-DIC (‰)	Average (‰)
C50_30	-30.49	-30.50 ± 0.00
	-30.50	
C50_65	-30.86	-30.71 ± 0.21
	-30.56	
C50_100	-29.13	-29.23 ± 0.14
	-29.33	
C100_30	-29.70	-29.78 ± 0.11
	-29.86	
C100_65	-30.08	-30.35 ± 0.38
	-30.62	
C100_100	-30.12	-30.22 ± 0.14
	-30.32	
C150_30	-29.76	-29.99 ± 0.33
	-30.22	
C150_65	-29.15	-29.52 ± 0.52
	-29.88	
C150_100	-30.92	-31.13 ± 0.30
	-31.35	

Table S7. Results of stable carbon isotope analysis of the cement powder carbonation experiments

Sample	$\delta^{13}C$ (‰)	Average (‰)
C50_30	-38.35 -38.31 -38.42	-38.36 ± 0.06
C50_65	-38.09 -38.28 -38.13	-38.16 ± 0.10
C50_100	-38.82 -38.88 -38.93	-38.88 ± 0.05
C100_30	-42.59 -42.83 -42.68	-42.70 ± 0.12
C100_65	-41.03 -41.01 -41.00	-41.01 ± 0.02
C100_100	-40.74 -40.65 -40.64	-40.67 ± 0.05
C150_30	-38.22 -38.52 -38.18	-38.30 ± 0.19
C150_65	-42.22 -42.44 -42.28	-42.31 ± 0.12
C150_100	-41.12 -41.28 -41.35	-41.25 ± 0.12

Table S8. Analysis of variance (ANOVA) of the effect of pressure and temperature on the DIC stable carbon isotope signature results

ANOVA - δ^{13}C-DIC versus Pressure					
Source	**DF**	**Adj SS**	**Adj MS**	**F-value**	**P-value**
Pressure	2	0.01543	0.007714	0.02	0.984
Error	6	2.83169	0.471949	-	-
Total	8	2.84712	-	-	-
ANOVA - δ^{13}C-DIC versus Temperature					
Source	**DF**	**Adj SS**	**Adj MS**	**F-value**	**P-value**
Temperature	2	0.02121	0.0106	0.02	0.978
Error	6	2.82591	0.47099	-	-
Total	8	2.84712	-	-	-

DF - Degrees of freedom; Adj SS - sum of squares; Adj MS - mean square; F-value - F-statistics and P-value - hypothesis testing

Table S9. Analysis of variance (ANOVA) of the effect of pressure and temperature on the $CaCO_3$ stable carbon isotope signature

ANOVA - δ^{13}C-$CaCO_3$ versus Pressure					
Source	**DF**	**Adj SS**	**Adj MS**	**F-value**	**P-value**
Pressure	2	14.31	7.157	3.82	0.085
Error	6	11.25	1.874	-	-
Total	8	25.56	-	-	-
ANOVA - δ^{13}C-$CaCO_3$ versus Temperature					
Source	**DF**	**Adj SS**	**Adj MS**	**F-value**	**P-value**
Temperature	2	0.7839	0.3919	0.09	0.911
Error	6	24.7774	4.1296	-	-
Total	8	25.5612	-	-	-

DF - Degrees of freedom; Adj SS - sum of squares; Adj MS - mean square; F-value - F-statistics and P-value - hypothesis testing

Table S10. Analysis of variance (ANOVA) of the effect of pressure and temperature on the isotopic fractionation between CO_2 and DIC

ANOVA - εDIC-CO_2 (δ^{13}C ‰) versus Pressure					
Source	**DF**	**Adj SS**	**Adj MS**	**F-value**	**P-value**
Pressure	2	0.01543	0.007714	0.02	0.984
Error	6	2.83169	0.471949	-	-
Total	8	2.84712	-	-	-
ANOVA - εDIC-CO_2 (δ^{13}C ‰) versus Temperature					
Source	**DF**	**Adj SS**	**Adj MS**	**F-value**	**P-value**
Temperature	2	0.02121	0.0106	0.02	0.978
Error	6	2.82591	0.47099	-	-
Total	8	2.84712	-	-	-

DF - Degrees of freedom; Adj SS - sum of squares; Adj MS - mean square; F-value - F-statistics and P-value - hypothesis testing

Table S11. Analysis of variance (ANOVA) of the effect of pressure and temperature on the isotopic fractionation between DIC and $CaCO_3$

ANOVA - $\varepsilon$$CaCO_3$-DIC ($\delta^{13}$C ‰) versus Pressure					
Source	**DF**	**Adj SS**	**Adj MS**	**F-value**	**P-value**
Pressure	2	14.36	7.181	2.59	0.154
Error	6	16.61	2.768	-	-
Total	8	30.97	-	-	-
ANOVA - $\varepsilon$$CaCO_3$-DIC ($\delta^{13}$C ‰) versus Temperature					
Source	**DF**	**Adj SS**	**Adj MS**	**F-value**	**P-value**
Temperature	2	0.5607	0.2803	0.06	0.947
Error	6	30.4087	5.0681	-	-
Total	8	30.9694	-	-	-

DF - Degrees of freedom; Adj SS - sum of squares; Adj MS - mean square; F-value - F-statistics and P-value - hypothesis testing

Table S12. Analysis of variance (ANOVA) of the effect of pressure and temperature on the isotopic fractionation between CO_2 and $CaCO_3$

ANOVA - $\varepsilon CaCO_3$-CO_2 ($\delta^{13}C$ ‰) versus Pressure					
Source	**DF**	**Adj SS**	**Adj MS**	**F-value**	**P-value**
Pressure	2	14.31	7.157	3.82	0.085
Error	6	11.25	1.874		
Total	8	25.56			
ANOVA - $\varepsilon CaCO_3$-CO_2 ($\delta^{13}C$ ‰) versus Temperature					
Source	**DF**	**Adj SS**	**Adj MS**	**F-value**	**P-value**
Temperature	2	0.7839	0.3919	0.09	0.911
Error	6	24.7774	4.1296		
Total	8	25.5612			

DF - Degrees of freedom; Adj SS - sum of squares; Adj MS - mean square; F-value - F-statistics and P-value - hypothesis testing

Table S13. Geochemical parameters estimated by PHREEQC for the reaction conditions of the carbonation experiments

Sample	**Pre. (bar)**	**Temp. (°C)**	**pH**	**$CO_{2\ (aq)}$ (mol/L)**	**CO_3^{2-} (mol/L)**	**HCO_3^- (mol/L)**	**$\alpha CO_{2\ (aq)}$**	**αCO_3^{2-}**	**αHCO_3^-**	**αH_2O**
C50_30	50	30	3.13	1.19E+00	5.75E-11	7.77E-04	0.076	-10.288	-3.119	0.979
C50_65	50	65	3.26	6.08E-01	8.13E-11	5.77E-04	-0.216	-10.138	-3.249	0.989
C50_100	50	100	3.40	4.18E-01	7.82E-11	4.16E-04	-0.379	-10.152	-3.391	0.992
C100_30	100	30	2.94	2.99E+00	5.94E-11	1.22E-03	0.476	-10.273	-2.918	0.948
C100_65	100	65	3.06	1.53E+00	8.38E-11	9.14E-04	0.184	-10.131	-3.049	0.973
C100_100	100	100	3.21	1.05E+00	7.99E-11	6.58E-04	0.021	-10.151	-3.192	0.981
C150_30	150	30	2.87	4.42E+00	6.04E-11	1.47E-03	0.646	-10.260	-2.833	0.923
C150_65	150	65	2.98	2.26E+00	8.51E-11	1.11E-03	0.,354	-10.125	-2.964	0.960
C150_100	150	100	3.13	1.55E+00	8.08E-11	7.99E-04	0.191	-10.147	-3.108	0.972

Table S14. Correlation index between the variables

Variables	Pre.	Temp.	pH	Cond.	DIC	$CaCO_3$	δ^{13}C-DIC	δ^{13}C-$CaCO_3$	$\varepsilon_{DIC\text{-}CO2}$	$\varepsilon_{CaCO3\text{-}DIC}$	$\varepsilon_{CaCO3\text{-}CO2}$ (δ^{13}C)	pH (initial)	CO_2	CO_3^{2-}	HCO_3^-	$\alpha\ CO_2$	αCO_3^{2-}	αHCO_3^-	αH_2O
Pre.																			
Temp.	0.00																		
pH	0.13	-0.04																	
Cond.	-0.85	-0.14	0.07																
DIC	-0.51	-0.10	0.15	0.82															
$CaCO_3$	-0.24	0.49	-0.53	-0.03	0.12														
δ^{13}C-DIC	-0.05	-0.07	0.47	-0.05	0.17	0.22													
δ^{13}C-$CaCO_3$	-0.52	-0.12	0.03	0.66	0.40	-0.39	-0.15												
$\varepsilon_{DIC\text{-}CO2}$	-0.05	-0.07	0.47	-0.05	0.17	0.22	1.00	-0.15											
$\varepsilon_{CaCO3\text{-}DIC}$	-0.46	-0.08	-0.12	0.62	0.31	-0.42	-0.44	0.95	-0.44										
$\varepsilon_{CaCO3\text{-}CO2}$ (δ^{13}C)	-0.52	-0.12	0.03	0.66	0.40	-0.39	-0.15	1.00	-0.15	0.95									
pH (initial)	-0.70	0.69	-0.07	0.57	0.40	0.44	-0.01	0.39	-0.01	0.36	0.39								
CO_2	0.68	-0.63	0.17	-0.56	-0.39	-0.49	0.18	-0.19	0.18	-0.23	-0.19	-0.91							
CO_3^{2-}	0.12	0.78	-0.24	-0.28	-0.17	0.50	-0.07	-0.25	-0.07	-0.20	-0.25	0.43	-0.53						
HCO_3^-	0.69	-0.69	0.13	-0.57	-0.39	-0.46	0.14	-0.31	0.14	-0.32	-0.31	-0.98	0.97	-048					
αCO_2	0.77	-0.61	0.12	-0.63	-0.44	-0.45	0.02	-0.41	0.02	-0.38	-0.41	-0.98	0.94	-0.44	0.98				
αCO_3^{2-}	0.10	0.79	-0.24	-0.27	-0.17	0.50	-0.05	-0.21	-0.05	-0.17	-0.21	0.46	-0.53	1.00	-0.49	-0.47			
αHCO_3^-	0.71	-0.68	0.08	-0.58	-0.41	-0.45	0.03	-0.38	0.03	-0.36	-0.38	-1.00	0.92	-0.43	0.98	0.99	-0.46		
αH_2O	-0.69	0.63	-0.17	0.57	0.39	0.49	-0.18	0.20	-0.18	0.23	0.20	0.91	-1.00	0.52	-0.97	-0.94	0.52	-0.92	

Table S15. Results of DIC quantification from the portlandite (CH) and calcium silicate hydrate (C-S-H) carbonation experiments

Sample		DIC	
		Concentration (Na_2CO_3-eq ppm)	**Average concentration (Na_2CO_3-eq ppm)**
CH_R1	1	1866.9	2011.9 ± 205.1
	2	2157.0	
CH_R2	1	1436.5	1470.7 ± 48.4
	2	1504.9	
C-S-H_R1	1	1915.5	1983.1 ± 95.5
	2	2050.6	
C-S-H_R2	1	1310.0	1679.3 ± 522.4
	2	2048.7	

Table S16. CO_2 isotopic signature used in the portlandite (CH) and calcium silicate hydrate (C-S-H) carbonation experiments

Sample		$\delta^{13}C$ (‰)	S.D (‰)	Average (‰)	S.D (‰)
CO_2 (Cylinder)	**1**	-36.70	0.03	-36.69	0.06
	2	-36.62	0. 06		
	3	-36.76	0.04		

Table S17. Results of DIC isotopic signatures from the portlandite (CH) and calcium silicate hydrate (C-S-H) carbonation experiments

Sample	$\delta^{13}C$-DIC (‰)	S.D (‰)	Average (‰)	S.D (‰)
CH-R1	-22.96	0.20	-22.74	0.24
	-22.77	0.14		
	-22.48	0.19		
CH-R2	-23.39	0.13	-22.96	0.60
	-23.20	0.19		
	-22.27	0.19		
C-S-H-R1	-25.83	0.13	-25.60	0.92
	-26.39	0.19		
	-24.59	0.05		
C-S-H-R2	-24.58	0.15	-24.32	0.62
	-24.77	0.14		
	-23.61	0.44		

Table S18. Results of $CaCO_3$ isotopic signatures from the portlandite (CH) and calcium silicate hydrate (C-S-H) carbonation experiments

Sample	$\delta^{13}C$ (‰)	S.D (‰)	Average (‰)	S.D (‰)
CH-R1	-36.05	0.04	-36.45	0.20
	-36.59	0.15		
	-36.40	0.02		
	-36.38	0.03		
	-36.57	0.10		
	-36.58	0.11		
	-36.55	0.22		
CH-R2	-36.62	0.13	-36.91	0.21
	-37.08	0.18		
	-36.90	0.03		
	-37.04	0.05		
C-S-H-R1	-34.29	0.04	-34.24	0.22
	-34.15	0.06		
	-34.53	0.03		
	-34.01	0.06		
C-S-H-R2	-33.80	0.02	-33.83	0.08
	-33.92	0.10		
	-33.77	0.03		

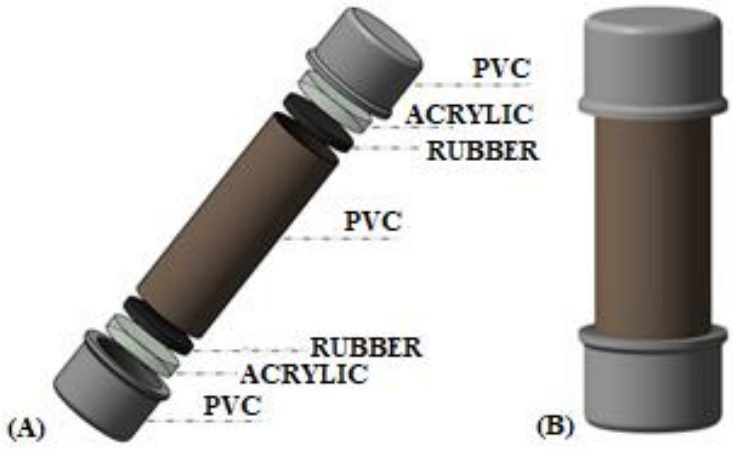

Figure S1. Mold used to prepare cement paste samples

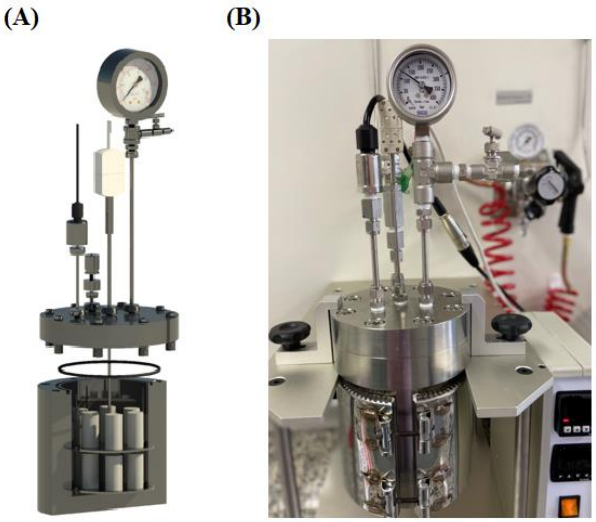

Figure S2. Carbonation experiments: (A) reactor design and (B) high pressure-high temperature (HPHT) autoclave

Figure S3. Hydrated class G cement powder: (A) non-carbonated cement powder (mag: 10000 X) and (B) carbonated cement powder (mag: 10000 X)

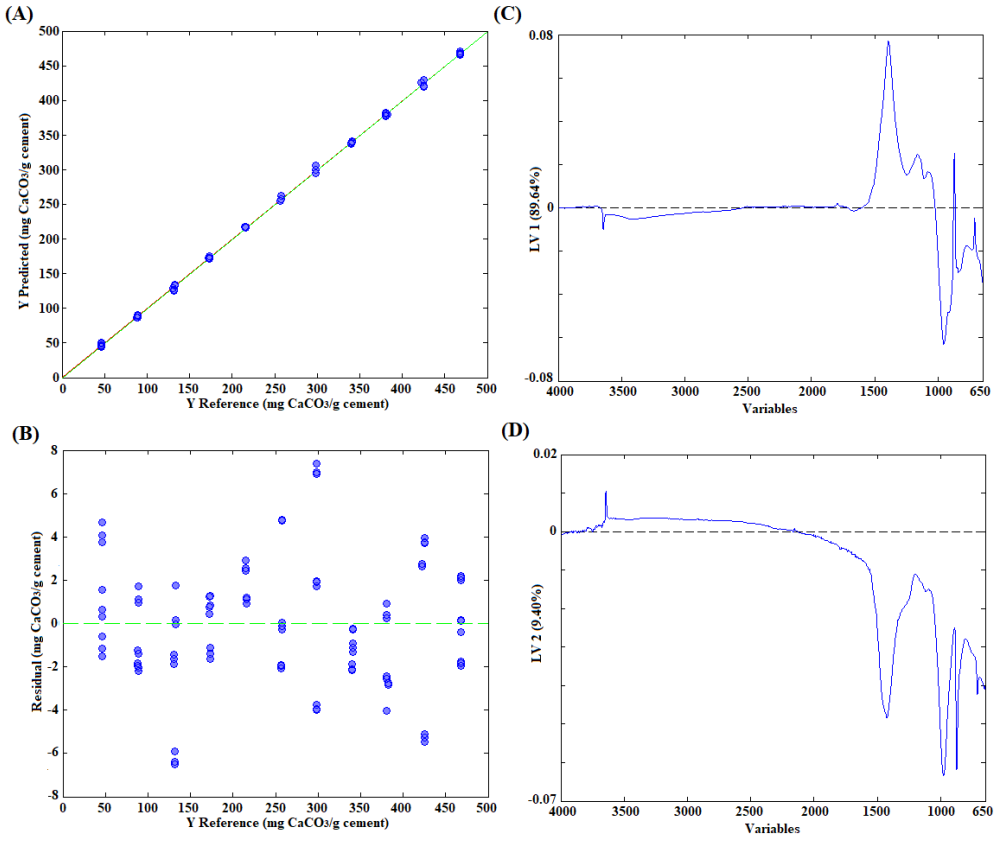

Figure S4. PLS regression from FTIR to quantify $CaCO_3$ in cement powder: (A) predicted vs. reference plot, (B) residual plot, (C) PLS loading (LV 1) and (D) PLS loading (LV 2)

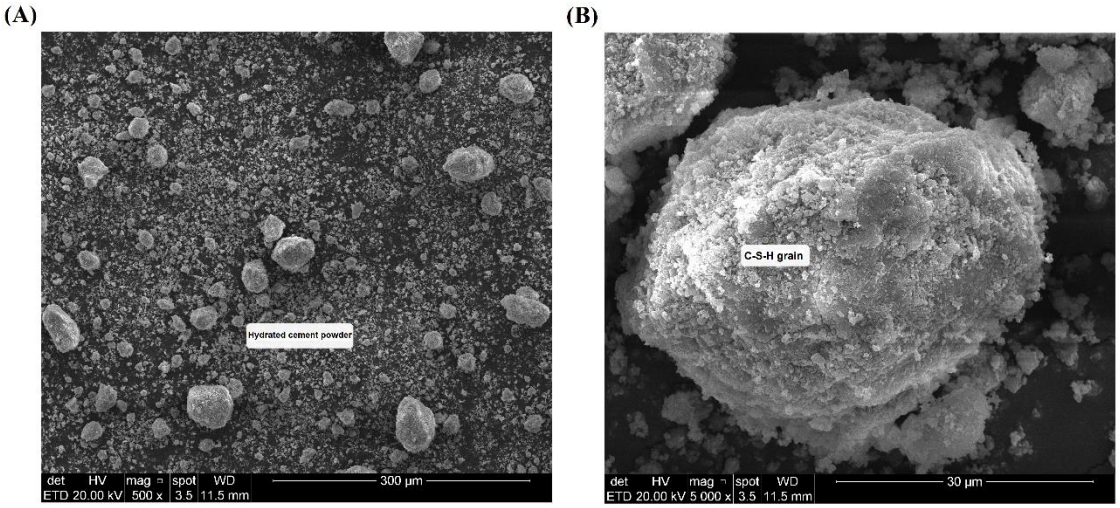

Figure S5. Hydrated class G cement powder: (A) 500x magnification and (B) 5000x magnification

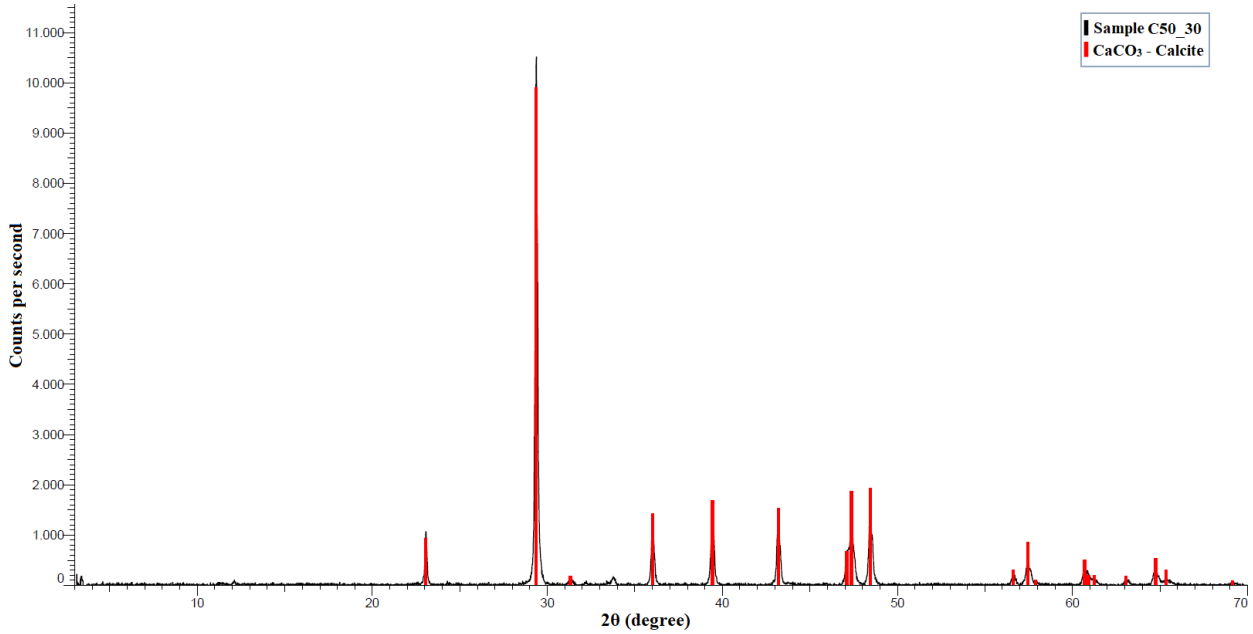

Figure S6. X-ray diffraction pattern of C50_30 carbonated cement powder sample

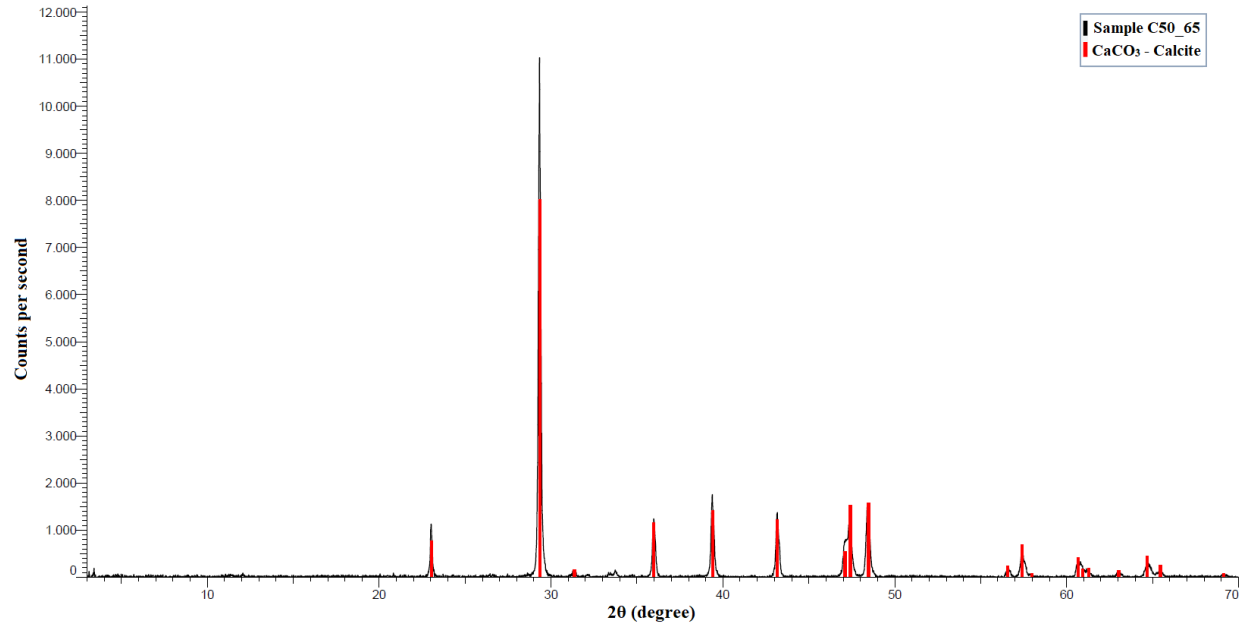

Figure S7. X-ray diffraction pattern of C50_65 carbonated cement powder sample

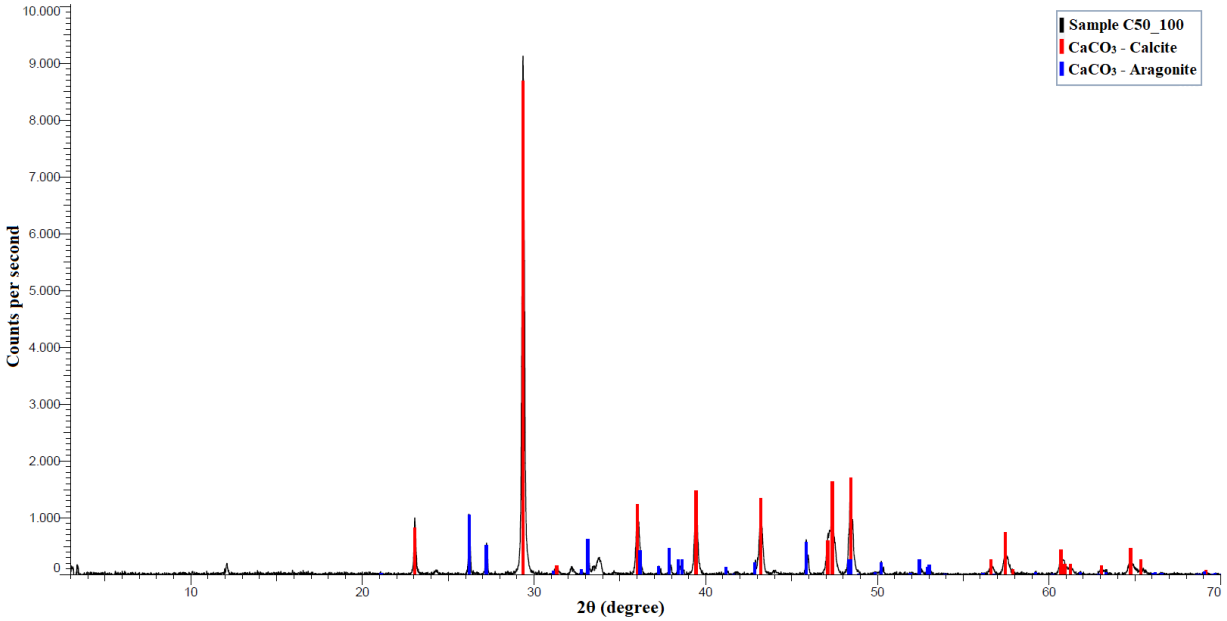

Figure S8. X-ray diffraction pattern of C50_100 carbonated cement powder sample

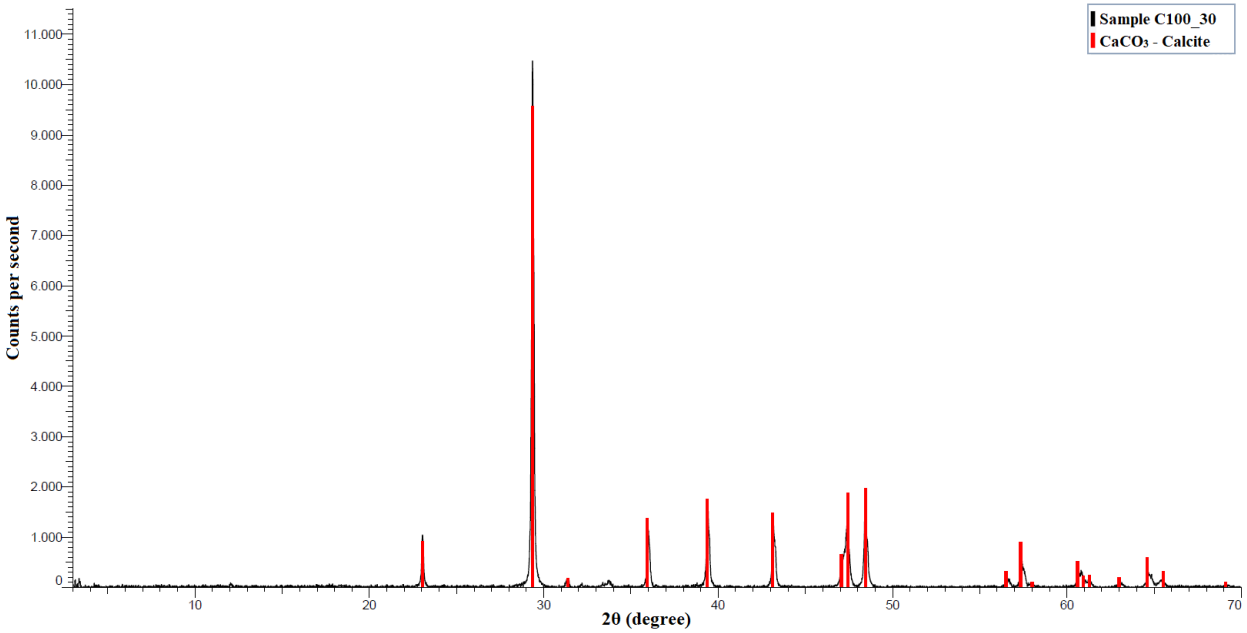

Figure S9. X-ray diffraction pattern of C100_30 carbonated cement powder sample

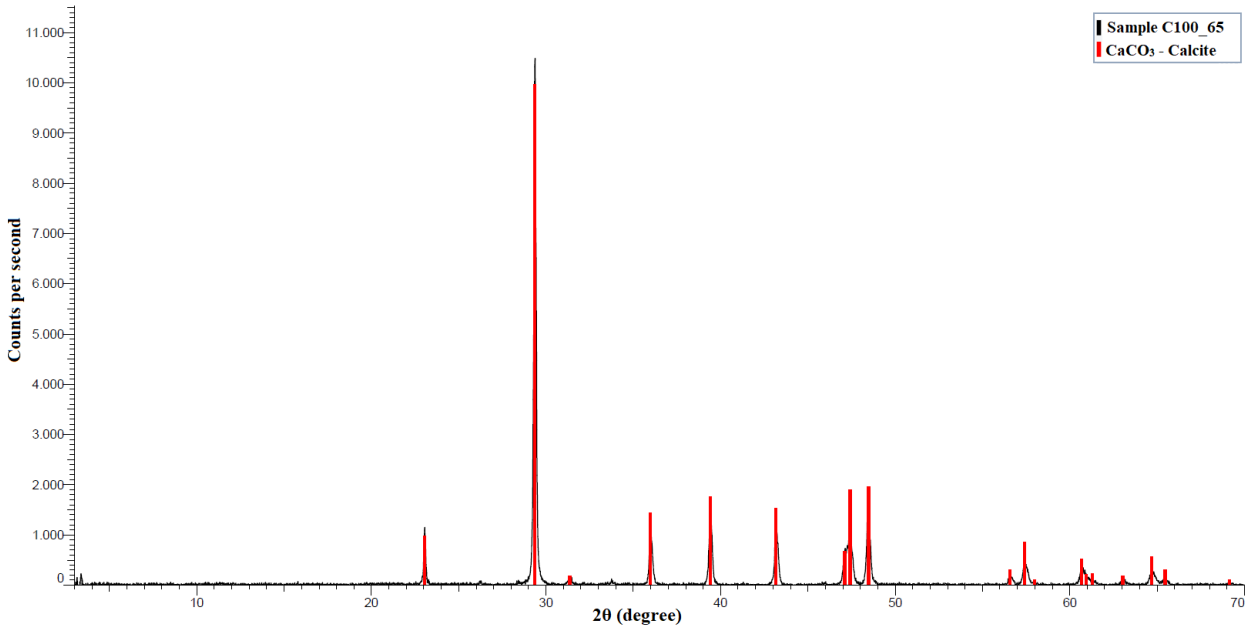

Figure S10. X-ray diffraction pattern of C100_65 carbonated cement powder sample

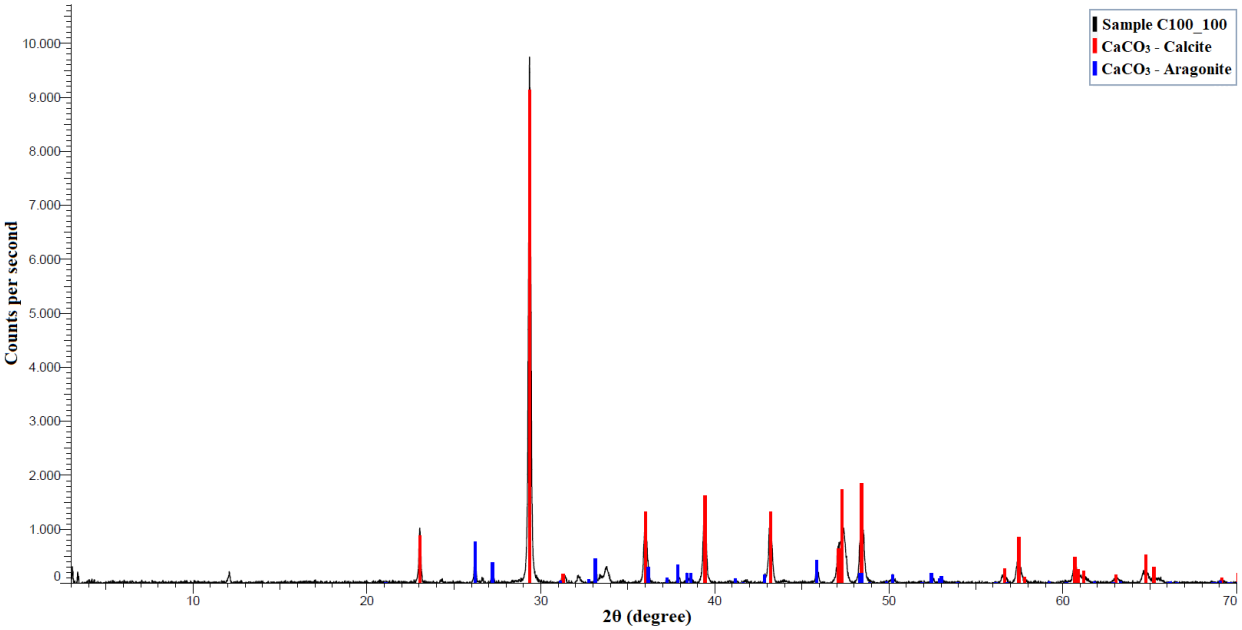

Figure S11. X-ray diffraction pattern of C100_100 carbonated cement powder sample

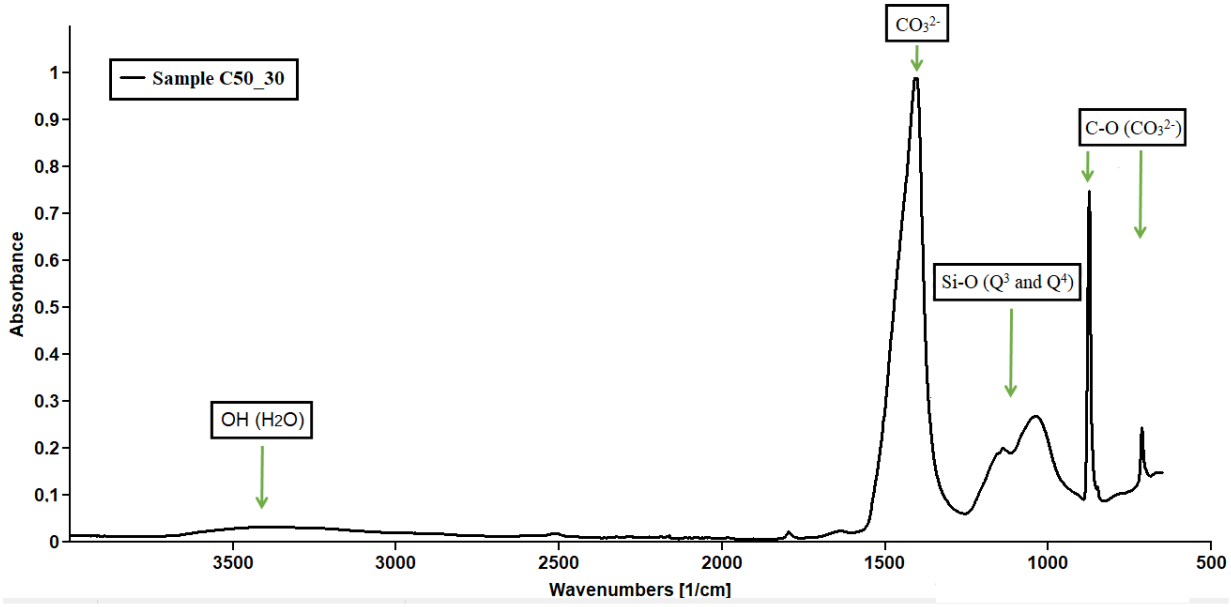

Figure S12. Infrared spectrum of C50_30 carbonated cement powder sample

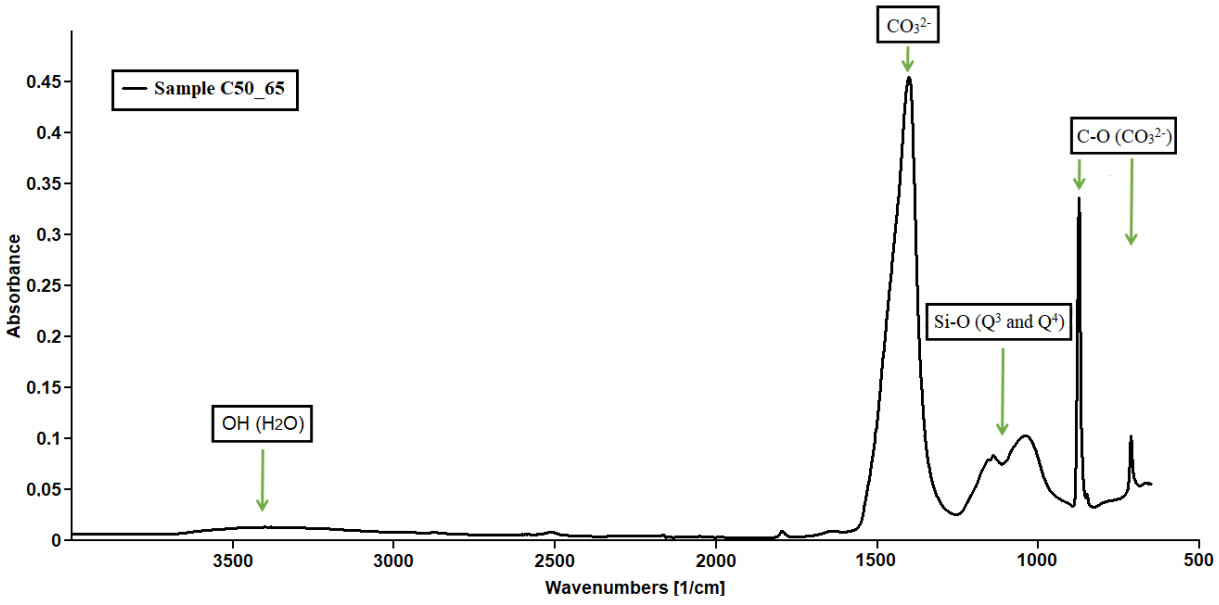

Figure S13. Infrared spectrum of C50_65 carbonated cement powder sample

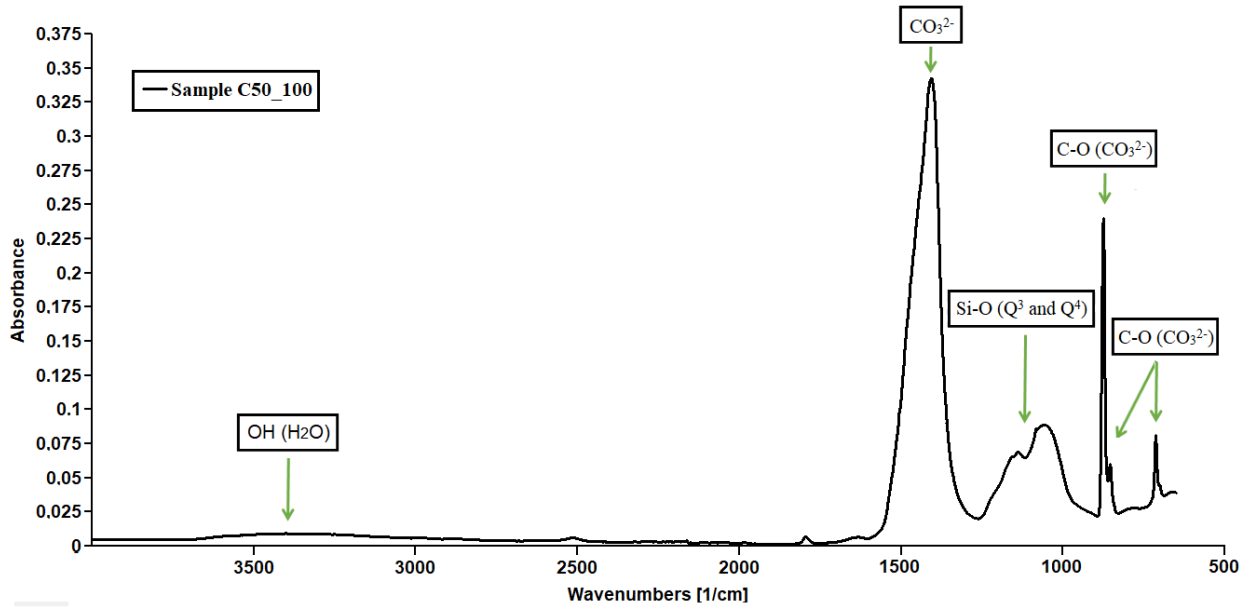

Figure S14. Infrared spectrum of C50_100 carbonated cement powder sample

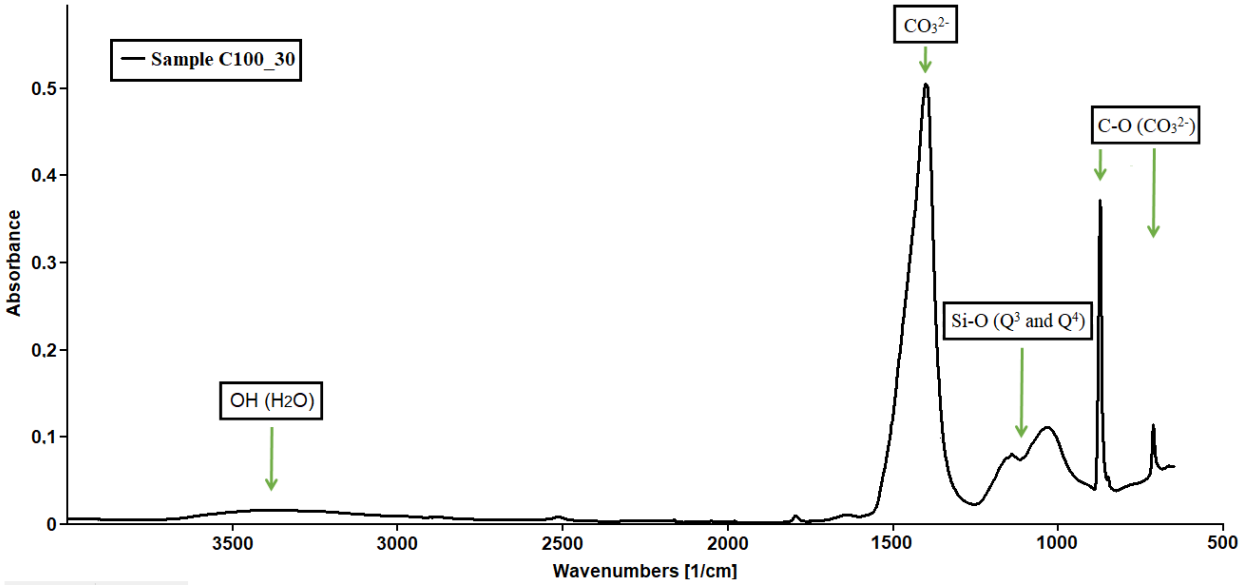

Figure S15. Infrared spectrum of C100_30 carbonated cement powder sample

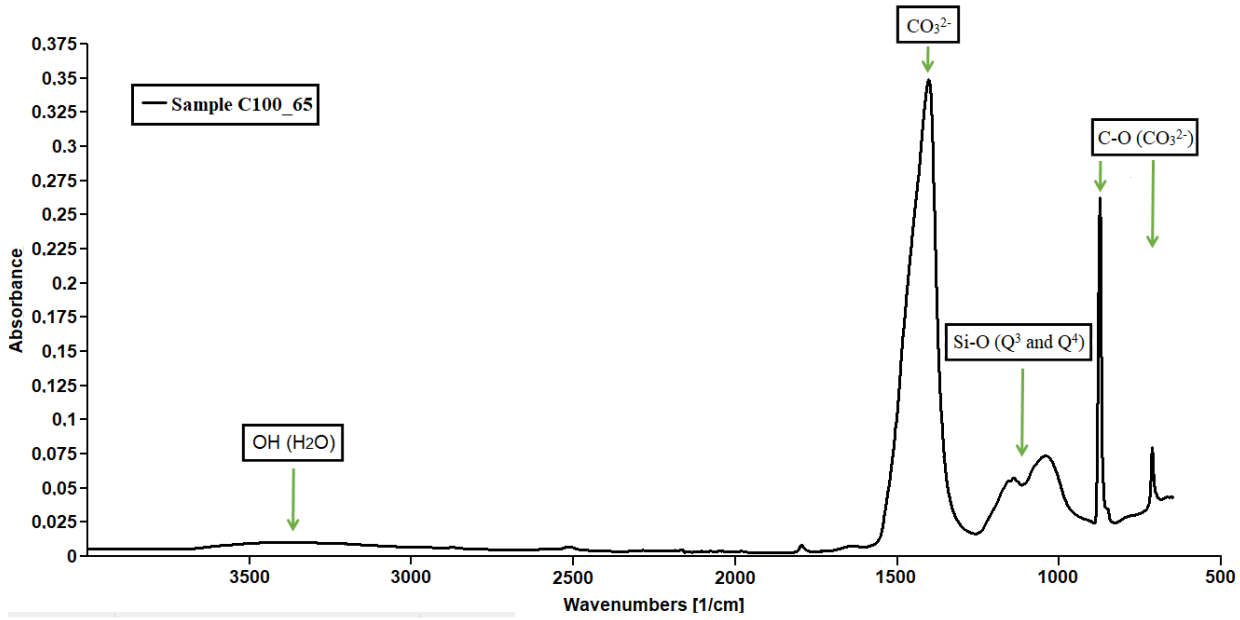

Figure S16. Infrared spectrum of C100_65 carbonated cement powder sample

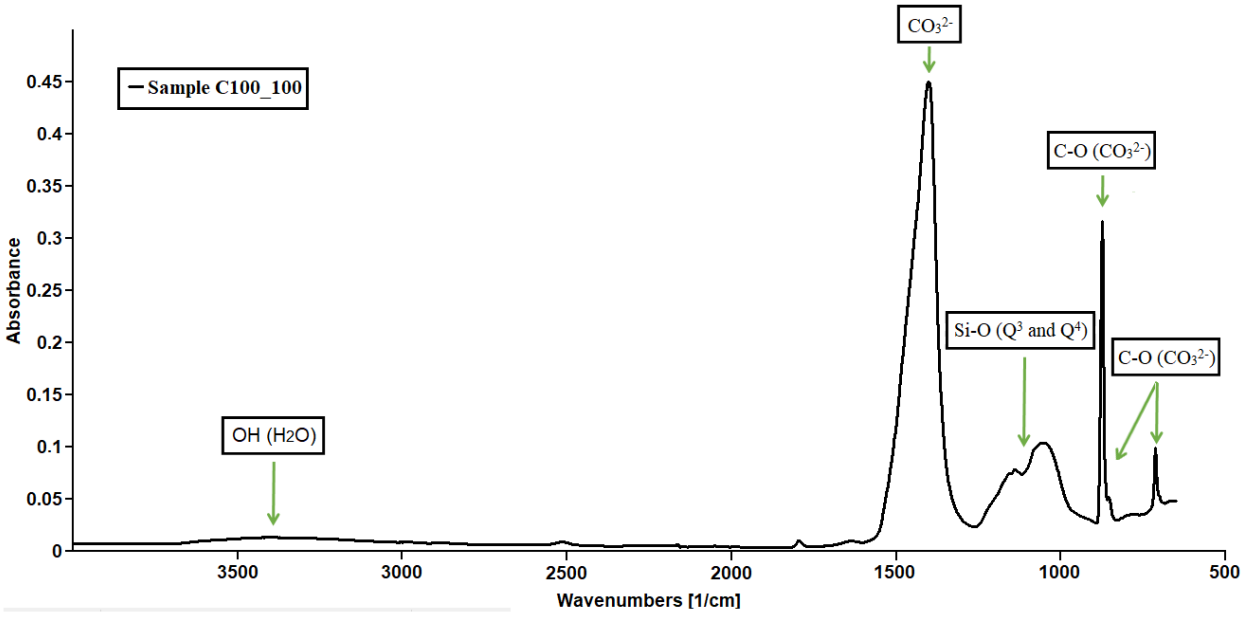

Figure S17. Infrared spectrum of C100_100 carbonated cement powder sample

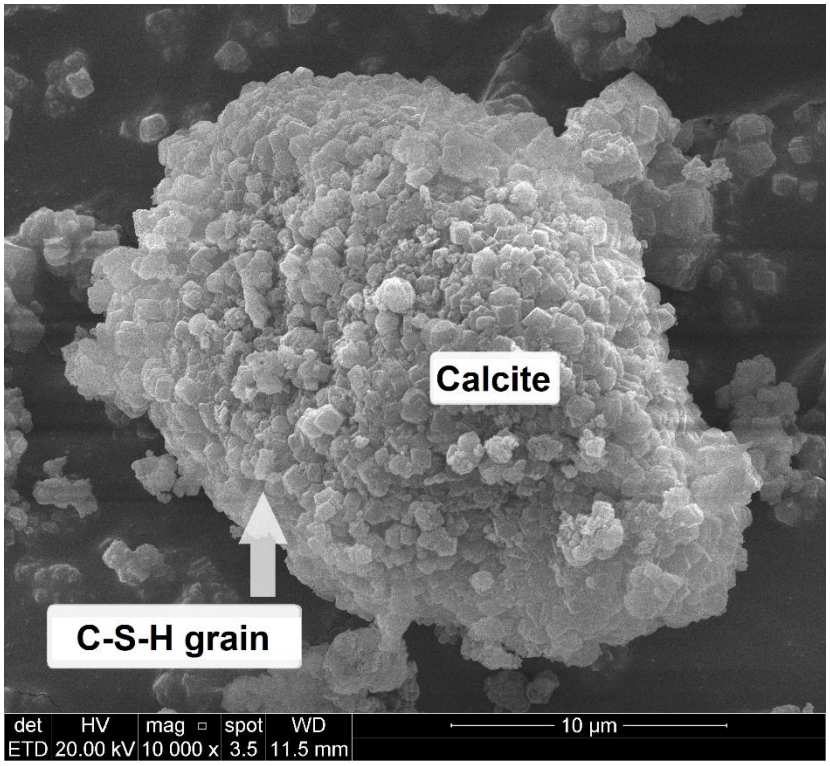

Figure S18. SEM image of C50_30 carbonated cement sample (mag: 10000 X)

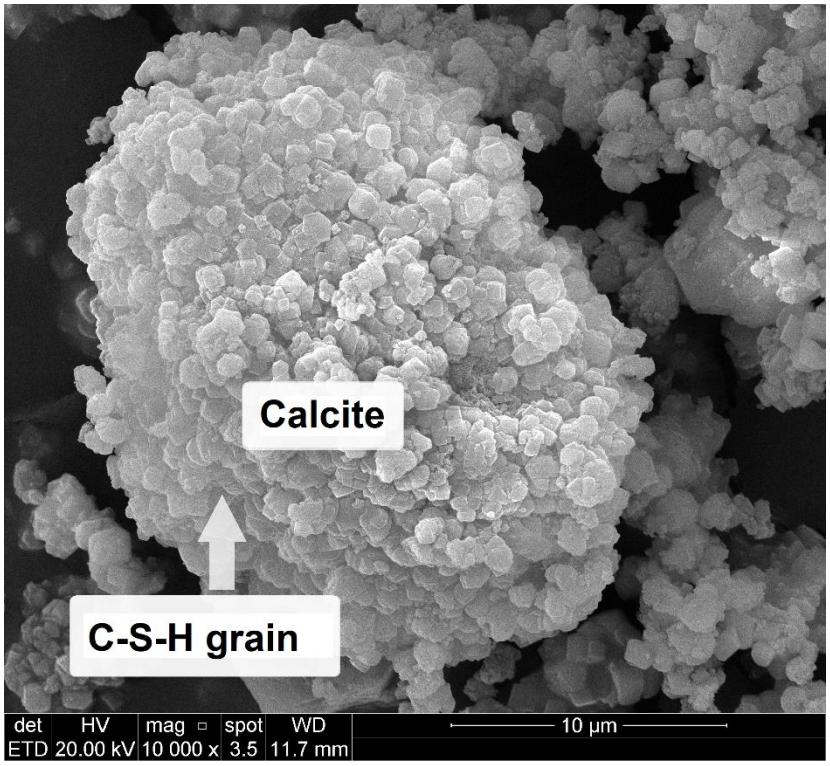

Figure S19. SEM image of C50_65 carbonated cement sample (mag: 10000 X)

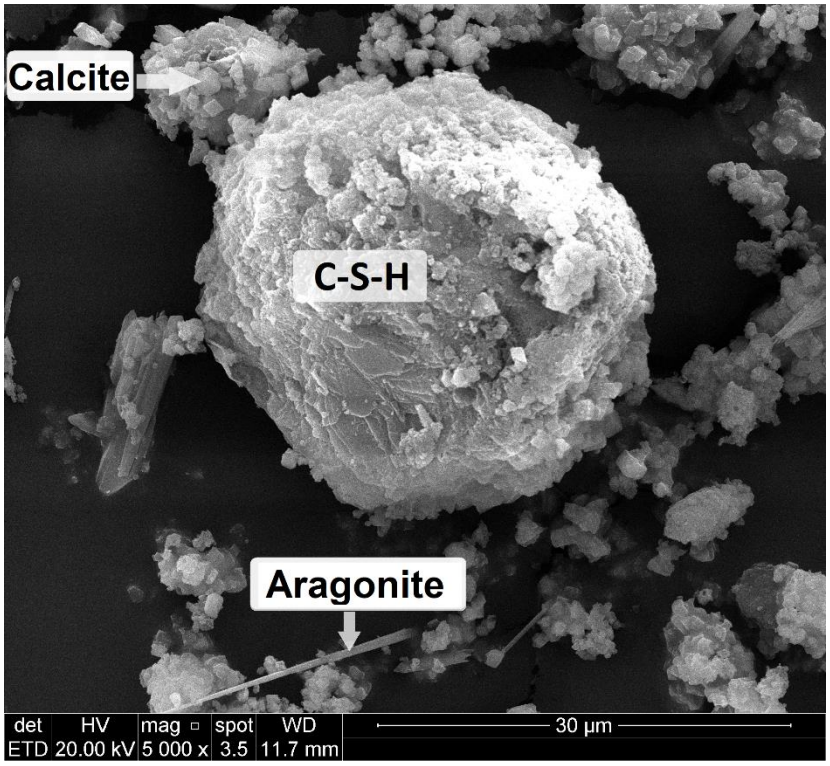

Figure S20. SEM image of C50_100 carbonated cement sample (mag: 5000 X)

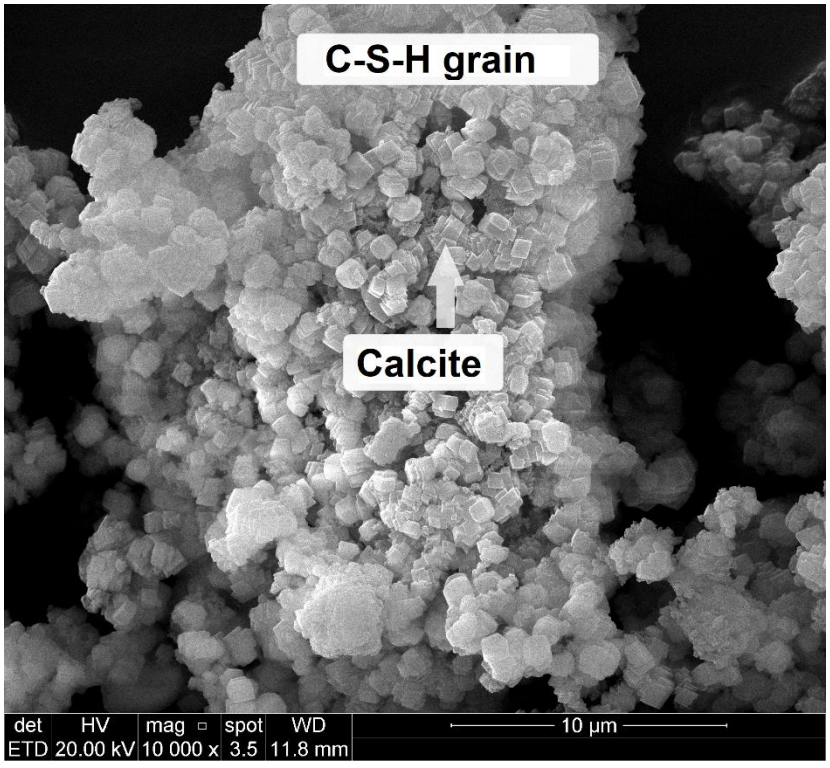

Figure S21. SEM image of C100_30 carbonated cement sample (mag: 10000 X)

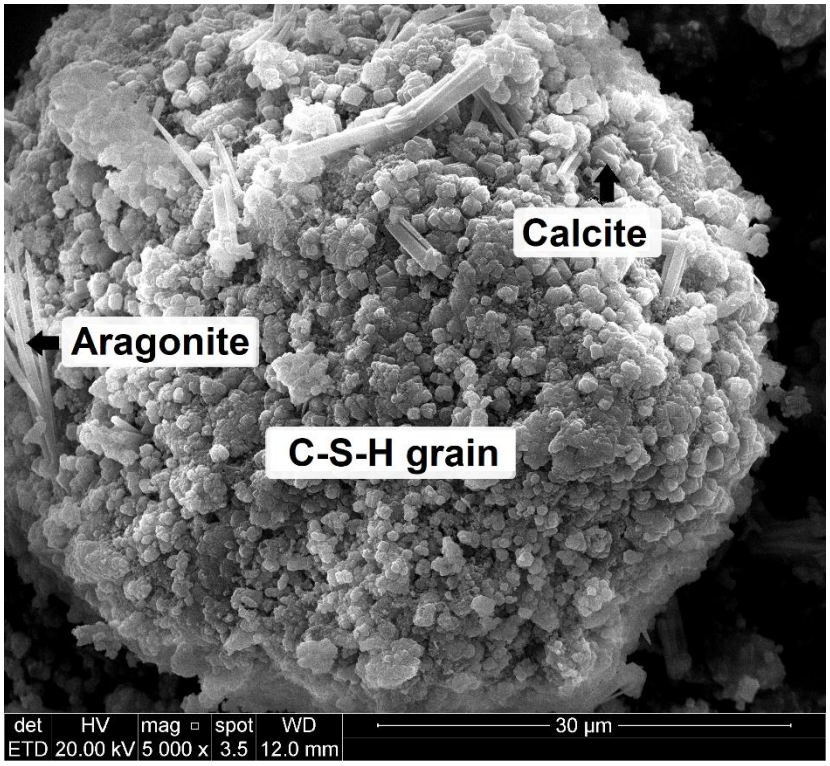

Figure S22. SEM image of C100_65 carbonated cement sample (mag: 5000 X)

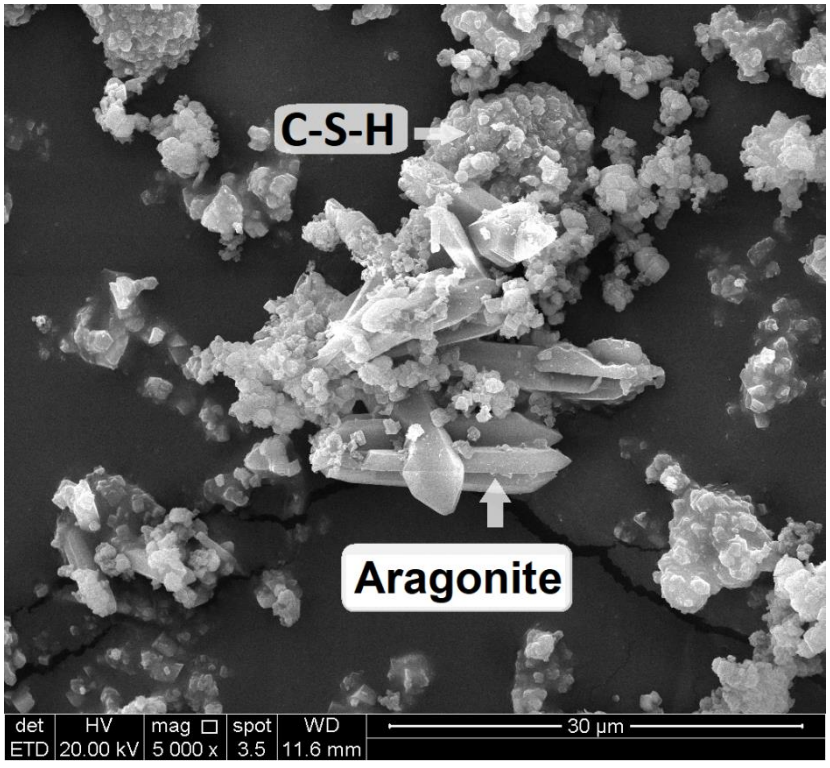

Figure S23. SEM image of C100_100 carbonated cement sample (mag: 5000 X)

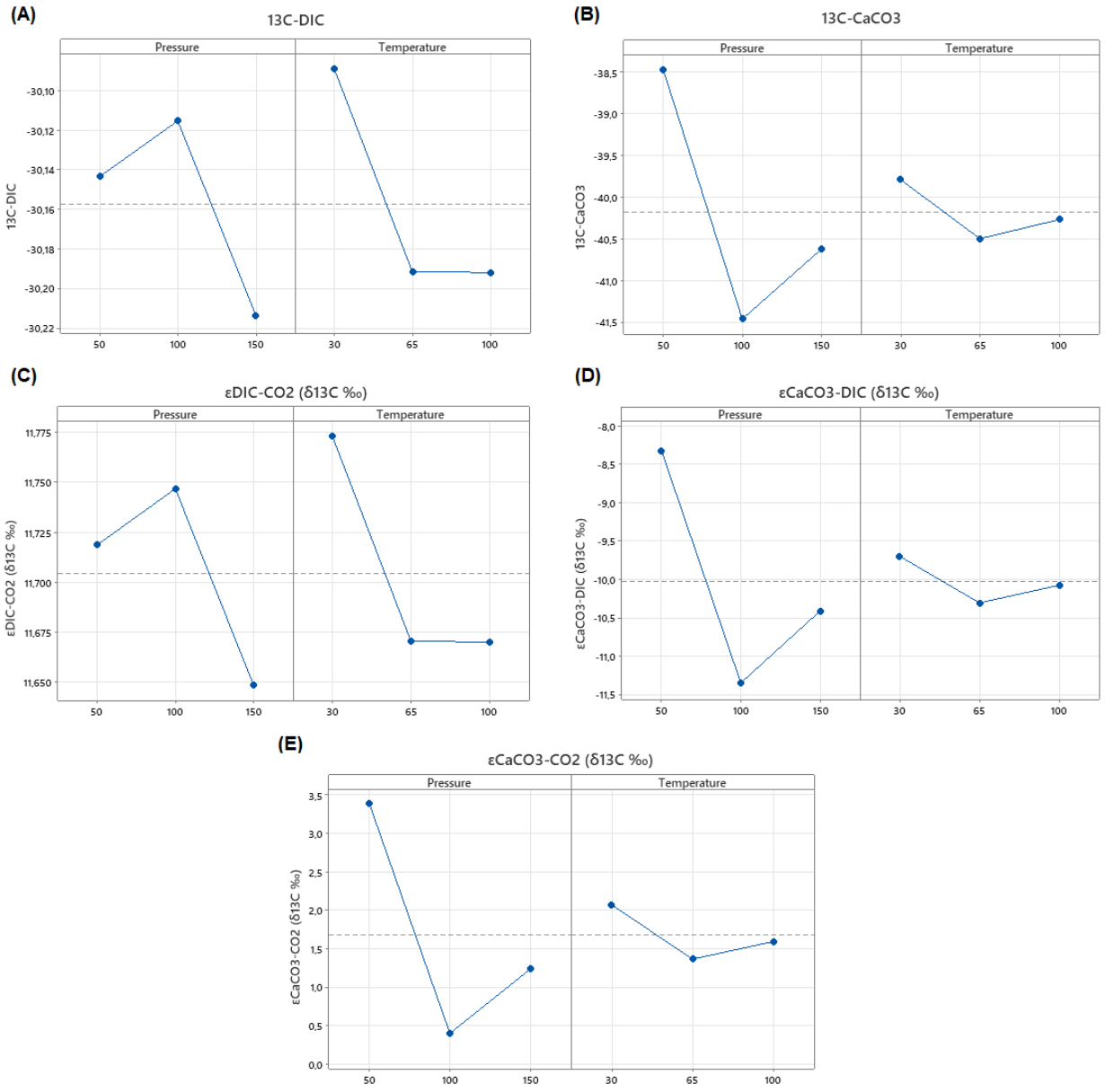

Figure S24. Temperature and pressure effect factorial plot on the: (A) DIC isotopic signature, (B) $CaCO_3$ isotopic signature, (C) DIC-CO_2 isotopic fractionation, (D) $CaCO_3$-DIC isotopic fractionation and (E) $CaCO_3$-CO_2 isotopic fractionation

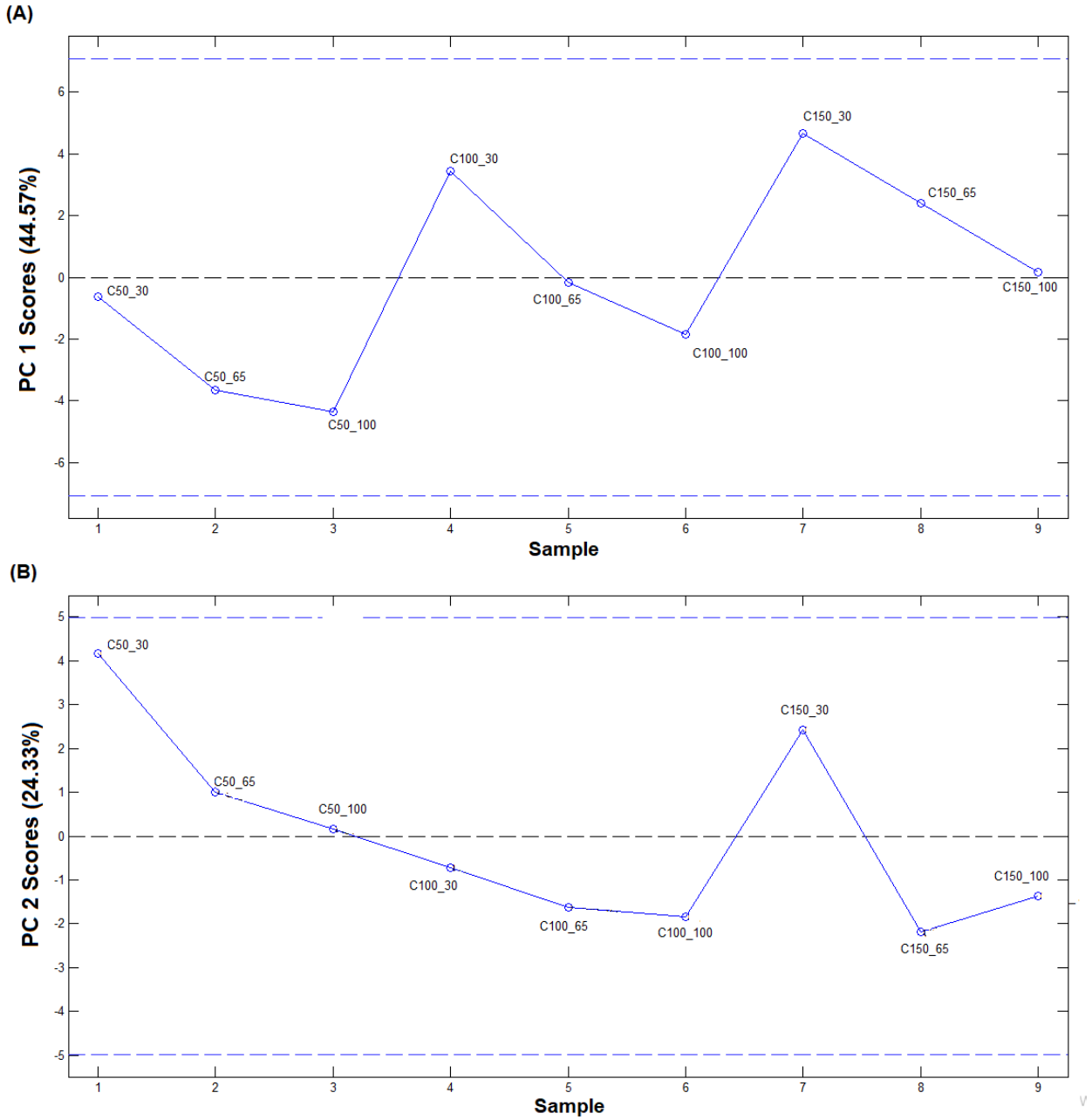

Figure S25. Principal component analysis (PCA) scores: (A) scores on PC-1 and (B) scores on PC-2

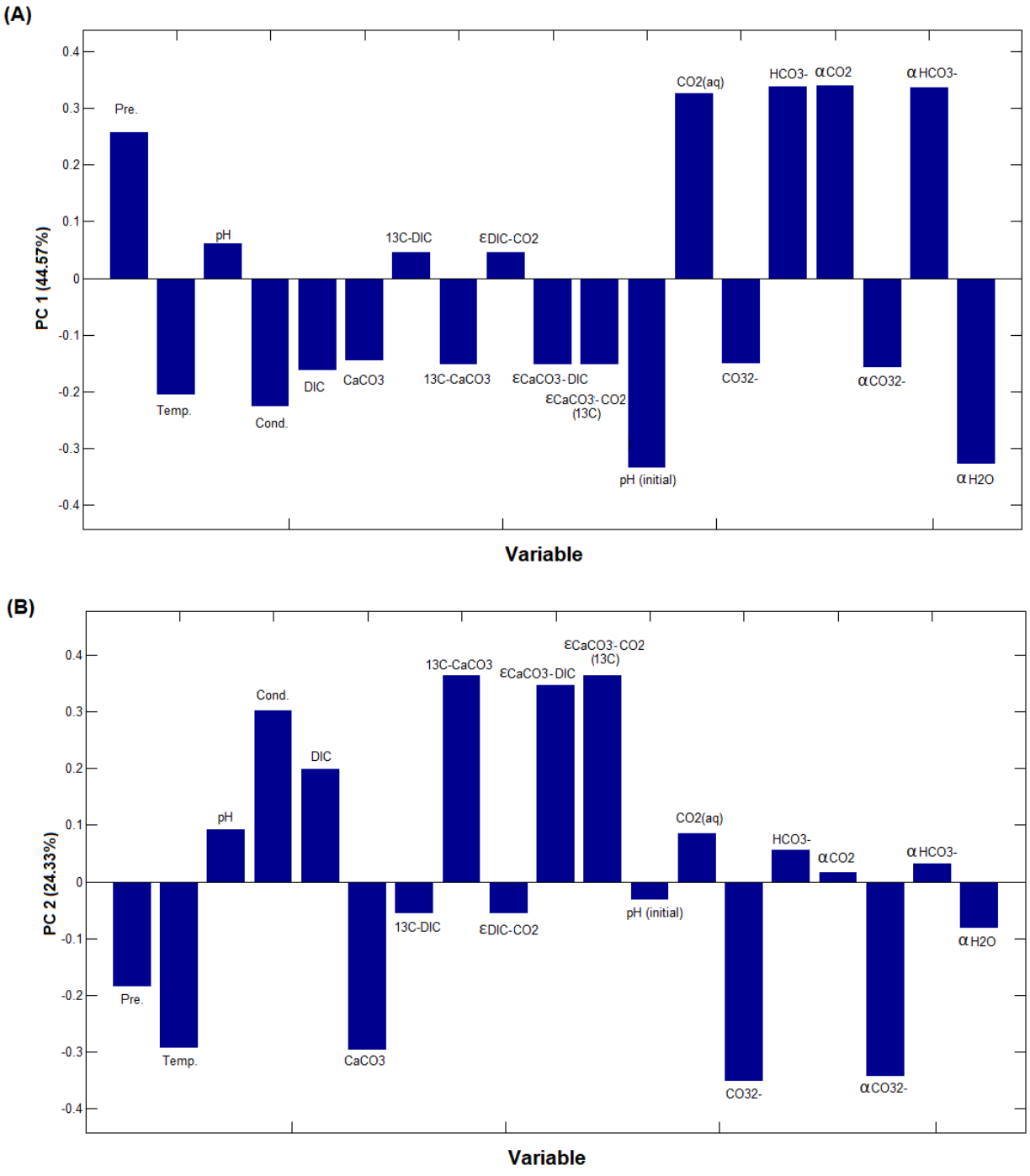

Figure S26. Principal component analysis (PCA) loadings: (A) variables loadings on PC-1 and (B) variables loadings on PC-2

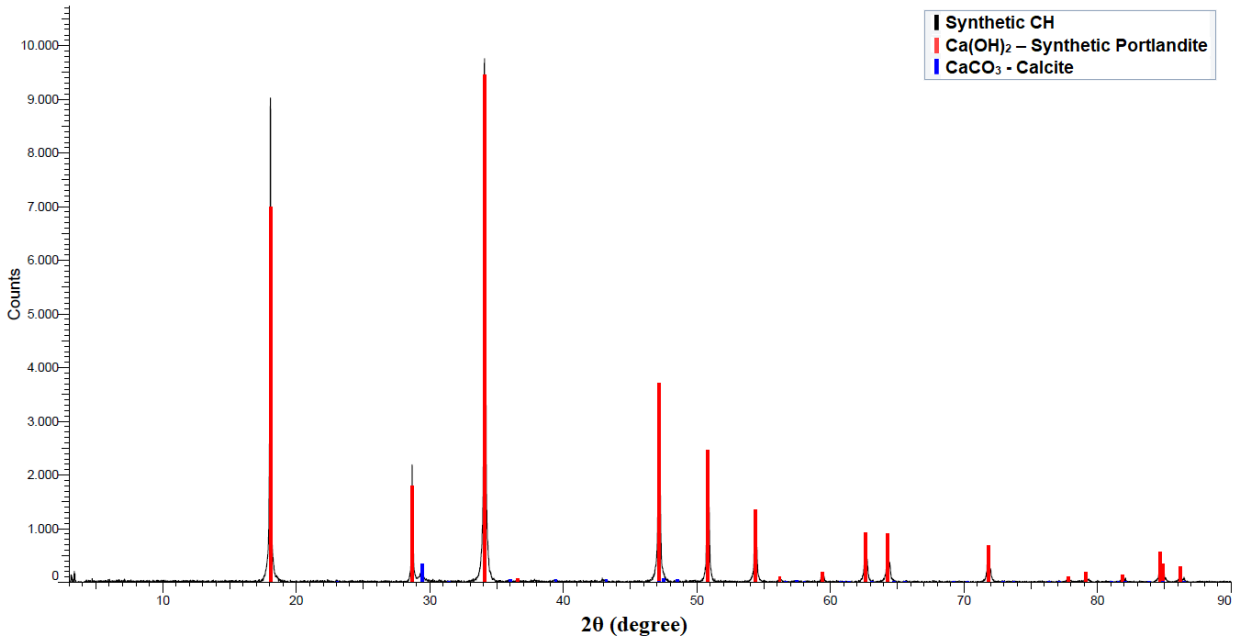

Figure S27. X-ray diffraction pattern of synthetic portlandite (CH)

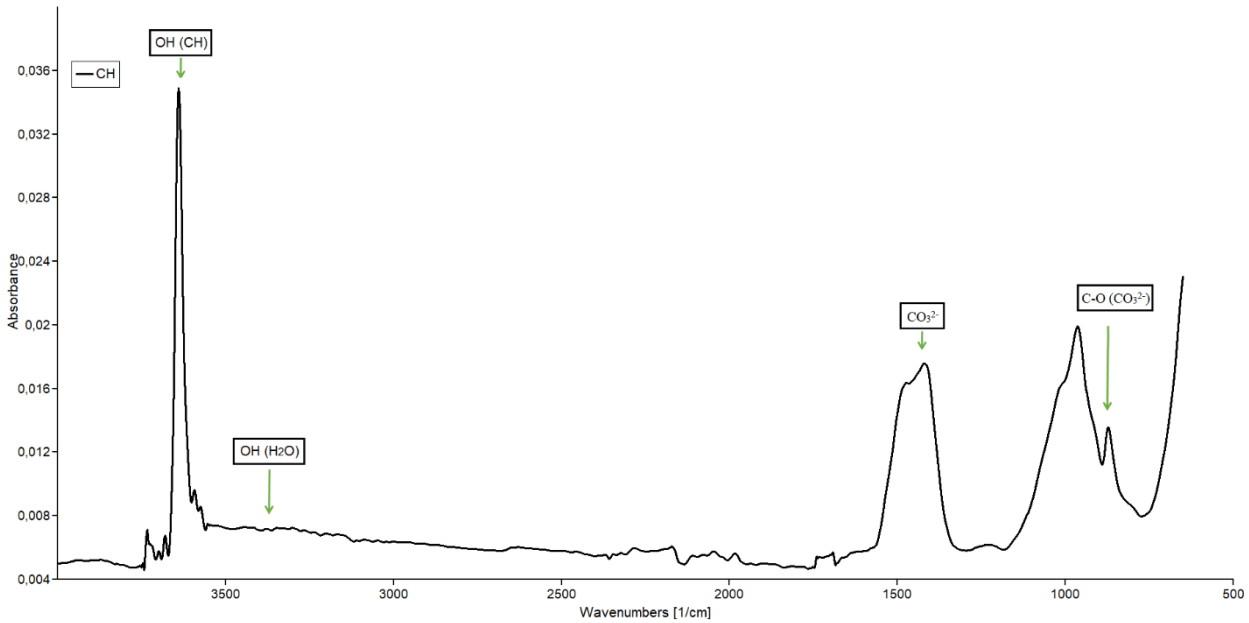

Figure S28. Infrared spectrum of synthetic portlandite (CH)

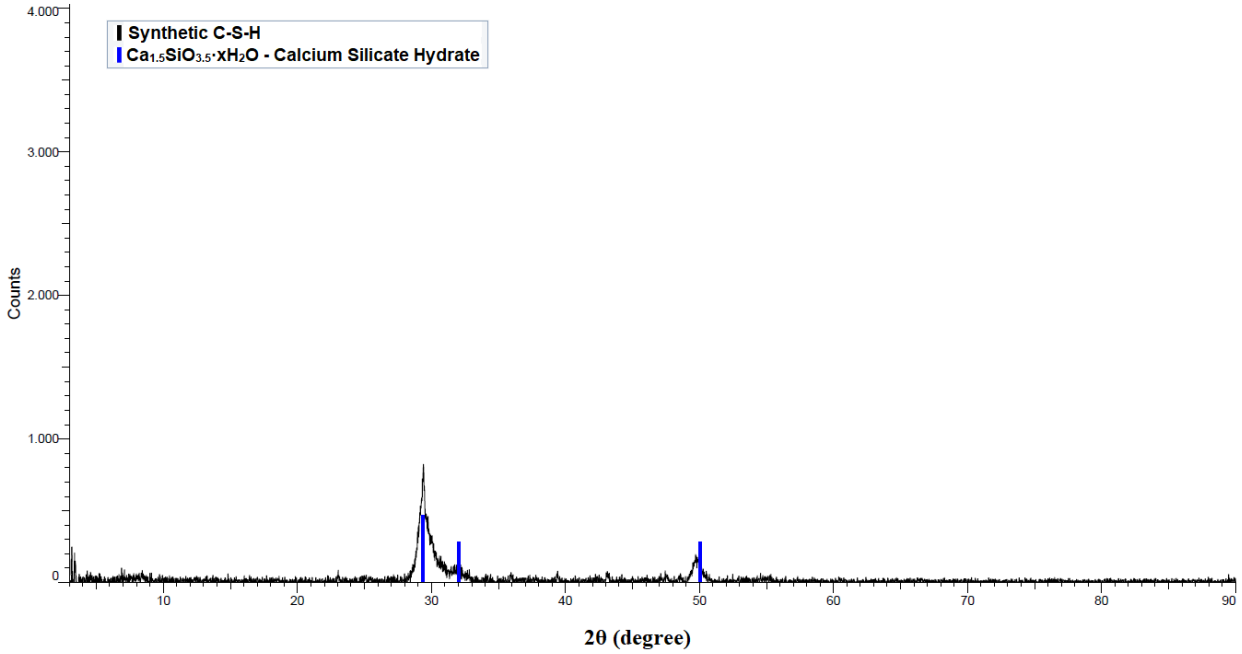

Figure S29. X-ray diffraction pattern of synthetic calcium silicate hydrate (C-S-H)

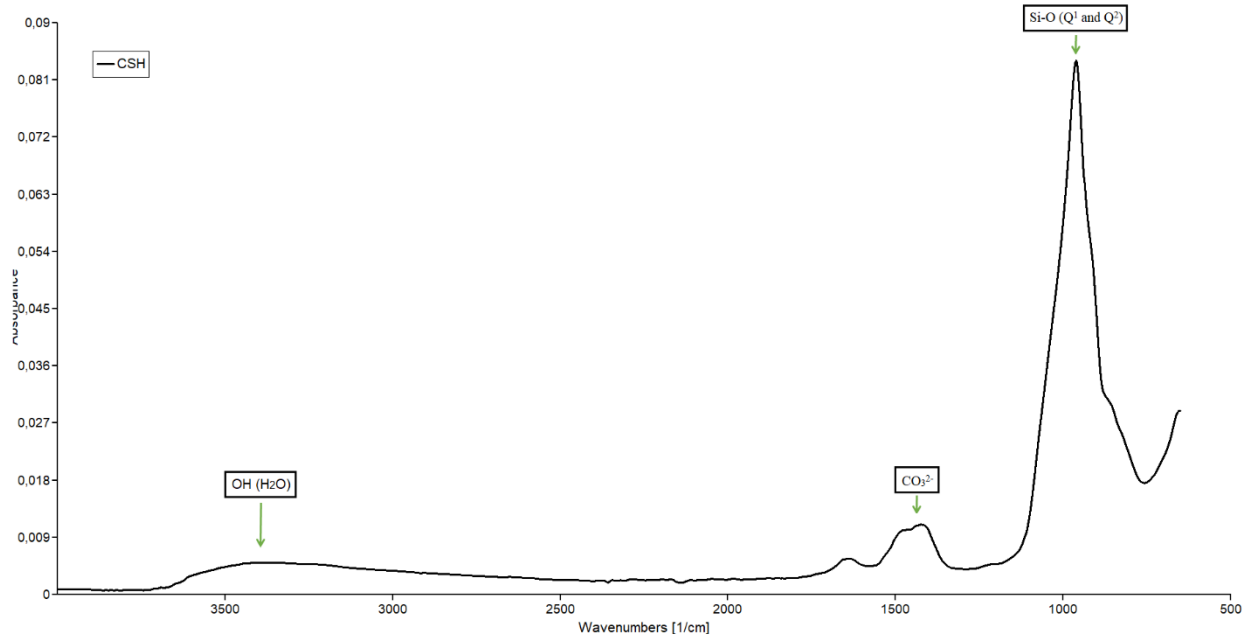

Figure S30. Infrared spectrum of synthetic calcium silicate hydrate (C-S-H)

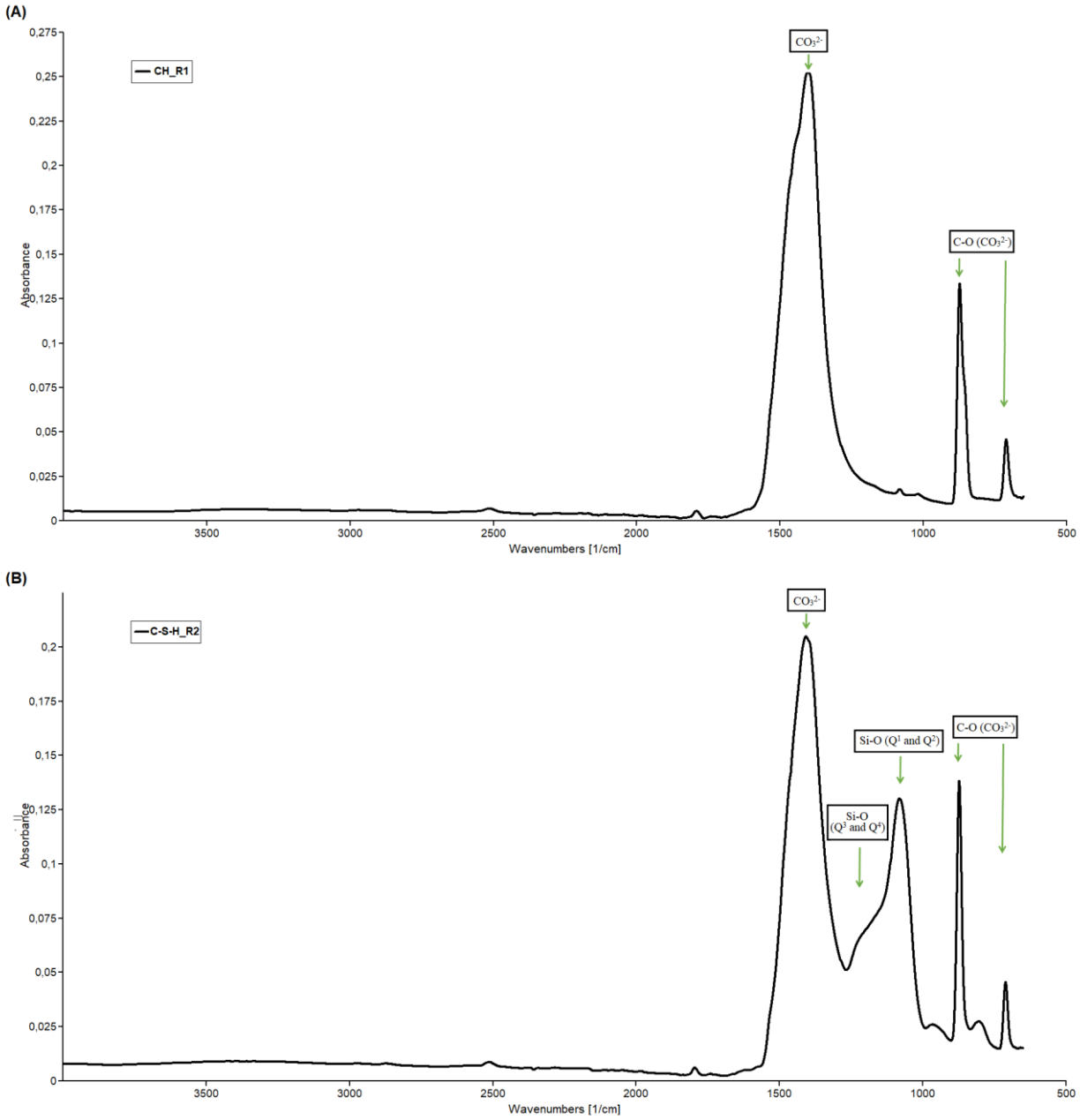

Figure 31. Infrared spectrum of the cement phase carbonation experiment: (A) carbonated portlandite (CH_R1) and (B) carbonated calcium silicate hydrate (C-S-H_R2)

5. CONCLUSÕES

Os métodos de monitoramento são essenciais para a obtenção de informações relevantes e necessárias para as empresas tomarem decisões orientadas por dados. Assim, a presente tese propôs-se a estudar soluções para monitorar a integridade das pastas de cimentos de poços expostos a ambientes ricos em CO_2. Dentro deste escopo, o trabalho foi dividido em dois tópicos, compreendendo: (*i*) o desenvolvimento de método quantitativo para o monitoramento da carbonatação da pasta de cimento e (*ii*) o estudo dos métodos de geoquímica isotópica para aprofundar os conhecimentos sobre o processo de carbonatação da pasta de cimento em ambientes ricos em CO_2.

No estudo de desenvolvimento de método quantitativo, foram propostos modelos de regressão parcial de mínimos quadrados (PLS) com base nos dados de infravermelho (FTIR) para quantificar o conteúdo de $CaCO_3$ em pasta de cimento que passaram pelo processo de carbonatação com CO_2 supercrítico. A partir dos resultados obtidos, conclui-se que é necessário considerar as transformações físicas e químicas induzidas pelo processo de carbonatação na matriz cimentícia para desenvolver modelos confiáveis para estimar o conteúdo de $CaCO_3$ no material. Ao longo do trabalho, observou-se que o consumo de portlandita (CH), o aumento do teor de $CaCO_3$ e a descalcificação-polimerização do C-S-H são as transformações químicas do cimento mais relevantes ao longo do processo de carbonatação. Os modelos PLS desenvolvidos foram calibrados e validados e os resultados da regressão apresentaram bom coeficiente de correlação (R^2 = 0,9995) e baixo erro de medição (RMSEP = 3,61 mg $CaCO_3$/g cimento). Assim, concluiu-se que: (*i*) é possível obter modelos rápidos e confiáveis para quantificar $CaCO_3$ por FTIR e (*ii*) o método é aplicável ao estudo de materiais cimentícios carbonatados.

No estudo de geoquímica isotópica, identificou-se que o pH do meio reacional e a solubilidade e pH das fases minerais dos materiais cimentícios (CH e C-S-H) são os principais parâmetros que influenciam nos fatores cinéticos e termodinâmicos e no equilíbrio/distribuição dos isótopos de carbono (^{13}C e ^{12}C) ao longo do sistema reacional. Assim, as seguintes conclusões foram obtidas: (*i*) as assinaturas de $\delta^{13}C$-DIC mais enriquecidas e os maiores fracionamentos isotópicos entre as fases de CO_2 e DIC ($\varepsilon_{DIC\text{-}CO2}$) estão relacionados aos meios reacionais com pH mais alto, (*ii*) as assinaturas de $\delta^{13}C$-$CaCO_3$ mais enriquecidas e os maiores fracionamentos isotópicos entre as fases de DIC e $CaCO_3$ ($\varepsilon_{CaCO3\text{-}DIC}$) indicam a precipitação de carbonato de cálcio ($CaCO_3$) em condições de maior equilíbrio termodinâmico e estão associados aos meios reacionais com maiores teores de DIC, maiores condutividade elétrica e pH mais baixos, (*iii*) os carbonatos minerais ($CaCO_3$) gerados a partir da carbonatação dos materiais cimentícios (cimento, CH e C-S-H) preservam a assinatura isotópica do gás de origem ($\delta^{13}C$-CO_2), apresentando fracionamentos isotópicos pequenos ou insignificantes entre as fases de CO_2 e o $CaCO_3$ ($\varepsilon_{CaCO3\text{-}CO2}$) e (*iv*) o fracionamento isotópico entre as fases de DIC e o $CaCO_3$ ($\varepsilon_{CaCO3\text{-}DIC}$) do sistema reacional regulam o fator de enriquecimento isotópico global do processo de carbonatação dos materiais cimentícios ($\varepsilon_{CaCO3\text{-}CO2}$).

No que tange aos objetivos (geral e específicos) do presente trabalho, pode-se concluir que foram obtidos resultados consistentes que levaram à proposição de novas alternativas para estudar e monitorar a integridade das pastas de cimento de poços expostos a ambientes ricos em CO_2. Assim, na presente tese de doutorado: (*i*) foram desenvolvidas soluções rápidas e confiáveis para monitorar o conteúdo de $CaCO_3$ em pastas de cimento carbonatado e (*ii*) foi confirmado o potencial dos dados de isótopos estáveis de carbono ($\delta^{13}C$) para diferenciar a origem do CO_2 que induziu o processo de degradação das pastas de cimento de poços. Dessa forma, o presente trabalho pôde contribuir para o desenvolvimento da área de engenharia e tecnologia de materiais cimentícios para aplicação em poços de O&G e de CCS.

6. PROPOSTA PARA TRABALHOS FUTUROS

Ao longo da presente tese de doutorado foram observadas oportunidades para ampliar o escopo do estudo e dar continuidade ao trabalho desenvolvido. Abaixo estão listados algumas das propostas para trabalhos futuros.

- Avaliar o potencial de utilizar de métodos de análise exploratória multivariada para triar potenciais materiais cimentícios suplementares (MCS);

- Estudar o preparo de compósitos de pasta de cimento com a adição de MCS, avaliando o efeito da carga inorgânica na resistência química dos materiais cimentícios frente ao CO_2;

- Realizar estudos de modelagem numérica e computacional do processo de carbonatação da pasta de cimento com a adição de MCS;

- Aprofundar as questões relacionadas ao processo de carbonatação da pasta de cimento de poços a partir dos dados de geoquímica isotópica e de modelagem numérica e dinâmica molecular.

7. REFERÊNCIAS BIBLIOGRÁFICAS

ABID, K. *et al.* A methodology to improve nanosilica based cements used in CO_2 sequestration sites. **Petroleum**, v. 4, n. 2, p. 198–208, jun. 2018.

ABID, K.; GHOLAMI, R.; MUTADIR, G. A pozzolanic based methodology to reinforce Portland cement used for CO_2 storage sites. **Journal of Natural Gas Science and Engineering**, v. 73, n. March 2019, p. 103062, jan. 2020.

AGBASIMALO, N.; RADONJIC, M. Experimental study of Portland cement/rock interface in relation to wellbore stability for carbon capture and storage (CCS). In: **46th US Rock Mechanics / Geomechanics Symposium 2012**, v. 3, p. 2212–2220, 2012.

AHDAYA, M. S. *et al.* New formulation of fly ash class C based geopolymer for oil well cementing. In: **International Petroleum Technology Conference**, 22 mar. 2019. Disponível em: <http://www.onepetro.org/doi/10.2523/19393-MS>.

AJAYI, T.; GUPTA, I. A review of reactive transport modeling in wellbore integrity problems. **Journal of Petroleum Science and Engineering**, v. 175, n. December 2018, p. 785–803, abr. 2019.

ANDRADE, J. J. DE O. *et al.* Evaluation of mechanical properties and carbonation of mortars produced with construction and demolition waste. **Construction and Building Materials**, v. 161, p. 70–83, fev. 2018.

ANDREW, R. M. Global CO_2 emissions from cement production. **Earth System Science Data**, v. 10, n. 1, p. 195–217, 26 jan. 2018.

API SPECIFICATION. API 10A - Specification for cements and materials for well cementing. **American Petroleum Institute**, v. 2009, n. December 2010, p. 50, 2010.

ARAUJO RODRIGUES, L.; LUÍS SAUER, I. Exploratory assessment of the economic gains of a pre-salt oil field in Brazil. **Energy Policy**, v. 87, p. 486–495, 2015.

ARTIOLI, G.; BULLARD, J. W. Cement hydration: the role of adsorption and crystal growth. **Crystal Research and Technology**, v. 48, n. 10, p. 903–918, out. 2013.

ASHRAF, W. Carbonation of cement-based materials: challenges and opportunities. **Construction and Building Materials**, v. 120, p. 558–570, set. 2016.

ASTM INTERNATIONAL. ASTM C150/C150M – 09: standard specification for Portland cement. **ASTM Standard, West Conshohocken**, p. 1–10, 2019.

BACHU, S.; ADAMS, J. J. Sequestration of CO_2 in geological media in response to climate change: capacity of deep saline aquifers to sequester CO_2 in solution. **Energy Conversion and Management**, v. 44, n. 20, p. 3151–3175, dez. 2003.

BAGHERI, M. *et al*. A review of oil well cement alteration in CO_2-rich environments. **Construction and Building Materials**, v. 186, p. 946–968, out. 2018.

BAI, M. *et al.* Well completion and integrity evaluation for CO_2 injection wells. **Renewable and Sustainable Energy Reviews**, v. 45, p. 556–564, maio 2015a.

BAI, M. *et al.* Evaluation of mechanical well integrity during CO_2 underground storage. **Environmental Earth Sciences**, v. 73, n. 11, p. 6815–6825, 14 jun. 2015b.

BAI, M.; ZHANG, Z.; FU, X. A review on well integrity issues for CO_2 geological storage and enhanced gas recovery. **Renewable and Sustainable Energy Reviews**, v. 59, p. 920–926, jun. 2016.

BALDISSERA, A. F. *et al.* Epoxy-modified Portland cement: effect of the resin hardener on the chemical degradation by carbon dioxide. **Energy Procedia**, v. 114, n. November 2016, p. 5256–5265, jul. 2017a.

BALDISSERA, A. F. *et al.* Epoxy resin-cement paste composite for wellbores: evaluation of chemical degradation fostered carbon dioxide. **Greenhouse Gases: Science and Technology**, v. 7, n. 6, p. 1065–1079, dez. 2017b.

BARTH, J. A. C. *et al.* Monitoring of cap-rock integrity during CCS from field data at the Ketzin pilot site (Germany): evidence from gas composition and stable carbon isotopes. **International Journal of Greenhouse Gas Control**, v. 43, p. 133–140, dez. 2015.

BATISTA, G. DOS S. *et al.* Chemical resistance and mechanical properties of nanosilica addition in oil well cement. **Journal of Petroleum Science and Engineering**, v. 196, n. August 2020, p. 107742, jan. 2021.

BENHELAL, E.; SHAMSAEI, E.; RASHID, M. I. Challenges against CO_2 abatement strategies in cement industry: a review. **Journal of Environmental Sciences**, v. 104, p. 84–101, jun. 2021.

BJØRGE, R. *et al.* Carbonation of silica cement at high-temperature well conditions. **International Journal of Greenhouse Gas Control**, v. 82, n. January, p. 261–268, mar. 2019.

BU, Y. *et al.* Experimental study on the thermal expansion property and mechanical performance of oil well cement with carbonaceous admixtures. **RSC Advances**, v. 7, n. 46, p. 29240–29254, 2017.

BULLARD, J. W. *et al.* Mechanisms of cement hydration. **Cement and Concrete Research**, v. 41, n. 12, p. 1208–1223, dez. 2011.

CAREY, J. W. *et al.* Analysis and performance of oil well cement with 30 years of CO_2 exposure from the SACROC Unit, West Texas, USA. **International Journal of Greenhouse Gas Control**, v. 1, n. 1, p. 75–85, abr. 2007.

CARROLL, S. *et al.* Review: role of chemistry, mechanics, and transport on well integrity in CO_2 storage environments. **International Journal of Greenhouse Gas Control**, v. 49, p. 149–160, jun. 2016.

CELIA, M. *et al.* Quantitative estimation of CO_2 leakage from geological storage: analytical models, numerical models, and data needs. In: **Greenhouse Gas Control Technologies 7**. Elsevier, 2005. v. Ip. 663–671.

CHANG, R. *et al.* Calcium carbonate precipitation for CO_2 storage and utilization: a review of the carbonate crystallization and polymorphism. **Frontiers in Energy Research**, v. 5, n. July, p. 1–12, 10 jul. 2017.

CHOI, Y. *et al.* Wellbore integrity and corrosion of carbon steel in CO_2 geologic storage environments: a literature review. **International Journal of Greenhouse Gas Control**, v. 16, p. S70–S77, jun. 2013.

CONDE SILVA, J.; MILESTONE, N. B. Cement/rock interaction in geothermal wells: the effect of silica addition to the cement and the impact of CO_2 enriched brine. **Geothermics**, v. 73, n. November 2017, p. 16–31, maio 2018a.

CONDE SILVA, J.; MILESTONE, N. B. The effect of the rock type on the degradation of well cements in CO_2 enriched geothermal environments. **Geothermics**, v. 75, n. February, p. 235–248, set. 2018b.

COSTA, B. L. DE S. *et al.* Carbonation in oil well Portland cement: influence of hydration time prior to contact with CO_2. **Construction and Building Materials**, v. 159, p. 252–260, jan. 2018.

COSTA, B. L. DE S. *et al.* Evaluation of density influence on resistance to carbonation process in oil well cement slurries. **Construction and Building Materials**, v. 197, p. 331–338, fev. 2019.

DA COSTA FRAGA, C. T. *et al.* Brazilian pre-salt: an impressive journey from plans and challenges to concrete results. In: **Offshore Technology Conference**, maio 2015.

DALLA VECCHIA, F. *et al.* Wellbore integrity in a saline aquifer: experimental steel-cement interface degradation under supercritical CO_2 conditions representative of Brazil's Parana basin. **International Journal of Greenhouse Gas Control**, v. 98, n. May, p. 103077, jul. 2020.

DE ALMEIDA, A. S. *et al.* CCGS opportunities in the Santos basin pre-salt development. In: **Society of Petroleum Engineers - International Conference on Health, Safety and Environment in Oil and Gas Exploration and Production 2010**, v. 2, p. 840–849, 2010.

DE SENA COSTA, B. L. *et al.* Study of carbonation in a class G Portland cement matrix at supercritical and saturated environments. **Construction and Building Materials**, v. 180, p. 308–319, ago. 2018.

DESHPANDE, A.; PATIL, R. Applications of nanotechnology in oilwell cementing. In: **SPE Middle East Oil & Gas Show and Conference**, Society of Petroleum Engineers, 6 mar. 2017. Disponível em: <https://www-onepetro-org.ezproxy.lib.ou.edu/download/conference-paper/SPE-183727-MS?id=conference-paper%2FSPE-183727-MS>.

DING, Q. *et al.* Insight on the mechanism of sulfate attacking on the cement paste with granulated blast furnace slag: an experimental and molecular dynamics study. **Construction and Building Materials**, v. 169, p. 601–611, abr. 2018.

DONG, X.; DUAN, Z.; GAO, D. Assessment on the cement integrity of CO_2 injection

wells through a wellbore flow model and stress analysis. **Journal of Natural Gas Science and Engineering**, v. 74, n. October 2019, p. 103097, fev. 2020.

DORN, T.; BLASK, O.; STEPHAN, D. Acceleration of cement hydration – a review of the working mechanisms, effects on setting time, and compressive strength development of accelerating admixtures. **Construction and Building Materials**, v. 323, n. January, p. 126554, mar. 2022.

DUGGAN, A. R. *et al.* The use of carbonation depth techniques on stabilized peat. **Geotechnical Testing Journal**, v. 40, n. 6, p. 20160223, 1 nov. 2017.

DUGUID, A.; RADONJIC, M.; SCHERER, G. W. Degradation of cement at the reservoir/cement interface from exposure to carbonated brine. **International Journal of Greenhouse Gas Control**, v. 5, n. 6, p. 1413–1428, nov. 2011.

EKOLU, S. O. A review on effects of curing, sheltering, and CO_2 concentration upon natural carbonation of concrete. **Construction and Building Materials**, v. 127, p. 306–320, nov. 2016.

ENGELMANN, P. DE M. *et al.* Environmental monitoring of a landfill area through the application of carbon stable isotopes, chemical parameters and multivariate analysis. **Waste Management**, v. 76, p. 591–605, jun. 2018.

FAROOQUI, N. M. *et al.* Understanding CO_2-brine-wellbore cement-rock interactions for CO_2 storage. **Energy Procedia**, v. 114, n. November 2016, p. 5206–5211, jul. 2017.

FLUDE, S. *et al.* The inherent tracer fingerprint of captured CO_2. **International Journal of Greenhouse Gas Control**, v. 65, n. January, p. 40–54, out. 2017.

GABOREAU, S. *et al.* In-situ interaction of cement paste and shotcrete with claystones in a deep disposal context. **American Journal of Science**, v. 312, n. 3, p. 314–356, 1

mar. 2012.

GARCIA FERNANDEZ, S. *et al.* Characterization of wellbore microannuli. **Journal of Natural Gas Science and Engineering**, v. 62, n. December 2018, p. 13–25, fev. 2019.

GASTALDI, D. *et al.* Near-infrared spectroscopy investigation on the hydration degree of a cement paste. **Journal of Materials Science**, v. 45, n. 12, p. 3169–3174, 4 jun. 2010.

GU, T. *et al.* Coupled effect of CO_2 attack and tensile stress on well cement under CO_2 storage conditions. **Construction and Building Materials**, v. 130, p. 92–102, jan. 2017.

GUATAME-GARCIA, A.; BUXTON, M. The use of infrared spectroscopy to determine the quality of carbonate-rich diatomite ores. **Minerals**, v. 8, n. 3, p. 120, 20 mar. 2018.

HA, J. H. *et al.* Changes in geochemical and carbon isotopic compositions during reactions of CO_2-saturated groundwater with aquifer materials. **International Journal of Greenhouse Gas Control**, v. 95, n. May 2019, p. 102961, abr. 2020.

HAN, J. *et al.* Degradation of cement-steel composite at bonded steel-cement interfaces in supercritical CO_2 saturated brines simulating wellbore systems. In: **NACE - International Corrosion Conference Series.** 2012.

HANSEN, T.; GARDELER, B.; MATTHIESSEN, B. Technical note: precise quantitative measurements of total dissolved inorganic carbon from small amounts of seawater using a gas chromatographic system. **Biogeosciences**, v. 10, n. 10, p. 6601–6608, 22 out. 2013.

HEINZ, O.; HEINZ, H. Cement interfaces: current understanding, challenges, and opportunities. **Langmuir**, v. 37, n. 21, p. 6347–6356, 1 jun. 2021.

HENRY, D. G.; WATSON, J. S.; JOHN, C. M. Assessing and calibrating the ATR-FTIR approach as a carbonate rock characterization tool. **Sedimentary Geology**, v. 347, p. 36–52, 2017.

HIDALGO, A. *et al.* Microstructural changes induced in Portland cement-based materials due to natural and supercritical carbonation. **Journal of Materials Science**, v. 43, n. 9, p. 3101–3111, 1 maio 2008.

HIGL, J. *et al.* Detailed in situ ATR-FTIR spectroscopy study of the early stages of C-S-H formation during hydration of monoclinic C_3S. **Cement and Concrete Research**, v. 142, n. October 2020, p. 106367, abr. 2021.

HOEFS, J. **Stable Isotope Geochemistry**. Berlin, Heidelberg: Springer Berlin Heidelberg, 2004.

HORGNIES, M.; CHEN, J. J.; BOUILLON, C. Overview about the use of Fourier transform infrared spectroscopy to study cementitious materials. In: **WIT Transactions on Engineering Sciences**. 4 jun. 2013. Disponível em: <http://library.witpress.com/viewpaper.asp?pcode=MC13-022-1>.

HUGHES, T. L. *et al.* Determining cement composition by Fourier transform infrared spectroscopy. **Advanced Cement Based Materials**, v. 2, n. 3, p. 91–104, maio 1995.

HWANG, J. *et al.* Shear bond strength of oil well cement in carbonic acid environment. **Journal of CO_2 Utilization**, v. 27, n. February, p. 60–72, out. 2018.

IGLESIAS, R. S. *et al.* Modeling CO_2 flow in support of a shallow subsurface controlled leakage field test. **Greenhouse Gases: Science and Technology**, v. 9, n. 5, p. 1027–1042, 20 out. 2019.

JOHN, E.; MATSCHEI, T.; STEPHAN, D. Nucleation seeding with calcium silicate hydrate – a review. **Cement and Concrete Research**, v. 113, n. June 2017, p. 74–85,

nov. 2018.

JOHNSON, G. *et al.* Tracing the movement of CO_2 injected into a mature oilfield using carbon isotope abundance ratios: the example of the Pembina Cardium CO_2 monitoring project. **International Journal of Greenhouse Gas Control**, v. 5, n. 4, p. 933–941, jul. 2011.

JOHNSON, G.; MAYER, B. Oxygen isotope exchange between H_2O and CO_2 at elevated CO_2 pressures: implications for monitoring of geological CO_2 storage. **Applied Geochemistry**, v. 26, n. 7, p. 1184–1191, jul. 2011.

JOSE, A. *et al.* Characterization of cement stabilized pond ash using FTIR spectroscopy. **Construction and Building Materials**, v. 263, p. 120136, dez. 2020.

KAROLYTĖ, R. *et al.* The influence of oxygen isotope exchange between CO_2 and H_2O in natural CO_2-rich spring waters: implications for geothermometry. **Applied Geochemistry**, v. 84, p. 173–186, set. 2017.

KHALIFEH, M. *et al.* Geopolymers as an alternative for oil well cementing applications: a review of advantages and concerns. **Journal of Energy Resources Technology**, v. 140, n. 9, p. 092801, 29 maio 2018.

KIRAN, R. *et al.* Identification and evaluation of well integrity and causes of failure of well integrity barriers (a review). **Journal of Natural Gas Science and Engineering**, v. 45, n. June, p. 511–526, set. 2017.

KMIEĆ, M. *et al.* Laboratory research on the influence of swelling clay on the quality of borehole cementing and evaluation of clay-cutting wellbore tool prototype. **Applied Clay Science**, v. 164, n. February 2017, p. 13–25, nov. 2018.

KOUKOUZAS, N. *et al.* Geochemical modeling of carbonation of hydrated oil well cement exposed to CO_2-saturated brine solution. **Applied Geochemistry**, v. 85, p.

35–48, out. 2017.

KUMAR, M. *et al.* Identification and evaluation of hydrogeochemical processes in the groundwater environment of Delhi, India. **Environmental Geology**, v. 50, n. 7, p. 1025–1039, 20 ago. 2006.

KUPWADE-PATIL, K. *et al.* Use of silica fume and natural volcanic ash as a replacement to Portland cement: micro and pore structural investigation using NMR, XRD, FTIR and X-ray microtomography. **Construction and Building Materials**, v. 158, p. 574–590, jan. 2018.

KUZIELOVÁ, E. *et al.* Effect of additives on the performance of Dyckerhoff cement, class G, submitted to simulated hydrothermal curing. **Journal of Thermal Analysis and Calorimetry**, v. 133, n. 1, p. 63–76, 7 jul. 2018.

KUZIELOVÁ, E. *et al.* Development of G-oil well cement phase composition during long therm hydrothermal curing. **Geothermics**, v. 80, n. March, p. 129–137, jul. 2019.

LEAVITT, S. W. Carbon Isotopes, Stable. In: GORNITZ, V. **Encyclopedia of Paleoclimatology and Ancient Environments**. Encyclopedia of Earth Sciences Series. Dordrecht: Springer Netherlands, 2009. p. 133–136.

LEDESMA, R. B. *et al.* Zeolite and fly ash in the composition of oil well cement: evaluation of degradation by CO_2 under geological storage condition. **Journal of Petroleum Science and Engineering**, v. 185, n. October 2019, p. 106656, fev. 2020.

LEGODI, M. A. *et al*. Quantitative determination of $CaCO_3$ in cement blends by FT-IR. **Applied Spectroscopy**, v. 55, n. 3, p. 361–365, 31 mar. 2001.

LESTI, M.; TIEMEYER, C.; PLANK, J. CO_2 stability of Portland cement based well cementing systems for use on carbon capture & storage (CCS) wells. **Cement and Concrete Research**, v. 45, n. 1, p. 45–54, mar. 2013.

LI, Y.; NYGAARD, R. A numerical study on the feasibility of evaluating CO_2 injection wellbore integrity through casing deformation monitoring. **Greenhouse Gases: Science and Technology**, v. 8, n. 1, p. 51–62, fev. 2018.

LI, Z.-P. *et al.* Determination of isotope composition of dissolved inorganic carbon by gas chromatography-conventional isotope-ratio mass spectrometry. **Chinese Journal of Analytical Chemistry**, v. 35, n. 10, p. 1455–1458, out. 2007.

LIAUDAT, J. *et al.* Modelling acid attack of oilwell cement exposed to carbonated brine. **International Journal of Greenhouse Gas Control**, v. 68, n. March 2017, p. 191–202, jan. 2018.

LIU, B. *et al.* New perspectives on utilization of CO_2 sequestration technologies in cement-based materials. **Construction and Building Materials**, v. 272, p. 121660, fev. 2021a.

LIU, L. *et al.* Study on high-efficiency CO_2 absorption by fresh cement paste. **Construction and Building Materials**, v. 270, p. 121364, fev. 2021b.

LIU, W. *et al.* XRD and ^{29}Si MAS NMR study on carbonated cement paste under accelerated carbonation using different concentration of CO_2. **Materials Today Communications**, v. 19, n. May, p. 464–470, jun. 2019.

LIU, X. *et al.* Estimation of carbonate, total organic carbon, and biogenic silica content by FTIR and XRF techniques in lacustrine sediments. **Journal of Paleolimnology**, v. 50, n. 3, p. 387–398, 20 out. 2013.

LOREK, A.; LABUS, M.; BUJOK, P. Wellbore cement degradation in contact zone with formation rock. **Environmental Earth Sciences**, v. 75, n. 6, p. 499, 15 mar. 2016.

LOTHENBACH, B.; SCRIVENER, K.; HOOTON, R. D. Supplementary cementitious

materials. **Cement and Concrete Research**, v. 41, n. 12, p. 1244–1256, dez. 2011.

LUZINOVA, Y. *et al.* Detection of cold seep derived authigenic carbonates with infrared spectroscopy. **Marine Chemistry**, v. 125, n. 1–4, p. 8–18, jul. 2011.

MANCEAU, J. C. C. *et al.* Well integrity assessment by a 1:1 scale wellbore experiment: exposition to dissolved CO_2 and overcoring. **International Journal of Greenhouse Gas Control**, v. 54, n. Part 1, p. 258–271, nov. 2016.

MANGADLAO, J. D.; CAO, P.; ADVINCULA, R. C. Smart cements and cement additives for oil and gas operations. **Journal of Petroleum Science and Engineering**, v. 129, n. April 2010, p. 63–76, maio 2015.

MÁRQUEZ, G. *et al.* Attack of carbonic anhydride and hydrogen sulfide on API class H cement slurries exposed to saline formation waters. **Materiales de Construcción**, v. 61, n. 303, p. 371–384, 30 set. 2011.

MARSHDI, Q. S. R. Benefits of using mineral additives, as components of the modern oil-well cement. **Case Studies in Construction Materials**, v. 8, n. March, p. 455–458, jun. 2018.

MAYER, B. *et al.* Assessing the usefulness of the isotopic composition of CO_2 for leakage monitoring at CO_2 storage sites: a review. **International Journal of Greenhouse Gas Control**, v. 37, p. 46–60, jun. 2015.

MAZURANA, L. *et al.* Determination of CO_2 capture in rendering mortars produced with recycled construction and demolition waste by thermogravimetry. **Journal of Thermal Analysis and Calorimetry**, n. 0123456789, 3 jan. 2021.

MECOZZI, M. *et al.* Determination of carbonate in marine solid samples by FTIR-ATR spectroscopy. **Analyst**, v. 126, n. 2, p. 144–146, 2001.

METZ, B. *et al.* **IPCC special report on carbon dioxide capture and storage**, Working Group III of the Intergovernmental Panel on Climate Change, Cambridge University Press, Cambridge, United Kingdom and New York, NY, USA, 2005.

MIDDELBURG, Jack J. **Marine carbon biogeochemistry: a primer for earth system scientists**. Springer Nature, 2019.

MISHRA, R. K. *et al.* Cemff : a force field database for cementitious materials including validations, applications and opportunities. **Cement and Concrete Research**, v. 102, n. September, p. 68–89, dez. 2017.

MOCZYDLOWER, B. *et al.* Development of the Brazilian pre-salt fields - when to pay for information and when to pay for flexibility. In: **SPE Latin American and Caribbean Petroleum Engineering Conference Proceedings**, v. 1, n. Figure 1, p. 872–882, 2012.

MOON, E.-J.; CHOI, Y. C. Carbon dioxide fixation via accelerated carbonation of cement-based materials: potential for construction materials applications. **Construction and Building Materials**, v. 199, p. 676–687, fev. 2019.

MORAES, M. K.; COSTA, E. M. DA. Effect of adding organo-modified montmorillonite nanoclay on the performance of oil-well cement paste in CO_2-rich environments. **Cement and Concrete Composites**, v. 127, n. February 2020, p. 104400, mar. 2022.

MUCCIO, Z.; JACKSON, G. P. Isotope ratio mass spectrometry. **The Analyst**, v. 134, n. 2, p. 213–222, 2009.

MURTAZA, M. *et al.* Experimental Investigation of the Impact of Modified Nano Clay on the Rheology of Oil Well Cement Slurry. In: **International Petroleum Technology Conference**, 22 mar. 2019. Disponível em: <http://www.onepetro.org/doi/10.2523/IPTC-19456-MS>.

MUSTAPHA, A. *et al.* Surface water quality contamination source apportionment and physicochemical characterization at the upper section of the Jakara basin, Nigeria. **Arabian Journal of Geosciences**, v. 6, n. 12, p. 4903–4915, 25 dez. 2013.

MYERS, M. B. *et al.* An experimental investigation into quantifying CO_2 leakage in aqueous environments using chemical tracers. **Chemical Geology**, v. 511, n. February, p. 91–99, abr. 2019.

NAKANO, K. *et al.* Observation of cement/sandstone interface after reaction with supercritical CO_2 using SEM-EDS, μ-XRD, and μ-Raman spectroscopy. **e-Journal of Surface Science and Nanotechnology**, v. 14, n. 0, p. 198–203, 2016.

NASRAZADANI, S.; SPRINGFIELD, T. Application of Fourier transform infrared spectroscopy in cement alkali quantification. **Materials and Structures**, v. 47, n. 10, p. 1607–1615, 16 out. 2014.

OMOSEBI, O. *et al.* Investigating temperature effect on degradation of well cement in HPHT carbonic acid environment. **Journal of Natural Gas Science and Engineering**, v. 26, p. 1344–1362, set. 2015.

OMOSEBI, O. *et al.* Degradation of well cement in HPHT acidic environment: Effects of CO_2 concentration and pressure. **Cement and Concrete Composites**, v. 74, p. 54–70, nov. 2016.

OMOSEBI, O. A. *et al.* Cement degradation in CO_2 - H_2S environment under high pressure-high temperature conditions. In: **SPE Bergen One Day Seminar**, 5 abr. 2017. Disponível em: <http://www.onepetro.org/doi/10.2118/185932-MS>.

OTSUKA, Y. *et al.* Effect of carbon dioxide on self-setting apatite cement formation from tetracalcium phosphate and dicalcium phosphate dihydrate; ATR-IR and chemoinformatics analysis. **Colloid and Polymer Science**, v. 293, n. 10, p. 2781–2788, 2 out. 2015.

PAIVA, M. D. M. *et al.* A geopolymer cementing system for oil wells subject to steam injection. **Journal of Petroleum Science and Engineering**, v. 169, n. June, p. 748–759, out. 2018.

PARIS, J. M. *et al.* A review of waste products utilized as supplements to Portland cement in concrete. **Journal of Cleaner Production**, v. 121, p. 1–18, maio 2016.

PARK, S. *et al.* Reaction of hydrated cement paste with supercritical carbon dioxide. **Construction and Building Materials**, v. 281, p. 122615, abr. 2021.

PIAO, J. *et al.* Dynamic behavior of CO_2 in a wellbore and storage formation: wellbore-coupled and salt-precipitation processes during geologic CO_2 sequestration. **Geofluids**, v. 2018, p. 1–20, 2018.

PONZI, G. G. D. *et al.* Basalt powder as a supplementary cementitious material in cement paste for CCS wells: chemical and mechanical resistance of cement formulations for CO_2 geological storage sites. **International Journal of Greenhouse Gas Control**, v. 109, n. March, p. 103337, jul. 2021.

QIN, L.; GAO, X.; CHEN, T. Influence of mineral admixtures on carbonation curing of cement paste. **Construction and Building Materials**, v. 212, p. 653–662, jul. 2019.

RANJAN, A.; KUMAR, R.; MOHAN, D. Comparative analysis of phenolphthalein indicator, XRDA and FTIR methods for measurement of carbonation depth of concrete. **International Journal of Civil Engineering and Technology**, v. 9, n. 5, p. 315–320, 2018.

REBOUÇAS, J. P.; ROHWEDDER, J. J. R.; PASQUINI, C. Near infrared emission spectroscopy for rapid compositional analysis of Portland cements. **Analytica Chimica Acta**, v. 1024, p. 136–144, set. 2018.

ROSÉN, P. *et al.* Fourier transform infrared spectroscopy, a new method for rapid determination of total organic and inorganic carbon and biogenic silica concentration in lake sediments. **Journal of Paleolimnology**, v. 43, n. 2, p. 247–259, 2 fev. 2010.

SAILLIO, M. *et al.* Effect of supplementary cementitious materials on carbonation of cement pastes. **Cement and Concrete Research**, v. 142, n. November 2020, p. 106358, abr. 2021.

SALEHI, S. *et al.* Investigation of mix design and properties of geopolymers for application as wellbore cement. **Journal of Petroleum Science and Engineering**, v. 178, n. March, p. 133–139, jul. 2019.

SANTOS, V. H. J. M. DOS *et al.* Application of Fourier transform infrared spectroscopy (FTIR) coupled with multivariate regression for calcium carbonate ($CaCO_3$) quantification in cement. **Construction and Building Materials**, v. 313, n. October, p. 125413, dez. 2021.

ŠAVIJA, B.; LUKOVIĆ, M. Carbonation of cement paste: understanding, challenges, and opportunities. **Construction and Building Materials**, v. 117, p. 285–301, ago. 2016.

SCHNEIDER DOS SANTOS, R.; ROLIM, S. B. A.; HEPP PULGATI, F. Application of visible and near infrared spectroscopy in non-destructive evaluation of cement materials. **International Journal of Remote Sensing**, v. 36, n. 3, p. 917–938, 1 fev. 2015.

SCHÜTZ, M. K. *et al.* Chemical degradation of reinforced epoxy-cement composites under CO_2-rich environments. **Polymer Composites**, v. 39, n. S4, p. E2234–E2244, dez. 2018.

SCHÜTZ, M. K. *et al.* Evaluation of CO_2 attack in wellbore class G cement: influence of epoxy resins, composites and minerals as additives. **Greenhouse Gases: Science**

and Technology, v. 9, n. 6, p. 1276–1287, 23 dez. 2019.

SHAH, V. *et al.* Changes in microstructure characteristics of cement paste on carbonation. **Cement and Concrete Research**, v. 109, n. April, p. 184–197, jul. 2018.

SHAHRIAR, A.; NEHDI, M. L. Effect of supplementary cementitious materials on rheology of oil well cement slurries. **Advances in Civil Engineering Materials**, v. 3, n. 1, p. 20120027, 27 ago. 2014.

SHI, T. *et al.* FTIR study on early-age hydration of carbon nanotubes-modified cement-based materials. **Advances in Cement Research**, v. 31, n. 8, p. 353–361, set. 2019.

SHIN, W.-J. *et al.* Monitoring the movement of artificially injected CO_2 at a shallow experimental site in Korea using carbon isotopes. **Journal of Environmental Management**, v. 258, n. January, p. 110030, mar. 2020.

ŠILER, P. *et al.* The influence of particle size of cement and different additives on the properties of Portland cement pastes. **Materials Science Forum**, v. 851, p. 104–109, abr. 2016.

SILVA, S. R. DA; DE OLIVEIRA ANDRADE, J. J. Investigation of mechanical properties and carbonation of concretes with construction and demolition waste and fly ash. **Construction and Building Materials**, v. 153, p. 704–715, out. 2017.

SKOCEK, J.; ZAJAC, M.; BEN HAHA, M. Carbon capture and utilization by mineralization of cement pastes derived from recycled concrete. **Scientific Reports**, v. 10, n. 1, p. 5614, 27 dez. 2020.

ŚLIWIŃSKI, M. G. *et al.* In situ $\delta^{13}C$ and $\delta^{18}O$ microanalysis by SIMS: a method for characterizing the carbonate components of natural and engineered CO_2-reservoirs. **International Journal of Greenhouse Gas Control**, v. 57, p. 116–133, fev. 2017.

STARK, J. Recent advances in the field of cement hydration and microstructure analysis. **Cement and Concrete Research**, v. 41, n. 7, p. 666–678, jul. 2011.

SUKMAK, P. *et al.* Sulfate resistance of clay-Portland cement and clay high-calcium fly ash geopolymer. **Journal of Materials in Civil Engineering**, v. 27, n. 5, p. 04014158, maio 2015.

SUWAN, T. Categories and types of raw materials using in geopolymer cement production: an overview. **Solid State Phenomena**, v. 280, p. 481–486, ago. 2018.

SZABÓ-KRAUSZ, Z. *et al.* Wellbore cement alteration during decades of abandonment and following CO_2 attack – a geochemical modelling study in the area of potential CO_2 reservoirs in the Pannonian basin. **Applied Geochemistry**, v. 113, n. June 2019, p. 104516, fev. 2020.

TATZBER, M. *et al.* An alternative method to measure carbonate in soils by FT-IR spectroscopy. **Environmental Chemistry Letters**, v. 5, n. 1, p. 9–12, 29 jan. 2007.

TAVARES, L. M. *et al.* Effect of calcium carbonate on low carbon steel corrosion behavior in saline CO_2 high pressure environments. **Applied Surface Science**, v. 359, p. 143–152, dez. 2015.

TEODORIU, C.; BELLO, O. A review of cement testing apparatus and methods under CO_2 environment and their impact on well integrity prediction – where do we stand? **Journal of Petroleum Science and Engineering**, v. 187, n. September 2019, p. 106736, abr. 2020.

TIONG, M.; GHOLAMI, R.; RAHMAN, M. E. Cement degradation in CO_2 storage sites: a review on potential applications of nanomaterials. **Journal of Petroleum Exploration and Production Technology**, v. 9, n. 1, p. 329–340, 31 mar. 2019.

TORSÆTER, M.; TODOROVIC, J.; LAVROV, A. Structure and debonding at cement–

steel and cement–rock interfaces: effect of geometry and materials. **Construction and Building Materials**, v. 96, p. 164–171, out. 2015.

TREMOSA, J. *et al.* Experimental assessment of well integrity for CO_2 geological storage: a numerical study of the geochemical interactions between a CO_2-brine mixture and a sandstone-cement-steel sample. **Applied Geochemistry**, v. 78, p. 61–73, mar. 2017.

TU, Z.; SHI, C.; FARZADNIA, N. Effect of limestone powder content on the early-age properties of CO_2-cured concrete. **Journal of Materials in Civil Engineering**, v. 30, n. 8, p. 04018164, ago. 2018.

VALLIANT, E. M. *et al.* Fourier transform infrared spectroscopy as a tool to study the setting reaction in glass-ionomer cements. **Materials Letters**, v. 185, p. 256–259, dez. 2016.

VAN GELDERN, R. *et al.* Field-based stable isotope analysis of carbon dioxide by mid-infrared laser spectroscopy for carbon capture and storage monitoring. **Analytical Chemistry**, v. 86, n. 24, p. 12191–12198, 16 dez. 2014.

VANCE, K. *et al.* Direct carbonation of $Ca(OH)_2$ using liquid and supercritical CO_2 : implications for carbon-neutral cementation. **Industrial & Engineering Chemistry Research**, v. 54, n. 36, p. 8908–8918, 16 set. 2015.

VEERASINGAM, S.; VENKATACHALAPATHY, R. Estimation of carbonate concentration and characterization of marine sediments by Fourier transform infrared spectroscopy. **Infrared Physics and Technology**, v. 66, p. 136–140, set. 2014.

VERMEUL, V. R. *et al.* An overview of the monitoring program design for the FutureGen 2.0 CO_2 storage site. **International Journal of Greenhouse Gas Control**, v. 51, p. 193–206, ago. 2016.

WAKEEL, S. AL *et al.* The effect of introducing nanoparticles on the fracture toughness of well cement paste. **International Journal of Greenhouse Gas Control**, v. 84, n. August 2018, p. 147–153, maio 2019.

WANG, C. *et al.* Can nanosilica sol prevent oil well cement from strength retrogression under high temperature? **Construction and Building Materials**, v. 144, p. 574–585, jul. 2017.

WANG, J.; WEN, X.; LI, S. Differentiated correction on the signal intensity dependence of GasBench II-IRMS from blank effect and instrument nonlinear effect. **International Journal of Mass Spectrometry**, v. 422, p. 80–87, nov. 2017.

WELCH, S. A. *et al.* Assessing geochemical reactions during CO_2 injection into an oil-bearing reef in the Northern Michigan basin. **Applied Geochemistry**, v. 100, n. December 2018, p. 380–392, jan. 2019.

WIESE, B. *et al.* Well-based hydraulic and geochemical monitoring of the above zone of the CO_2 reservoir at Ketzin, Germany. **Environmental Earth Sciences**, v. 70, n. 8, p. 3709–3726, 15 dez. 2013.

WIGAND, M. *et al.* Geochemical effects of CO_2 sequestration on fractured wellbore cement at the cement/caprock interface. **Chemical Geology**, v. 265, n. 1–2, p. 122–133, jul. 2009.

WILBERFORCE, T. *et al.* Progress in carbon capture technologies. **Science of The Total Environment**, v. 761, p. 143203, mar. 2021.

WITKOWSKI, H.; KONIORCZYK, M. New sampling method to improve the reliability of FTIR analysis for self-compacting concrete. **Construction and Building Materials**, v. 172, p. 196–203, maio 2018.

WU, B.; YE, G. Study of carbonation rate of synthetic C-S-H by XRD, NMR and FTIR.

Heron, v. 64, n. 1–2, p. 21–38, 2019.

XIAO, T. *et al.* Quantification of CO_2-cement-rock interactions at the well-caprock-reservoir interface and implications for geological CO_2 storage. **International Journal of Greenhouse Gas Control**, v. 63, n. May, p. 126–140, ago. 2017.

YADAV, S.; MEHRA, A. A review on ex situ mineral carbonation. **Environmental Science and Pollution Research**, v. 28, n. 10, p. 12202–12231, 6 mar. 2021.

ZHA, X. *et al.* Numerical modeling of supercritical carbonation process in cement-based materials. **Cement and Concrete Research**, v. 72, p. 10–20, jun. 2015.

ZHAN, B. J. *et al.* Characterization of C–S–H formed in coupled CO_2–water cured Portland cement pastes. **Materials and Structures**, v. 51, n. 4, p. 92, 4 ago. 2018.

ZHANG, D.; GHOULEH, Z.; SHAO, Y. Review on carbonation curing of cement-based materials. **Journal of CO_2 Utilization**, v. 21, n. June, p. 119–131, out. 2017.

ZHANG, T. *et al.* CO_2 capture and storage monitoring based on remote sensing techniques: a review. **Journal of Cleaner Production**, v. 281, p. 124409, jan. 2021.

ZHOU, Y. *et al.* Analytical methods and application of stable isotopes in dissolved organic carbon and inorganic carbon in groundwater. **Rapid Communications in Mass Spectrometry**, v. 29, n. 19, p. 1827–1835, 2015.

ZHUANG, X. Y. *et al.* Fly ash-based geopolymer: clean production, properties and applications. **Journal of Cleaner Production**, v. 125, p. 253–267, jul. 2016.

ZIMMER, M. *et al.* Monitoring of the gas composition and stable carbon isotopes during side track drilling in Ktzi 203 at the Ketzin CO_2 storage pilot site, Germany. **Advances in Geosciences**, v. 45, n. Ktzi 203, p. 7–11, 16 jul. 2018.

Pontifícia Universidade Católica do Rio Grande do Sul
Pró-Reitoria de Graduação
Av. Ipiranga, 6681 - Prédio 1 - 3º. andar
Porto Alegre - RS - Brasil
Fone: (51) 3320-3500 - Fax: (51) 3339-1564
E-mail: prograd@pucrs.br
Site: www.pucrs.br